地下水流動特性を考慮した
水質形成モデルの構築

（核燃料サイクル開発機構 契約業務報告書）

2003年3月

三菱商事株式会社

2003年3月

地下水流動特性を考慮した水質形成モデルの構築

（核燃料サイクル開発機構 契約業務報告書）

杉田 健一郎* Richard Metcalfe**

要約

本報告書は、岐阜県（中部日本に位置する）東濃地区における地下水流動特性を考慮した水質形成モデルの構築を行ったものである。水と岩石との相互作用、および地下水の化学的性質を変化させる混合過程との連関を理解する事を本プロジェクトの目的とする。結果に基づき、以下を目標とした。

- 筋道の通ったモデルを構築するため、水文地質学的情報と地球化学的情報を統合する包括的な研究方法を提案する。
- 自然界の水文地質学的情報に基く地下水のフローモデルのテストとして、地球化学的情報を利用する包括的な研究方法を提唱する。
- 性能評価（PA）の時間尺度（一般的に10^5－10^6年）から見た場合、フローと連関した水と岩石との相互作用が、岩石－水の系に対し、その物理的、化学的特性を著しく変化させうるか否かを評価する。

連関したシミュレーションを実行できるコンピュータコードはいくつか存在する。しかしながら極めて単純化した地下水／岩石系であっても、シミュレーションを行うには、非現実的な長い時間を要することがよくある。それ故、起こりうるすべての連関プロセスを組み込んだ単一の数値モデルを構築されることはなかった。代わりに連関の異なる面を調べるため、モデルがいくつか構築されたのである。

フローと化学反応の連関は、バッチシミュレーションと 1 次元連関シミュレーションで調べた。バッチシミュレーションは、（フローの経路に沿って条件が異なることを表すため）異なる条件で行った。フローの表現は極めて単純化されていたため、計算時間を適度に短くしている間も比較的複雑な水／岩石反応を考慮することができた。

---

* 三菱商事株式会社

** 株式会社クインテッサジャパン

大量移行（地下水混合過程）とフローの連関は、3次元シミュレーションおよび2次元シミュレーションで調べた。これらのシミュレーションは、水／岩石反応を考慮しなかったため、地下水のフローを比較的複雑に表現し、計算時間を比較的短縮することができた。

以下のコードを利用し化学反応とフローの連関を調べた。

- 平衡計算と動力学的反応経路計算を行うため、「地球化学的モデリング」(Geochemist's Workbench)（GWB）3.2.1版（イリノイ大学；Bethke、1996）を利用。
- 酸化還元フロントと塩分の移動を調べるため、オゾン（O3）（Quintessa）を利用。
- 動力学がない場合は、フローと反応の連関を調べるため、PHREEQC Interactive2.8版（米国地質調査；Parkhurst and Appelo、1999）を利用。
- 動力学を考慮し、フローと反応の連関を調べるため、Raiden2（Quintessa）を利用。

地下水のフローはコードFEMWATER3.0版（Lin他、2001）を利用し、シミュレーションを行った。大量移行は考慮しなかった。しかし大量移行の計算を初期化するため、コードSUTRA（Voss、1984）によりアウトプット操作を利用した。モデル化は、3次元領域モデル（40×30×10km）から2次元局所（9×3km）可変密度フローおよび溶質移行モデルへと進歩した。

重要な涵養地帯と考えられるため3次元領域モデルには笠置山を含めた。また3次元領域モデルは最も重要な河川まで広げた。なぜならこれらの河川は流出帯と考えられるためである。加えて笠置山は、新建設地（NCS）まで主要な分布区域を支配している。NCSはこの地域の主要な2つの河川の間に位置するが、土岐川の堆積盆地に属する。

この領域モデルは、ほぼNCSを中心に展開する局在性3次元モデルの境界条件を明らかにするために利用された。局所モデルは、木曽川（北部）と土岐川（南部）の分水界に囲まれた地域から広がっていた。側方への限界はフローラインと一致した。底部は平面であり、地表より約3km下に位置した。結果として生じたブロックは9×6×3kmであった。この局所モデルは、領域3次元モデルと異なり、花崗岩の水力学的特性とその上に重なる堆積岩の水力学的特性を識別することができた。

2次元モデルは、局所3次元モデルを通じ、長さ10kmの横断面を考慮した。モデル変域の主な流出は、土岐川の両側に対してであった。月吉断層とともに堆積岩の層が示された。沈積によって生じた遮蔽物は、5層の要素で示された。そのため初期塩分のフラッシングは、先駆的な3次元モデルでの場合より一貫性をもってシミュレーションすることが可能となった。

これらの様々な化学反応（および地下水のフローに関する）モデルは、東濃地区地下水の

化学的性質の漸進的変化に関し、起こりうるシナリオの 1 つを評価するために利用した。これらのシナリオは、最初は、入手可能な地下水の化学的性質に関するデータを利用し、創り出したものである。

土岐川流域近くの深部河水における総溶解性物質（TDS）の含有量は、調査地域中、最大である。これらの地下水の優性成分は Na－（Ca）－Cl であるが、対照的に Na－Ca－HCO_3が優性成分である深部地下水はさらに北方で標本としたものである。これらの水の起原に関し起こりうるシナリオを以下に展開した。

- 「化石」海水のフラッシング
- 「化石」熱水のフラッシング
- 「化石」岩漿のフラッシング
- 現在の熱水との混合
- 現在の岩漿との混合
- 上述のシナリオの組み合わせ

たとえあるにせよ、これらの可能性のうち、いずれが正しいかは断定できない。しかしながら過去にこの地域で海洋性塩分が存在したという明確な証拠は存在する。一方、他のシナリオに関する証拠は薄弱である。それ故、数値モデル化は、以下の密接な関係を評価することに焦点を合わせた。

- 土岐花崗岩に海水が均等に染み込む
- 同等の多孔性媒質として水力学的に振る舞う各岩石構成物
- 現在の水力学的条件とほぼ類似した水力学的条件下で、塩分のない地下水がフラッシュする土岐花崗岩

1 次元、2 次元、3 次元モデル化の結果を統合し、評価するため、証拠に基づく支持論理（ESL）を利用した。研究方法は、筋が通る水文地質学的、地球化学的な理解が存在するという仮説に賛成、または反対する 1 つの証拠として、各モデルのアウトプットを処理することであった。

特筆すべき結果は以下の通りである。

- 評価したシナリオの水文地質学的、地球化学的な結果は相反する。それ故そのシナリ

オは却下しなければならない。特に現在と類似した水力学的パラメータによれば、およそ 1 万 5000 年以内には地下水の塩分はフラッシュされると思われる。しかし海水は、まだ、この時間枠内ではこの地域に浸入していない。

- 岩石塊の発現（たとえば二重有孔性媒質）に変化があれば、塩分は数千万年もの長期にわたり保存されると推測される。

- 鉱物学上の変化があっても、地下水系の全体的な有孔性に大規模な変化が生じることはないと予測される。

- pH と PCO_2の漸進的変化を説明するには動力学的モデルが必要である。不確定性を考慮すると、Raiden の結果は、滞留時間が増すにつれ、フロー経路に沿って pH が増し、PCO_2が減少する事象と一致する。

- 新しい花崗岩が涵養されると、減少条件は、涵養地帯の数十メートルの範囲内で極めて速やかに達成されよう。いかなる時でも酸化還元フロントが浸透する実際の深さは、岩石中に存在する黒雲母の量で制御されると思われる。

- 連関シミュレーションでは、この酸化還元フロントは、真水と塩水との混合地帯の移動する場合と比べ、岩床を通って数倍ゆっくりと移動した。

- 酸素を運搬する水の浸透については、塩性地下水をフラッシュするのに必要な期間中、観察とモデルの間に矛盾がある。モデルから、酸素化された水は、観察されているよりも遙かに深く浸透すると予測される。

- 粘土鉱物による石灰長石の交代作用は、重要事となりえよう。この過程で方解石を形成する pH は低下するであろう。しかし方解石は極めて少量しか形成されず、ある環境下では、その後すぐに再び溶解すると予想される。

以下に推奨点を上げる。

- 堆積物のフラッシングについては、適切な尺度でモデル化しなければならない。

- モデル上での水の進入は、シミュレーション中に変更しなければならない。

- 上記の事項を行うためには、（最近の地形学の評価に基づき）境界条件の変化率を正しく理解する必要がある。

- 海水に起原を持つ塩分に対し、既存のものに代わる起原をいくつか考慮する必要がある。

- 塩分は、それぞれが別個の起原を持ついくつかの成分の混合物である、という可能性を考慮する必要がある。

結果から、水分地質学的解釈と地球化学的解釈を統合するにはいくつかの包括的な考え方が考えられる。

- 初期の境界条件を解釈するには、古水文地質学的情報が必須である。

- たとえ水文地質学上の特性と地球化学上のパラメータが極めて判然としないものであっても、地下水の漸進的変化について既存のものに代わるシナリオを創り出し、テストを行えば、有益な洞察を行える。

- 最適な研究方法は、連関の異なる面を調べる一連のコンピュータモデルを構築し、モデルで得られた結果が互いにどの程度まで一致するかを評価することである。

- 入手可能なコンピュータコードが多くの連関過程をシミュレーションできるが、地下水のフローに関し完全に連関したただ一つのモデルを構築することは、通常、不適当である。理由は下記の通りである。

  ✓ 計算に長時間を要し、不確定性について適切な評価を行えない。

  ✓ 多くの場合本質的に定量できない不確定性が多数存在する。

  ✓ 現場データの空間的分布状態は、そうしたモデルから得られる結果を直接比較するには、たいてい、不適切である

Abstract

This report describes a coupled geological geochemical/hydrogeological model of the groundwater system in the Tono area of Gifu ken, central Japan. The project aimed to understand the coupling between water/rock interactions and mixing processes that cause variations in groundwater chemistry. Based on the results it was aimed to:

- suggest generic approaches for integrating hydrogeological and geochemical information so as to produce self-consistent models;
- suggest generic approaches for using geochemical information as a test of groundwater flow models based on physical hydrogeological information;
- evaluate whether or not water/rock interactions coupled to flow can cause significant variations to the physical and chemical properties of rock-water system over Performance Assessment (PA) time scales (typically 10^5 to 10^6 years).

There are several computer codes that can perform coupled simulations. However, even highly simplified groundwater/rock systems often take impractically long times to simulate. Therefore, a single numerical model incorporating all possible coupled processes was not constructed. Instead, several models were developed to investigate separate aspects of coupling.

The coupling between flow and chemical reactions was investigated by batch simulations conducted for different conditions (to represent different conditions along a flow path) and by 1D coupled simulations. Because the representation of flow was very simplified, relatively complex water/rock reactions could be considered while keeping calculation times reasonably short.

The coupling between mass transport (groundwater mixing processes) and flow was investigated by 3D and 2D simulations. These simulations did not consider water/rock reactions, enabling relatively complex representations of groundwater flow and relatively short calculation times.

Coupling between chemical reactions and flow was investigated by using the following codes:

- Geochemist's Workbench (GWB) v. 3.2.1 (University of Illinois; Bethke, 1996) was used for equilibrium calculations and kinetic reaction-path calculations.
- Ozone (O3) (Quintessa) was used to investigate the migration of redox fronts and salinity.
- PHREEQC Interactive v. 2.8 (United States Geological Survey; Parkhurst and Appelo, 1999) was used to investigate the coupling between flow and reactions in the absence of kinetics.
- Raiden 2 (Quintessa) was used to investigate the coupling between flow and reactions, taking into account kinetics.

Groundwater flow was simulated using the code FEMWATER v3.0 (Lin et al., 2001). Mass transport was not considered, but the output was used to initialise mass transport calculations using the code SUTRA (Voss, 1984). The modelling progressed from a 3D regional model (40 x 30 x 10 km) to a 2D local (9 x 3 km) variable density flow and solute transport model.

The 3D regional model included Mt. Kasagi, which is thought to be an important recharge zone, and extended to the most important rivers, which are considered to be discharge zones. In addition, Mt. Kasagi exerts a control over the head distribution as far as the New Construction Site (NCS), which is located between the two main rivers of the area, but in the Toki river basin.

This regional model was used to define the boundary conditions for a localised 3D model centred approximately on the NCS. The local model extended from the watershed division between the Kiso river (North) and the Toki river (South). Lateral limits were coincident with flow lines. The

bottom face was planar and located some 3 km below the land surface. The resulting block was 9 x 6 x 3 km. Unlike the regional 3D model this local model distinguished between the hydraulic properties of the granite and those of the overlying sedimentary rocks.

The 2D model considered a 10 km long cross section through the local 3D model. The main discharge of the model domain was to both sides of the Toki river. The sedimentary rock layers and with the Tsukiyoshi fault were represented. The sedimentary cover was represented by 5 layers of elements, which enabled the flushing of initial salinity to be simulated more consistently than in the precursor 3D model.

These various chemical reaction- and groundwater flow- models were used to evaluate one of several possible scenarios for the evolution of groundwater chemistry in the Tono area. These scenarios were developed initially, using the available groundwater chemical data.

The total dissolved solid (TDS) contents of the deeper waters near the Toki River valley are the highest encountered in the investigation area. These groundwaters are dominated by Na-(Ca)-Cl, whereas contrasting Na-Ca-HCO_3 dominated deep groundwater has been sampled further north. The following possible scenarios for the origin of these waters were developed:

- flushing of 'fossil' seawater;
- flushing of 'fossil' hydrothermal water;
- flushing of 'fossil' magmatic fluid;
- mixing with present hydrothermal fluid;
- mixing with present magmatic fluid;
- a combination of the above scenarios.

It is uncertain which of these possibilities, if any, is correct. However, there is clear evidence that marine salinity occurred in the area in the past, whereas evidence for the other scenarios is more tenuous. Therefore, the numerical modelling focused on evaluating the implications of:

- the Toki granite being uniformly saturated with seawater;
- each of the rock formations behaving hydraulically as equivalent porous media;
- the Toki granite being flushed by fresh groundwater under hydraulic conditions broadly similar to those of the present.

Evidential Support Logic (ESL) was used to integrate and evaluate the results from the 1D, 2D and 3D modelling. The approach was to treat each model's output as a piece of evidence for or against the hypothesis that there is a self-consistent hydrogeological/geochemical understanding.

Important results are:

- The hydrogeological and geochemical consequences of the evaluated scenario are inconsistent and therefore the scenario must be rejected. Notably, hydraulic parameters similar to the present would cause groundwater salinity to be flushed within around 15,000 years, but seawater has not entered the area within this time frame.
- Variations in the rock mass's representation (e.g. as a dual porosity medium) could lead to much longer preservation of the salinity, even to a times of several 10's of millions of years.

- Variations in mineralogy are not predicted to cause a large change in the overall porosity of the groundwater system.

- Kinetic models are required to explain the progressive evolution of pH and PCO_2. When uncertainties are taken into account, Raiden results are consistent with pH increasing and PCO_2 decreasing along a flow path as residence times increase.

- If fresh granite is recharged, reducing conditions would be attained very rapidly, within a few 10's of metres of a recharge zone. The actual depth of penetration of the redox front at any time will be controlled by the amount of biotite present in the rock.

- In the coupled simulations, this redox front migrated through the rock up to several orders of magnitude slower than the migration of the mixing zone between fresh and saline water.

- There is an inconsistency between the observed and modelled penetration of oxygen-bearing water during the time taken to flush the saline groundwater. The model predicts that oxygenated water would penetrated much more deeply than is observed.

- Replacement of calcic feldspar by clay minerals could be significant. This process could lead to a reduction of pH which could cause calcite to form, but calcite would form in only very small amounts and could, under some circumstances, dissolve again soon afterwards.

The following recommendations are made:

- The flushing of the sediments should be modelled at an appropriate scale.

- The ingress of water in the model should be changed during the simulation.

- To do so, a proper understanding of the changing rates of the boundary conditions is needed (based on an evaluation of recent geomorphology).

- Several alternative origins to salinity of seawater origin need to be considered.

- The possibility that the salinity is a mixture of several components, each with a distinct origin, needs to be considered.

The results have several generic implications for integrating hydrogeological and geochemical interpretations.

- Palaeohydrogeological information is essential to interpret the initial boundary conditions.

- Even if hydrogeological characteristics and geochemical parameters are very uncertain, developing and testing alternative groundwater evolution scenarios can give useful insights.

- The most appropriate approach is to construct a series of computer models that investigate different aspects of coupling, and then to evaluate the degree to which the models' results are consistent with one another.

- Even though available computer codes can simulate many coupled processes, it is usually inappropriate to construct a single, fully-coupled model for groundwater flow because:

  - long computation times are required, preventing adequate evaluation of uncertainties;

  - there are many uncertainties that are often inherently unquantiable;

  - the spatial distribution of site data is usually inappropriate for direct comparison with the results of such a model.

A coupled geochemical/hydrogeological model of the Tono area

Report to JNC (JNC Cpmd Integrate 101203v1.doc Issue 1)

R. Metcalfe
D. Savage
S.J. Benbow
H. Takase
T. Noguchi

Quintessa Japan

Jordi Guimerà
Eduardo Ruiz
Miguel Luna
David Arcos
Salvador Jordana

ENVIROS

March 2003

ENVIROS

Quintessa

Contents

Part 1: Alternative concepts and 1D coupled water/rock interactions models

Part 2: 2D and 3D coupled models of salinity distributions

Part 3: Integrated evaluation of results from 1D, 2D and 3D coupled models

Tables

Figures

Part 1: Alternative concepts and 1D coupled water/rock interactions models

1 Introduction

This part of the report describes a coupled geological geochemical/hydrogeological model of the groundwater system in the Tono area of Gifu ken, central Japan.

The work builds on results from earlier geochemical studies undertaken by JNC in the Tono area, notably the Tono Geochemistry Research Project (TGRP). This latter project has identified several water/rock interaction processes that control the chemistry of groundwaters around Tono. Additionally, it has been recognised that in and around the Toki River valley (Figure 1), in the south of the Tono area, there is groundwater that is chemically distinct from groundwater sampled further north. The total dissolved solid (TDS) contents of the deeper waters near the Toki River valley are the highest encountered in the investigation area. These groundwaters are dominated by Na-(Ca)-Cl, whereas contrasting Na-Ca-HCO_3 dominated waters have been sampled further north.

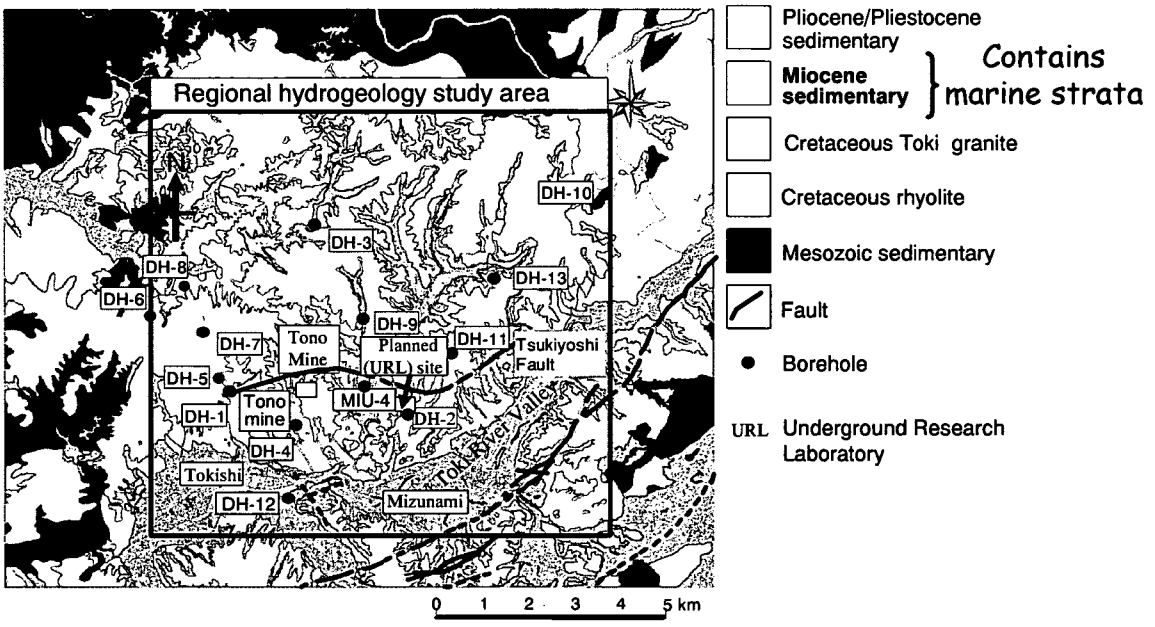

Figure 1. Simplified geological map of the Tono area showing the locations of selected boreholes. MSB-series boreholes (not shown) are located within the planned URL site.

The project described here aims to understand further the coupling between water/rock interactions and mixing processes that are responsible for these variations in groundwater chemistry. Based on the resulting improved understanding of the practicalities of constructing a coupled model it is aimed to:

- suggest generic approaches for integrating hydrogeological and geochemical information so as to produce self-consistent models for groundwater flow;
- suggest generic approaches for using geochemical information as a test of groundwater flow models based on physical hydrogeological information;
- develop and demonstrate approaches for evaluating whether or not water/rock interactions coupled to flow can cause significant variations to the physical and chemical properties of rock-water system over the time scales of PA (typically 10^5 to 10^6 years).

The first two aims are important because self-consistent models for groundwater flow based on both chemical and physical information will generally be more robust than models based on physical data alone.

The third aim is important because PA models generally tend to assume invariant rock properties for any particular scenario over the timescale of an assessment. The validity of this hypothesis needs to be evaluated on a site-by-site basis.

The following aspects of the work were undertaken by Quintessa:

- compiling relevant data for the project;
- development of alternative conceptual models;
- simulating the coupling between flow and chemical reactions in 1D;
- integration of the final results and preparation of the final report.

Staff of the Barcelona office of ENVIROS have developed coupled 2D and 3D models of salinity distributions in the Tono area under subcontract to Quintessa. These models are described separately in Part 2 of the report. Part 3 integrates the results from the two sets of models.

2 Approach

2.1 Developing a conceptual model

The basic approach involved the following steps.

- The available geochemical and geological data from the Tono area were compiled.
- Alternative conceptual models for the initial distribution of the groundwater salinity and the processes controlling the chemical evolution of the groundwater were then developed, based only upon:
  - the chemical compositions of the groundwaters and the spatial distributions of chemically distinct groundwater types;
  - the geological history of the Tono area.
- The conceptual model that is most consistent with the chemical characteristics and spatial distribution of chemically distinct groundwaters was then used as a basis for coupled numerical simulations of different types. The aim of the simulations was to evaluate the consistency of the chemical variations and the characteristics of groundwater flow based on hydrogeological information.

2.2 The computational approach

Simulations of the coupling between groundwater/rock interactions and groundwater flow are inherently complex. Several computer modelling codes exist that can in principle simulate the

coupling between flow and many different types of water/rock interactions. However, in practice, numerical models of even highly simplified groundwater/rock systems can require considerable computing time to complete. For this reason, the present project did not attempt to construct a single numerical model that incorporates all possible couplings. Instead, several models were developed to investigate separate aspects of the coupling. These models used various complementary computer codes and approaches, as listed in Table1.

To ensure consistency with previous modelling, simulations employing the codes Geochemist's Workbench (GWB), Raiden and PHREEQC used thermodynamic databases developed by JNC as follows:

- The GWB and Raiden simulations used the database 'thermo.tap'. This is an adaptation of the GWB database, 'thermo.dat', which is supplied with the GWB package. The 'thermo.dat' database was checked for consistency with JNC's thermodynamic database 'sprons.jnc' during the Tono Geochemistry Research Project (Arthur, 2003) and where necessary data where modified. Subsequently, during the Tono Natural Analogue Project (TAP), this database was further modified by R.A. Arthur to include more recent data for uranium minerals and thereby produce the database 'thermo.tap' that was used in this work.

- The PHREEQC simulations were made using a modified version of the database '990900c0.tdb', which was obtained from JNC's web page. Data for $Fe(OH)_3(am)$ from the GWB database 'thermo.tap' were added to '990900c0.tdb'.

Table 1. Summary of the computer codes used in the project.

Code	Source	Nature of Code	Application in project	Advantages (as applied in this project)[1]	Limitations (as applied in this project)[2]
Geochemist's Workbench (GWB) version 3.2.1	University of Illinois (Bethke, 1996).	Chemical speciation and water/rock interaction simulation code	Understanding importance of reaction kinetics and mineral evolution Non-coupled batch reaction and 'flush simulations	• Relatively rapid calculations allowing large number of alternative cases • Can handle redox, pH, chemical speciation complex water chemistry • Can handle wide range of minerals	• No coupling between transport and chemistry
Ozone (O_3)	Quintessa K.K.	Performance Assessment (PA) code with 1D transport and chemical simulation capabilities (extendable to 2D and 3D)	Understanding the evolution of redox conditions coupled to flushing of saline water by fresh water	• Relatively rapid calculations allowing large number of alternative cases • Evolution of redox conditions and gross salinity can be calculated	• Relatively simplified representation of chemical reactions • No coupling between hydraulic and chemical properties
PHREEQC Interactive version 2.8	United States Geological Survey (Parkhurst and Appelo, 1999)	Chemical speciation and water/rock interaction code with 1D semi-coupled transport simulation capabilities	Understanding evolution of groundwater salinity and rock mineralogy over short time-scales (to 1000's of years) and short spatiagl scales (100's of m) during saline water flushing by fresh water	• Relatively easy to simulate complex groundwater chemistry and a wide range of mineral reactions	• Very long calculation times (several days to weeks for even simple chemical systems) • Only a limited range of alternative cases can be simulated • No coupling between porosity and mineralogical evolution • Very simple transport capability
Raiden version 2	Quintessa K.K.	1D fully coupled flow and reaction code (extendable to 2D and 3D)	Undertanding full coupling between hydraulic properties, evolution of groundwater salinity and rock mineralogy during flushing of saline water by fresh water over long time scales (to 1 million years) and spatial scales (to 10 km)	• Full coupling between transport, groundwater chemistry, mineralogy and porosity	• Very long calculation times (several days to weeks for even simple chemical systems) • Only a limited range of alternative cases can be simulated • In practice considerably simplified chemical system required (no redox)

Notes:

[1,2] These advantages and disadvantages relate to the particular use of each code in ***this project*** and would not necessarily apply to other uses. For example, Ozone(O_3) is a very flexible code and the complexity of a simulation is decided by the user. Other applications of this code could involve much more complex calculations, with much larger degrees of coupling and/or greater representation of chemical processes (e.g. speciation, water/rock reactions etc). In such a case, simulation times would probably be much greater.

3 Data compilation

The primary data used in the project are summarised in Table 2.

Table 2. Summary of data compiled for the present project.

Data Title	Description	Source
Maps and satellite images of the Tono area	Birds-eye view of the Togari site DH borehole localities and the area for which groundwater flow modelling has been carried out Map of the Shoba sama site Map showing borehole locations in the regional hydrogeology study area –DH, SN-An-, KA- boreholes Map showing the locations of boreholes in the regional hydrogeology study area – MC boreholes Map showing the locations of boreholes around Tono mine Landsat images (2) of the Tono area and the surrounding countryside	JPEG files: 'BirdViewOfTogariSite' 'TGC_All_2' 'TGC_All_3' 'TGC_All_4' 'TGC_All_5' 'TGC_All_6' 'TGC_All_7' 'TGC_All_8'
Details of river details flows etc	Catchment and flow rates of major rivers in the study area.	Excel file 'RiverInfo.xls'
Borehole locations	Locations of boreholes numbered in the following series: A-, AN-, C-, E-, F-, G-, H-, HN-, Hy-, IWA-, J-, K-, Kn-, Ms-, Mt-, S-, Tu-, Z-	Excel file 'LocationBH.xls'
Borehole locations	Locations of boreholes numbered in the following series: DH- AN- MIU- SN- TH- MSB-	Excel file 'Borehole.xls'
Flow calculation mesh information	Grid used previously in flow calculations. Files containing X, Y, Z coordinates of mesh nodes.	Folder 'DEM20m' containing Excel files Folder 'DEM50m' containing Excel files
Water balance information	Includes rainfall and data for stream flows, discharge, recharge etc	Excel file 'balance_moni'
Head data	Head data for boreholes MIU-1, MIU-2, MIU-3, MIU-4, AN-1, AN-3, DH-9, DH-11, DH-13	Excel file 'Head_1'
Head data	Data for multi-piezometers, boreholes TH-1, TH-2, TH-3, TH-4(1), TH-4(2), TH-5(1), TH-5(2), TH-6, TH-7(1), TH-7(2), TH-8(1), TH-8(2), AN-6, SN-4, DH-3, DH-7	Excel file 'Head_2'
Hydraulic test results (hydraulic conductivity and transmissivity)	DH-1, DH-2, DH-3, DH-4, DH-5, DH-6, DH-7, DH-8, DH-9, DH-10, DH-11, DH-12, DH-13 AN-1, AN-3, MIU-1, MIU-2, MIU-3	Excel files: 'Hydoraulic_test_DH' 'Hydraulic_test_AN,MIU_1v2' 'status'
Compilation of water chemical data	All routine groundwater, surface water, onsen, stream water, drilling fluid and rain water analyses	Excel file 'Table_gwchem_ver up.xls 1'
Hotspring data	Historical data (pre-JNC) for hot springs	Excel file 'chemicaldata'
MSB-Borehole data	Chemical data for the MSB boreholes in the New Constrution Site (NCS)	Excel files: 'MSB-2 GW chem sum' 'MSB-4 GW chem sum'
Borehole DH-2 data	Groundwater chemistry Physical chemical parameters	Excel files: 'DH-2 chem sum' '物理化学パラ'

Table 2. Continued

Data Title	Description	Source
Borehole MIU-4 data	Geological, hydrogeological and geochemical information from borehole MIU-4	Files (Excel, Adobe Acrobat) in folders: '0.Overview' '2.Geology' '4.Hydrogeology' '6.Additional Investigation' 'Rock Mechanics' '1.Drilling' '3.Geophysical log' '5.HydrochemistryAppendix'
Electro-magnetic survey data	Data used for estimating the boundary between sedimentary rocks and basements using an electromagnetic method	Folder 'Unc', containing JPEG and Word files

4 Alternative conceptual model development

4.1 Present groundwater chemistry

In the part of the Tono groundwater system that is dominated by Ca-Na-HCO_3 fresh water, the groundwater salinity can be explained largely as a consequence of progressive water/rock interactions (e.g. Iwatsuki and Yoshida, 1999; JNC, 2000; Iwatsuki et al. 2002 and references therein). These reactions are thought to include cation exchange, most probably on clay minerals such as smectite, which may explain a general decrease in Ca/Na ratios with depth/inferred distance along a flow path.

Towards the south of the investigation area, in and around the valley of the Toki river (Figure 1), the slightly more saline (though only brackish[1] at its most concentrated) Na-(Ca)-Cl dominated water is of much less certain origin. A possible origin is seawater since the sedimentary rocks of the Akeyo Formation in particular are marine in origin, indicating that marine water has been in the area in the past. Additionally, stable isotopic evidence suggests that marine water has penetrated into the underlying Toki Granite in the past (Iwatsuki et al 2002). However, as pointed out by Metcalfe et al. (2003), the present salinity clearly does not have the chemical signature of seawater. This can be appreciated by considering the ratios of dissolved constituents (Table 3). However, it is instructive to consider whether it is ***possible*** that the salinity originated in seawater, but has since been modified, by water/rock reactions and/or by mixing with other groundwater. Some simple calculations with this goal in mind are presented in the following section.

[1] Here, the classification of Carpenter (1978) is used to describe salinity, following the practice of other studies (e.g. Nirex, 1997). Fresh water has Total Dissolved Solids (TDS) < 1000 mgl^{-1}; brackish water has TDS = 1000 and < 10,000 mgl^{-1}; saline water has TDS = 10,000 and < 100,000 mgl^{-1}; and brines have TDS = 100,000 mgl^{-1}.

Table 3. Comparison between selected chemical ratios for Tono groundwater (GW) and seawater (SW).

Samples	Na/Cl	Br/Cl	Na/Ca	Mg/Ca	Na/K
	Mass	Mass	Mass	Mass	Mass
Average of all except older (1980s) analyses from U-exploration boreholes and waters with <10 ppm Cl	1.00	2.06E-03	9	7.03E-03	166
Standard Dev of all except older (1980s) analyses from U-exploration boreholes and waters with <10 ppm Cl	0.87	3.80E-04	11.22	5.26E-03	87.08
Number analyses except older (1980s) analyses from U-exploration boreholes and waters with <10 ppm Cl	30	30	30	25	30
Average of all except MSB-2, MSB-4, DH-2, older U-Exploration boreholes	1.74	3.86E-03	13	1.56E-02	148
Standard Deviation of all except MSB-2, MSB-4, DH-2, older U-Exploration boreholes	1.54	6.54E-03	14.71	2.82E-02	79.73
Number of analyses except MSB-2, MSB-4, DH-2 older U-Exploration boreholes	17	17	17	13	17
Average of MSB-2, MSB-4 and DH-2	0.67	1.83E-03	5	6.57E-03	169
Standard Deviation of MSB-2, MSB-4 and DH-2	0.10	1.69E-04	0.85	3.12E-03	102.31
Number analyses from MSB-2, MSB-4 and DH-2	15	15	15	14	15
MSB-2 - 79 to 130.5 m	0.69	1.87E-03	7	1.20E-02	465
MSB-2 - 132 to 154 m	0.58	1.88E-03	5	4.07E-03	68
MSB-2 - 171.50 to 175.50 m	0.58	1.32E-03	4	8.52E-03	100
MSB-4 - 99.50 to 99.00 m	0.77	1.88E-03	5	<0.00714	322
Mean Seawater	**0.56**	**3.45E-03**	**26**	**3.13E+00**	**28**

4.2 Theoretical constraints on geochemical trends

4.2.1 Major solutes

Further insights can be gained by calculating likely ranges of species concentrations in groundwater assuming equilibrium between the granite minerals and chloride-bearing fluids. In this approach it is assumed that Cl is a conservative or 'mobile' ion unconstrained by mineral-fluid equilibria (i.e. following the approach of Giggenbach, 1984). Here, pH was

calculated from charge balance constraints and the granite minerals were used to constrain minerals as shown in Table 4. The code GWB was used to carry out the calculations.

Table 4. Constraints on a model for the equilibration of groundwater with granite.

Species	Constraint
Temperature, °C	25, 50, 100, 150, 200, 250
pH	Charge balance
Na	Albite
K	K-feldspar
Ca	Laumontite
Mg	Phlogopite
Al	Kaolinite
SiO_2	Quartz
HCO_3	Calcite
Cl, $mgkg^{-1}$	10, 100, 1000, 10000
Temperature, °C	25, 50, 100, 150, 200, 250

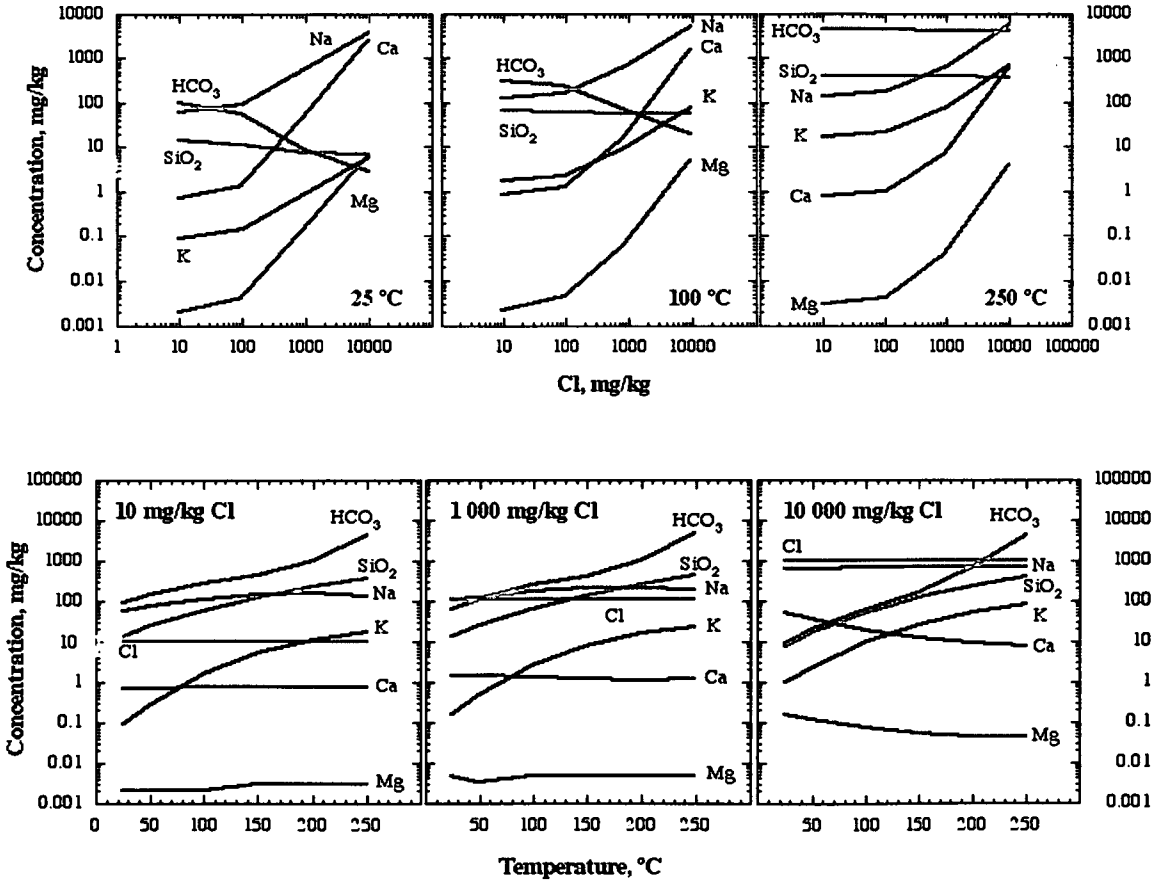

Figure 2. Variations in major cations and ions as functions of temperature and Cl concentration, assuming equilibrium between the water and the granite.

The results of these calculations are summarized in Figure 2 and reveal that:

- Na is the dominant cation under all conditions.
- Ca becomes increasingly important with increasing Cl.

- At all temperatures, concentrations of Ca and Mg increase strongly with Cl, while Na and K increase less markedly.
- HCO_3 decreases with increasing Cl at all temperatures.
- SiO_2 is not very sensitive to Cl concentrations.
- HCO_3, SiO_2 and K increase strongly with temperature at all concentrations of Cl.
- Concentrations of Ca and Mg are invariant or decrease with increasing temperature.

Water/rock interactions involving dilute groundwaters would tend to cause higher Na/Cl than seawater. However, if the Cl contents are high, the Na/Cl ratio produced by water/rock interactions could be comparable to that of seawater. Therefore, the higher Na/Cl ratio of the Tono groundwaters compared to seawater could possibly be explained by water/rock interactions provided there was substantial dilution of seawater first.

Water/rock interactions at any Cl content would produce a higher Na/K ratio than seawater for any reasonable Cl. Therefore, water/rock reactions may explain the higher Na/K ratios of the groundwater compared to seawater. The increase in the ratio would be enhanced even further if the water/rock interactions occurred at the same time as a decrease in temperature along a moderate temperature gradient.

The Mg/Ca ratios of the groundwater are very much smaller than that of seawater. Initial equilibration of seawater with granite would cause a decrease in this ratio. Any subsequent dilution would not change the ratio very much.

Na/Ca ratios of the groundwater are also very much lower than seawater. Movement of seawater towards equilibrium with the rock would decrease the ratio, but subsequent dilution of this water while maintaining continuous equilibrium with the rock would cause the ratio to increase again. Variations in temperature would not have much effect.

Taken together these results illustrate the possibility that an initial seawater, undergoing a combination of dilution and water/rock interaction in a granitic rock could plausibly produce groundwater with the presently observed chemistry.

4.2.2 Stable isotopes and Br/Cl ratios

The isotopic data indicate a dominantly meteoric origin for all the groundwater. However, while stable isotopic data may be good indicators for the origins of the ***water***, they are less sensitive to the origins of the dissolved solutes. This can be appreciated from some simple illustrative mixing calculations (Figure 3 and Figure 4). From these figures it can readily be seen that the meteoric isotopic composition of the Tono groundwaters does not rule out an origin of the salinity in seawater. The most saline water encountered in the Tono area, at Takasago Onsen in Mizunami, has around 1600 $mgkg^{-1}$ TDS. This is only 4.5% of seawater salinity. In other words, if the water is indeed a mixture of meteoric water and seawater, more than 95% of the mixture is meteoric water. The small seawater component would cause an oxygen isotope deviation of < 0.5 ‰ from meteoric values. Any small seawater component would be indistinguishable using the stable isotopic data.

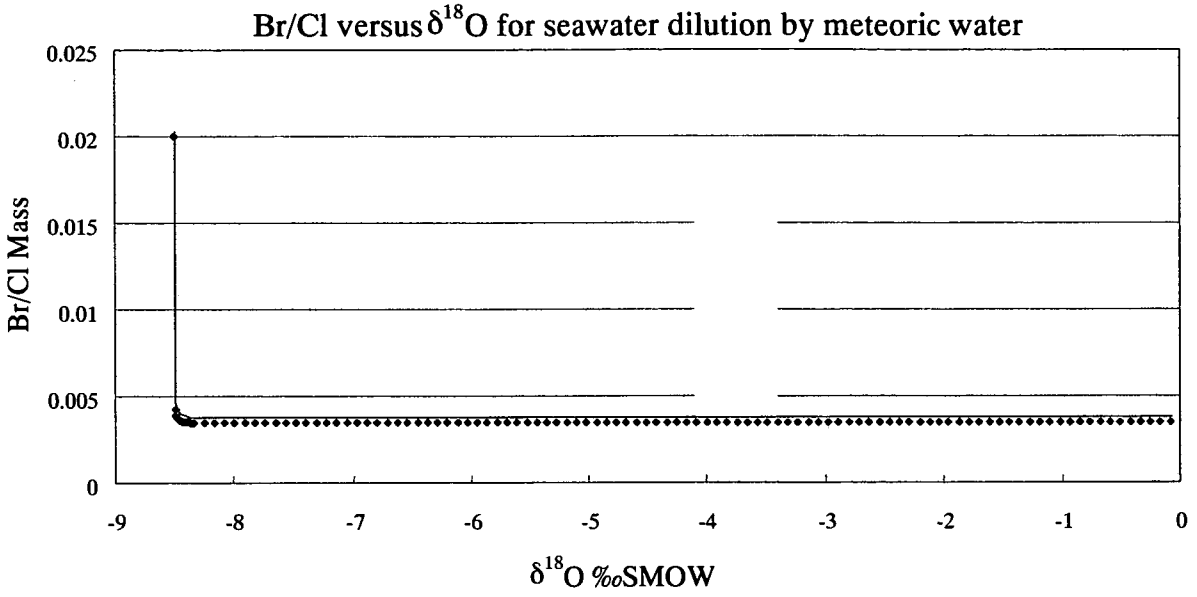

Figure 3. Fresh water (Br = 0.02 mgkg^{-1}, Cl = 1 mgkg^{-1}, $\delta^{18}O_{SMOW}$ = -8.5 ‰) mixes with seawater (Br = 67 mgkg^{-1}, Cl = 19500 mgkg^{-1} Cl, $\delta^{18}O_{SMOW}$ = 0 ‰). Over a very wide range of oxygen isotopic compositions, the mixture has effectively the same Br/Cl ratio as seawater.

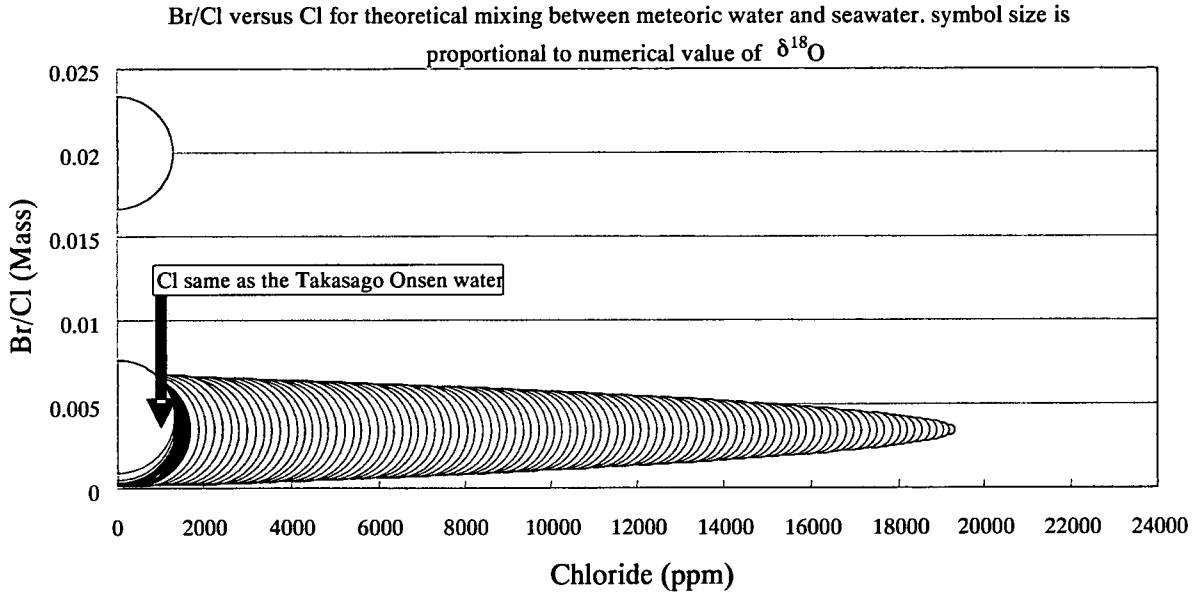

Figure 4. Theoretical mixing between fresh water and seawater. The compositions used were the same as those employed to calculate the curve in Figure 3. It can be appreciated that water with the same salinity as that occurring in Takasago Onsen, would have a stable isotopic composition very similar to meteoric water.

Ratios of dissolved Br and Cl are often used to distinguish the origin of groundwater salinity (e.g. Hanor, 1994, Nirex, 1997). Both Br and Cl are often relatively unreactive in water/rock systems (at least compared to cations like Mg^{2+}, Na^{+}, Ca^{2+} and anions such as HCO_3^{-} and SO_4^{2-}). Often, the concentrations of Br and Cl in groundwater are higher than concentrations of Br and Cl in the surrounding rock. In these cases, water/rock interactions will have little effect on the water's Br/Cl ratio, which will instead depend on the origins of the salinity acquired before the water moved into the sampled rock formation.

In contrast, water/rock interactions could have a major effect on the Br/Cl ratio if the water is sufficiently dilute and/or there are rocks containing soluble evaporite minerals (notably halite, NaCl),. In these cases, Br/Cl ratios cannot be used to evaluate any origins of salinity outside the sampled rock formation.

More specific causes of variations in Br/Cl ratios are:

- A dominantly seawater origin for salinity will produce water with Br/Cl mass ratios around 0.0035 (e.g. Hanor, 1994).

- Halite dissolution may cause waters to have very low Br/Cl because Br does not locate readily within the halite crystal structure (e.g. groundwaters in northwest England have Br/Cl ratios around 0.0005, caused by halite dissolution; Nirex, 1997).

- Evaporation of seawater to halite saturation may produce residual brine with even higher Br/Cl ratios than seawater. Potentially, these dense brines could descend into underlying rock formations, thereby forming high Br/Cl groundwaters.

- Evaporation of continental waters will also produce saline water with low Br/Cl mass ratios (e.g. saline lake waters in Australia, produced by evaporation; Vengosh et al., 1990).

- Recrystallisation of halite may cause any small amount of NaBr within the halite structure to partition into the aqueous phase, producing relatively high Br/Cl residual waters (Stoessell and Carpenter, 1986).

- Water/rock interactions with organic matter could affect Br. In the U.K. Carboniferous Coal Measures typically contain water with relatively high Br/Cl, possibly reflecting the release of Br from organic matter during later diagenesis (Edmunds, 1975; Edmunds, 1996).

- Water/rock interactions in certain rocks (notably mafic and ultramafic rocks (Kamineni et al., 1992)), and granite with fresh biotite (Edmunds et al., 1985) may produce water with relatively high Br/Cl ratios. These rocks may contain significant Br.

- Input of magmatic fluids to hydrothermal waters has been suggested as a cause of Br/Cl ratios that are lower than seawater (e.g. for hot springs in northern Japan; Uzumasa, 1965).

- Membrane filtration has been suggested as a mechanism by which halogen ratios may be varied. If water is forced through a low-permeability formation such as a mudrock that acts as a membrane, the Br/Cl ratio on the upstream side will theoretically increase. There is expected to be a decrease in the ration on the down-stream side. The significance of this process is uncertain however (Hanor, 1994).

- Incorporation of marine aerosols into rainfall will tend to produce rainwater with relatively high Br/Cl ratios (Edmunds, 1996). The relatively elevated Br in the aerosols is thought to come from Br-enriched marine lipids.

- Burning of fossil fuels may release Br to the atmosphere and this Br may find its way into the groundwater system (Edmunds, 1996).

- Addition of salt to roads during the winter and the use of certain fertilisers may also cause the Br/Cl ratios of recharge water to vary locally.

The mean ratio for the Tono groundwater samples, excluding recent analyses from the New Construction Site (NCS) and older analyses from the uranium exploration boreholes is close

to the modern seawater ratio. However, this result reflects the very large ratios of the dilute samples (Br/Cl was up to 842% of the seawater value in one water sample that contained only 2.74 $mgkg^{-1}$ chloride). In contrast, all the Na-(Ca)-Cl dominated waters have ratios that are significantly lower than the seawater ratio, the mean being c. 60% of the seawater value. Together with the strong correlation between Br and Cl concentrations (Figure 5), this finding suggests the presence of a source of a distinct source of groundwater salinity other than seawater.

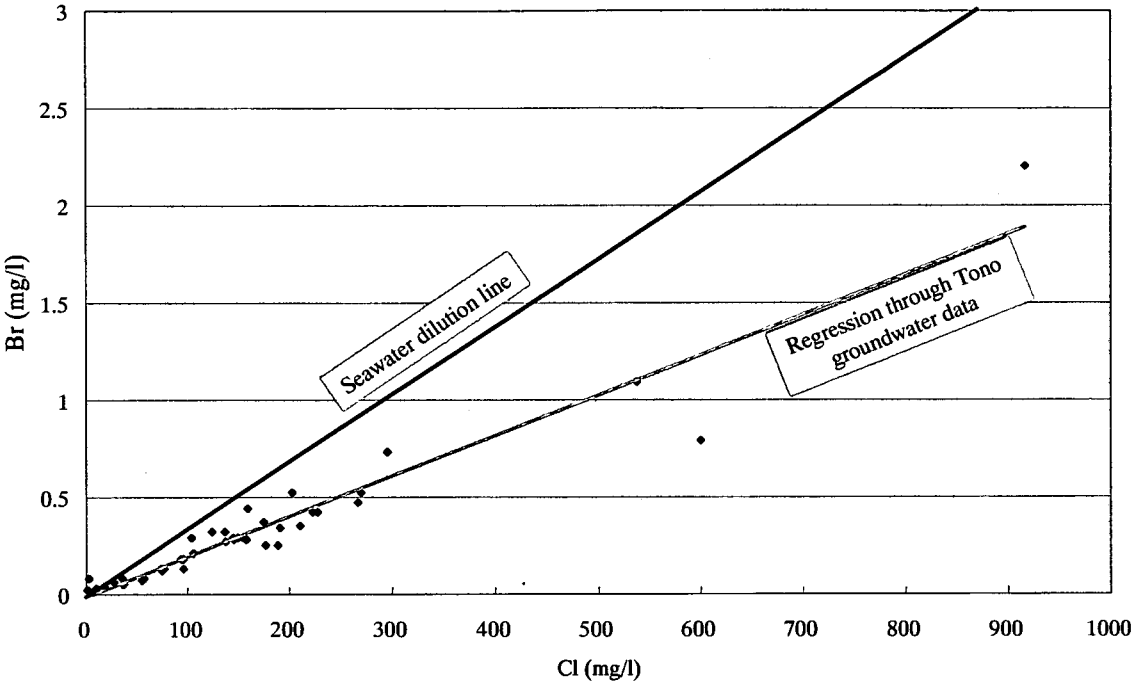

Figure 5. Plot showing the strong correlation between concentrations of Br and Cl in Tono groundwater samples and the difference between a regression line through these data and a seawater dilution line.

Of the other processes listed above, those involving the precipitation or dissolution of evaporite minerals are unlikely to be important in the Tono area, or indeed in Japan more generally, where large evaporate deposits are absent. Most of the other reported processes would tend to produce Br/Cl ratios that are higher than seawater. The process that at face value seems most likely to explain the relatively low ratios is the introduction of a source of Cl derived from a magmatic source.

The occurrence of onsen in the Toki river valley, and in particular the occurrence of the most saline Na-(Ca)-Cl dominated water at Takasao Onsen, apparently supports this hypothesis. However, the more saline onsen waters originate from uncertain depth in boreholes. It is not clear that the locations of these onsen actually reflect especially high geothermal gradients. Thus, there is no clear indication of a magmatic fluid source or an unusual hydrothermal heat source in the Toki river valley area. Nevertheless, it is possible that fluids originating at considerable depth and/or a considerable lateral distance from the study area could be involved. Alternatively, any component of magmatic fluid could be 'fossil' water, reflecting palaeo-conditions.

Based on occurrences of high Br/Cl waters in granitic rocks, several publications have suggested that relatively high Br/Cl ratios would be caused by water/rock reactions in such rocks (e.g. Edmunds et al. 1985). However, usually the origins of the waters themselves are open to debate in such cases and there are actually very few analyses of Br and Cl in coexisting rocks or minerals with which to support this hypothesis. Furthermore, the few data

that are available show that the Br and Cl contents of relatively reactive minerals such as biotite may be very variable. There are consequently large uncertainties in this hypothesis.

During the MIU-4 investigations, analyses of Br and Cl were made on whole-rock samples. Only one sample gave Cl above the detection limit of 200 ppm and no samples gave Br above the detection limit of 20 ppm. Thus, the data for the Tono area are inconclusive and cannot be used to confirm or refute the hypothesis that water/rock reactions might explain the observed Br and Cl chemistry of the Na-(Ca)-Cl dominated waters.

Taken together, these considerations mean that the possible modification of seawater salinity by water/rock reactions cannot be ruled out entirely.

Simple scoping calculations are useful to evaluate the ***plausibility*** of this hypothesis further. Here, these calculations assume that the rock contributes only Cl to the water during water/rock reactions, and that the rock contains 150 ppm Cl (c.f. Toki Granite analyses of 22 ppm (Yoshida et al. 1994) and 230 ppm (MIU-4 borehole report; EXCEL file 'Rock major&minor' received from JNC on 26th January 2003) and analyses up to 526 ppm for the Lower Toki Formation (Yoshida et al. 1994)). In this case, undiluted seawater would acquire Br/Cl ratios similar to those observed only after rather large degrees of water/rock reaction (Figure 6). In contrast, seawater that had first been diluted to a similar level of salinity as that observed at Takasago onsen could subsequently acquire the observed Br/Cl ratios after only relatively small degrees of water/rock interaction (Figure 7).

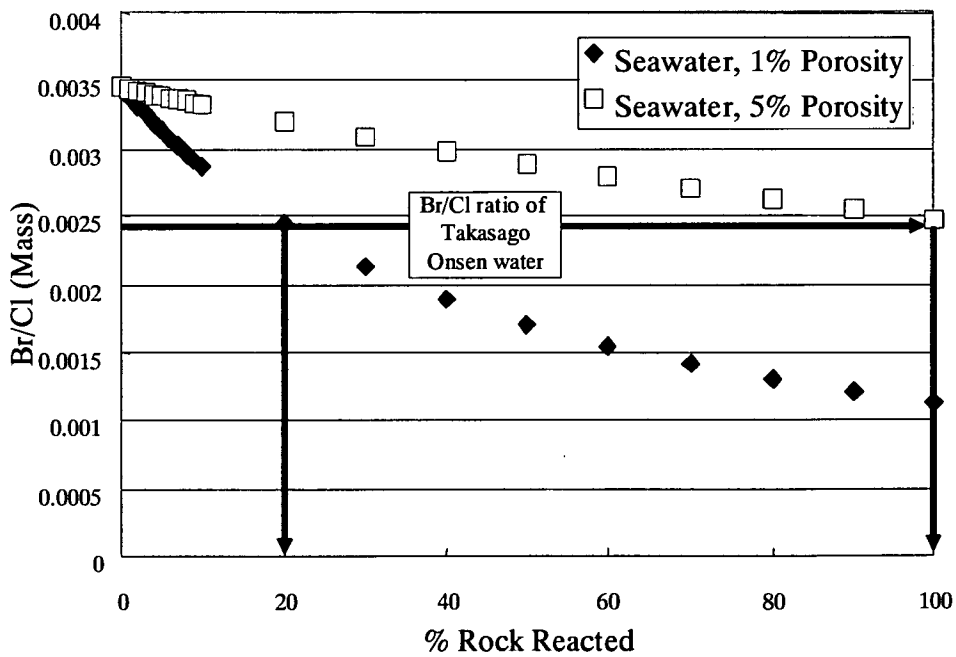

Figure 6. Results of scoping calculations showing the possible effect of water/rock reactions on the Br/Cl ratio of seawater. Granite containing 150 $mgkg^{-1}$ Cl and no Br reacts with seawater having 67 Br $mgkg^{-1}$ and 19400 $mgkg^{-1}$ Cl.

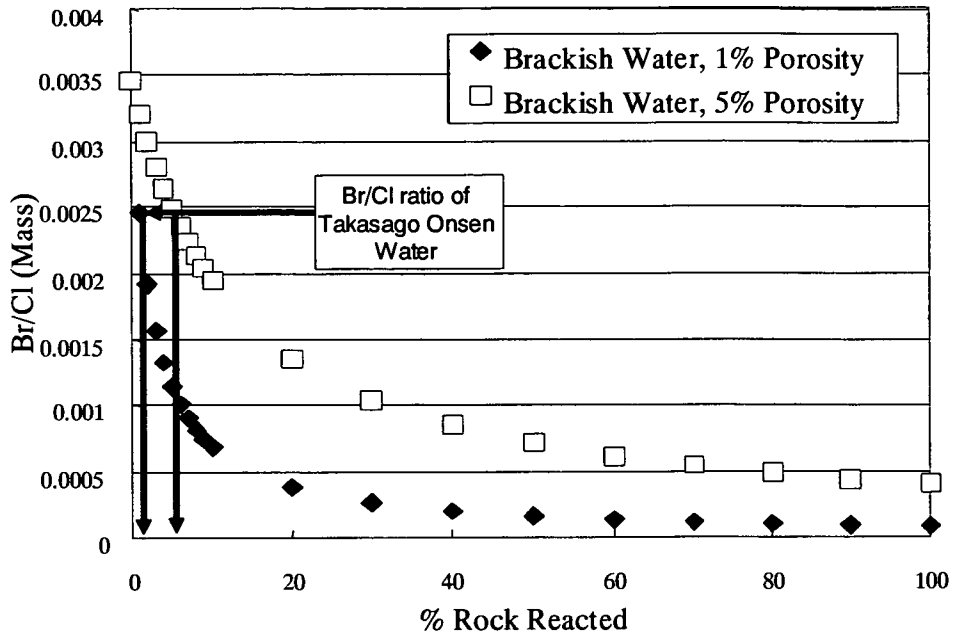

Figure 7. Results of scoping calculations showing the possible effects of water/rock reactions on the Br/Cl ratio of brackish water. Granite containing 150 $mgkg^{-1}$ Cl and no Br reacts with water having 3.45 Br $mgkg^{-1}$ and 1000 $mgkg^{-1}$ Cl (i.e. a brackish water with the same Br/Cl mass ratio as seawater, 3.45×10^{-3}).

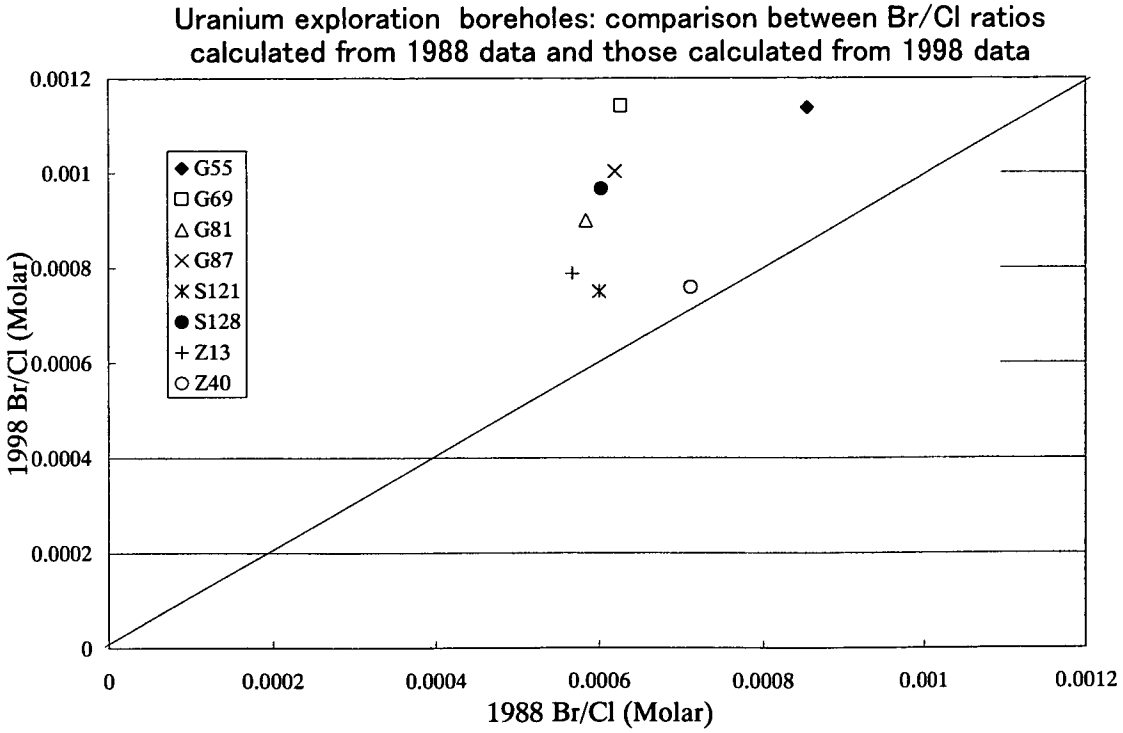

Figure 8. Comparison between analyses made in 1988 and 1998.

Finally, it is pointed out that there are also uncertainties associated with the Br and Cl analyses, which complicate interpretation of these data and the determination of the origins of salinity. Many of the analyses are close to the limit of detection for Br and consequently there may be relatively large errors in the Br/Cl ratios. However, there is no information with which to estimate such errors. Duplicate analyses for groundwaters from 8 of the uranium

exploration boreholes are also considerably different from one another (Figure 8). One analysis of each pair was performed in 1988, while the other was undertaken in 1998. Each of the latter gave a substantially higher ratio than the corresponding earlier analysis.

It is also highlighted that even in the most saline water, from Takasago onsen, the Br concentration is very low, only 2.2 $mgkg^{-1}$. This value would only need to be erroneously lower than the actual value by 0.96 $mgkg^{-1}$ to explain the observed departure from the seawater value.

4.2.3 Summary evidence for the origin of Na-Cl dominated groundwater salinity

The origin of the Na-Cl dominated groundwater salinity remains uncertain. It is possible that the observed cation and anion ratios dominantly reflect water/rock interactions rather than the original origins of the salinity. In this case the key issue is the origin of the Cl, which is likely to have been affected relatively little by these reactions.

It is possible that the Cl had an origin initially in seawater, but other origins can also be suggested, including high-temperature water/rock interactions or an influx of magmatic fluids. The main difficulty with these other possibilities lies in the lack of evidence for elevated geothermal gradients in the south of the area, relative to the north of the area.

Thus, while there is clear evidence that marine Cl was present in the area in the past, the evidence for the presence of Cl of other origins is marginally more tenuous.

4.3 Alternative conceptual models

Based on the review and discussion in Section 5.1, several alternative conceptual models have been constructed for the origin of the Na-(Ca)-Cl dominated water in the south of the study area (Figures 9, 10, 11, 12 and 13). It should be noted that:

- These alternative concepts can be viewed as 'limiting' concepts.
- In detail many variants on these basic models could be suggested.
- Any one concept may not apply across the whole area. For example, there is no evidence for a present magmatic or hydrothermal source of salinity in the NCS. However, one possible concept variant is for the salinity here to have a 'palaeo-magmatic' or 'palaeo-hydrothermal' origin. If this is the case, it does not rule out the possible on-going input of hydrothermal or magmatic fluid into the groundwater system further south.
- The concepts are not mutually exclusive. For example, one alternative possibility is that a component of magmatic Cl was added to salinity of seawater origin, which was then further modified by water/rock interactions.

A summary of the main features of these concepts and evidence for and against each one is given in Table 5.

Figure 9. Schematic diagram illustrating a possible origin of salinity in seawater. Here the salinity is passive and is being gradually removed over time.

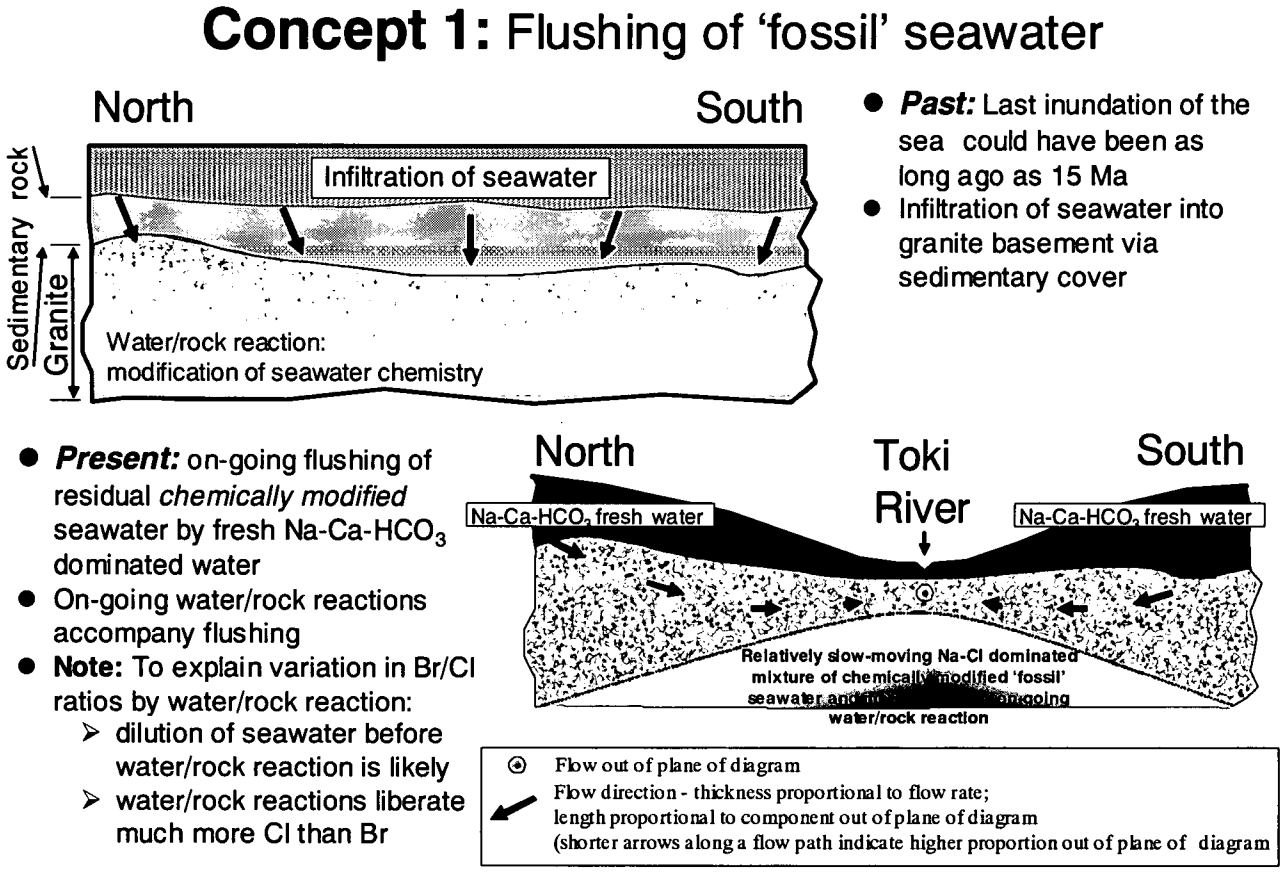

Figure 10. Schematic illustration of a possible origin of salinity in an ancient hydrothermal system. Again the present salinity is passive and is being gradually removed over time.

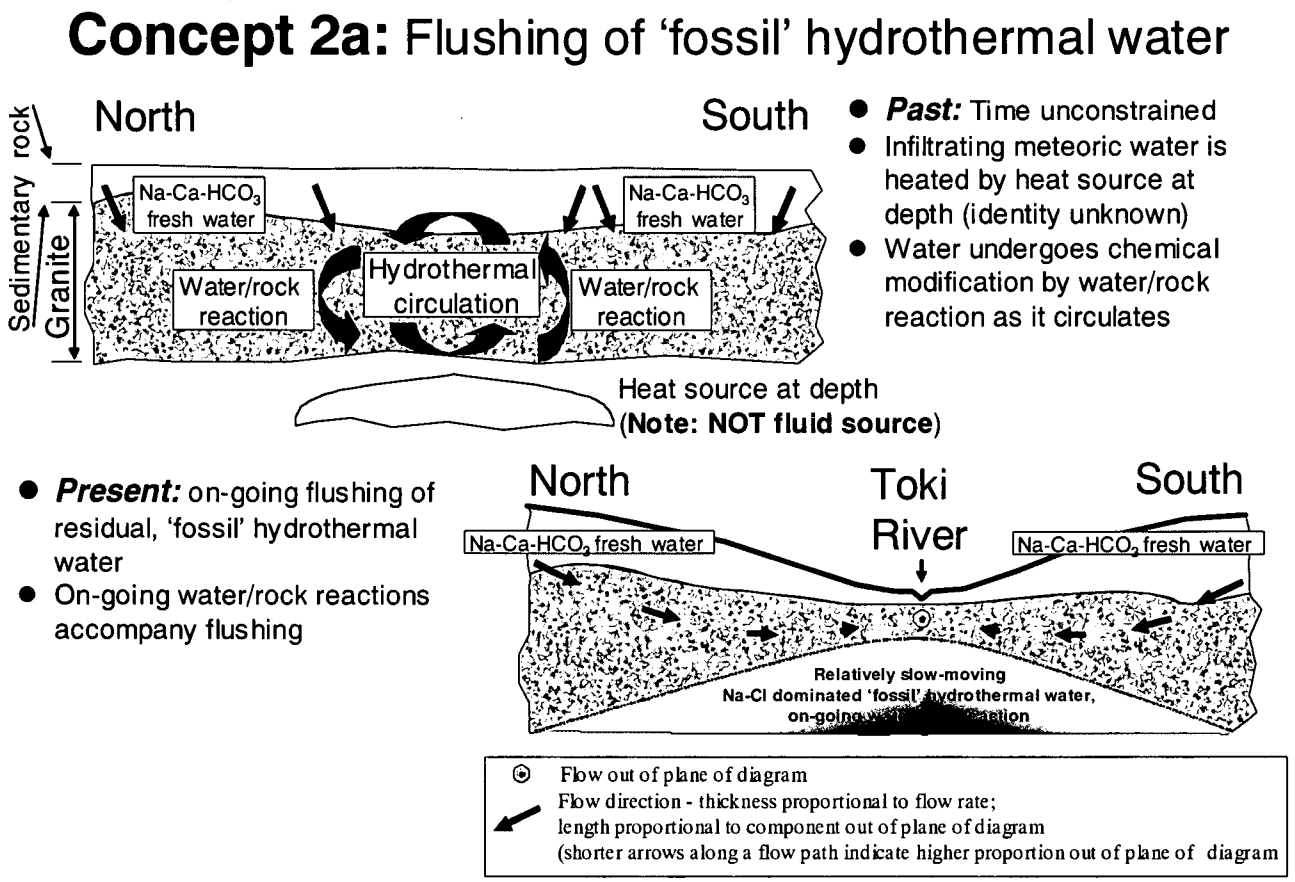

Figure 11. Schematic illustration of a possible origin of salinity in fossil magmatic fluid. Again the present salinity is passive and is being gradually removed over time.

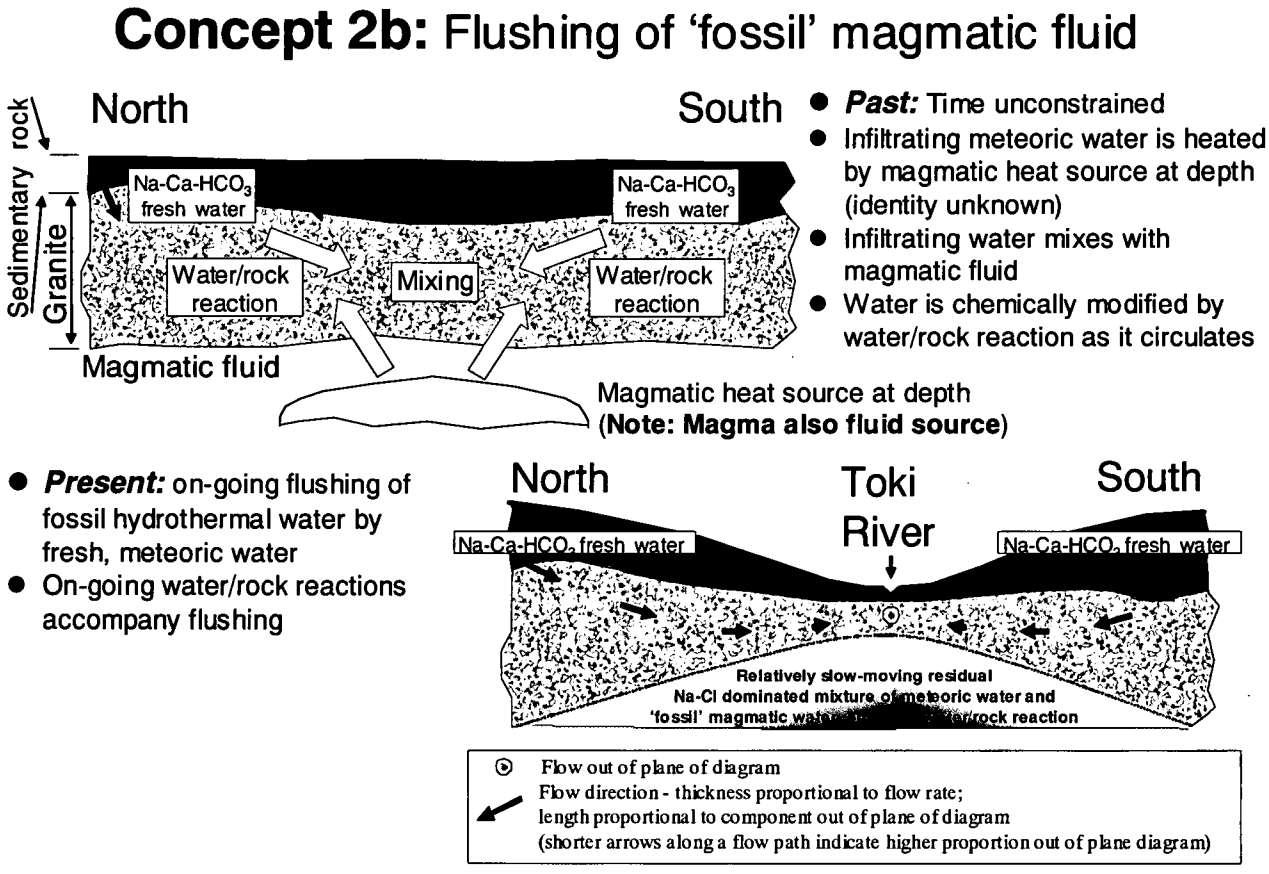

Figure 12. Schematic illustration of a possible source of salinity in active hydrothermal circulation. In this case, the salinity is actively forming and is not being gradually decreased over time.

Concept 3a: Mixing with present hydrothermal water

- ***Present:*** on-going formation of hydrothermal water at depth
- On-going water/rock reactions accompany hydrothermal circulation
- Note:
  - geothermal gradient not necessarily very high
  - heat source unknown

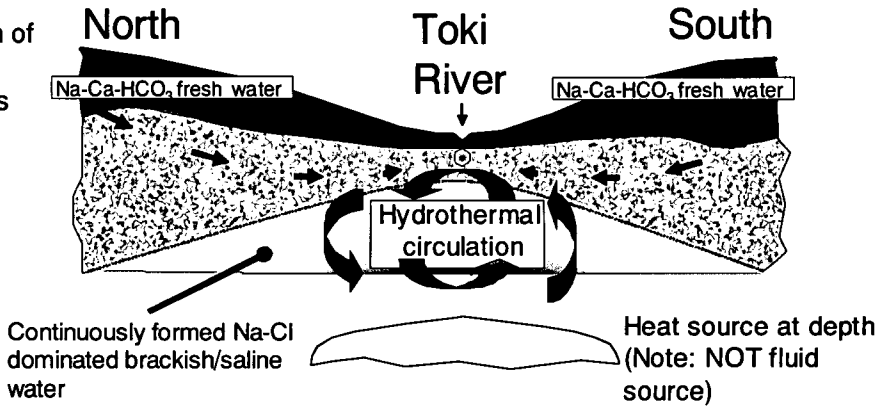

Figure 13. Schematic illustration of a possible origin of salinity in an active magma system. Again the salinity is active and is not decreasing gradually over time.

Concept 3b: Mixing with present magmatic fluid

- ***Present:*** on-going mixing with present magmatic fluid at depth
- On-going water/rock reactions accompany mixing
- Note:
  - geothermal gradient not necessarily very high
  - magma source unknown, ***could be a considerable distance away***

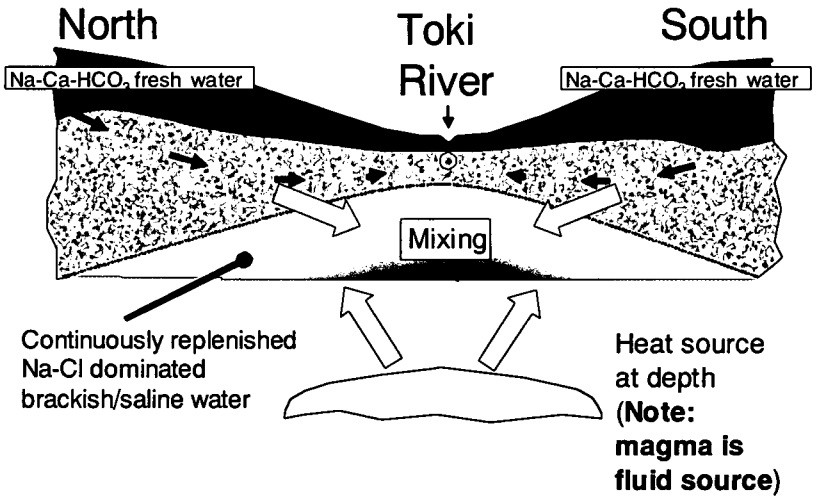

Table 5. Summary of the main 'end-member' concepts for the origins of the Na-(Ca)-Cl dominated salinity.

No	Concept Name	Description	Key evidence for	Key evidence against
1	Flushing of 'fossil' seawater	Seawater infiltrated the Toki granite via the sedimentary cover sequence and has since been flushed by dilute Na-Ca-HCO_3-dominated fresh water, accompanied by water/rock reactions	Marine sedimentary rocks occur Stable isotopic data for fracture-filling calcite in the granite are consistent with marine water	Major and minor constituents have ratios different from those of seawater
2a	Flushing of 'fossil' hydrothermal water	Water/rock reactions at elevated temperature in a hydrothermal system generate Na-Ca-Cl dominated salinity which is then flushed by dilute Na-Ca-HCO_3-dominated fresh water, accompanied by water/rock reactions	Theoretical considerations imply may be feasible	No clear evidence for a fossil hydrothermal system in many localities (e.g. the NCS) where Na-Ca-Cl dominated water occur Difficulty of explaining distribution of salinity in both the Toki Granite and in the overlying sedimentary rocks
2b	Flushing of 'fossil' magmatic fluid	Relatively Cl-enriched fluid of magmatic origin entered the groundwater system in the past and has since been flushed by dilute Na-Ca-HCO_3-dominated fresh water, accompanied by water/rock reactions	Modern hydrothermal systems in northern Japan, where there is good evidence for a component of magmatic fluid, have water with relatively low in Br/Cl (e.g. Uzamasa, 1965)	No clear evidence of magmatism required to produce the low Br/Cl fluid
3a	Mixing with present hydrothermal fluid	On-going water/rock reactions at elevated temperature in a hydrothermal system in the Toki River valley generate Na-Ca-Cl dominated salinity which then mixes with dilute Na-Ca-HCO_3-dominated fresh water, accompanied by water/rock reactions	Most saline water occurs in Takasago onsen, which contains relatively hot water	Apparently elevated temperature of onsen water may reflect the water's origin at depth in a borehole rather than a locally elevated geothermal gradient Difficulty of explaining distribution of salinity both in the Toki Granite and in the sedimentary rocks where there is clearly no present hydrothermal activity

Table 5. Continued.

No	Concept Name	Description	Key evidence for	Key evidence against
3b	Mixing with present magmatic fluid	Relatively Cl-enriched fluid of magmatic origin is entering the groundwater system and is mixing with dilute Na-Ca-HCO_3-dominated fresh water, accompanied by water/rock reactions	Modern hydrothermal systems in northern Japan, where there is good evidence for a component of magmatic fluid, have water with relatively low in Br/Cl (e.g. Uzamasa, 1965)	Difficulty of explaining distribution of salinity both in the Toki Granite and in the sedimentary rocks (e.g. in the NCS there is higher salinity in the Lower Toki Formation than in the immediately underlying granite)

From the perspectives of the origin(s) and distribution of the Na-(Ca)-Cl dominated salinity these alternative concepts can be summarised as shown in Table 6.

Table 6. Summary of key features of alternative concepts.

Timing of Generation	Initial Distribution	
	Localised (south of the study area)	Dispersed (throughout the study area)
Continuous source of salinity, on-going	Present hydrothermal fluid Present magmatic fluid	None
Palaeo-source, present flushing	'Fossil' hydrothermal water; 'Fossil' magmatic fluid	'Fossil' seawater

5 Modelling flow and water/rock reactions in the present groundwater system

5.1 Features of the flow system to be modelled

While several alternative concepts are consistent with the data, as discussed in Section 4, the balance of evidence suggests that seawater was present in the area in the past. For this reason, the numerical modelling focuses on evaluating the geochemical implications of:

- the Toki granite being uniformly saturated with seawater;
- the Toki granite subsequently being flushed by fresh groundwater.

However, it is noted that this modelling also helps to understand the alternative cases in which ***palaeo***-salinity of hydrothermal or magmatic origin is being flushed at the present.

The work focuses on calculating values for parameters that be compared with actual site data and/or which would be relevant to PA. These parameters are:

- Salinity (Cl concentrations and effect on water/rock reactions);

- pH;
- Eh;
- $fCO_2(g)$.

Previous work as part of the TGRP (Arthur, 2003) has identified a correlation between pH and log $fCO_2(g)$ (Figure 14) in the site data. It was suggested that the pH of the groundwater becomes more alkaline along any particular flow path and that the correlation between pH and log $fCO_2(g)$ reflects subsequent equilibration of the groundwater with calcite under open-system conditions. However, the chemical processes responsible for causing the variations pH were not identified. Additionally, there was no direct evidence that the pH is positively correlated with the residence time of the groundwater. This would be the case, if this simple model is correct.

An aim of the modelling carried out here was therefore to evaluate further the relationship between groundwater flow, pH evolution and log $fCO_2(g)$ variation. One aspect of this was to assess how these variations would fit into the overall concept of flushing of marine water by fresh groundwater.

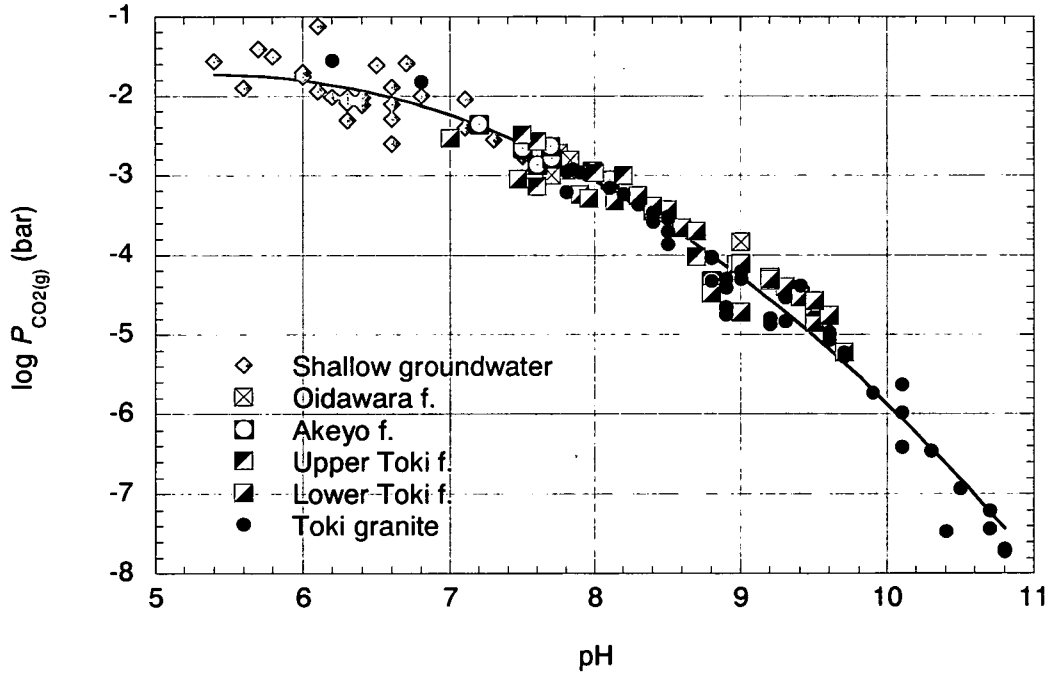

Figure 14. Correlation between pCO_2 and pH for groundwaters in the Tono area. The solid line is the best fit to the data (From Arthur, 2003).

For these reasons, it was important to make each model a plausible representation of a possible flow path in the present Tono groundwater system. Therefore, initially the results of particle tracking calculations supplied by JNC, were assessed.

The results of particle tracking calculations undertaken using the code FracAffinity 2.2 were evaluated (Table 7). As is to be expected, these tracks show considerable variability, both in length and orientation. However, it is clear that, other than the borehole in which it originates, none of the tracks passes close to several boreholes. This means that simulated variations in groundwater chemistry along a particular flow path cannot be compared with observed variations in groundwater chemistry along the same flow path.

Table 7. Summary of particle tracks supplied by JNC on 2nd May 2005. The paths are from a simulation that covers an area of 35km2 and that includes the Tsukiyoshi Fault.

Path	Borehole	Total Distance (m)	Total Time (s)	Coordinates of path termination at borehole			Coordinates of path end furthest from borehole		
				X	Y	Z	X	Y	Z
49	MIU-4	75.7117	1.18E+08	5543.37	-68703.8	150.08	5523.9	-68764.1	191.585
16	DH-11	127.554	-1.49E+08	7831.93	-67634.5	204.48	7777.38	-67656.9	317.169
41	MSB-2	145.895	2.79E+08	6720	-69418.2	68	6689.24	-69473.3	196.937
61	DH-12	157.799	2.38E+08	4200	-70900	-26.74	4188.23	-70911.1	129.392
42	MSB-2	173.599	4.17E+08	6720	-69418.2	44.5	6664.67	-69486.2	190.503
5	DH-10	178.283	-3.21E+08	11217.3	-64094.3	354.06	11282	-63991.5	484.569
4	DH-10	188.6	-3.27E+08	11217.3	-64094.3	414.06	11279.4	-63986.4	555.768
43	MSB-2	197.778	4.96E+08	6720	-69418.2	23	6654.77	-69497.6	186.917
6	DH-10	230.897	-4.40E+08	11217.3	-64094.3	134.06	11259.3	-63967.3	315.325
56	MIU-4	243.575	-4.76E+08	5583.39	-68615.5	-22.24	5654.18	-68396.7	58.0502
55	MIU-4	248.625	-3.81E+08	5551.4	-68686.1	115.5	5576.23	-68448.4	87.1725
19	DH-2	273.864	7.41E+08	6708.8	-69474.1	-16.17	6621.28	-69602.6	183.022
62	DH-12	274.992	5.11E+08	4200	-70900	-142.79	4167.95	-70907.8	127.711
54	MIU-4	292.136	-4.42E+08	5543.37	-68703.8	150.08	5577.7	-68435.2	154.871
20	DH-2	316.375	1.04E+09	6708.8	-69474.1	-43.67	6672.54	-69659.4	159.716
63	DH-12	340.371	7.05E+08	4200	-70900	-207.29	4154.75	-70908.6	127.031
60	DH-4	354.023	-9.03E+08	4343.19	-69602.4	78.08	4336.65	-69339.6	246.625
17	DH-11	358.309	-9.95E+08	7831.93	-67634.5	-128.12	7759.57	-67624	220.066
64	DH-12	382.065	8.27E+08	4200	-70900	-249.79	4145.14	-70904.9	125.927
7	DH-13	402.191	8.71E+08	8897.29	-65673.8	257.01	8518.79	-65683.6	290.506
65	DH-12	426.659	9.76E+08	4200	-70900	-292.12	4135.44	-70911.8	126.337
8	DH-13	437.372	9.06E+08	8897.29	-65673.8	203.36	8498.02	-65678.5	258.952
66	DH-12	469.964	1.12E+09	4200	-70900	-335.12	4128.51	-70913.9	126.223
50	MIU-4	517.004	9.00E+08	5551.4	-68686.1	115.5	5678.51	-69107.9	187.865
21	DH-2	584.966	2.76E+09	6708.8	-69474.1	-111.37	6633.87	-69880.8	175.312
22	DH-2	590.654	2.81E+09	6708.8	-69474.1	-114.22	6632.5	-69888.8	174.446
23	DH-2	596.418	2.83E+09	6708.8	-69474.1	-118.37	6632.61	-69892.3	173.968
24	DH-2	601.001	2.84E+09	6708.8	-69474.1	-121.67	6632.7	-69895.1	173.588
25	DH-2	623.065	2.95E+09	6708.8	-69474.1	-135.07	6630.39	-69914.3	171.386
47	MSB-4	680.371	3.15E+09	6741.56	-69123.3	115.45	6244.47	-69042.2	193.161
51	MIU-4	698.718	1.24E+09	5583.39	-68615.5	-22.24	5765.34	-69144.5	169.253
26	DH-2	703.69	3.43E+09	6708.8	-69474.1	-156.47	6611.47	-70004.6	170.146
44	MSB-2	709.676	-2.01E+09	6720	-69418.2	68	7262.9	-69269.1	256.057
52	MIU-4	770.446	2.66E+09	5641.25	-68487.8	-271.44	6158.8	-68368.8	212.723
27	DH-2	781.913	3.83E+09	6708.8	-69474.1	-174.17	6572.58	-70083.5	173.839
53	MIU-4	827.632	2.65E+09	5666.31	-68432.5	-379.375	6216.33	-68393.5	198.486
9	DH-13	890.956	2.78E+09	8897.29	-65673.8	-164.54	8289.58	-65827.1	261.261
48	MSB-4	918.579	-1.91E+09	6741.56	-69123.3	115.45	7084.74	-68395.1	86.782
46	MSB-2	927.491	-3.61E+09	6720	-69418.2	23	7276.96	-69052.7	297.589
45	MSB-2	948.581	-3.63E+09	6720	-69418.2	44.5	7278.44	-69058.9	309.401

Table 7. Continued.

Path	Borehole	Total Distance (m)	Total Time (s)	Coordinates of path termination at borehole			Coordinates of path end furthest from borehole		
				X	Y	Z	X	Y	Z
31	DH-2	983.713	-3.99E+09	6708.8	-69474.1	-43.67	7282.2	-69044.4	296.37
30	DH-2	996.112	-3.99E+09	6708.8	-69474.1	-16.17	7283.11	-69046.7	301.504
10	DH-13	1064.2	-3.01E+09	8897.29	-65673.8	257.01	9069.46	-64824.7	393.343
28	DH-2	1121.52	5.80E+09	6708.8	-69474.1	-254.67	6564.45	-70374.1	154.203
11	DH-13	1147.31	-3.44E+09	8897.29	-65673.8	203.36	9080.85	-64695.3	403.427
59	DH-4	1185.28	3.09E+09	4343.19	-69602.4	78.08	4254.02	-70653.1	150.068
29	DH-2	1213.71	6.36E+09	6708.8	-69474.1	-266.37	6563.08	-70478.2	170.837
40	DH-2	1383.81	-4.38E+09	6708.8	-69474.1	-266.37	7302.11	-68379	13.5139
39	DH-2	1393.87	-4.42E+09	6708.8	-69474.1	-254.67	7321.73	-68378.6	19.3806
38	DH-2	1572.55	-4.64E+09	6708.8	-69474.1	-174.17	7232.23	-68327.2	52.4236
37	DH-2	1586.09	-4.59E+09	6708.8	-69474.1	-156.47	7242.29	-68321.4	46.9898
13	DH-11	1610.6	6.03E+09	7831.93	-67634.5	204.48	8700.81	-68107	219.941
33	DH-2	1617.71	-4.87E+09	6708.8	-69474.1	-114.22	7604.88	-68324.9	224.971
36	DH-2	1629.08	-4.74E+09	6708.8	-69474.1	-135.07	7699.21	-68327.1	78.9633
32	DH-2	1629.8	-4.91E+09	6708.8	-69474.1	-111.37	7611.68	-68319.7	206.385
34	DH-2	1632.57	-4.79E+09	6708.8	-69474.1	-118.37	7713.81	-68336.7	103.48
35	DH-2	1632.82	-4.79E+09	6708.8	-69474.1	-121.67	7714.34	-68337.2	101.38
12	DH-13	1934.48	-5.77E+09	8897.29	-65673.8	-164.54	9419.8	-64093	452.051
15	DH-11	2019.12	1.75E+10	7831.93	-67634.5	-667.62	6437.66	-68359.8	191.392
14	DH-11	2456.25	2.29E+10	7831.93	-67634.5	-128.12	6455.54	-68488.7	173.991
1	DH-10	3316.8	1.31E+10	11217.3	-64094.3	414.06	10970.8	-66780.7	-794.305
2	DH-10	4369.72	1.71E+10	11217.3	-64094.3	354.06	10671.1	-67183.6	68.9214
3	DH-10	4598.95	1.80E+10	11217.3	-64094.3	134.06	10723.8	-67366.8	104.413
18	DH-11	6496.23	-4.49E+10	7831.93	-67634.5	-667.62	10037.1	-62709.2	599.974
58	MIU-4	8458.96	-9.01E+10	5666.31	-68432.5	-379.375	7506.99	-63255	421.686
57	MIU-4	10049.4	-9.40E+10	5641.25	-68487.8	-271.44	8721.03	-62306	674.791
70	DH-12	25416.4	-7.06E+11	4200	-70900	-249.79	21275.5	-66482.3	192.42
69	DH-12	25561.2	-6.76E+11	4200	-70900	-207.29	21277.7	-66577.1	378.565
68	DH-12	26321.3	-7.03E+11	4200	-70900	-142.79	21384.8	-66698.1	785.256
71	DH-12	28428	-8.32E+11	4200	-70900	-292.12	20978.6	-66183.6	455.031
72	DH-12	28624.2	-8.15E+11	4200	-70900	-335.12	20973.7	-66174.8	472.39
67	DH-12	34894.3	-1.29E+12	4200	-70900	-26.74	21814.6	-68087.6	1627

Additionally, uncertainty in the characteristics of groundwater flow paths was investigated during a separate project 'Development of uncertainty judgment methods for Tono' which was undertaken at the same time as the present work. The results of this project highlight considerable uncertainty in the precise lengths and orientation of flow paths relative to the locations of actual groundwater sampling points (Figure 15).

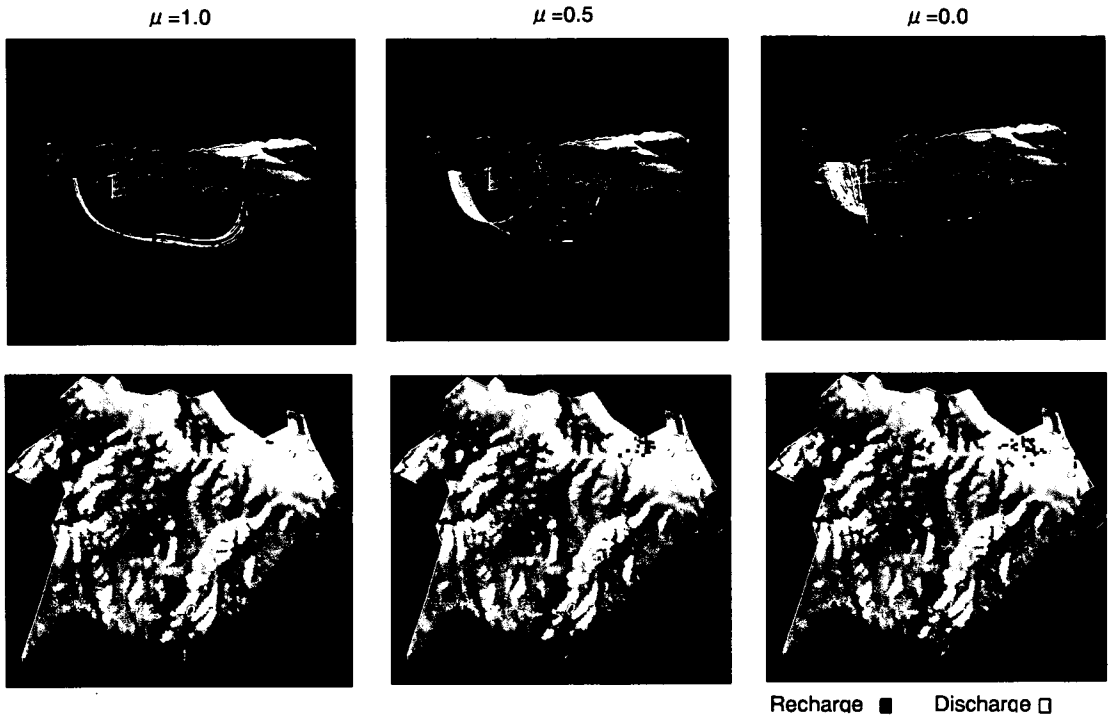

Figure 15. Uncertainty in groundwater migration pathways in the central part of the area. Each figure shows the results of 100 particle tracking simulations, each one using hydraulic parameters sampled randomly from ranges that depended upon the particular fuzzy membership class (μ). Particles are tracked from a point at 1414 m depth in the centre of the NCS forwards (red lines) towards the discharge points (red points), and backwards (blue lines) towards the recharge points (blue points). The uncertainty in the location of the recharge areas and discharge areas increases from left to right as the rock mass is modelled with increasingly dual-porosity characteristics. Details are explained in the report of project 'Development of uncertainty judgment methods for Tono'.

For these reasons, rather than attempt to simulate one particular flow path, the present work uses the results of the particle tracking as a basis for constructing generic 1D flow models. The particle tracking results are used to ensure that path lengths are reasonable and that temperature variations considered by the modelling are reasonable, given the maximum depths of the particle tracks.

The major part of the transport modelling considered a path of 10 km length, which is similar to the maximum length of a northerly-directed track derived from the FracAffinity 2.2 modelling (Track 57 from MIU-4; Table 7). Longer tracks were calculated, from DH-12, but these are directed in an easterly direction and lie mostly outside the present investigation area.

At these length scales, the sedimentary cover sequence is considered to have an insignificant effect on the groundwater chemistry. Modelling instead focuses upon the granitic rocks.

5.2 Equilibrium geochemical models

When developing coupled models it is necessary to consider only the minimum number of chemical reactions necessary to answer the questions being addressed. This is because even small increases in the complexity of a model can produce very large increases in the time required to undertake a simulation. Highly complex simulations often take too long to allow meaningful alternative cases to be explored.

Simple chemical scoping calculations are therefore valuable to identify which chemical reactions are likely to be most important. Subesquent coupled modelling can then focus on these.

Equilibrium geochemical calculations were carried out using the 'Tact' and 'Act' modules of GWB, to evaluate the importance of various mineral buffers as possible controls on pH and $pCO_2(g)$ (Table 8, Figures 16 and 17).

A key observation is that the CO_2 fugacity could potentially be buffered by pH-independent reactions (Table 8 and Figure 16). It can be envisaged that as temperature increases along a flow path, the CO_2 fugacity will also decrease, owing to the water moving progressively towards equilibrium with higher-temperature mineral assemblages (i.e. the water would move from bottom right of Figure 16 towards the top left). There is no need for pH to be an independent variable that controls the fugacity of CO_2.

On the other hand, pH could also be controlled by progressive reactions with one or more of the minerals in the rock (Table 8, Figure 17). Reaction with feldspar to produce clay minerals such as kaolinite or montmorillonite would consume H^+, leading to an increase in pH. However, at the low temperatures of the present groundwater system, this process would not reach equilibrium, as can be appreciated from the large, positive equilibrium constants of the pH-influencing reactions in Table 8.

Figures 17B and 17C illustrate that over much of the range of CO_2 fugacity and pH in the present groundwater system, calcite is stable relative to anorthite. Additionally, depending upon the concentration at which dissolved Ca is buffered, the solubility of calcite could result in pH values which, for a given CO_2 fugacity, are similar to those observed (c.f. Figure 14 and Figure 17C).

In this case, the mineral reaction controlling the dissolved Ca concentration is uncertain. However, a mixture of kinetically controlled, non-equilibrium and equilibrium reactions could potentially control the overall evolution of chemical conditions. One possible combination of processes are described below.

- Along a flow path, dissolution of feldspar (a non-equilibrium process) and formation of clay minerals may cause the concentration of dissolved Ca and pH to increase.
- Eventually, the solubility limit of calcite is exceeded and calcite precipitates.
- Thereafter, the pH is controlled by reactions involving the calcite (an equilibrium process).
- At the same time as these reactions, the CO_2 fugacity moves towards equilibrium with the calcite-bearing mineral assemblage, though equilibrium may not be attained.

The coupled modelling described in Sections 5.5 and 5.6 was designed to shed further light on the feasibility of these processes.

Table 8. A selection of possible CO_2- and pH- controlling mineral phase assemblages.

Equilibrium Relation	Equilibrium Equation	Equilibrium Constants			
		0°C	25°C	60°C	100° C
Laumontite+CO_2(g) = Calcite +Kaolinite+2*Quartz +2*H_2O	logK=2*loga[H_2O]-logf[CO_2(g)]	6.5394	5.1929	3.6638	2.2955
Laumontite+CO_2(g) =Calcite+ Kaolinite+2*Chalcedony+2*H_2O	logK=2*loga[H_2O]-log f[CO_2(g)]	5.9474	4.6505	3.1784	1.8621
Laumontite+CO_2(g)=Calcite+Kaolinite +2*SiO_2(am)+2*H_2O	logK=2*loga[H_2O]-logf[CO_2(g)]	3.5236	2.6215	1.5304	0.5077
Anorthite+2.79*Quartz+ 1.066*H_2O+0.1317*Phlogopite+ 0.8024*CO_2(g)=0.8024*Calcite +1.198* Montmor-Ca +0.1317* K-feldspar	logK=-1.066*loga[H_2O]- 0.8024*log f[CO_2(g)]	11.5058	9.6455	7.4907	5.5022
Anorthite + H^+ + H_2O + HCO_3^- = Calcite + Kaolinite	log K = - log a[H^+] – log a[H_2O] - log a[HCO_3^-]	19.9482	17.9192	15.6292	13.5837
Anorthite + 0.01198*H^+ + 2.79*Quartz + 0.7904*H_2O + 0.8024*HCO_3^- + 0.3952*Mg^{++} = 0.8024*Calcite + 1.198*Montmor-Ca	log K = - 0.01198*log a[H^+] - 0.7904*log a[H_2O] - 0.8024*log a[HCO_3^-] - 0.3952*log a[Mg^{++}]	12.0914	10.9466	9.6743	8.5516
Albite + H^+ + 0.5*H_2O = 0.5*Kaolinite + Na^+ + 2*Quartz	log K = - log a[H+] + log a[Na^+] - 0.5*log a[H_2O]	8.0277	7.3580	6.5912	5.9030
Albite + 0.4072*H^+ + 0.3952*H_2O + 0.0988*Ca^{++} + 0.1976*Mg^{++} = 0.5988*Montmor-Ca + Na^+ + 0.6048*Quartz	log K = - 0.4072*log a[H^+] + log a[Na^+] - 0.3952*log a[H_2O] - 0.0988*log a[Ca^{++}] - 0.1976*log a[Mg^{++}]	3.8794	3.6891	3.4821	3.3104

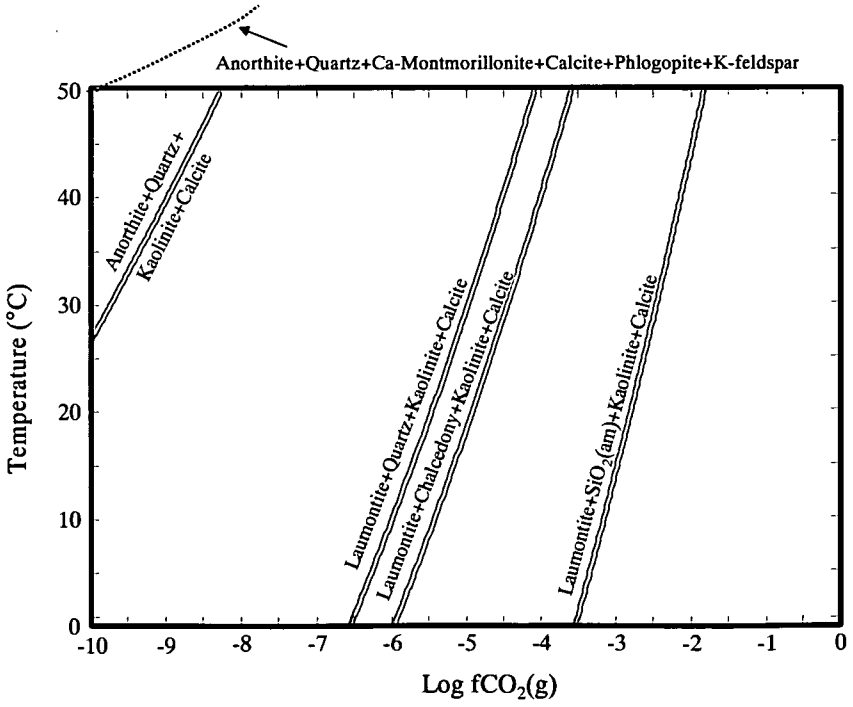

Figure 16. Relationships between temperature and log fCO_2(g) for various possible buffering assemblages. The equilbria were calculated using the 'Tact' module of the code GWB.

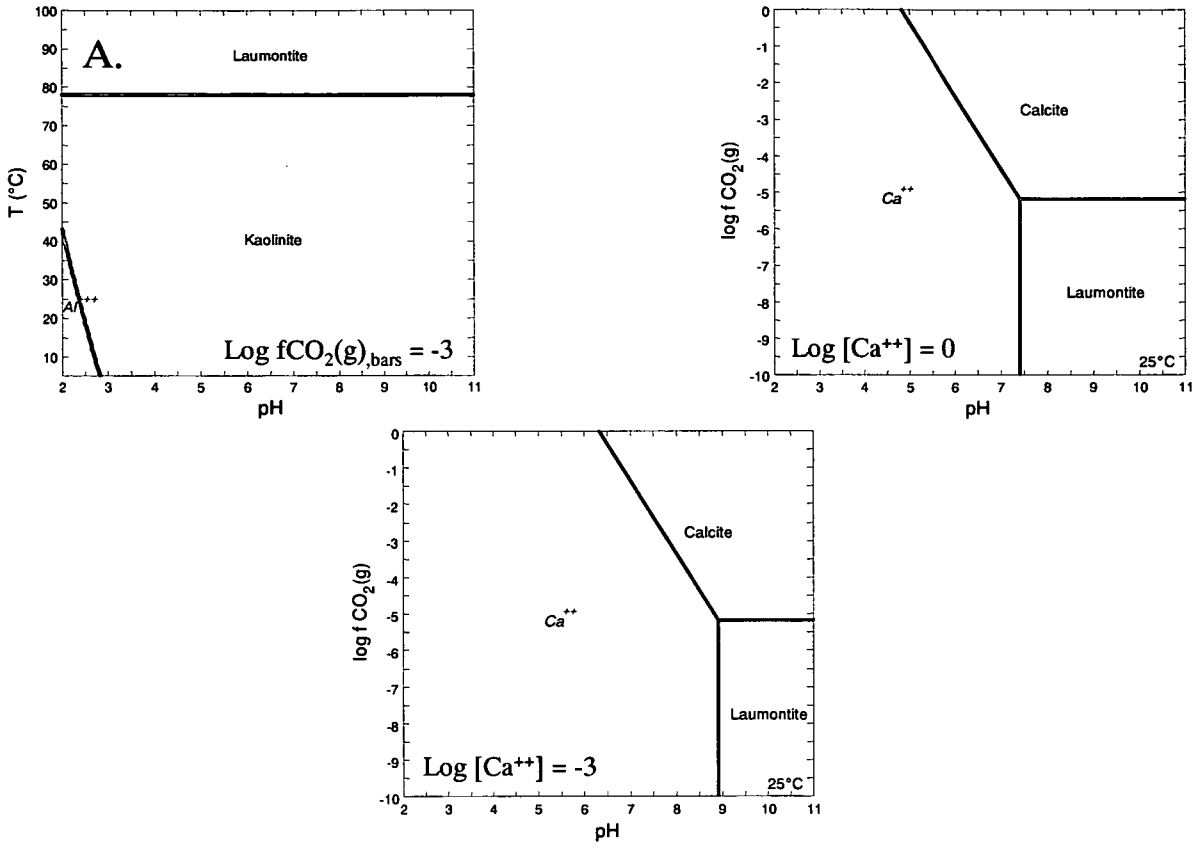

Figure 17. A. Stability relations between temperature and pH in the presence of quartz and calcite. B. and C. stability of calcite and laumontite in CO_2 fugacity – pH space in the presence of kaolinite and quartz. In B., the coexisting anorthite is pure. In C. the coexisting anorthite has an activity of only 0.001. The equilbria were calculated using the 'Tact' (A.) and 'Act' (B. and C.) modules of the code GWB.

5.3 Reaction path models

Kinetic reaction path calculations were carried out using GWB to gain further insights into the role of reaction kinetics, prior to constructing the fully-coupled models.

The code was run in 'flush' simulation mode at 25 °C (Figure 18). In this simulation, 1 kg of saline water, with a composition modified from that of seawater (Table 9) was equilibrated with granite minerals (Table 9) and then flushed by 5 kg fresh water (Table 10) over a time interval of 10 000 years.

There are uncertainties associated with the:

- thermodynamic and kinetic models used;
- thermodynamic and kinetic data;
- representation of natural minerals.

Generally, each natural mineral must be represented within a model by the most similar mineral for which there are data. Thus, the anorthite component of natural plagioclase might be represented by thermodynamic data for pure anorthite. The significance of these approximations is considered qualitatively when interpreting the output from the calculations.

Laboratory data for mineral reaction kinetics were used for primary minerals (Table 11) and simple geometrical relationships were used to estimate reactive mineral surface areas. These areas were calculated by assuming that 1 kg of water (the default amount with which GWB carries out calculations) occupies a planar fracture with an aperture of 1 mm. This gives a rock surface area of 2 m^2 in contact with the water. The surface area of a mineral was then calculated by dividing this total surface area by the mineral's fractional molar abundance.

Secondary minerals were assumed to precipitate or dissolve instantaneously, once they become over-saturated or under-saturated respectively.

While highly simplified, this approach to calculating surface areas is considered adequate for assessing the significance of the ***relative*** rates of mineral reactions. These calculations in turn form a basis for setting up the fully coupled simulations described in Section 5.6. The limitations of the reaction kinetics treatment are discussed more fully in Section 5.6.

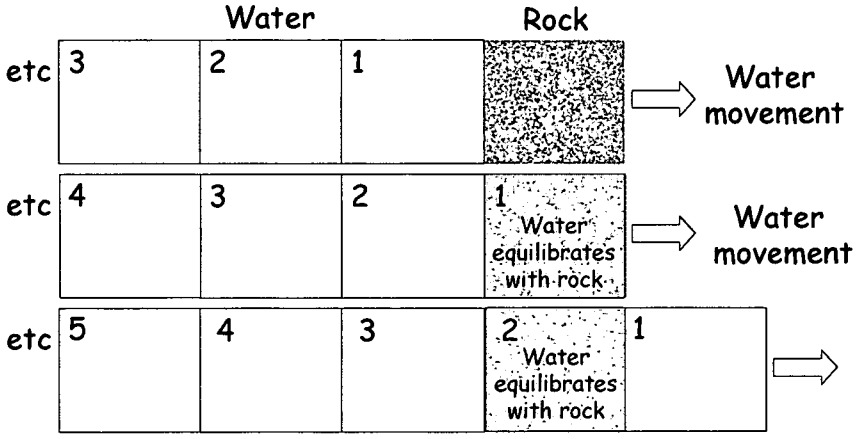

Figure 18. Schematic illustration of a 'flush' model as implemented in GWB.

Table 9. Summary of constraints on the composition of groundwater initially present in the Toki Granite.

Component	Constraint	Aqueous Concentration	[1]Abundance of constraining mineral	Reactive area of constraining mineral
		Moles kg^{-1} water	Moles kg^{-1} water	m^2 kg^{-1} water
Na	Charge balance	0.565	[2]N.A.	N.A.
Ca	[3]Seawater	0.01	N.A.	N.A.
K	K-feldspar	N.A.	21	0.22
Fe	Annite	N.A.	2	0.02
Mg	Phlogopite	N.A.	0.4	0.004
Si	Quartz	N.A.	132	1.38
Cl	Seawater	0.545	N.A.	N.A.
S	Seawater	0.028	N.A.	N.A.
C	Seawater	0.002	N.A.	N.A.

Notes:

[1]Mineral abundances are calculated to be consistent with the whole-rock analysis from 738 .12 m in MIU-4 (coarse-grained, un-weathered biotite granite), supplied by JNC in EXCEL file 'Rock major&minor', on 16th January 2003. This sample has the lowest Fe(III) content among all the samples from this borehole. The calculation assumes that all P is located in apatite, all Ti is in ilmenite, all Na is in albite, all Ca not in apatite is in anorthite, all Fe(II) not in ilmenite or pyrite is in annite, all Mg is in phlogopite, all K not in these other minerals is in K-feldspar, all Si not in these other minerals is in quartz, all sulphur is in pyrite, and all Fe(III) is in amorphous Fe-oxyhydroxide.

[2]Not Applicable.

[3]Modified from a mean seawater composition reported in Henderson (1982).

Table 10. Summary of the recharge water composition used in the simulation of flushing of seawater by fresh water.

Component	Constraint	Concentration
		moles
pH	[1]MC-21	5.4
fO_2, bars	Atmosphere	0.2
Na	MC-21	7.48e-5
K	MC-21	3.27e-5
Ca	MC-21	2.00e-5
Mg	MC-21	2.06e-6
Fe	MC-21	3.76e-6
SiO_2	MC-21	2.59e-4
Cl	MC-21	3.86e-5
HCO_3^-	[2]Log $fCO_2(g)_{,bars}$ = -1.50	4.50e-4
SO_4	MC-21	1.11e-5

Notes:

[1] Most acidic soil water reported in Microsoft Excel file 'Table_gwchem_ver up.xls 1', which was supplied by JNC and which contains all the groundwater from the Tono area that were available on 25th February 2003.

[2] CO_2 fugacity set to be 100 times greater than the atmosphere, to reflect the fact that soil-zone CO_2 concentrations are higher than concentrations controlled by the atmosphere.

Table 11. Summary of information used to calculate the rates of reaction in simulations of flushing of a seawater-saturated Toki granite by fresh water.

Mineral	log k	Surface area, A	Source of log k
	k in mol m^{-2} s^{-1}	m^2	
Anorthite	-11.6	0.06	Brady and Walther (1989)
K-feldspar	-12.5	0.22	Schweda (1989)
Annite	-7.3	0.02	Malmström and Banwart (1997)
Phlogopite	-7.3	0.004	Malmström and Banwart (1997)
Quartz	-13.4	1.38	Knauss and Wolery (1988)

Reaction rates were modelled using the rate law:

$$Rate = k.A.\left(1-\frac{Q}{K}\right) \quad (1)$$

where:
A = surface area (m^2)
Q = activity quotient for the reaction
K = equilibrium constant for the reaction

The results of these calculations are summarized in Figures 19 to 24.

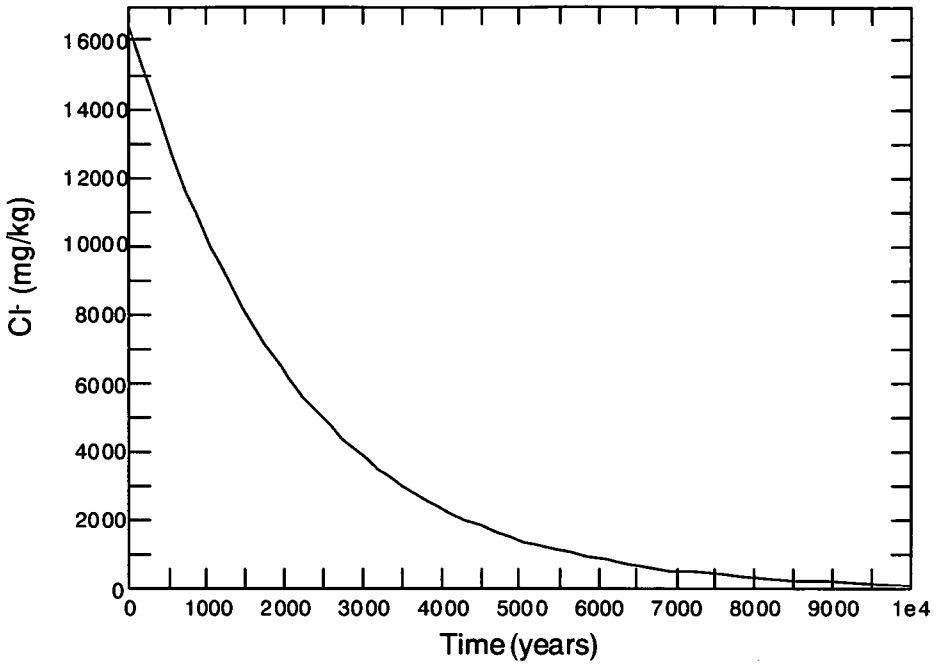

Figure 19. The variation in Cl concentration of groundwater as 1 kg of seawater (containing Na, Ca, SO_4, Cl, HCO_3), equilibrated with granite minerals (quartz, annite, phlogopite, anorthite, K-feldspar) is flushed by 5 kg fresh recharge water over 10 000 years.

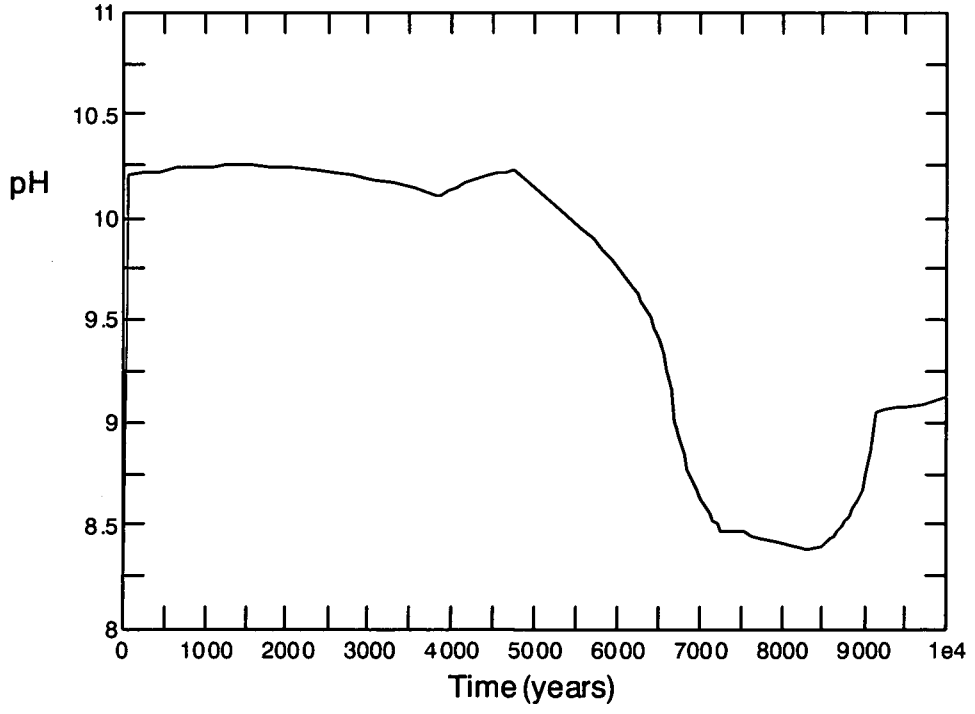

Figure 20. Variations in pH accompanying the flushing shown in Figure 19. A rapid increase in pH from 5.4 to 10.2 occurs in <100 years due to silicate mineral hydrolysis. A later decrease to pH 8-9 is associated with the growth of sheet silicates.

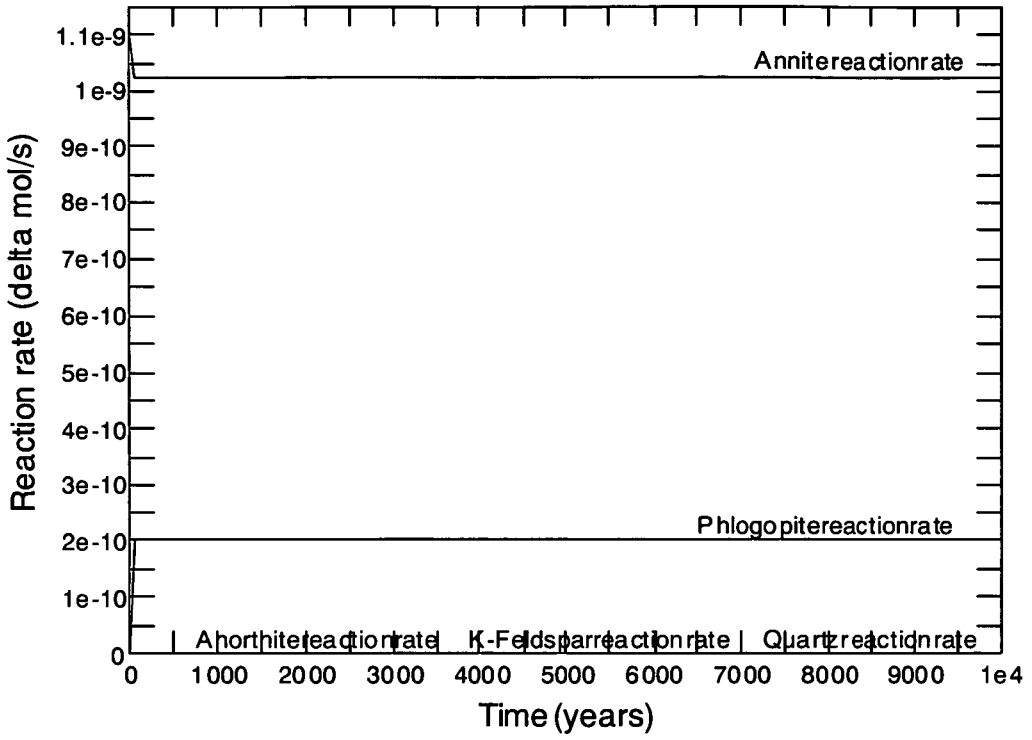

Figure 21. Reaction rates during reactions accompanying the flushing shown in Figure 19.

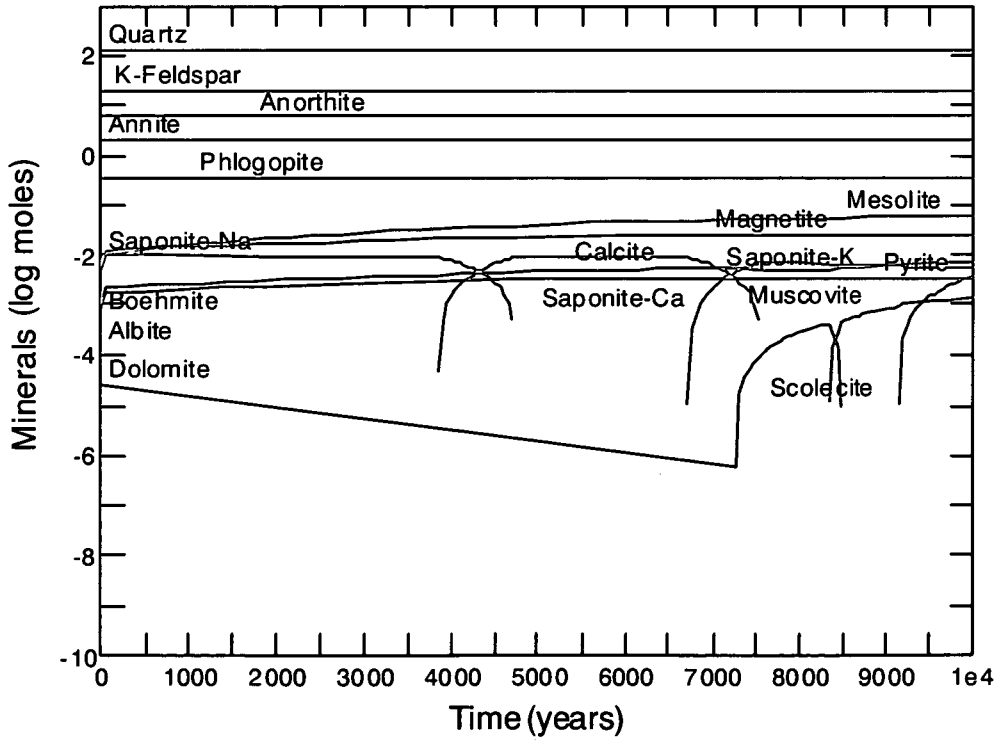

Figure 22. Variations in the mineral assemblage accompanying the flushing shown in Figure 19. All primary minerals except K-feldspar show progressive dissolution with time. Secondary minerals characterised by carbonates, sheet silicates, zeolites, pyrite and magnetite, but the amounts of secondary minerals are small (<0.1 moles over 104 years).

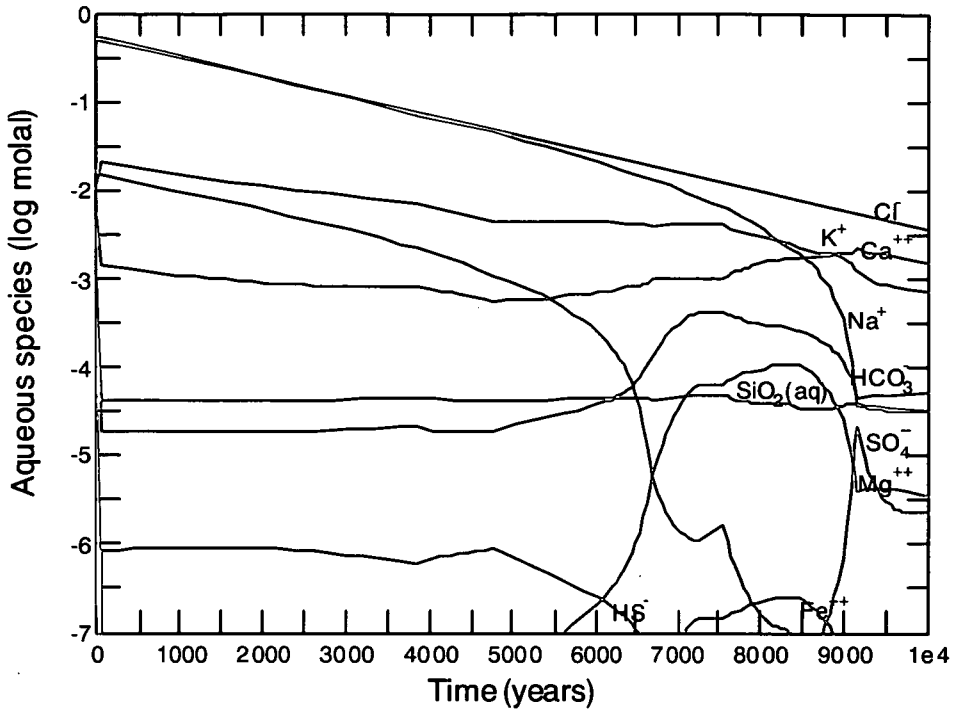

Figure 23. Variations in the aqueous species concentrations accompanying the flushing shown in Figure 19. Cl shows progressive dilution in accord with flush model (final concentration = 125 mg kg^{-1}). Other seawater species show greater decreases due to precipitation reactions, e.g. Na, SO_4.

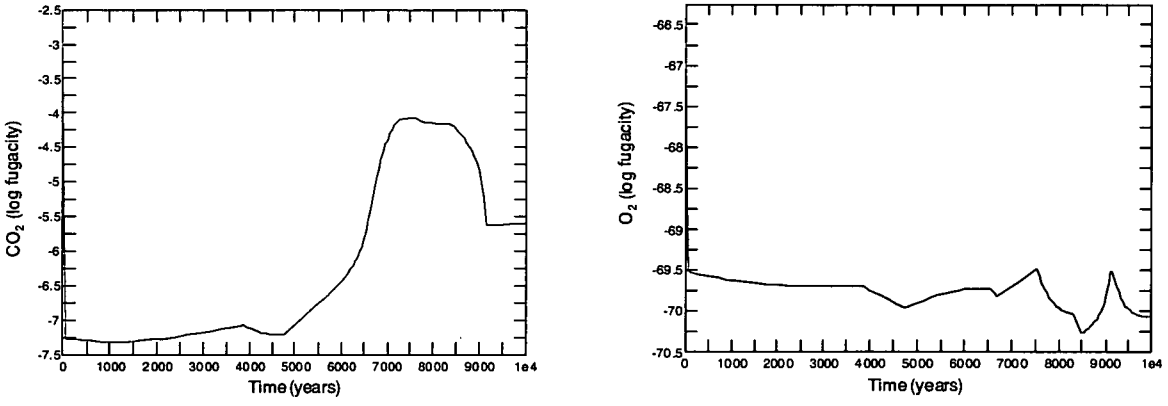

Figure 24. Variations in the CO_2 and O_2 accompanying the flushing shown in Figure 19. fCO_2 mirrors pH behaviour. fO_2 decreases rapidly in first 100 years of simulation due to annite dissolution.

The most important aspects of these results are:

- Mineral reaction rates are dominated by biotite (annite and phlogopite; Figure 21).
- Simulated flushing of seawater from the granite by fresh water reproduces some features of Tono mineralogy (pyrite, sheet silicates, zeolite precipitation; Figure 22). However, although kaolinite is actually present in the rock (Iwatsuki and Yoshida, 1999; Gillespie et al. 2000), this mineral is not predicted by the model.
- Calcite appears (c. 3500 a) and then disappears (c. 8000 a) (Figure 22).

- The modelled groundwater chemistry has significant differences from the observed chemistry (Ca > Na; K > Na; Figure 23).

- Reducing conditions (Eh ~-350 mV) are attained very rapidly and reflect dissolution of annite and precipitation of amorphous $Fe(OH)_3$ and/or pyrite (Figure 24).

- The modelled CO_2 and pH are inversely correlated, as seen in the actual groundwater system, but actually show a relationship with respect to age that is the opposite of the conceptual model developed by Arthur (2003) and expanded further in Section 5.2.

Several of the major differences between the modelled and actual water-mineral systems could be due to the short timescale of the simulation compared to the timescale over which the actual groundwater system has been flushed. Additionally, the assumption of instantaneous precipitation could explain why no kaolinite forms, but instead other sheet silicates precipitate.

The simulation time of 10,000 years is comparable to the timescale over which the groundwater system (horizontal length scale 10 km, depth 2 km) could be flushed once by inflowing water (see Part 2). However, the initial mineralogy in the model is pristine granite. In contrast, the rock has probably been flushed many times and the present mineralogy of the rock at present reflects a long history of water/rock reactions.

It can be concluded from the calculations that clay minerals would have formed early in the history of the groundwater flow system. They are therefore expected to have been important parts of the system throughout most of the system's evolution and to remain so at the present.

The abundances of the secondary phases are all small compared to the abundances of primary phases. The overall chemical buffering capacity of the primary silicate mineral assemblage is unlikely to be exhausted during the timescales of interest to PA (1 million years).

The tendency of biotite to dissolve relatively quickly has two important implications for the coupled simulations:

- Other minerals will tend to be 'protected' by this dissolution, because the aqueous concentrations of dissolved constituents will be maintained at relatively high levels. Any kinetic coupled simulation that does not include Fe-biotite will tend to over-estimate the dissolution rates of other silicates.

- Oxygen consumption by the Fe(II) released from biotite oxidation is likely to be an important control on the migration of redox fronts.

These results indicate that coupled models need to include a representation of clay minerals and to allow silicate mineral hydrolysis and calcite precipitation. Oxygen consumption by the oxidation of Fe obtained from silicate minerals must also be considered.

5.4 Coupled 1D models of redox and salinity variations

5.4.1 Modelling approach

Simulations of both redox-dependent and non-redox dependent reactions that are fully coupled to flow are computationally highly complex. The Raiden code used in this project (Section 5.6) is able to perform such computations. However, several weeks may be required for a single simulation. Therefore, instead of coupling many transport processes and water/rock interactions an alternative, more rapid approach was adopted. The evolution of total groundwater salinity and the penetration of oxygenated groundwater into the rock were

simulated separately along a single flow line (1D) using the code 'Online-Object-Oriented PA Environment (OZONE(O3); Figure 25).

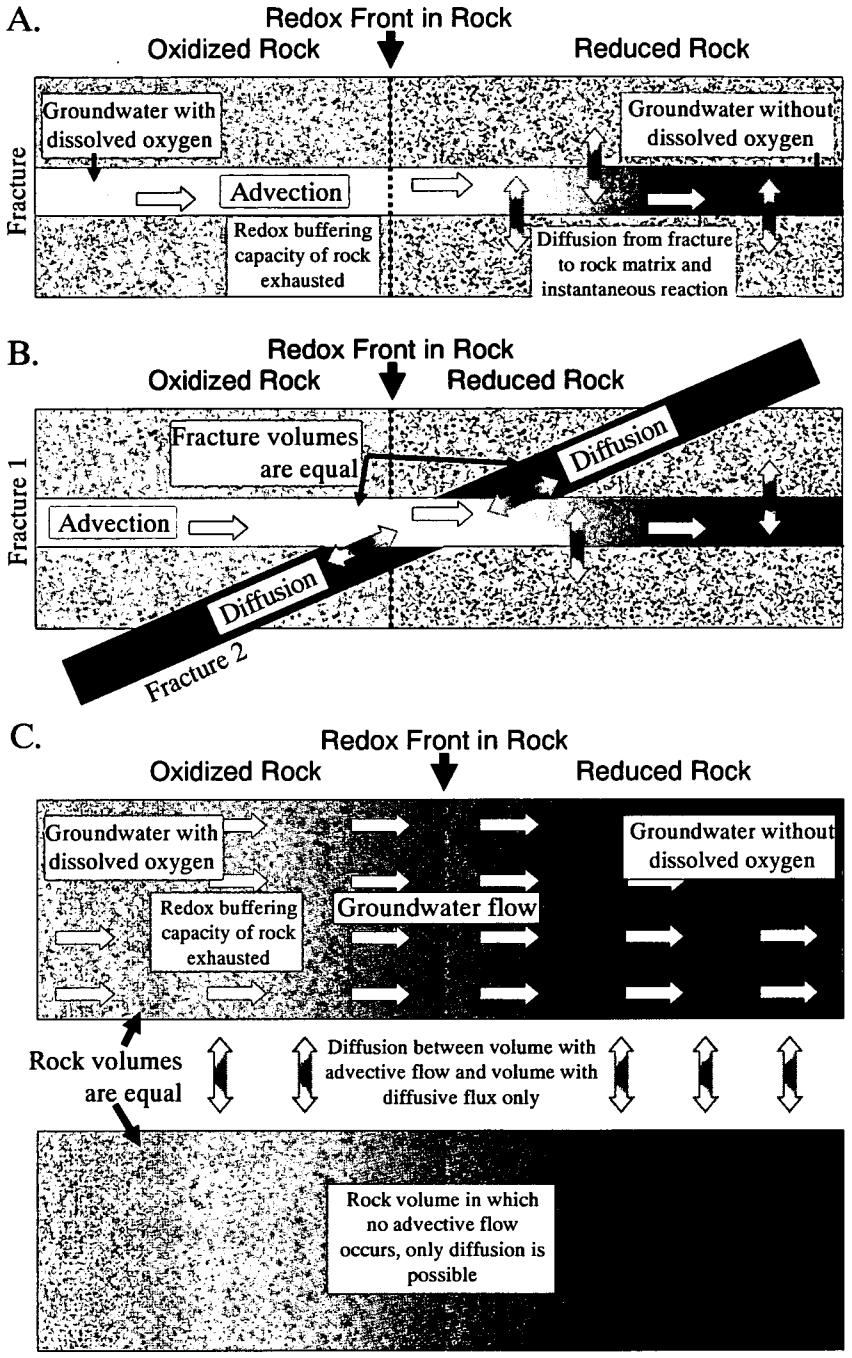

Figure 25. Schematic illustration of the Ozone(O3) simulation cases. Configuration **A.** was used to evaluate both salinity evolution and redox front migration. Configurations **B.** and **C.** were used to evaluate only salinity evolution. **A.** shows only a single fracture for clarity and corresponds to the results in Figures 26 ('f-cases') 27 and 28. **B.** is similar, but each fracture conducting flowing water is cut by a second fracture of equal volume that contains stagnant, reducing water (Figure 26 't-fract'). The stagnant water exchanges by diffusion with the flowing water. In **C.** water flows through the rock matrix (upper) and exchanges by diffusion with stagnant, reducing water in a separate but equal volume of matrix (lower; Figure 26 'p-fract). In some simulations, this stagnant volume was absent (Figure 26 'p-cases').

The different model cases are tabulated in Table 12 and the results are summarised in Figures 26, 27 and 28. The Reference Case is based on the Reference Case of the H12 PA reported in JNC (2000). Case 1 is similar to the 2D base case simulation of groundwater flow in the Tono area that was undertaken by Enviros (Part 2).

Table 12. Summary of simulations using Ozone. For the Reference Case and cases 1 to 4 there are corresponding 'f-' and 'p-' sub-cases in Figure 26. The 'p-cases' were the same as the 'f-cases' except that the fracture was not represented (the 'p-cases' correspond to Figure 25C, without the matrix volume containing stagnant water). There are also 't-frac' and 't-porous' sub-cases corresponding to the Reference Case.

Analysis component		[1]Reference	[2]Case 1	Case 2	[3]Case 3	[3]Case 4	[4]Case 5	[4]Case 6
Length (Salinity calculation)	[m]	10000	10000	10000	10000	10000	Not Applicable	
Dispersion length (Salinity calculation)	[m]	1000	1000	1000	1000	1000	Not Applicable	
Length (Redox calculation)	[m]	1000	1000	1000	Not Applicable		1000	1000
Dispersion length (Redox calculation)	[m]	100	100	100	Not Applicable		100	100
Distribution coefficient	[$m^3 kg^{-1}$]	0	0	0	0	0	0	0
Flow cell number (Salinity calculation)	[-]	500	500	500	500	500	Not Applicable	
Flow cell number (Redox calculation)	[-]	100	100	100	Not Applicable		100	100
Matrix proportion	[-]	10	10	10	10	10	10	10
Fracture (not applicable to 'p-cases' in Figure 26)								
Hydraulic gradient	[$m\ m^{-1}$]	0.01	0.1	0.01	0.01	0.01	0.01	0.01
Coefficient of transmissivity	[$m^2 s^{-1}$]	1.02E-10	1.00E-08	1.00E-08	1.00E-08	1.00E-08	1.00E-09	1.02E-10
[5]Aperture width	[m]	2.02E-05	0.0002	0.0002	0.0002	0.0002	6.32E-05	2.02E-05
Fracture frequency	[m^{-1}]	0.3	0.3	0.3	0.3	0.3	0.3	0.3
Matrix								
Porosity	[-]	0.02	0.02	0.02	0.02	0.02	0.02	0.02
Diffusion depth	[m]	1	1	1	1	1	1	0.1
Contribution proportion	[%]	50	50	50	50	50	50	50
Density	[$kg\ m^{-3}$]	2640	2640	2640	2640	2640	2640	2640
Effective diffusion coefficient	[$m^2 s^{-1}$]	3.00E-12	3.00E-12	3.00E-12	3.00E-13	3.00E-14	3.00E-12	3.00E-12
Coeff. of hydraulic conductivity	[$m\ s^{-1}$]	3.07E-11	3.00E-09	3.00E-09	3.00E-09	3.00E-09	3.00E-10	3.07E-11
Darcy velocity	[$m\ y^{-1}$]	9.69E-06	0.00947	0.000947	0.000947	0.000947	9.47E-05	9.69E-06
Flow line velociy	[$m\ y^{-1}$]	1.60	158	15.8	15.8	15.8	5.00	1.60
Aperture area per unit section area	[$m^2 m^{-2}$]	6.07E-06	0.00006	0.00006	0.00006	0.00006	1.90E-05	6.07E-06
Diffusion area per unit volume	[$m^2 m^{-3}$]	1.65E+05	1.67E+04	1.67E+04	1.67E+04	1.67E+04	5.27E+04	1.65E+05
Diffusion coefficient	[$m^2 y^{-1}$]	4.73E-03	4.73E-03	4.73E-03	4.73E-04	4.73E-05	4.73E-03	4.73E-03
Effective diffusion coefficient	[$m^2 y^{-1}$]	9.47E-05	9.47E-05	9.47E-05	9.47E-06	9.47E-07	9.47E-05	9.47E-05

Notes:

[1] Reference Case values are from the PA Reference Case described in the H12 report (JNC, 2000).

[2] The rock properties used in Case 1 are closest to the base case for the simulations of groundwater flow in the Tono area undertaken by Enviros and reported in Part 2.

[3] Only applicable to simulation of salinity evolution.

[4] Only applicable to simulation of redox front migration.

[5] Apertures for the fractures are effective apertures, calculated to be consistent with the transmissivities. The values are substantially less than the actual observed apertures of the fractures.

5.4.2 Salinity variations

The simulations of salinity evolution aimed to evaluate the influence of varying rock properties on the time taken to flush saline water from the rock. It was assumed that water/rock reactions would have a negligible effect on the total salinity and that density effects could be neglected. Consequently the precise level of the salinity in the model was not significant and therefore the rock was initially saturated with water containing 1 mol m^3 of total dissolved solids. The rock was then flushed by fresh water containing no solutes.

Figure 26 shows the normalised flux of saline water on a log scale and the most important features of the diagram are the points where the salinity begins to decrease. These points can be thought of as representing the time where the inflowing fresh water breaks through to the end of the flow path, 10 km distant from recharge. The initial fluxes are different, reflecting the different rock properties and hydraulic gradients of the different cases.

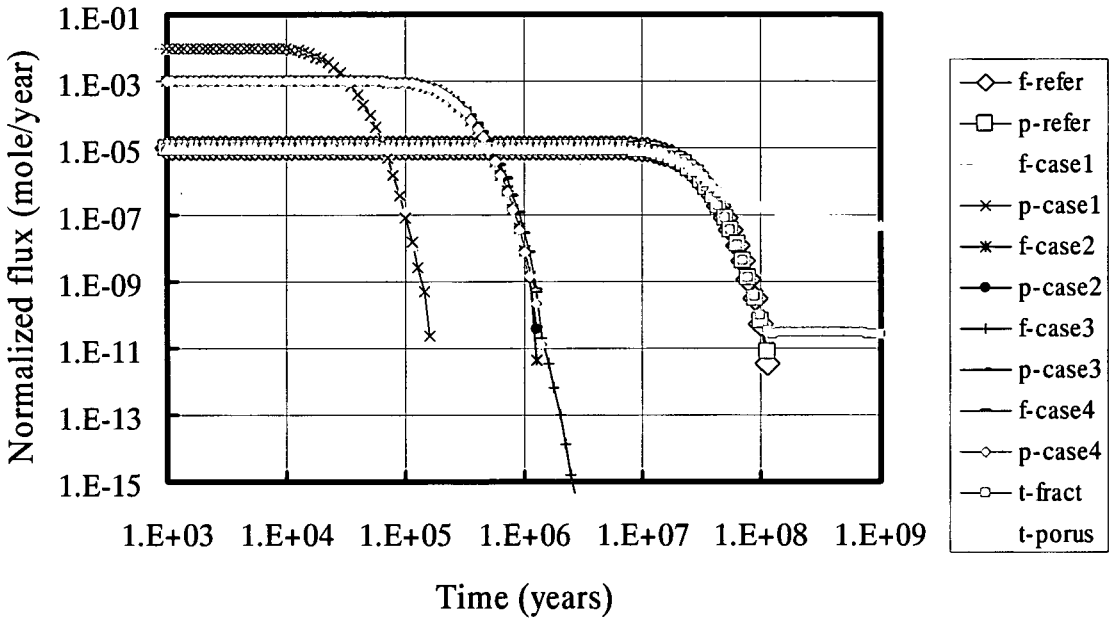

Figure 26. Variations in flux of salinity versus time, normalized to a total dissolved salt content of 1 mole in the entire transport field.

There is little difference between each pair of simulation results (the 'p-case' and corresponding 'f-case'). This reflects the fact that the fracture properties were constrained to produce the bulk hydraulic properties of the rock. Thus, the two models are very similar from the point of view of simulating the distribution of salinity.

The flushing time for Case 1 is in the order of 10^4 years, similar to the flushing time calculated by Enviros for the 2D base case (Part 2). The Cases 2, 3, and 4 give flushing times that are in the order of 10^5 years, which are still comparable with some of the alternative cases considered by Enviros (reduced flux Case 9; Part 2).

In contrast, the Reference Case, and the 't-fract' case based upon it, have fractures with very low transmissivities and corresponding small apertures, compared to the other cases. These constraints are reflected in the very long times required for the salinity of water leaving the flow line to decrease significantly from the initial value. Approximately 30 Ma is required, which is greater than the age of the sedimentary rocks in the Tono area.

The cases with stagnant water volumes ('t-fract' and 't-porous') take the same time for lower salinity water to break through as the Reference Case on which they are based. However, both

The cases with stagnant water volumes ('t-fract' and 't-porous') take the same time for lower salinity water to break through as the Reference Case on which they are based. However, both these cases with stagnant water volumes have long 'tails' in their flushing curves. These extend to 1000 Ma, the limit of the simulation time. In the 't-frac' case, the tail occurs at a very low flux, in the order of 10^6 lower than the initial flux. Therefore in this case the final flux and the corresponding salinity are effectively zero. However, the tail in the 't-porous' curve is only 10^2 lower than the initial flux.

These results illustrate that a very wide range of flushing times may be possible, depending upon the particular rock parameters and the model that is chosen to represent the permeability characteristics of the rock. If Case 1 is an accurate representation of the Toki Granite, then an initial seawater origin of the salinity is unlikely. In this case, any seawater salinity would be flushed in a very short time compared to the time since seawater is known to have been present in the area. However, if the other cases are in fact more representative of the bulk granite, then an original seawater source for the groundwater salinity cannot be ruled out. More information is needed concerning the permeability distribution in the granite in order to reach a firm conclusion about the flushing time.

5.4.3 Redox variations

The simulations of redox variations were based on several assumptions.

- The rate of oxygen consumption by water/rock reactions was assumed to be fast compared to the rate of oxygen supply by advective groundwater flow. The calculations carried out with GWB in section 5.3 support this conclusion (Figure 24).

- The water/rock reactions were assumed to be controlled by the accessibility of reactive minerals to the dissolved oxygen-bearing water.

- All the minerals in the rock were assumed to be available for reaction, once they come into contact with oxygenated water.

- Diffusion from fractures, where the water moves by advection, was assumed to transport oxygenated water into the rock matrix, where redox reactions may take place.

These assumptions meant that it was unnecessary to represent the mineralogy of the rock explicitly within the calculations. Instead, the total oxygen uptake capacity of each unit rock volume was calculated from a reported bulk-rock chemical analysis. An analysis of a sample from DH-10 was used (Table 13), since this sample had the largest apparent concentration of reduced elements reported for the granite in the Tono area.

The assumptions mean that for a given permitted matrix diffusion depth, the redox front propagation distance in a given time for a given inflowing oxygen concentration is a minimum value. The propagation of the redox front will be more rapid if one or more of the following occurs:

- the rate of oxygen consumption by the rock is slower than the rate of supply by advection;

- the effective capacity of the rock to uptake oxygen is lower, than assumed by the model, which will occur if:

  - the actual reduced minerals in the rock are less abundant;

  - the actual reduced minerals in the rock are less accessible to oxygenated water;

- the depths over which matrix diffusion may occur is less.

Table 13. Derivation of the whole-rock composition used in the Ozone, PHREEQC and Raiden modelling.

Whole-rock analysis		[1]Calculated mineral composition			
Borehole	**DH-10**	**Mineral**	**Wt% (Calculated)**	**Moles Mineral in Rock (allowing for 10% porosity)**	**Starting composition used in the models**
Depth (mabh)	**645.5m**			**mol kg^{-1} H_2O**	**mol kg^{-1} H_2O**
Rock Type	Altered biotite granite				
Component					
SiO_2	76.71	**Quartz**	44.36	179.61	179.61
TiO_2	0.05				
Al_2O_3	12.25				
FeO	0.59	**Annite**	0.20	0.096	0.10
Fe_2O_3	0.48	**$Fe(OH)_3$(am)**	0.67	1.52	0.00
Fe^{2+}/Fe^{3+}	1.3661				
MnO	0.00				
MgO	0.01	**Phlogopite**	0.04	0.02	0.02
CaO	0.09	**Anorthite**	0.40	0.35	0.35
Na_2O	1.86	**Albite**	16.38	15.20	15.20
K_2O	6.04	**K-Feldspar**	37.02	32.36	32.36
P_2O_5	0.01				
H_2O^+	0.95				
H_2O^-	<0.76				
CO_2	-				
S	0.4137	**Pyrite**	0.81	1.63	1.63
C	-				
Totals	100.21		99.88		

Notes:

[1]Mineral abundances are calculated to be consistent with the whole-rock analysis analysis of sample from 645.5 m in DH-10, from Table 2.5.9 of Iwatsuki et al. (2000). This sample has the highest redox buffering capacity (Fe(II)/Fe(III)) of any of the samples. The calculation assumes that all P is located in apatite, all Ti is in ilmenite, all Na is in albite, all Ca not in apatite is in anorthite, all Fe(II) not in ilmenite or pyrite is in annite, all Mg is in phlogopite, all K not in these other minerals is in K-feldspar, all Si not in these other minerals is in quartz, all sulphur is in pyrite, and all Fe(III) is in amorphous Fe-oxyhydroxide.

In all the simulations, the redox front at which dissolved oxygen effectively disappears, migrated through the rock up to several orders of magnitude slower than the mixing zone between fresh and saline water (c.f. Figures 26, 27 and 28; note that the flow lines used to simulate salinity and redox variations were 10 km and 1 km long respectively). However, the penetration depths of the redox front are still substantial given the timescales considered. For example, in Case 1, the redox front propagated around 200 m from the recharge zone in the same time interval as it took for fresh recharge water to flush through the 10 km flow line. If this situation persisted for PA-relevant timescales of around 1 Ma, then the rock would be oxidised throughout the flow path (Figure 27).

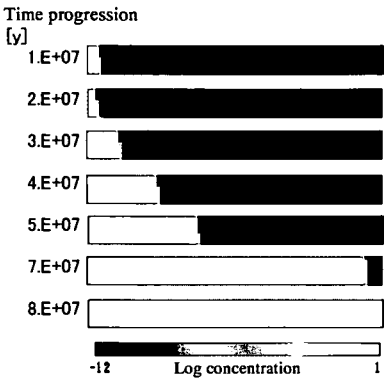

Dissolved oxygen concentration (mol/m³) distribution in the fractured medium **Reference Case**
Horizontal: Flow direction Length 1000 m 100 cells
Perpendicular: Matrix diffusion Depth 1 m 10cells
Vertical and horizontal scales different.
Figure showing output after 6.E+07 years omitted.

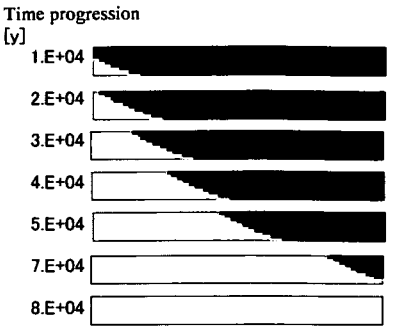

Dissolved oxygen concentration (mol/m³) distribution in the fractured medium **Case 1**
Horizontal: Flow direction Length 1000 m 100 cells
Perpendicular: Matrix diffusion Depth 1 m 10cells
Vertical and horizontal scales different.
Figure showing output after 6.E+04 years omitted.

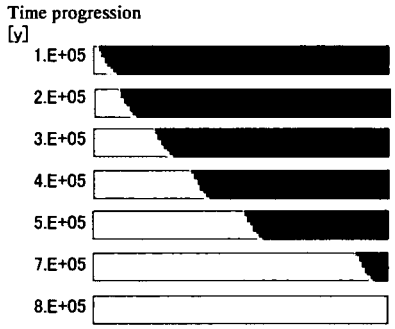

Dissolved oxygen concentration (mol/m³) distribution in the fractured medium **Case 2**
Horizontal: Flow direction Length 1000 m 100 cells
Perpendicular: Matrix diffusion Depth 1 m 10cells
Vertical and horizontal scales different.
Figure showing output after 6.E+05 years omitted.

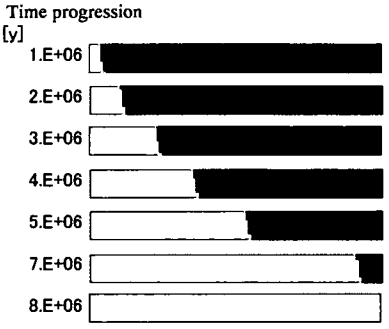

Dissolved oxygen concentration (mol/m³) distribution in the fractured medium **Case 5**
Horizontal: Flow direction Length 1000 m 100 cells
Perpendicular: Matrix diffusion Depth 1 m 10cells
Vertical and horizontal scales different.
Figure showing output after 6.E+06 years omitted.

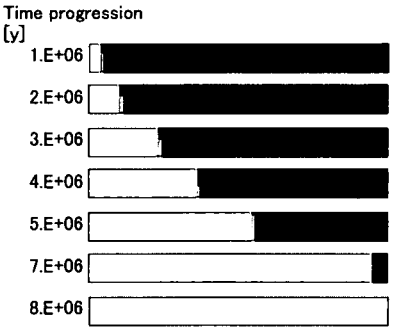

Dissolved oxygen concentration (mol/m³) distribution in the fractured medium **Case 6**
Horizontal: Flow direction Length 1000 m 100 cells
Perpendicular: Matrix diffusion Depth 0.1 m 10cells
Vertical and horizontal scales different.
Figure showing output after 6.E+06 years omitted.

Figure 27. Calculation of O_2(aq) concentration as fresh water moves through fractures and exchanges by diffusion with porewater in the matrix. This porewater becomes instantaneously reducing owing to its reaction with minerals in the rock. The cases are those described in Table 12. Note that the length of the flow line is 0.1 times that in the salinity simulations of Figure 26.

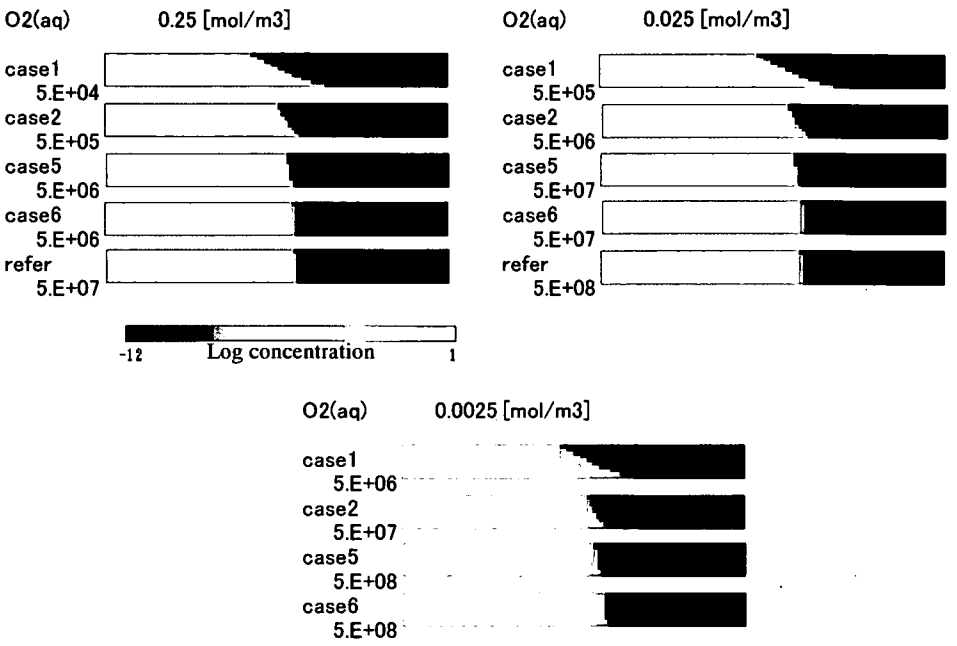

If the Case 1 flow rate is taken as a standard, that of Case 2 is 1/10, that of Case 5 is 1/100 and that of the reference case is approximately 1/1000. The flow-dependent O_2(aq) influx in the Case 2 at the upper left and Case 1 in the upper right are equal. The diffusion-dependent fluxes are different.

Figure 28. Comparison between the results from Case 1 and the results from the other cases. The cases are those described in Table 12. The upper left diagram compiles results from Figure 27. The other results illustrate the effect of decreasing the oxygen content of the in-flowing water by one order of magnitude (upper right) and two orders of magnitude (bottom). Note that the length of the flow line is 0.1 times that in the salinity simulations of Figure 26.

This result is inconsistent with the site observations. Possible explanations for the apparent discrepancy are:

- The rock properties assumed for Case 1 are in fact different to the actual properties of the Toki Granite.
- The oxygen content of the inflowing water has in reality been lower than was assumed by Case 1.

The simulated variability in rock properties caused substantial variations in the rates of redox front propagation (Figures 27 and 28). If the bulk Toki granite in fact behaves more like 'average' granite (e.g. the Reference Case) then more reasonably slow redox front propagation rates would result. In this case, even in 30 million years the redox front would penetrate only around 150 m.

The depth of diffusion is an important control on the propagation rate. However, it is likely that the 1 m depth assumed in all cases except for Case 6 overestimates the likely diffusion depth. Evidence for this comes from the observed depths of reddening around fractures, both in the Toki Granite and elsewhere. If the diffusion depth is in reality substantially less than 1 m, propagation rate could more rapid than calculated (c.f. Case 6 where diffusion could occur to only 0.1 m with the Reference Case where diffusion could occur to 1 m; Figures 27 and 28).

The oxygen content of 8 mgl^{-1} in the calculations illustrated in Figure 27 is consistent with air saturation and is therefore a maximum value. It is expected that the actual oxygen content water flowing into the granite would be less than this, owing to redox reactions occurring in the soil zone and possibly organic-rich sedimentary rocks. Such reduction in oxygen contents

was found as Äspö in Sweden (Banwart et al., 1996). The calculations in the present study demonstrate that an order of magnitude reduction in oxygen content would result in an order of magnitude decrease in the rate of redox front propagation (Figure 28).

5.5 Semi-coupled flow and salinity transport models using PHREEQC

5.5.1 Purpose of PHREEQC simulations and their relationship to Raiden simulations

Even when chemical reactions are considered independently of redox reactions, simulations of the coupling between reactions and flow are computationally challenging and require considerable time. A major cause of the long times required is the need to include rate laws describing reaction kinetics.

Test simulations were carried out using both the USGS code PHREEQC and Quintessa's own code Raiden (see Section 5.6), in order to establish how best to optimise the speed of the simulations. Both these codes can carry out simulations of 1D transport using user-defined rate laws. However, the representation of transport by PHREEQC is very simple in comparison with the representation in Raiden.

In PHREEQC transport simulations the flow path is divided into cells of equal length and volume. ***At each step of the simulation all the contents of one cell are transferred to the next cell.*** Thus, if the time step needs to be very short in order for the simulation to converge to a solution (which is usually the case during complex simulations), many cells are needed to represent a reasonable overall transport time. A consequence of this is that overall computation times are large. The durations are particularly long if dispersion is considered, because PHREEQC represents dispersion as a mixing process between adjacent cells. If the cell size is very small in order to achieve realistic overall transport times when the time step is short, a geologically reasonable dispersion length may require the mixing calculation to consider many cells.

In contrast, Raiden transport calculations are fully coupled. The cells need not be all of the same length and volume and only a proportion of the contents of each cell need be transported at each time step. This is because the code calculates flow explicitly, using input values for the hydraulic properties of the rock and hydraulic gradient. Thus, if the time step duration needs to become short to achieve convergence of the simulation, the volume of water transported at each step also becomes small. This in turn means that very small cells are not a pre-requisite to achieve realistic travel times. Simulations that incorporate dispersion may therefore be more rapid than equivalent simulations using PHREEQC.

However, to make kinetic calculations run to completion in a reasonable time requires a very simplified representation of the reacting mineral assemblage. It is highly desirable to understand the significance of such simplifications by first undertaking non-kinetic coupled simulations incorporating a more realistic mineral assemblage. Unfortunately, Raiden cannot readily be used for this purpose owing to the numerical approach that it uses to solve the relevant equations. If kinetics are not included the simulations are less likely to converge and in any case will tend to take longer. In contrast, PHREEQC can more readily handle transport simulations with instantaneous reactions involving a complex mineralogy.

5.5.2 PHREEQC simulation cases

The rock composition used in the PHREEQC simulations is summarised in Table 13. Each PHREEQC calculation reported here involved 1 kg of water and 1 kg of water was present in each cell. Therefore the abundances of minerals in each cell were set to be the same as listed

in the final column of Table 13. The water compositions used are summarised in Table 14. Both the initial saline water and the recharge water compositions were calculated using a combination of analytical data and theoretical constraints. The code GWB was used to do this.

The PHREEQC simulations evaluated the effects of varying dispersion and the effect of a temperature gradient along the flow line. The model cases are summarised in Table 15.

Table 14. Summary of the water compositions used in the PHREEQC modelling.

Component[2]	Units	Initial saline groundwater[1]		Recharge water	
		Constraint	Concentration	Constraint	Concentration
pH	pH	Seawater	8.0	MC-21[3]	5.4
Eh	mV	Pyrite	-240	Atmosphere	900
Na	molal	Seawater	4.58e-001	MC-21	7.48e-005
Al	molal	Kaolinite	1.14e-007	Kaolinite	3.96e-009
Ca	molal	Calcite	3.30e-003	MC-21	2.00e-005
K	molal	Seawater	9.49e-003	MC-21	3.27e-005
Fe	molal	Annite	2.57e-006	$Fe(OH)_3(am)$	8.34e-006
Mg	molal	Seawater	5.18e-002	MC-21	2.06e-006
Si	molal	Seawater	6.93e-005	MC-21	2.59e-004
Cl	molal	Charge Balance on Cl^-	5.20e-001	MC-21[4]	3.86e-005
S	molal	Seawater	2.76e-002	MC-21	1.11e-005
C	molal	Seawater	2.28e-003	Charge balance on HCO_3^-	1.00e-003

Notes:

[1] Modified from a mean seawater composition reported in Henderson (1982).

[2] Total concentration of the indicated element.

[3] Most acidic soil water reported in Microsoft Excel file 'Table_gwchem_ver up.xls 1', which was supplied by JNC and which contains all the groundwater from the Tono area that were available on 25th February 2003.

[4] Charge balanced on HCO_3^- when defining initial solution, but subsequently during the transport calculations charge was balanced on Cl^- for consistency with the charge balancing constraint on the initial modified seawater solution.

The model cases are summarised in Table 15.

Table 15. Summary of the coupled simulations undertaken using PHREEQC.

Simulation Number	No. of cells	Lengths of cells	Temperature	Dispersion	Diffusion coefficient	Porosity	Primary minerals	Secondary minerals	Initial groundwater Chemistry	Recharge water chemistry
		relative	°C	no of cells	$m^2\ yr^{-1}$					
JNC 2073A Phq coup inst v4	100	Arbitrary	25	0	0	0.1	Quartz, K-feldspar, Anorthite, Albite, Annite, Phlogopite, Pyrite	Calcite, Kaolinite, $Fe(OH)_3(am)$	Saline, modified seawater	Fresh, reducing
JNC 2073A Phq coup inst v5		Arbitrary	25	10						
JNC 2073A Phq coup inst v6		Arbitrary	25 to 40 (uniform gradient across 100 cells)	0						

5.5.3 Results of the PHREEQC simulations

The results of all the model cases are given in Appendix A1. The cell lengths and time steps are arbitrary since kinetics were not considered, the cell volumes are equal and flow rates are not calculated by the code. The results are therefore presented in terms of relative distances (percentages of the overall flow path length) and times (fractions or multiples of the time taken for the inflowing water to exit the flow line).

Key features of the results are:

- In each model the abundances of the minerals present initially in the rock change only in the first few percent of the flow line, except in the case of anorthite.

- Anorthite abundances decrease to zero over time and a front at which anorthite is lost completely propagates through the rock. After 100 pore volumes have passed, anorthite is absent from the flow line (Figure 29).

- The dissolution of anorthite is mirrored by the formation of calcite. A front of calcite precipitation propagates along the flow line. At high water/rock ratios, the calcite formed already begins to dissolve once more near the inflow. A second front, with calcite absent towards the upflow side therefore propagates through the rock (Figure 29).

- The abundances of the initial minerals decrease over time, with the exception of annite which shows an increase in abundance.

- This increase in annite abundance is an artefact of the thermodynamic data for the relevant phases and the fact that kinetics are not considered. The simulated precipitation of this phase illustrates the importance of considering kinetics. In reality dissolution of annite would probably occur much more rapidly than any other phase (Section 5.3, Figure 21) and therefore the abundance of this component would decrease. However, in the modelled case, the abundance of annite reflects only solubility constraints. Since the feldspars are more soluble than annite, the net effect is for these to dissolve very close to the inflow and for some of the dissolved components to be re-precipitated as annite slightly further along the flow path.

- The abundances of the dissolving and precipitating minerals are small. Overall, very little change in the porosity is predicted by the models, except very close to the inflow point after several 10s of pore volumes have flushed the system.

- Dispersion has a significant effect on the concentration gradients of dissolved species, but only a small effect on the abundances of minerals.

- In contrast temperature gradients have a relatively large effect on the abundances of secondary minerals, but a less significant effect on concentration gradients of dissolved species.

- The primary mineral assemblage would buffer the pH at very alkaline values, between about 9.5 and 11.1, depending upon the model case. Only when the anorthite is effectively removed does the pH begin to drop. A front where the pH falls towards the upstream, side propagates through the rock.

- The simulations illustrate that the value chosen for the dispersion coefficient could influence the relationship between CO_2 fugacity and pH.

- When dispersion is neglected, the relationship between pH and CO_2 fugacity is similar to that identified by Arthur (2003), except where the pH is calculated to be buffered at very alkaline values by the initial silicate mineral assemblage (Figure 30). This discrepancy

between the model results and the groundwater observations suggest that in the Tono area, the pH-CO_2 fugacity relationship is effectively controlled by equilibrium with calcite, whereas the evolution of pH is controlled by a kinetic process; equilibrium with the silicate assemblage is approached but not attained.

- The pH increases away from the inflow point. This is consistent with water of longer residence time having higher pH and lower CO_2 fugacity.

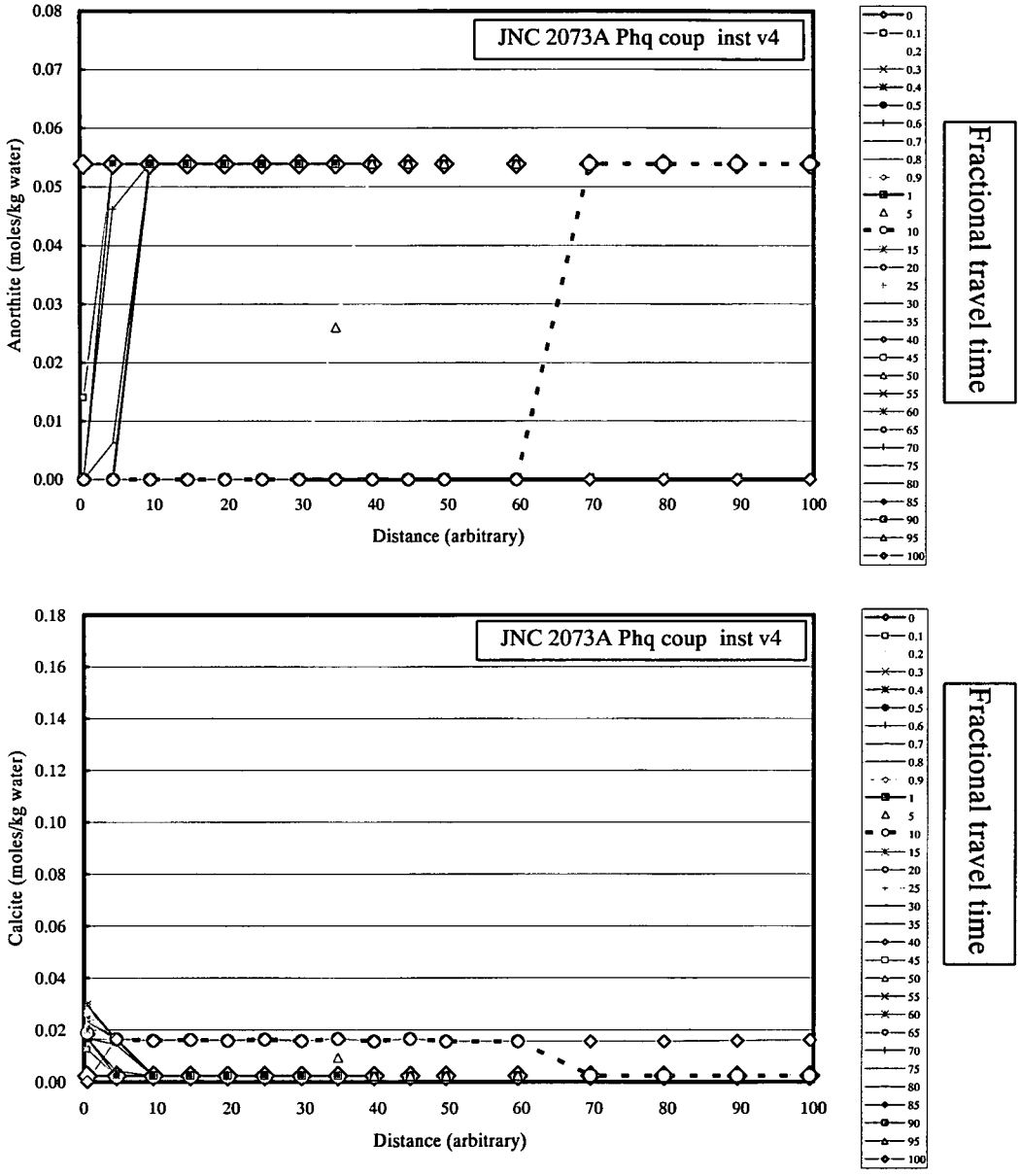

Figure 29. Propagation of fronts at which anorthite dissolves (upper) and calcite dissolves or precipitates (lower). The output is from case JNC 2073A Phq coup inst v4.

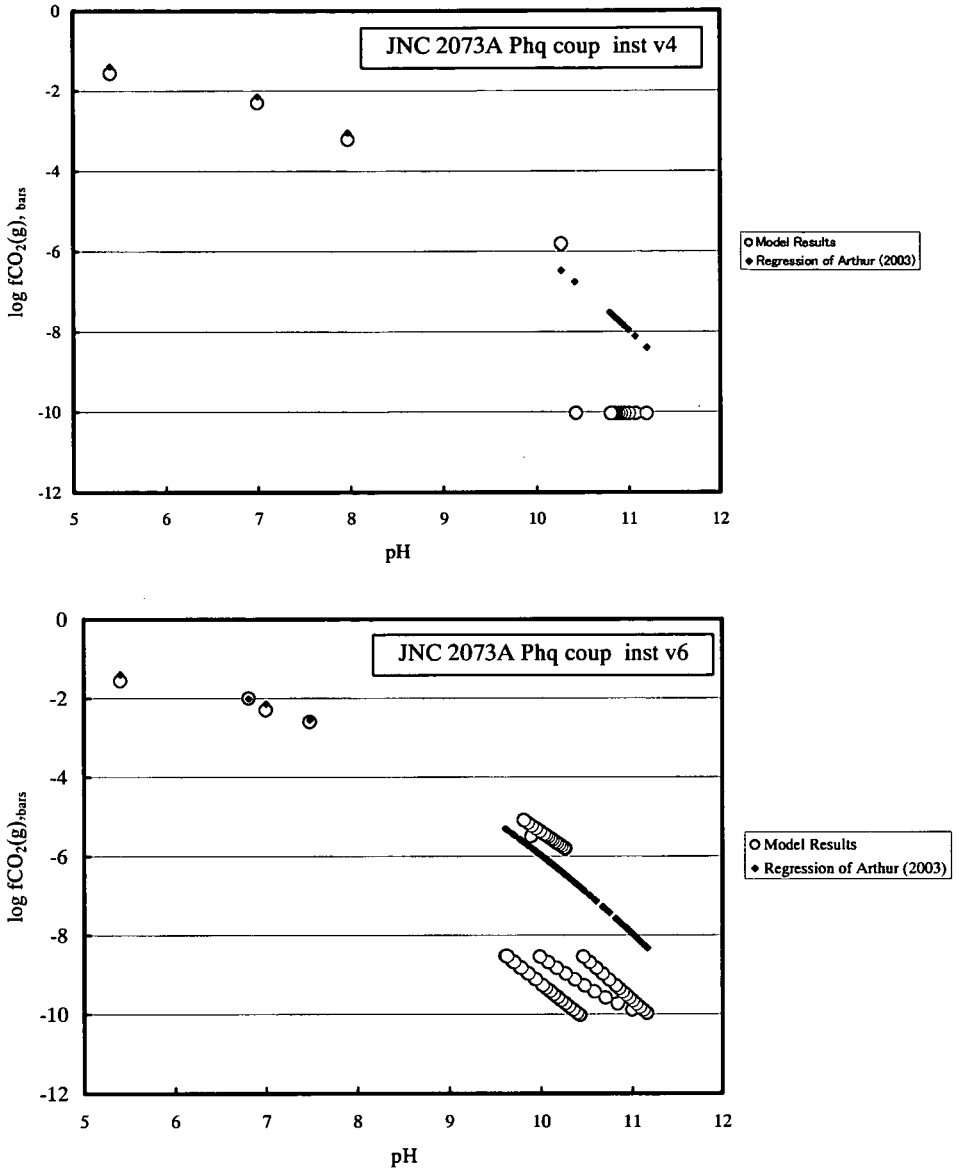

Figure 30. Simulated relationships between CO_2 fugacity and pH calculated for simulations JNC 2073A Phq coup inst v4 (upper) and JNC 2073A Phq coup inst v4 (lower).

5.6 Fully-coupled flow and salinity transport models using Raiden

5.6.1 Purpose of Raiden simulations

The GWB and PHREEQC models described in Sections 5.3 and 5.5 indicate that the simplest fully-coupled kinetic models that might simulate major features of the groundwater/rock system should include:

- replacement of anorthite by clay minerals;
- precipitation and dissolution of calcite.

These reactions are also consistent with observed mineral textures (e.g. Iwatsuki and Yoshida, 1999; Gillespie et al. 2000).

The Raiden calculations described here were designed to investigate the coupling between groundwater flow and these reactions. An aim was to evaluate the degree to which this coupling could explain the major observed variations in groundwater chemistry in the Toki Granite.

Similar uncertainties to those that applied to the GWB simulations described in Section 5.3 also apply to the Raiden calculations. As previously, these uncertainties were taken into account qualitatively when interpreting the output from the calculations.

5.6.2 Raiden simulation cases

The mineral assemblages considered in the Raiden simulations were based on that given in the right hand column of Table 13. However, in each simulation, the mineral assemblage was simplified by removing some of the minerals and then adding quartz of equal volume to these removed minerals. In this way, the overall porosity of the mineral assemblage was preserved.

The simulations did not consider annite because it contains reduced iron. Therefore, inclusion of this mineral would have introduced the complexity of redox reactions, causing the time required to perform a simulation to become prohibitively long.

A major effect of neglecting annite would probably be that the dissolution rate of anorthite is over-estimated (Section 5.3). A consequence is, in turn, that the rate of calcite production at any location is likely to be a maximum value.

The water compositions used in the simulations are summarised in Table 16 and the modelled cases are described in Table 17.

Table 16. Summary of the water compositions used in the Raiden modelling.

Component[2]	Units	Initial saline groundwater[1]		Initial fresh groundwater		Recharge water	
		Constraint	Concentration	Constraint	Concentration	Constraint	Concentration
pH	pH	Seawater	8.0	Middle of observed range	8.5	MC-21	5.4
Na	Molal	Seawater	4.58e-001	MC-21[3]	7.48e-005	MC-21	7.48e-005
Al	Molal	Kaolinite	1.14e-007	Kaolinite	1.10e-007	Kaolinite	3.96e-009
Ca	Molal	Calcite	3.30e-003	Calcite	4.00e-004	MC-21	2.00e-005
K	Molal	Seawater	9.49e-003	MC-21	3.27e-005	MC-21	3.27e-005
Mg	Molal	Seawater	5.18e-002	MC-21	2.06e-006	MC-21	2.06e-006
Si	Molal	Seawater	6.93e-005	Quartz	1.09e-004	MC-21	2.59e-004
Cl	Molal	Charge Balance on Cl-	5.20e-001	MC-21	3.86e-005	MC-21	3.86e-005
S	Molal	Seawater	2.76e-002	MC-21	1.11e-005	MC-21	1.11e-005
C	Molal	Seawater	2.28e-003	Charge balance on HCO_3^-	8.00e-004	Charge balance on HCO_3^-	1.00e-003

Notes:

[1] Modified from a mean seawater composition reported in Henderson (1982).

[2] Total concentration of the indicated element.

[3] Most acidic soil water reported in Microsoft Excel file 'Table_gwchem_ver up.xls 1', which was supplied by JNC and which contains all the groundwater from the Tono area that were available on 25th February 2003.

Table 17. Summary of the coupled simulations undertaken using Raiden.

Simulation Number	No. of cells	Lengths of cells	Temperature	Dispersion	Diffusion coefficient	Hydraulic Conductivity	Head difference	Porosity	Primary minerals	Secondary minerals allowed to form	Initial groundwater Chemistry	Recharge water chemistry
		m	°C	m	$m^2\ yr^{-1}$	$m\ y^{-1}$	m					
fwpCO2pH25Kav1	1	10000	25	0	3.15e-03	20.4	950	0.1	Quartz, Anorthite	Kaolinite	Fresh, reducing	Fresh, oxidising
fwpCO2pH25Kap01v1								0.01				
fwpCO2pH25v2					3.16e-04			0.1				
fwpCO2pH25Kadfe5v1					3.15e-05	1.79	105	0.01				
fwpCO2pH25Kah105v1												
fwpCO2pH25Kak1.7v1												
fwpCO2pH25PhMmv1									Quartz, Anorthite, Phlogopite	Ca-Montmorillonite		
fwpCO2pH25PhMmv1a										Ca-Montmorillonite, Calcite		
fwpCO2pH25Lmd100v1				100					Quartz, Anorthite	Laumontite		
fwpCO2pH25Kad100										Kaolinite		
fwpCO2pH25Kad100a										Kaolinite, Calcite		
fwpCO2pH60Kad100v1			60							Kaolinite		
fwpCO2pH60Kad100v1a										Kaolinite, Calcite		
[redacted]	10	1000	25							[redacted]		
fwpCO2pH 25Ka 10 c 270803v1a										Kaolinite, Calcite		
[redacted]										[redacted]	Saline, modified seawater	
swpCO2pH 25Ka 10 c 270803v2a										Kaolinite, Calcite		
a28cv2	28	1st 20 of 100 m, then 8 of 1000 m										

The rock properties, hydraulic gradients and groundwater types in the 3D local model and the 2D base case of Enviros (Part 2) are represented in the multi-cell cases swpCO2pH 25Ka 10 c 270803v2, swpCO2pH 25Ka 10 c 270803v2a and a28cv2. Additionally the rock properties and hydraulic gradients in these Enviros simulations are represented in the cases fwpCO2pH25Lmd100v1, fwpCO2pH25Kad100, fwpCO2pH25Kad100a, fwpCO2pH60Kad100v1, fwpCO2pH60Kad100v1a, fwpCO2pH 25Ka 10 c 270803v1, fwpCO2pH 25Ka 10 c 270803v1a.

5.6.3 Incorporation of mineral reaction kinetics

The simplified modelling of reaction rates in Section 5.3 allowed the relative rates of the mineral reactions to be calculated and provided important insights into the mineral reactions that would control overall reaction rates. However, this approach is very much an approximation of the real world, notably:

- The reaction rates are appropriate for neutral conditions, but in fact the pH varies markedly from neutral (e.g. Figure 20).
- The geometrical approach gives minimum mineral surface areas available for reaction, assuming that all the surface area of each mineral species is in contact with the groundwater. In reality, the surface area could be much greater for some minerals and less for others (though in most cases it is likely that the geometrical surface area under-estimates the true surface area (e.g. White, (1995)).
- The kinetics of secondary mineral precipitation are not considered.

The Raiden modelling attempted to produce a more realistic representation of the real world by:

- using rate laws that take into account pH variations;
- specifying rate laws for precipitating minerals.

Additionally, since the surface areas used in the GWB modelling probably under-estimate the actual reactive surface areas, ***experimental*** surface areas were chosen from the literature, consistent with producing:

- realistic *relative* reaction rates;
- *reasonable* overall degrees of reaction within the timescale considered.

The aim was not to use more ***realistic*** surface areas since there are too many uncertainties to evaluate whether the surface areas are in fact 'realistic'. Instead, the aim was to use ***plausibly*** large surface areas to provide a basis for comparison with the earlier results and hence gain insights into the significance of uncertainties in surface areas.

The dissolution of silicate minerals is strongly dependent upon pH, due to catalysis by surface reactions involving protons and hydroxyl ions (Brady and Walther, 1989). Typically, the following dissolution regimes can be defined:

- an 'acidic pH regime' where rates increase with increasing H+ concentrations;
- a 'neutral pH regime' where rates are independent of pH;
- an 'alkaline pH' regime' where rates increase with decreasing H+ concentrations.

The extent of each of these regimes is mineral specific and relates to mineral structure and composition.

The GWB modelling described in Section 5.3 did not take into account this pH-dependence of the rate law and instead used rate constants appropriate for a 'neutral pH regime' (Table 11). In contrast, the Raiden modelling implemented more sophisticated rate laws that took into account this pH-dependence.

An empirical rate law for silicate dissolution under far-field conditions was defined as follows, where dissolution behaviour is separated into H^+-catalysed (k_H), pH-independent (k_0) and hydroxyl-catalysed (k_{OH}) regimes:

$$fe\_rate = k_H A\left(H^+\right)^m + k_0 A + k_{OH} A\left(H^+\right)^n \quad (2)$$

where:
fe_rate is the rate under far-from equilibrium conditions;
A is the mineral surface area (m^2);
m and n are coefficients describing the dependency of rate upon H^+;

Dissolution kinetics data for anorthite and quartz are presented in Table 17.

Table 18. Dissolution rate constants and reaction coefficients for silicate minerals at 25 °C (mol m^{-2} s^{-1}), as defined by release of Si.

Mineral	log k_H	m	log k_0	log k_{OH}	n	Source
Anorthite	-4.8	1.7	-11.6	-13.5	-0.3	Brady and Walther (1989)
[1]Biotite	-4.5	0.9	-7.3	-11.3	-0.5	Malmström and Banwart (1997)
Quartz	-	-	-13.4	-16.3	-0.5	Knauss and Wolery (1988)

Notes:
[1] The biotite composition was: $K_{0.79}(Mg_{0.83}Fe^{II}_{1.03}Fe^{III}_{0.19}Al_{0.58})(Si_{3.17}Al_{0.67}Fe^{III}_{0.16})O_{10}(OH)_2$. The data were assumed to be applicable to phlogopite in the simulations here.

To allow for the decrease in mineral precipitation rate as equilibrium is approached, the rate calculated by this equation was found by:

$$Rate = fe\_rate.\left(1 - \frac{Q}{K}\right) \quad (3)$$

where:
Q is the activity quotient for the reaction;
K is the equilibrium constant for the reaction

The formation of secondary silicate minerals was assumed to be fast compared to the dissolution of the primary minerals and was modelled using the rate law:

$$Rate = k.A.\left(1 - \frac{Q}{K}\right) \quad (4)$$

where:
k is the rate constant

Here log k was set to -2, thereby ensuring that the precipitation rate is fast compared to the dissolution rate (numerical convergence is aided by treating all reactions kinetically).

Calcite dissolution and growth were simulated using an overall rate law described by Plummer et al. (1978):

$$rate = A.\left(k_1\left[H^+\right] + k_2\left[H_2CO_3^*\right] + k_3\left[H_2O\right] - k_4\left[Ca^{2+}\right]\left[HCO_3^-\right]\right) \quad (5)$$

where at 25 °C:
$\log k_1 = -0.29$;
$\log k_2 = -3.47$;
$\log k_3 = -4.88$;
$[H_2CO_3^*] = [H_2CO_3] + [CO_2(aq)]$;
k_4 is a function of both temperature and PCO_2 and can be expressed as:

$$k_4 = \frac{K_2}{K_{sp}}\left[k_1' + \frac{1}{a_{H^+}}\left(k_2 a_{H_2CO_3} + k_3 a_{H_2O}\right)\right] \quad (6)$$

where:
K_2 is the second dissociation constant of carbonic acid (i.e. $HCO_3^- = H^+ + CO_3^{2-}$; -10.30 at 25°C);
K_{sp} is the equilibrium constant for calcite (-8.475 at 25°C);
k'_1 is the first-order mechanistic rate constant for H^+ attack (here approximated by k_1, but note that $k'_1 > k_1$);
and k_2 and k_3 are as defined above.

The units of the rate constants are mol m^{-2} s^{-1}.

Table 19. Summary of mineral surface area data.

Mineral	Surface Area	Source	Comments
	$m^2 g^{-1}$		
Quartz	2.5	White (1995)	Middle of range quoted for fresh quartz.
Anorthite	0.3	White (1995)	Data in White (1995) suggest that feldspar and quartz crystals of similar size would have similar specific surface areas. However, the anorthite here represents the calcic component of dominantly sodic plagioclase. Therefore, the surface area was scaled according to the compositional boundary between albite and oligoclase (10% anorthite).
Kaolinite	15	Santamarina et al. (2002)	The choice of log k means that the rate of precipitation will be high relative to the dissolution rate of anorthite, irrespective of the choice of surface area.
Calcite	0.02	White (1995)	Calcite is a secondary mineral and was predicted to form in only very small quantities, which makes an evaluation of surface area even more uncertain than for other phases. Consequently, the surface area used corresponds to a grain size of 1 mm, chosen arbitrarily, on a regression through measured surface area versus grain size for various minerals.
Phlogopite	0.5	Appelo and Postma (1994)	Surface area reported for biotite.
Montmorillonite	600	Santamarina et al. (2002)	The choice of log k means that the rate of precipitation will be high relative to the dissolution rate of anorthite, irrespective of the choice of surface area.
Laumontite	20	Wilkin and Barnes (2000)	The choice of log k means that the rate of precipitation will be high relative to the dissolution rate of anorthite, irrespective of the choice of surface area.

The Raiden simulations all used laboratory surface areas derived from the literature (Table 19). These areas are around 5 orders of magnitude larger than the surface areas calculated geometrically in Section 5.3 and given in Table 11.

5.6.4 Results of the Raiden simulations

The results of all the model cases are given in Appendix A1. The most important features are:

- Anorthite is replaced by kaolinite in the simulations where kaolinite is allowed to precipitate (Figure 31).

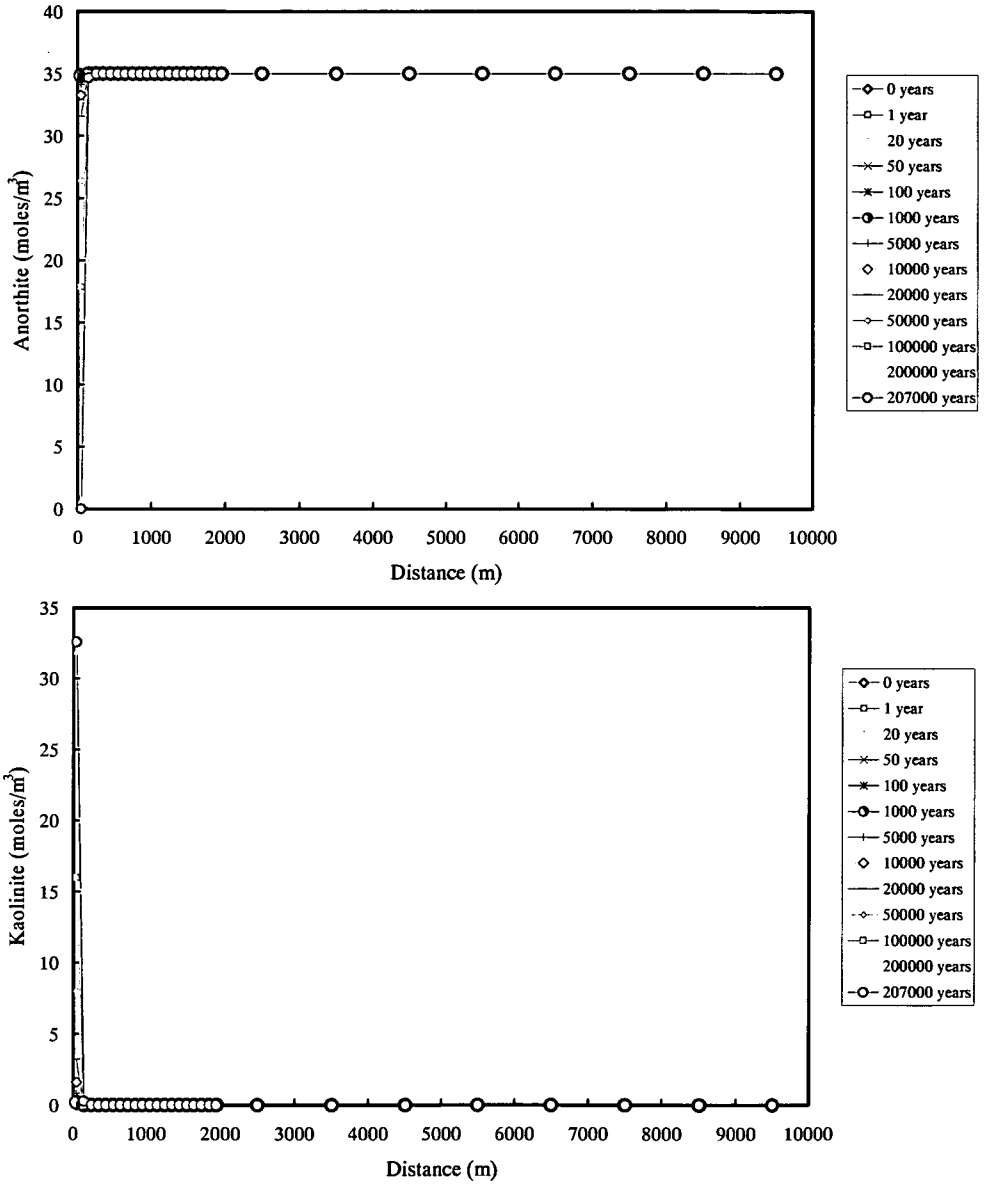

Figure 31. Simulated distributions of anorthite and kaolinite versus distance along a flow path at various time intervals. The simulation was carried out using Raiden, with a 10000 m long flow line discretised into 28 cells of varying lengths and the input constraints given in Table 18 (model a28cv2).

- As expected, the rate of anorthite replacement by kaolinite is proportional to the rate of water flow, which in turn depends on the head gradient and the hydraulic conductivity.

  - In 1 cell simulations where the head changes by 950 m along the 10 km flow path anorthite is replaced completely after 500000 years. In contrast when the head difference is only 100 m head difference only 25% of the anorthite is replaced after 1 million years.

  - Similarly, decreasing the hydraulic conductivity by an order of magnitude, decreases the dissolution rates of primary minerals by an order of magnitude.

- When the flow rate is varied, the duration for which the silicate mineral assemblage can control pH and logfCO_2 also varies. However, for as long as the actual silicate minerals present do not change, the values of pH and CO_2 remain invariant.

  - Single cell models with a large head gradient (950 m) have two steps in the curves of pH and log $fCO_2(g)$ versus time. These parameters decrease and increase respectively very rapidly initially, effectively instantaneously. They are then constant until 500,000 years at which point they decrease and increase respectively to constant values that are maintained until the end of the simulation at 1 Ma.

  - Single cell models with low head gradient (100 m) have effectively instantaneous decreases and increases of pH and log f $CO_2(g)$ respectively. These then remain constant until the end of the simulation.

- In simulations that allowed calcite to form only very small amounts were produced. These would have an insignificant effect on porosity.

- There are differences between the single cell and multi-cell cases that can be attributed to the averaging effect of mixing. In the single cell cases the volume of inflowing water at each time step is mixed with a very much larger volume of water that is already present. However in the multi-cell cases, the inflowing water at each time step mixes with only the proportion of the total water that is present in the first cell. These effects are readily appreciated by comparing the occurrences of calcite in the single cell:

  - In the single cell flushing cases that allowed calcite to form, calcite formed initially and then dissolved again within a few years to 10s of years. From the perspective of the 1 million year time scale considered this is effectively instantaneous.

  - In contrast, in the 10 cell and 28 cell flushing cases, calcite forms initially and is then removed from the rock as a front at which calcite disappears propagates along the flow line. This front reaches only 5000 m in 1 Ma (Figure 32).

- In the 28 cell model, all changes in silicate mineralogy occur within the first 100 m of the flow line (Figure 31).

- There are only small differences in the evolution of mineralogy, pH and pCO_2 between the cases which consider only fresh water and the cases that consider flushing of seawater by freshwater.

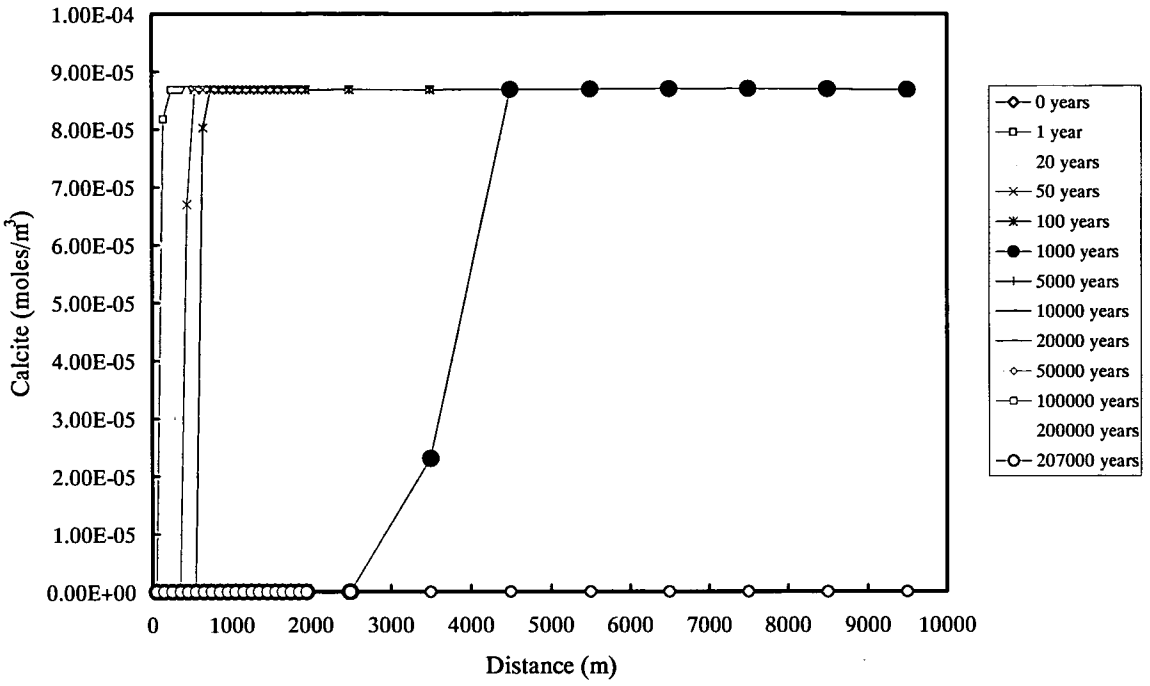

Figure 32. Illustration of the propagation of a front at which initially-formed calcite disappears in the 28 cell model (Table 18, model a28cv2). Note that only very small amounts of calcite are formed.

- Multi-cell models, either with or without calcite precipitation, show propagation of a front at which pH decreases and log fCO_2 increases (Figure 33). This front takes around 10,000 years to propagate to the end of the flow line at 10 km.

- Negligible amounts of calcite precipitates in the multi-cell models that allow calcite to form. These amounts effect the pH and pCO_2 buffering insignificantly. There is no step in the pH- or log fCO_2(g) versus distance curves that corresponds to the disappearance of calcite that is formed initially. The pH is buffered by the silicate mineral assemblage throughout.

- Porosity changes are almost always effectively zero and never greater than 2% of the initial porosity, even after 1000000 years.

- Changing the porosity along from 0.1 to 0.01 makes very little difference to the results.

- A temperature increase causes little change to the overall sequence of reaction, but does change the rate of reaction. The simulations at a temperature of 60°C produced kaolinite at about 1/3 of the rate as the corresponding 25 °C simulations. The pH tends to a value that is about 0.75 pH units lower in the 60 °C cases. Correspondingly, log fCO_2(g) is about 0.5 units higher in the higher temperature case. Calcite is formed very early at low temperatures, but is not formed at all at the higher temperature.

- When montmorillonite, rather than kaolinite is allowed to precipitate, none actually forms.

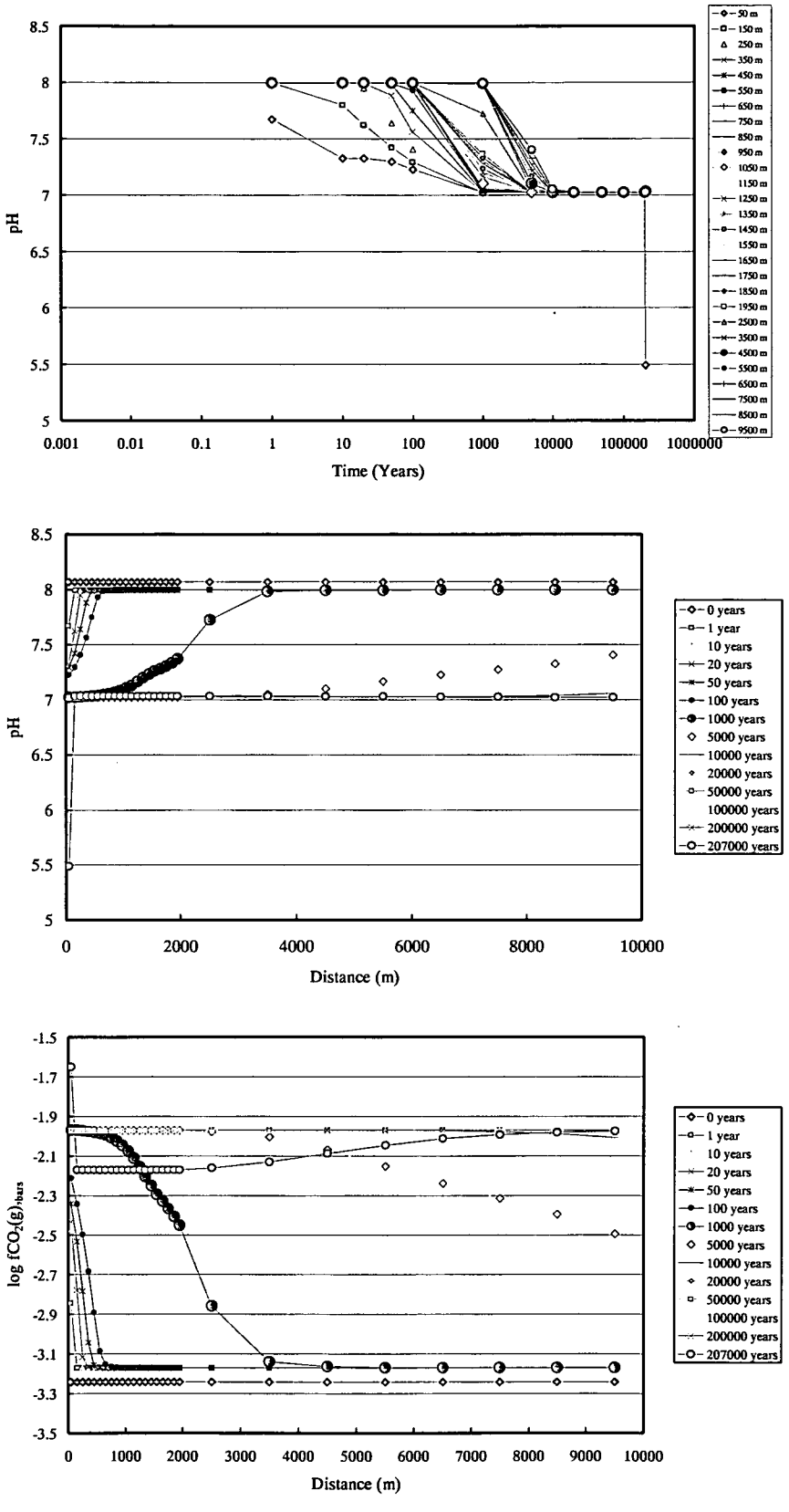

Figure 33. Simulated variations in pH and log $fCO_2(g)$ along the 10 km flow line in the 28 cell model. A front at which pH and CO_2 fugacity vary rapidly propagates along the flow line and takes about 10,000 years to reach the end. Once the anorthite in the rock is consumed near the beginning of the flow line a second front begins to propagate through the rock.

- If laumontite is allowed to precipitate then all the anorthite disappears in only a few 1000 years. This result reflects the relative solubilities of laumontite and anorthite.

It is impossible to fully quantify the significance of the various approximations underlying the models for the overall predicted mineral evolution. Particular causes of uncertainties are:

- the highly simplified representation of the natural mineral assemblage;
- crystallographic and chemical differences between natural minerals of interest and pure minerals used in the laboratory experiments from which thermodynamic and kinetic data were obtained;
- the validity of the rate laws is uncertain (considered to be the least significant uncertainty);
- unknown reactive surface areas of natural minerals.

However, the significance of these uncertainties can be gauged qualitatively.

A combination of the results from the GWB modelling reported in Section 5.3 and mineralogical observations suggests that the simplified mineral assemblage should allow the actual evolution of pH, pCO_2 and porosity to be determined, at least qualitatively.

As noted in Section 5.3, the actual dissolution of Fe-biotite in the real groundwater system would tend to slow the silicate dissolution of other silicate minerals. Therefore, the simulations that did not include biotite would tend to have over-estimated the dissolution rates of silicate minerals.

The most significant uncertainties related to mineral composition are due to:

- using pure anorthite to represent the calcic component of plagioclase;
- using phlogopite to represent biotite (two simulations only);
- using kaolinite or montmorillonite alone to represent a complex clay mineral assemblage.

The effect of plagioclase being dominantly sodic is partly taken into account by scaling the surface area (Table 18). However, the solubility calculated for pure anorthite in the simulation will be higher than the actual solubility of the plagioclase. Thus, the calculated dissolution rate will be higher, owing to the term (1-Q/K) in the rate law (Section 5.6.3).

Similarly, by using phlogopite to represent biotite the calculated rate of Mg release to the water will tend to over-estimate the actual release of Mg.

The net effect of these higher modelled release rates would tend to be increased precipitation rates of any Ca- and Mg-bearing minerals. Therefore, even though a very simplified mineral assemblage is modelled, the conclusion that calcite would form in very small quantities and be present for relatively short time scales is unaffected. Likewise, the conclusion that no montmorillonite will form is unaffected by this approximation.

The validity of using the simplified clay mineral assemblage is supported by actual observations. The dissolution of calcic feldspar coupled to the precipitation of kaolinite is consistent with textural information (Iwatsuki and Yoshida, 1999; Gillespie et al., 2003).

The rate laws and associated parameter values used in the work are appropriate for calculations at a temperature of 25°C. All except two of the simulations were undertaken at this temperature. Two simulations were undertaken at 60°C (fwpCO2pH60Kad100v1 and

fwpCO2pH60Kad100v1a). However, there is probably only a relatively small variation in rates between 25°C and 60°C. The chief effect of increasing the temperature would probably be to increase the overall reaction rates (rate constants) rather than the general form of the rate equation. Therefore, the simulations at the higher temperature probably over-estimate the actual rates.

The general forms of the rate laws used for dissolution of primary silicate minerals and calcite are fairly well known and relative variations in dissolution rates with respect to pH are considered to be well reproduced. The rate law of Plummer et al. (1978) is known from experimental data to be applicable to calcite precipitation while none of the primary minerals precipitate or else are close to equilibrium (quartz). The greatest uncertainty is in the validity of the rate law for simulating precipitation of secondary silicate minerals and the assumption that far-from equilibrium precipitation rates of these minerals are fast compared to the dissolution rates of primary minerals. If this assumption is incorrect, the chief effects will be that at any given time or distance along the flow path:

- the simulated pH is higher than the actual pH;
- the simulated fugacity of CO_2 will tend to be lower than the actual fugacity of CO_2;
- the simulated porosity will tend to be lower than the actual porosity.

The greatest uncertainties in the kinetic calculations concern the mineral surface areas. In nature, the surface areas can vary over several orders of magnitude.

The mineral surface areas that are available for reaction are a function of many un-quantified factors, including:

- crystal shape;
- crystal size (for a given mineral, smaller crystals have higher specific surface areas than larger crystals);
- crystal surface characteristics (e.g. whether fresh and smooth or weathered and irregular);
- petrographical relationships (e.g. whether or not a mineral is overgrown by another mineral and therefore isolated from the groundwater);
- structural setting (e.g. whether in the rock matrix or in a fracture).

Furthermore, a given mineral species may occur in different forms within a single rock. Therefore, the surface areas used in the present work are unlikely to accurately represent the actual reactive surface areas in the rock. However, the most likely implications of the uncertainties are as follows:

- The rate of anorthite reaction will tend to control the rate of calcite formation since anorthite dissolution adds Ca to the water and supplies Si and Al to the solution that are necessary for the formation of clay minerals (represented by kaolinite), which control the pH to be alkaline.
- In the simulations with phlogopite, the rates of anorthite dissolution are reduced relative to those in simulations without anorthite. This effect is due to the relatively rapid rate of phologopite dissolution. However, the extent to which this is important depends on the relative surface areas of phologopite and anorthite. Assuming that biotite and feldspar crystals had the same specific surface, the biotite dissolution rate would be about two to four orders of magnitude faster than the anorthite dissolution rate over most of the pH range considered. Thus, the specific surface area of phlogopite would need to be reduced

by the same order relative to that of anorthite, before the effect on calcite precipitation or dissolution rates would become significant.

- The surface area used for the calcite is likely to under-estimate the actual surface area. This means that the precipitation and dissolution rates will tend to be underestimated, leading to calcite being predicted to form earlier and dissolve later than would actually be the case.

- The specific surface area chosen for anorthite probably overestimates the actual surface area since it is appropriate for a small grain size of around 0.005 mm. Therefore, the dissolution rates would tend to be over-estimated, which would in turn tend to enhance the precipitation rate of calcite. This effect would lead to calcite being predicted to form earlier and dissolve later than would actually be the case.

6 Summary and Conclusions

6.1 Summary of modelling

Geochemical and physical hydrogeological information can be used ***together*** to model groundwater flow directions and fluxes more confidently than could be done with either type of information alone. A common approach is to:

- establish initial conditions for the spatial distribution of groundwater salinity at a time of interest in the past;

- using physical hydrogeological models, simulate the movement of the groundwater salinity to the present time;

- compare the predicted distribution of salinity with the observed distributions;

- compare calculated flow times with groundwater residence times estimated from geochemical data;

- if there are differences between predicted and observed salinity distributions, and/or differences between flow times estimated from the hydrogeological model and residence times calculated from geochemical data, then:

  - modify the initial geochemical conditions;

  - modify the physical hydrogeological model.

- Repeat the above process until self-consistency is achieved.

The approach is most easily applied when water/rock interactions do not significantly affect the salinity distribution during the timescale of the modeling. This situation may occur in saline groundwater systems and where the water chemistry is dominated by relatively un-reactive solutes such as Cl. However, if water/rock interactions are significant, this approach is much more difficult. Water rock reactions may be particularly important when the groundwater is dilute, as in the Tono area. In this case, it is necessary to consider coupling between groundwater flow and water/rock reactions. The work reported here has considered the best way to take this coupling into account.

In the Tono area there are large uncertainties concerning both hydrogeological and geochemical information, notably:

- the initial conditions, principally:
  - distribution of groundwater salinity;
  - hydraulic boundary conditions;
- the origins of the Na-Cl dominated groundwater salinity, principally:
  - whether salinity is being flushed passively (that is, salinity is not produced continuously) or produced continuously as it is being flushed;
  - alternatively whether salinity is being produced continuously at the same time as it is being flushed.

For these reasons, it was inappropriate to continuously adjust these model constraints to achieve consistency. There would be many valid solutions that match both physical and chemical information. Instead, the approach adopted was to consider a possible scenario for the characteristics of the flow system and then to evaluate whether or not this is self-consistent (and hence possibly correct) or inconsistent (and hence incorrect).

The evaluated scenario was that the area was initially uniformly saturated with seawater and then subsequently flushed by meteoric water. The rock permeability remained the same as the present throughout the flushing. Similarly, driving head gradients were similar to the present.

An important result from the modelling is that this scenario is inconsistent and must be rejected. The work has therefore resulted in a reduction in the number of valid scenarios.

The Na-Cl dominated water in the south of the area is chemically very different from seawater. However, it is possible that initially there was a component of seawater salinity that was then modified by water/rock interactions. In this case it is most likely that the water/rock interactions occurred after or during dilution of the original seawater salinity.

Groundwater flow modelling is reported in detail in Part 2. The present part of the report considers the coupling between the flow and chemical reactions.

The coupled models show that hydraulic parameters similar to the present (similar to the base cases in Part 2) would cause groundwater salinity to be flushed within around 15,000 years. This result is inconsistent with the conceptual model, since seawater has clearly not entered the area within this time scale. However, the modelling also shows that variations to head gradients within reasonable limits and/or variations in the representation of the rock mass could lead to the salinity being preserved for much longer, even to a time scale of several 10's of millions of years.

The CO_2 fugacity could potentially be buffered by pH-independent reactions. It can be envisaged that as temperature increases along a flow path, the CO_2 fugacity will also decrease, owing to the water moving progressively towards equilibrium with higher-temperature mineral assemblages. There is no need for pH to be an independent variable that controls the fugacity of CO_2.

On the other hand, pH could also be controlled by progressive reactions with one or more of the minerals in the rock. Reaction with feldspar to produce clay minerals such as kaolinite or montmorillonite would consume H^+, leading to an increase in pH. However, at the low temperatures of the present groundwater system, this process would probably not reach equilibrium.

Kinetic models are required to explain the progressive evolution of pH and PCO_2. When uncertainties are taken into account, the kinetic model results with Raiden are consistent with

pH increasing and PCO_2 decreasing along a flow path as residence times increase. This result is also consistent with the correlation identified by Arthur (2003) using site data.

The observed ranges of pH are not reproduced very well by the model. This may be due partly to an inaccurate representation of secondary clay minerals which in turn is partly due to uncertain kinetic data for these minerals.

Kinetic simulations suggest that if fresh granite is recharged, reducing conditions would be attained very rapidly, within a few 10's of metres of a recharge zone. However, this is due to the rapid reaction of the biotite, which is rapidly consumed. The actual depth of penetration of the redox front at any time will be controlled by the amount of biotite present in the rock.

In the coupled simulations, this redox front migrated through the rock up to several orders of magnitude slower than the migration of the mixing zone between fresh and saline water. However, there is an inconsistency between the observed and modelled penetration of oxygen-bearing water during the time taken to flush the saline groundwater from the system. The model predicts that oxygenated water would penetrated much more deeply into the groundwater system than is in fact observed. This result suggests one or a combination of the following:

- the hydraulic properties of the rock mass are represented incorrectly;
- the amount of oxygen in the water recharging the granite is actually lower than modelled (the model assumed atmospheric equilibration);
- the groundwater fluxes were actually lower than modeled (implying lower driving head gradients than modeled).

The modelling suggests that replacement of calcic feldspar by clay minerals could be significant. This process could lead to a reduction of pH which could cause calcite to form. However, calcite would form in only very small amounts and could, under some circumstances, dissolve again soon afterwards.

Variations in mineralogy are not predicted to cause a large change in the overall porosity of the groundwater system.

The concentration gradients of dissolved species would depend upon whether or not seawater is being flushed and upon dispersion. However, these processes would have only limited effects on the abundances of minerals. In contrast variations in temperature gradients have a relatively large effect on the abundances of secondary minerals, but a less significant effect on concentration gradients of dissolved species. Within a reasonable range of temperatures, the sequence of mineral formation would show little change, but the abundances of the secondary minerals would change.

6.2 Implications for integrating hydrogeological and geochemical interpretations

The work has several generic implications for integrating hydrogeological and geochemical interpretations.

- Palaeohydrogeological information is essential to interpret the initial boundary conditions to be used.
- Even if there are large uncertainties in both hydrogeological characteristics and geochemical parameters, useful insights can be gained by developing and testing scenarios for the possible evolution of the groundwater system.

- The most appropriate approach is to construct a series of computer models that investigate different aspects of coupling, and then to evaluate the degree to which the results of these models are consistent with one another.

- Even though available computer codes allow coupling of many processes to be simulated, it is inappropriate to aim to construct a single, fully-coupled model for groundwater flow because:

  - a great deal of computation time is required, which prevents adequate evaluation of uncertainties;

  - there are many uncertainties that are often inherently unquantiable;

  - the spatial distribution of site data is usually inappropriate for direct comparison with the results of such a model (e.g. in the present work, no single predicted flow line passed through several boreholes).

Part 2: 2D and 3D coupled models of salinity distributions

7 Introduction to coupled modelling of salinity distributions

7.1 Framework

This part of the report describes work done by ENVIROS-Spain for the project 'Development of a coupled geochemical/hydrogeological model of the Tono area (hydrocoupling)', under subcontract to Quintessa, K.K. for the JNC Tono Geosciences centre. The project aims at integrating the current knowledge of the geochemistry of the Tono area with the results of the hydrogeological investigations. It is intended that the results serve for methodological purposes in the context of PA exercises during the site investigation/selection for deep underground storage of radioactive waste in Japan.

A particular issue of the Tono area is the presence of salty water at considerable depths (>500 m) in certain boreholes. One of the tasks of the projects is to develop a conceptual understanding of such water. Such conceptualisation should be supported by a numerical model.

7.2 Scope and Objectives

The objective of this part of the report is to propose hypotheses and/or conjectures after a short discussion on the potential origins of salinity in groundwater in Tono, and to test one of these hypotheses/conjectures by means of a numerical approach.

To fulfil this objective, a methodology is proposed.

7.3 Methodology

First, the chemical composition provided by the client, essentially the file 'Table_gwchem_ver_up.xls', was reviewed. Data in this file have been checked and analysed to highlight potential explanations for the salinity.

The most significant contribution of ENVIROS-Spain to the project has been the numerical modelling of one of the plausible origins of salinity, which is seawater flushing. For this purpose, targeted numerical models at different scales are presented.

7.4 Structure of the document

Section 8 contains the description of some potential sources of groundwater salinity based on the data provided by the client. Since one of these possible sources is Tertiary seawater, when the sedimentary cover of the Toki granite was formed, numerical modelling of the evolution of this salinity has been performed. This is described in Section 9, where the specific methodology aimed at producing the detailed and regional models is presented. The discussion the modelling results is further expanded in Section 10, where they are placed in the framework of the project and in the light of PA exercises. Finally, some conclusions from the project of a methodological and targeted nature are outlined in Section 11 along with some recommendations.

8 Review of existing information

8.1 Existing chemical data

The first step of the methodology followed involved reviewing the chemical composition provided by the client, essentially the contents of the file 'Table_gwchem_ver_up.xls'. Data in this file have been checked and carefully analysed to highlight hydrogeochemical processes, i.e. plotting some components against other analytical data (isotopic, depth, etc.). The following section illustrates the most significant results.

8.2 Analysis of information

Figure 34 shows that most of the registered temperatures lie in a trend consistent with a normal geothermal gradient (30ºC km^{-1}). However, some samples deviate from this behaviour. One group of samples have a lower temperature than that corresponding to this geothermal gradient: they are surface waters (river waters) which have temperatures that vary according to seasonal changes. The other group of samples have higher temperature values: they are sampled from deep boreholes and their high temperatures (up to 32ºC) can only be explained by means of an underground heat source. While this may or may not be significant for the study, the fact that most groundwater temperatures fall in a normal geothermal gradient shows that the thermal source is either far from the sampling points, or that there is a high renovation rate with cold (meteoric) water.

Chloride content vs. depth could eventually show whether there is a clear origin of salts with depth. Actually, Figure 35 shows that in some cases there is such a trend (borehole DH-12) but it also shows that there are many other sampling points at lower depths displaying higher chloride contents than DH-12. In fact, several uranium exploration boreholes show chloride contents in the same range or even higher than the deepest samples from DH-12. Apparently, such boreholes are drilled in the sedimentary cover of the Toki granite.

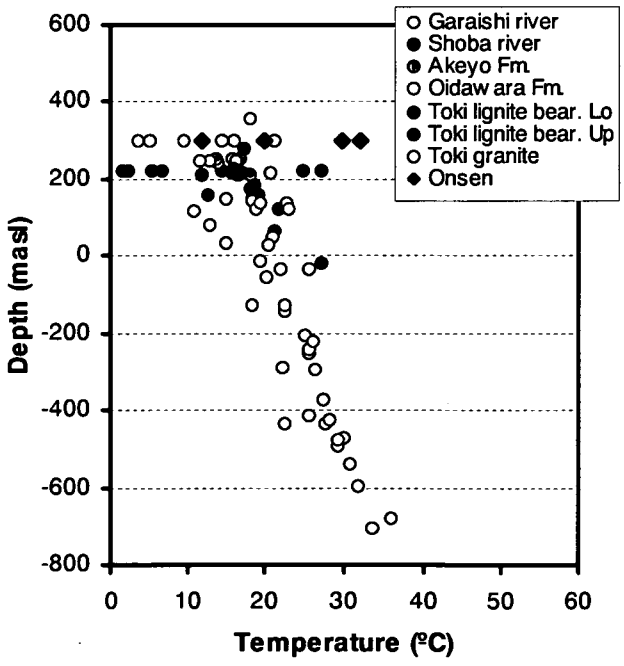

Figure 34. Temperature vs. depth graphic for samples from the Tono area. Note that the origin of Onsen samples is from uncertain depths in deep boreholes.

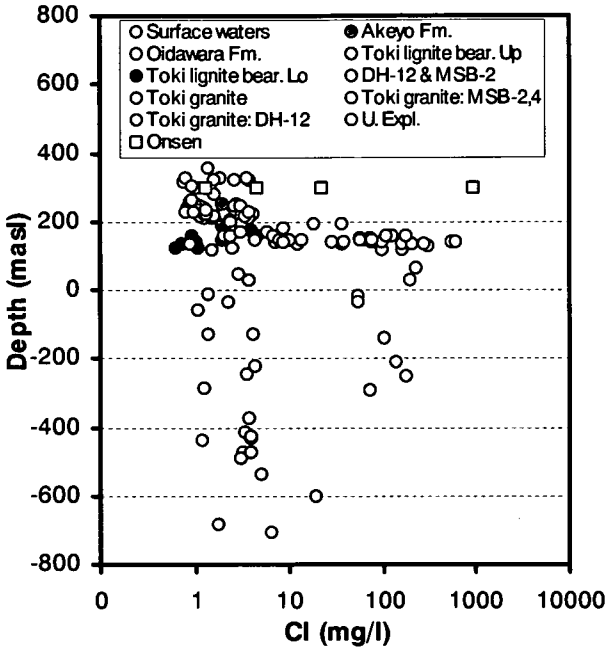

Figure 35. Chloride content (log scale) vs. depth in the Tono area.

Other relationships that are usually useful for discerning the origin of groundwater and its salinity are the stable isotopic ratios (Figure 36) and bromide/chloride ratios (Figure 37).

Figure 36 shows the stable isotope composition of waters of the area (rain and groundwater). For comparison, the seawater composition has been plotted. This figure shows that while the rainwater extends over 6 and 60 units of ^{18}O and D respectively, groundwater samples are concentrated over a 2 and 20 units interval, but within the same range of values as for rainwater. Such a range of concentrations favours a meteoric origin for the groundwater, but the seawater component lies much further away.

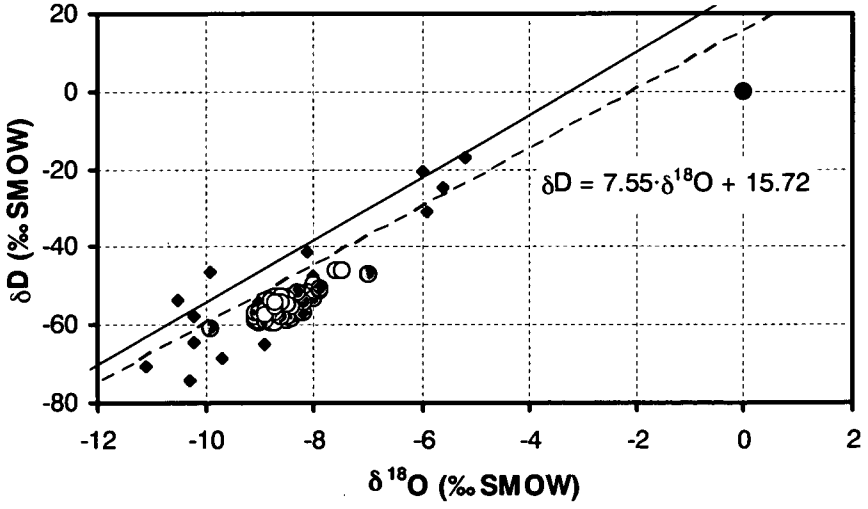

Figure 36. Stable isotopes plot. Blue diamonds are rainwater analyses. The black dot is the seawater composition and coloured circles are groundwater samples from the Tono area. The dashed line with a corresponding equation is the regression of the rain water samples and the solid line is the relationship for Japanese meteoric water (Sheppard, 1986).

Finally, Figure 37 displays the available bromide / chloride analyses. The highly linear regression coefficient points to a common origin for the salinity of all samples. For comparison with the conjectured origin of these conservative components, we plot the dilution line of seawater, which results from proportional dilution of seawater with chloride and bromide contents of 19,350 and 67 ppm respectively (Drever, 1997). The difference between these lines - seawater dilution line and samples' correlation line - is further discussed.

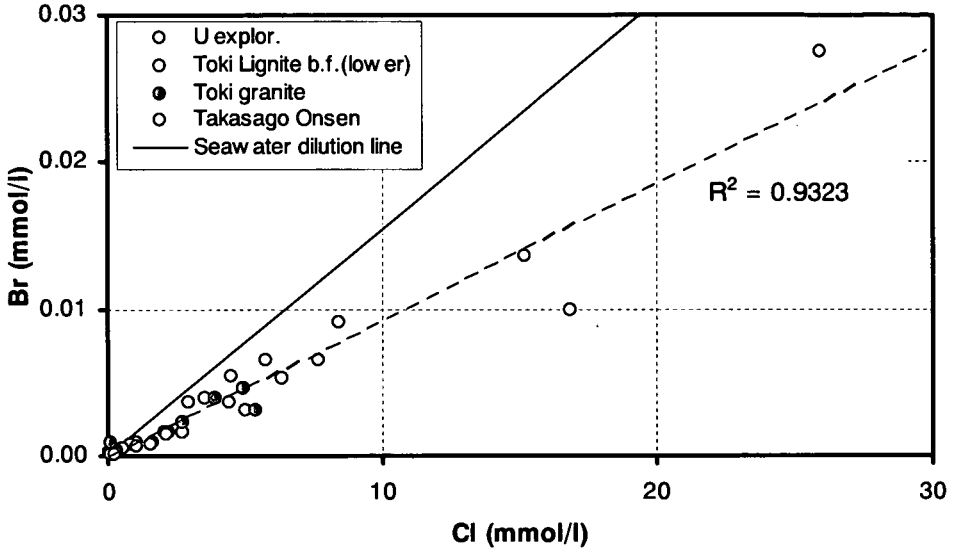

Figure 37. Chloride vs. bromide plot. The dashed line is the regression line for all available samples, whereas the continuous line represents seawater dilution.

Interpretative salinity contour lines are presented in Figure 39, together with some additional geological and hydraulic information.

8.3 Potential sources of groundwater salinity

The presence of salty water in the Tono area is indicated by samples taken from selected boreholes. Furthermore, anomalies in salt content are also displayed by a hot 'spring' in the area, in which the water is supplied by a deep borehole. The origin of water with such a composition is suggested to be:

- Residual seawater with a composition modified by water-rock interactions.
- Water rock interaction in an area of small water renovation close to a discharge zone (Toki river).
- Magmatic origin.

The first hypothesis is partially supported by carbon and oxygen isotopic data from calcite fracture fillings. While these data have not been used directly in the present interpretation, it is likely that during Miocene times, seawater intruded the Toki granite. However, the present samples indicate that the groundwater composition clearly departs from that of a water of marine origin. That is, if marine water is present, both the chloride/bromide plot and the stable isotopes would indicate it to be the case. In fact, Figure 36 and Figure 37 show that groundwater samples displaying a relatively high salinity do not have a clear link with present seawater composition, but this hypothesis deserves further consideration.

The second hypothesis can hardly explain the relatively high salinity observed. It is difficult to propose a mass balance in a system that by simple water – mineral weathering could explain chloride contents as high as determined in DH-12. Favouring this hypothesis however, is the fact that residence times might be long, since it is a discharge area close to a low groundwater renovation zone.

The third hypothesis is favoured by the fact that several hot springs exist in the area –at least seven spas are located in an area smaller than 10 x 10 km, which is the scale of the domain of some hydrogeological models-. It is well known that during magmatic crystallisation at depth high-salinity fluids are formed by the so-called secondary boiling process (Burnham & Ohmoto, 1980; Burnham, 1997). These brines usually stay in the upper part of the intrusive body and rarely migrate from this point due to their high density (Giggenbach, 1995; Roedder, 1984; Sasaki et al., 1998). Such fluids may become mixed and diluted by fresh water (Henley et al., 1984; Giggenbach, 1995, 1997; Mahon et al., 2000; Evans et al., 2002), which topographical driving forces cause to circulate down to depths of generally less than 1 km. Deeper than this threshold, topography or gravity driven flow may become negligible against density or compaction driven effects. Such dilution of magmatic waters, which leads to an increased salinity and temperature of meteoric waters, has also been observed in other areas of Japan (Shinohara et al., 1993; Sturchio et al., 1996).

A fourth explanation combines the most plausible hypotheses. In this case, observed salinities are mixtures of different proportions of salinity of different origin. Checking all the hypotheses in a quantitative manner falls beyond the scope of this project. Instead, the following sections are devoted to verifying or rejecting the first hypothesis, a potential ocean water origin for salinities detected in the Tono area.

9 Modelling of salinity flushing

This section deals with the performance of the models aimed at simulating the flushing of seawater from the domain of interest. The tasks progress from defining the objectives and approaches to the models produced: from 3D regional scale (some 35 x 35 x 10 km) groundwater flow to 2D local (9 x 3 km) variable density groundwater flow and solute transport models. The results are compared with existing data when available, and discussed in the context of the project and with the existing geochemical information presented in Section 8. Sensitivity analyses are also performed and discussed.

9.1 Objectives

The objective of this modelling exercise is to provide quantitative evidence of the likelihood that current salinity detected in the boreholes of the MIU site and surrounding areas, could or could not have a seawater origin.

9.2 Approach: from regional to local scale

We attempt to model the impact of the regression of ocean water that once covered the Tono area and the NCS during the Tertiary period. To do so, the uplift of the modelled area, the variable position of the coast line and consequently, the variable recharge rate over geological time needed to be considered. A consistent model that accounts for these processes needs to

incorporate realistic data on their values and variability and also, the modelled domain should extend from the present coast position to the MIU site and surrounding areas. This certainly would have been a challenging activity, and approaches should have followed those that have been employed to simulate groundwater flow in evolving basins (Mailloux et al., 1999; Wieck et al., 1995; Toupin et al., 1997 among others), where the natural boundary conditions can be changed according to known geological processes. However, it should be kept in mind that the target salinity samples are located in the sedimentary cover above the Toki granite and in the Toki granite itself. Therefore, such an extended model domain is simply not suitable for our purposes.

Hence a more restricted model around the area of interest is preferred, and the effects of the important processes mentioned above are taken into account in a lumped manner in the sensitivity analyses.

The restricted model in the area of interest is depicted in Figure 38. Such an area is considered suitable since it contains the main natural hydrogeological boundaries that currently affect the groundwater flow pattern in the vicinity of the NCS. At this point it should be noted that the available head values for the project (from files Hydraulic_test_DH.xls and Head_2.xls provided by the client) have been displayed in a cross section to gain some knowledge of the natural groundwater flow trends in the area. However, no clear trends are visible (Figure 39). Hence, we opted for a homogeneous domain, with flow boundaries far enough from the NCS site that they do not have a huge impact on the calculated values. This model was primarily used to define the local boundary conditions for groundwater flow.

A second, more restricted 3D model domain was selected in the vicinity of the NCS site (Figure 38) with the flow boundaries and initial conditions extracted from the regional model. Both models were performed at steady-state. The second model was more refined, and contained relevant information such as the sedimentary layers and the Tsukiyoshi fault. Also, the hydraulic conductivity of the granite and the sedimentary layers was considered to be anisotropic.

Despite the possibility of the code to cope with the selected model domain in 3D, in fact the problem could easily be represented in 2D. The advantages of such simplification are mainly connected with mesh definition (it can be more refined) and also of a computational nature.

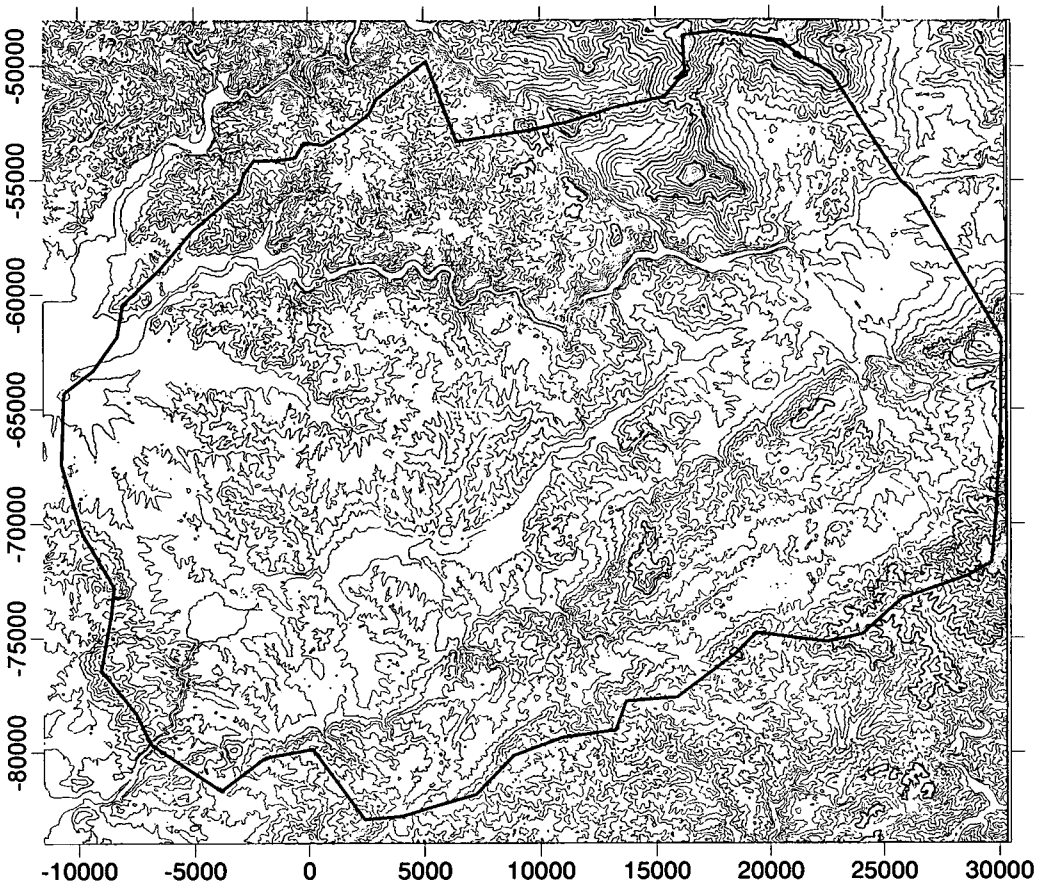

Figure 38. Selected model domain for the regional flow model in plan view (blue contour). In yellow, the local domain is also displayed.

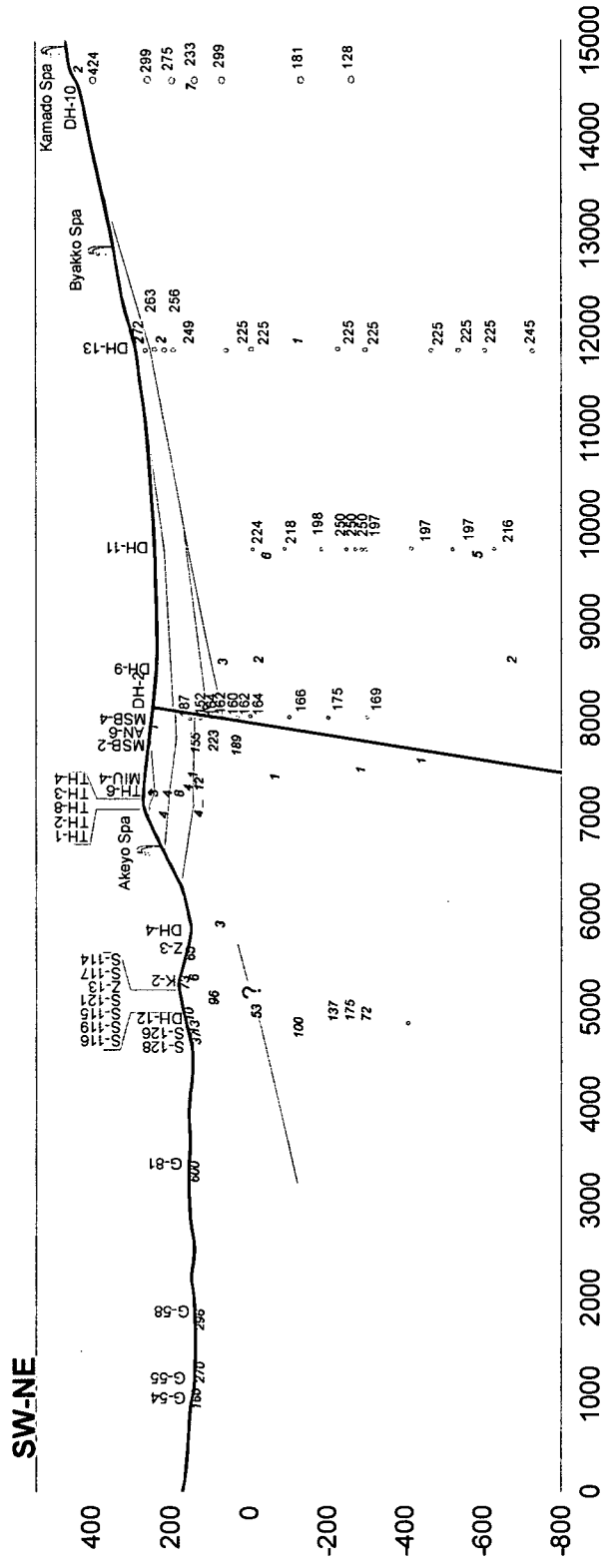

Figure 39. Cross section with head values and chloride content contour lines at selected boreholes.

9.3 Regional flow model

9.3.1 Conceptual model

The conceptual understanding of the model developed at a regional scale, which is based on scarce hard data with which to constrain model zones and parameters, is quite a simplification of reality. Hence, we opted for a fully saturated homogeneous and isotropic domain, where recharge occurs on the top with values according to data provided by the client (file balance_moni.xls) and discharges in naturally occurring discharge zones (present rivers). It is noted that from now on the boundary conditions as well as the models' parameters are kept constant through each simulation performed –they do not vary during one simulation-, and they are consistent with currently measured or estimated values. It is likely that such conditions, especially the boundaries, have changed during geological times. However, this is not explicitly considered in the calculations.

9.3.2 Domain and dimensions

Figure 38 shows the domain of interest for the regional model in plan view. It is worth noticing that it extends from Mt. Kasagi to the most important rivers, since they are considered to be important zones of recharge and discharge respectively. In addition, Mt. Kasagi exerts a control over the head distribution as far as the NCS. The site falls between the two main rivers of the area, but in the Toki river basin. Hence it is important to constrain the model in order to obtain local boundary conditions that are as realistic as possible.

The initially discussed dimensions (35 x 35 km in plan view) have finally turned out into 40 x 30 km, which is suitable for our purposes.

While the limits in plan view are supported by hydrogeological evidence, the bottom boundary is relatively arbitrary. Given that the depth of interest is restricted to the upper 1000 m, we opted for an extension down to 10 km. Hence, the modelled domain has an approximate volume of 12000 km^3.

9.3.3 Mesh

The regional groundwater flow model has been solved by the finite element (FE) method. Hence, a 2D mesh was created and refined to conform to the zones of interest, and was extended to depth, forming prisms in layers of variable thickness. The GMS v3.1 package (EMRL, 2001) has been used to create the mesh and the model has been solved with the code FEMWATER v3.0 (Lin et al., 2001).

Figure 40 shows the 2D mesh used with the local scale area of interest around the highlighted NCS. It should be noted that the extreme refinement in the centre results in more exact values being calculated, which permits their export and solution with a transport code. Such a mesh contains explicit nodes that follow the Mt. Kasagi and Toki and Kiso rivers, and which are considered to be boundaries of the domain.

Figure 41 shows the extension of the 2D mesh to depth. Note that the height of the prisms increases with depth to permit a higher definition close to the area of interest.

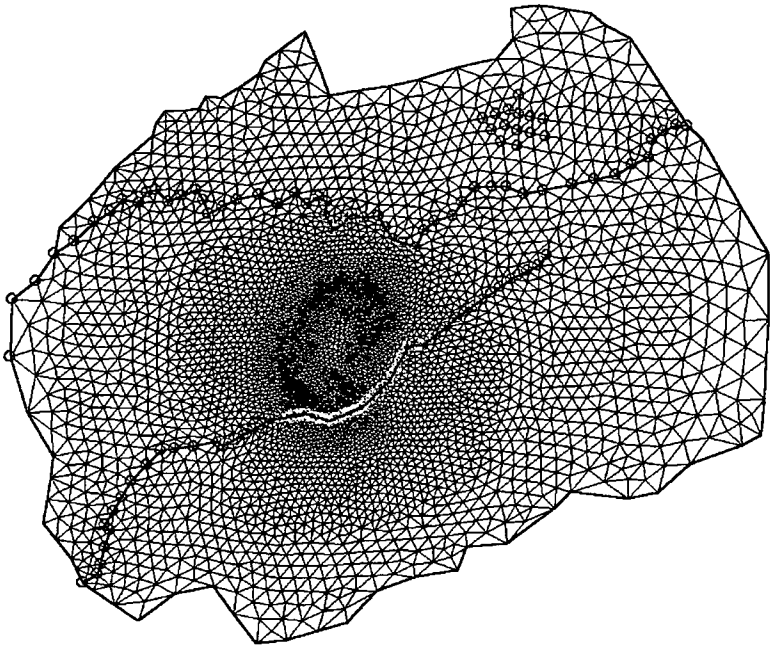

Figure 40. Plan view of the 3D finite element mesh used for the regional modelling (40 x 30 km) including Mt. Kasagi and the main rivers used as head boundary conditions (red circles). Note the refinement around the NCS.

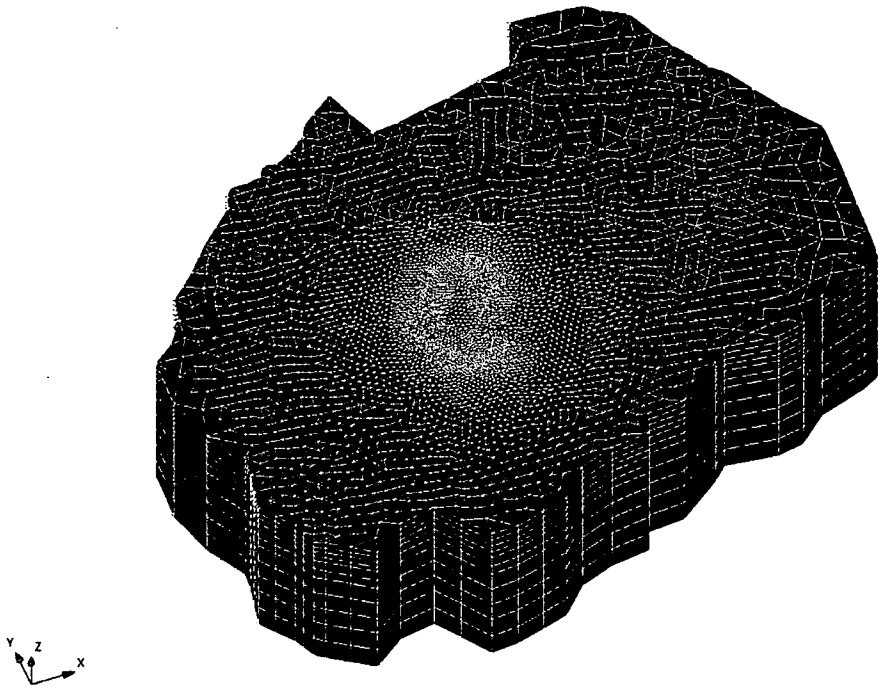

Figure 41. 3D mesh-of the regional-model (30x40x10 km). Note that the model is homogeneous.

9.3.4 Boundary conditions

The external boundary conditions of the domain have been taken to be prescribed flows at most of the nodes. Given that the domain satisfies the watershed divisions, this flow is nil at the lateral nodes. The external nodes that correspond to the Kiso and Toki river basins, have been assigned prescribed head values equal to 10 m below the corresponding elevation. The distance from these nodes to the NCS prevents major effects due to the arbitrary choice of the value. Nodes of the bottom face are also of prescribed flow, which are equal to zero. The nodes of the top face have been assigned a prescribed flow equal to the recharge (initially 250 mmy^{-1}), exceptions being made at the Kiso and Toki river nodes, which are of prescribed head, equal to the elevation. It should be noted that to permit mt. Kasagi to control the flow in the area, few nodes have been assigned prescribed heads equal to 10 m below the corresponding elevation.

9.3.5 Parameters

As mentioned in the conceptual model, the block has been considered as homogeneous and isotropic. Thus, the selected initial hydraulic conductivity falls in the range of values provided by the client. This value was $5.787 \cdot 10^{-6}$ ms^{-1}.

9.3.6 Results

Figure 42 and Figure 43 show the head results after some calibration on the hydraulic conductivity and recharge values. They have been finally selected as $5 \cdot 10^{-2}$ md^{-1} (5.787×10^{-7} ms^{-1}) and 125 mmy^{-1} (3.96×10^{-9} ms^{-1}) respectively and remained unchanged. Figure 44 shows the computed vs. measured head values of some key boreholes in the area. In spite of some values departing notably from the measurements, there is a remarkable correspondence for a such a simplistic model (homogeneous and isotropic), especially in the boreholes near the NCS (DH-9 and DH-11). This provides confidence in the initial values used for the local models as well as the boundary conditions.

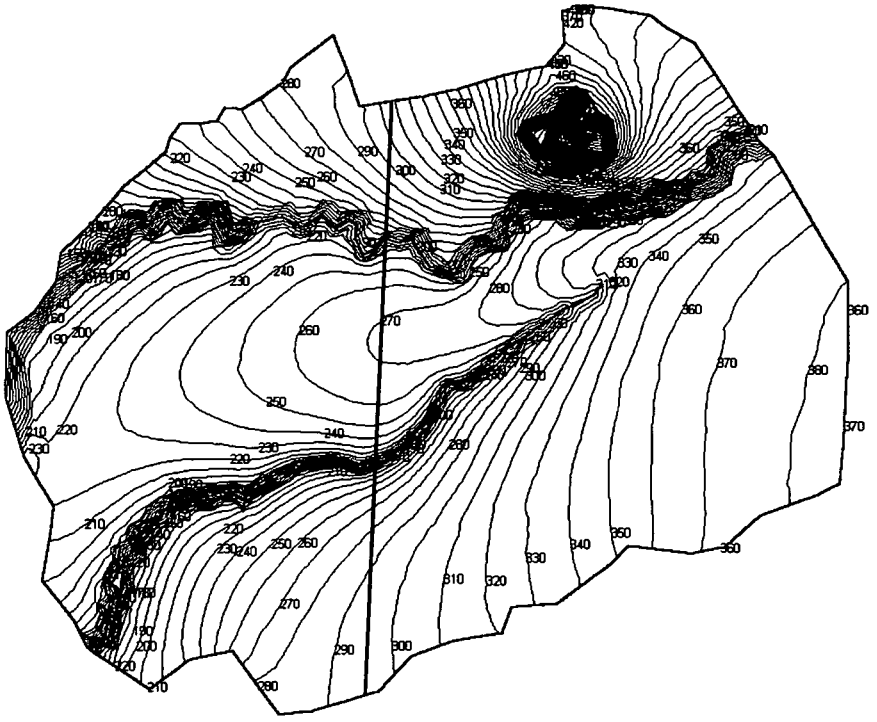

Figure 42. Head contour map of the regional flow model. The line depicts the position of the cross section shown in Figure 43.

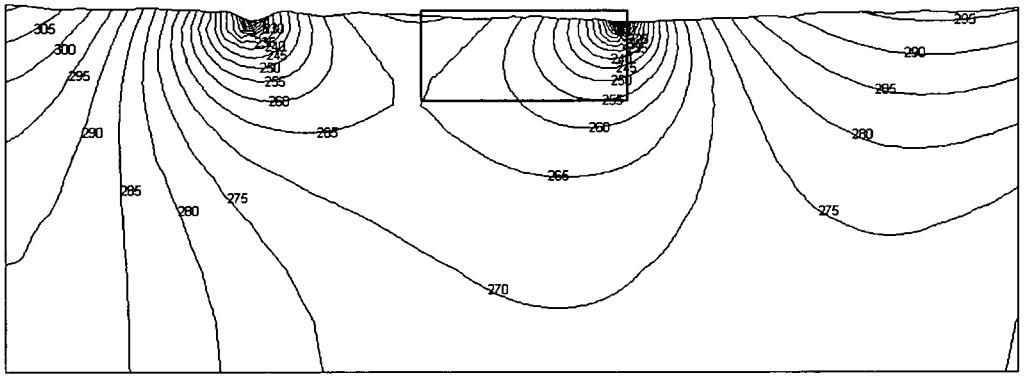

Figure 43. Steady piezometric head computed for the regional model (for a Toki River-transversing cross-section). The rectangle shows the area of interest in the local model.

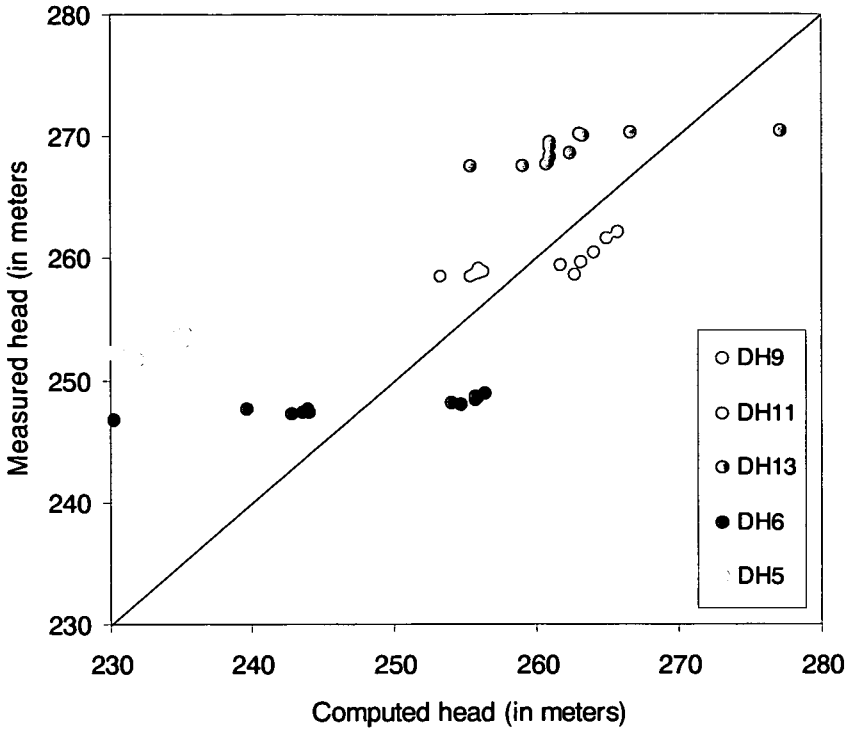

Figure 44. Computed vs. Measured head values (m.a.s.l.) of some of the relevant boreholes in the area. Note that in spite of some values departing by more than 20 m from the measured values, data from boreholes close to the NCS (DH-9 and DH-11) are reasonably reproduced.

9.4 Local 3D models

3D models at the local scale comprise groundwater flow-, variable density flow- and solute transport models. The first two have been performed to produce initial conditions for the last one. Due to the highly non-linear character of the problem and difference from conventional groundwater flow and solute transport models, variable density problems need to define the initial conditions more precisely, otherwise the risk of non-converging solutions is high.

9.4.1 Domain and dimensions

The domain of the local model has been carefully selected in order to obtain not only natural, but sensible boundary conditions for the variable density modelling. It should be noted for instance, that prescribed head boundaries are not suitable in variably density problems, if concentration is expected to change along them, since pressure will change during the simulation according to the change of concentration. Hence, based on the results of the regional flow model, all lateral and bottom faces have been selected to match a nil flow Base Case (BC). The domain extends from the watershed division between the Toki and Kiso rivers (North) to the Toki river (South). Lateral limits are coincident with flow lines. The bottom face is planar and located some 3 km below the topographic surface. The resulting block is of some 9 x 6 x 3 km.

9.4.2 Mesh

The code used to solve for the flow was FEMWATER while solute transport problems were solved using SUTRA (Voss, 1984). Both codes are based on the FE method. However, in contrast to FEMWATER, which was used for the regional flow model and for flow simulations, the elements in SUTRA need to be either quadrangular, in the cases of 2D problems, or hexahedrons in 3D. Hence, the mesh needed to be different to a locally refined version of the regional one, which used triangular prisms. At the local scale, the mesh was suitable to include zones of different parameter values from the granite ones, such as the Tsukiyoshi fault or the sedimentary layer. Figure 45 shows the block mesh, in which the fault and the sediments are displayed explicitly. The total number of elements and nodes is 7488 and 8778 respectively, which is a compromise imposed by the capabilities of the code and the duration of the runs. Such mesh dimensions did not permit, for example, a proper refinement at the discharge boundary in the Toki river. If the number of nodes was to have been maintained and a refinement included, then larger elements would have been needed far from such a boundary to compensate for the extra refinement. It should be noted, however, that the problems – parameters, mesh, stepping, etc. - should be posed so as to conform to the Courant (C) and Peclet (Pe) numbers:

$$Pe = \frac{|q|\Delta L}{\phi\, Dm + \alpha_L |q|} \tag{7}$$

where q stands for the Darcy flow, ΔL is the nodal distance in the flow direction, ϕ is porosity, Dm is the matrix diffusion term and αL is the longitudinal dispersion length. Usually, the term ϕ Dm can be neglected and the Peclet number is defined as.

$$Pe = \frac{\Delta L}{\alpha_L} \tag{8}$$

Traditionally, an upper bound is imposed to this ratio to ensure stability:

$$Pe = 2 \tag{9}$$

The Courant number is defined as:

$$C = \frac{|q|\Delta t}{\phi\, \Delta x} \tag{10}$$

where Δt is the time step selected for calculation (time interval) and Δx is the mesh size (similar to ΔL).

And the classical stability condition is:

$$C = 1 \tag{11}$$

Hence, large elements would need extra large dispersion coefficients to conform to the Peclet number, which in turn would have made transport by dispersion dominant over transport by advection or originating in density effects. Also, while the 2D solver of SUTRA permits the use of highly irregular meshes, the 3D solver does not permit the use of highly irregular quadrangular prisms. Thus, the mesh depicted in Figure 45 was the best solution to conform to the requirements of the project.

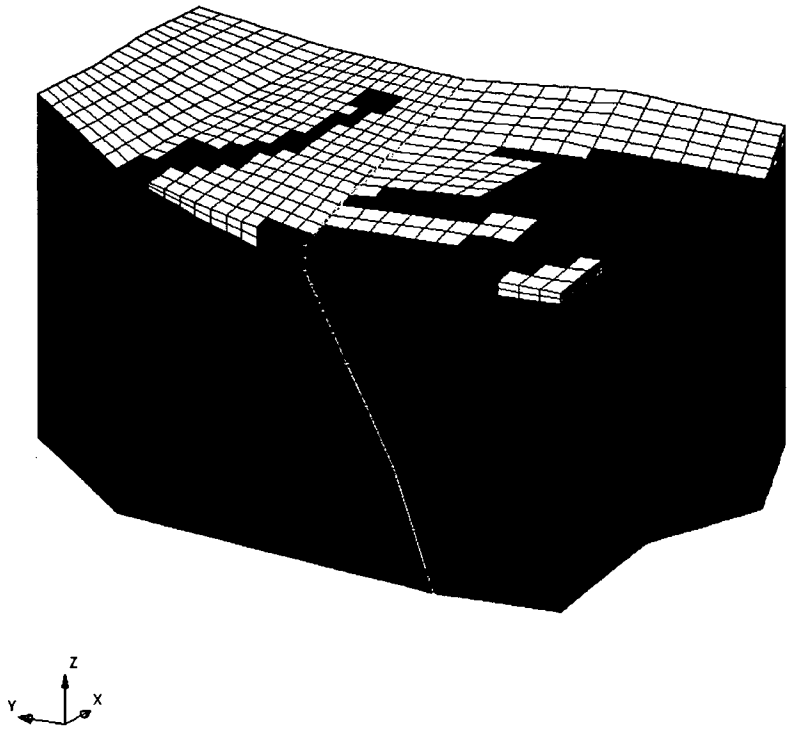

Figure 45. 3D mesh at local scale. Note the presence of the sedimentary layers on top, conforming to the mapped outcrops and the presence of the Tsukiyoshi fault. Also, the top altitudes correspond to the topography.

9.4.3 Boundary and initial conditions

Lateral and bottom faces were defined to have prescribed flows equal to zero. The reason was the resulting head distribution after regional simulations. Water entered into the domain through the top face with a prescribed flow value of 12.5 mmy^{-1} (recharge).

The recharge value provided by the client was initially 250 mmy^{-1}. We contended that such a value was very high for the present precipitation occurring in the area, which is 650 to 700 mmy^{-1}. Hence this value was reduced by a factor of half. It is not likely, however, that such water enters into the whole rock formation; rather, most of the infiltrated water in granite environments flows through the upper, weathered rock layer and only a very small proportion enters into the deeper rock mass (Carrera et al., 1996, 1997; Guimerà et al., 1997). Also, given the nature of the simulation, with constant recharge during the simulation, an averaged value, lower than the present one, was preferred. An order of magnitude lower was chosen because, although uncertain, it still permits the simulation results to be calibrated to lie within the range of measured head values, with the hydraulic parameters employed lying within the same orders of magnitude as the measured conductivities.

The recharge value (R_i) was distributed homogeneously and was proportional to the areas of the elements related to a given node, since SUTRA uses the recharge condition as a prescribed nodal flow:

$$R_i = 0.25 \cdot r \cdot \sum a_i \quad (12)$$

Where r is the recharge value [L/T] and a_i is the area of each element (irregular polygons) associated with the node i computed as follows:

$$a_i = abs\,[(x_o - x_1)\cdot(y_o - y_1) + (x_1 - x_2)\cdot(y_1 - y_2) + (x_2 - x_3)\cdot(y_2 - y_3) + (x_3 - x_o)\,x\,(y_3 - y_o)]\,/\,2 \quad (13)$$

x_i , y_i are the coordinates of node i (i =1,4 in adjacent order)

The concentration of dissolved solids in the recharge water was set to zero.

Nodes corresponding to the intersection of the lower end of the top face and the corresponding lateral boundary, the Toki river, were given prescribed head values, corresponding to the topographic elevation. Hence, water enters the domain through the top face and leaves the domain through this string of nodes.

Initial conditions for flow were those resulting from the regional flow simulations. In the transport simulations, the concentration was set equal to 20800 mgl^{-1} Cl^- which is the present day concentration of chloride in ocean waters. Given that transport simulations were of variably dependent density, initial pressure at each node for such simulations was corrected for density according to:

$$P_i = \rho \cdot g.h \quad (14)$$

The salt water density being 1027 gl^{-1}

9.4.4 Parameters

On the one hand, the parameter values were selected to be consistent with the regional model, which is the result of a given combination of recharge and a value which falls in the range of K values for the region. On the other hand, the local 3D model includes the top sedimentary layer and the Tsukiyoshi fault. Initially, the parameter values were those shown in Table 20.

Table 20. Initial hydraulic conductivity values for the 3D local model. Note that the K in the granite is reduced with respect to the regional model proportionally to the reduction in recharge.

Material	K_{xx} (ms^{-1})	K_{yy} (ms^{-1})	K_{zz} (ms^{-1})
Tsukiyoshi Fault	5.788×10^{-9}	5.788×10^{-9}	$5.788 \cdot 10^{-9}$
Sedimentary rock	$5.788 \cdot 10^{-8}$	5.788×10^{-8}	5.788×10^{-8}
Granite rock	7.810×10^{-7}	7.810×10^{-7}	7.810×10^{-7}

9.4.5 Results

Both the parameter values and the recharge BC were "tuned" (manually calibrated) to obtain a reasonable reproduction of the measured heads in borehole DH-9, which is a deep borehole

located in the center of the target area. Figure 46 shows the calculated vs. measured values and Table 21 the resulting values after calibration.

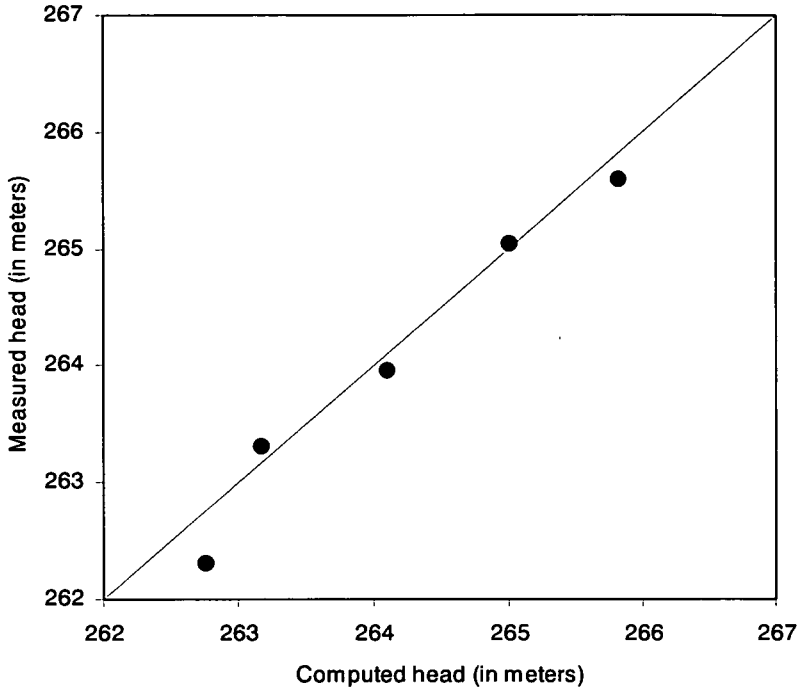

Figure 46. Calculated vs. measured values for borehole DH9.

Table 21. Initial and final parameter values of the 3D local model. Units in m and sec.

	Granite	Fault	Sediments
Kx ini	7.810×10^{-7}	5.788×10^{-9}	5.788×10^{-8}
Kx fin	7.810×10^{-8}	5.788×10^{-9}	2.890×10^{-8}
Ky ini	7.810×10^{-7}	5.788×10^{-9}	5.788×10^{-8}
Ky fin	5.670×10^{-8}	5.788×10^{-9}	2.890×10^{-8}
Kz ini	7.810×10^{-7}	5.788×10^{-9}	5.788×10^{-8}
Kz fin	7.810×10^{-8}	5.788×10^{-9}	5.780×10^{-9}
ϕ	1×10^{-2}	1×10^{-2}	2×10^{-1}
αL	1×10^{2}	1×10^{2}	1×10^{2}
αT	10	10	10

Despite the uncertainty of the K value for such a "homogeneous" model, which is highly conditioned by the recharge value, an outcome of this model is the convenience of using an anisotropic value of K, which points to a lower K value in the Y direction compared to the X

direction. This is coincident with the direction of the Tsukiyoshi fault. That the Kz is equally low, suggests that the K distribution with depth might spread over very low values.

Transport simulations with this model were performed over a simulation time of approximately 30000 years. Time discretisation, the variation of Δt within the simulation time, progresses from 0.1 years at the beginning, up to 500 years after 1000 years of simulation. Such progression in the time intervals is promoted to speed up the CPU times. It is important to note that such stepping is problem dependent.

Despite all precautions, the combination of large elements and reasonable dispersion coefficients and likely large Δt, lead to some numerical instability during the simulation. Such instabilities are evident at the end of the run. It is worth noticing that instabilities tend to speed up the rate of flushing. Having found it difficult to increase the size of the problem or its duration, this prompted us to explore the possibilities of the 2D simulations.

Despite the difficulties, it is worth noticing that the flushing of the domain is almost accomplished a long time before the end of the simulation (30000 years) and that a residual corner of salt water is left, due to the nature of the problem (the lowest renovation area).

9.5 Local 2D model with variable density

An outcome of the 3D local models with variable density was that the size of the problem required a much more refined mesh than that used and likely, the results were being affected by such restriction. Also, as depicted in the previous section, the 3D domain was selected in a way that could easily be reproduced in a 2D section (from the watershed division between rivers beyond the Toki river). Hence, a 2D section has been selected to model the salinity flushing at a local scale. The base case is described below and the sensitivity analyses are explained in the next section.

9.5.1 Domain and dimensions

The model domain is a cross section located in the vicinity of the NCS that is coincident with the regional groundwater flow direction returned by the regional and local 3D flow models. Figure 47 shows the position of the section in the overall context of the area of interest. It extends from surface to -3000 m.a.s.l vertically and from the watershed division between the Toki and Kiso rivers to the entire Toki river valley. Thus, the main discharge of the model domain is the Toki river and discharges from both sides: North and South. The longitudinal extension is of some 10 km.

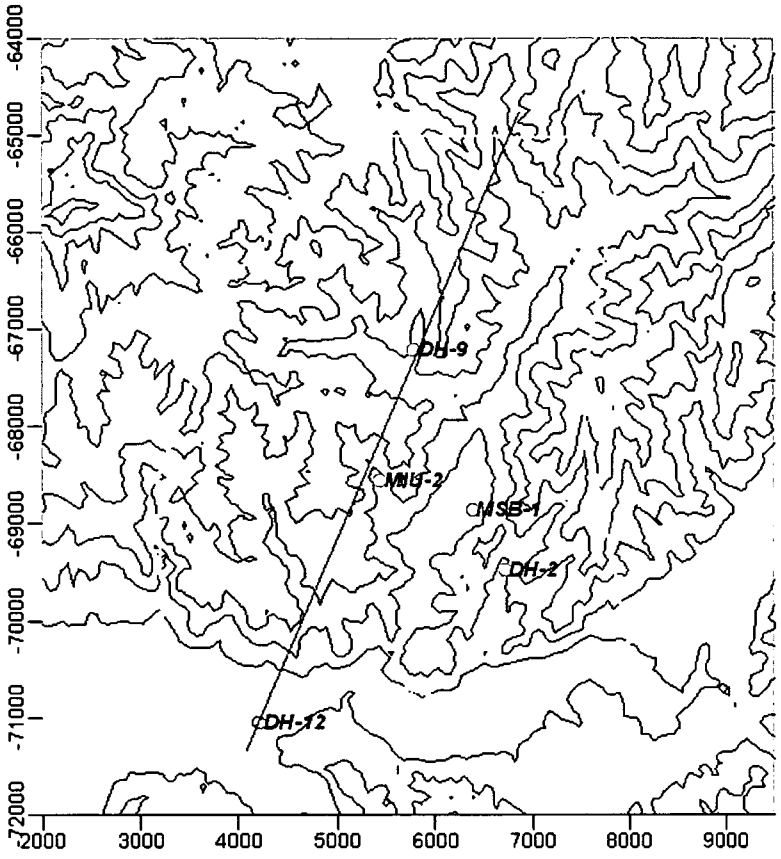

Figure 47. Location of the 2D section.

9.5.2 Mesh

The mesh has been structured to conform with the geometry of the sediment layers (upper 200 m when present) and with the presence of the Tsukiyoshi fault. The dimensions of the 2D domain permit a proper refinement close to the target areas with a reasonable problem size: the total number of elements and nodes is 3594 and 3785 respectively. The sedimentary cover is represented by 5 layers of elements, which will reproduce the flushing of the initial salinity in a more consistent manner than in the former 3D model. The mesh is depicted in Figure 48, along with the distributions of the different materials considered.

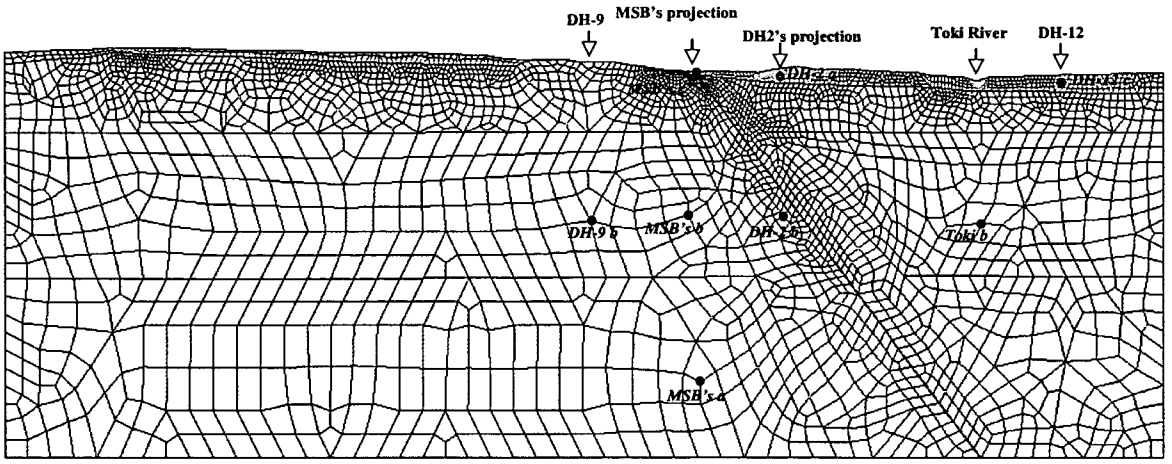

Figure 48. 2D mesh used for the variable density dependent problem. Note the location of the different materials and the position of "observation" points along the domain, which will be used to show the evolution of the salinity along the runs.

9.5.3 Boundary and initial conditions

Lateral and bottom boundary conditions are of prescribed flow equal to zero. The recharge occurs on top of the domain (the upper string of nodes) according to the equation (12) with the value discussed in Section 9.4.3 (12.5 mmy^{-1}). Concentration of chloride in recharge water is zero and the initial pressure conditions are provided by the steady state with pressures according to the fluid with corresponding ocean salinity.

9.5.4 Parameters

Initially, parameters selected for the base case were in agreement with those resulting from the local 3D models. No calibration was performed in this case, and porosity was assigned to be 0.01 in the granite and in the fault and 0.2 in the sedimentary cover (Table 22).

Table 22. Parameter values used for the 2D base case. Values in m and s.

	Granite	Fault	Sediments
Ky	5.670×10^{-8}	5.788×10^{-9}	2.890×10^{-8}
Kz	7.810×10^{-8}	5.788×10^{-9}	5.780×10^{-9}
ϕ	1×10^{-2}	1×10^{-2}	2×10^{-1}
αL	1×10^{2}	1×10^{2}	1×10^{2}
αT	10	10	10

9.5.5 Results

The results of this run are shown on a plot of relative concentration evolution with time at selected nodes (Figure 49) and some selected cross sections of concentration at different times during the simulation (Figure 50).

Considering the nature of the problem, the simulation times were initially selected to be 10^6 (1M) years, in order not to restrict the salinity flushing by the duration of the run. It is clear however, that complete flushing is achieved much earlier. In fact, with the exception of MSB-c, MSB-a and Toki, the observation points achieve 80% of flushing after 5000 years and complete flushing at 10000 years. MSB-c is located in an area of highly active flow and hence, achieves complete flushing much earlier than the rest of the domain. In contrast, the points located below the Toki river and MSB-a are in a slow flow-renovation area, and salinity is displaced more slowly than in the rest of the domain.

Figure 49 illustrates that those granitic zones in the upper part of the domain are flushed very effectively due to the combination of both high conductivity and low porosity. In contrast, the sedimentary cover is flushed more slowly than the granite, which is consistent with the parameters assigned to this material. The observation points situated 1000 m deep, however, achieve the same flushing rates as the sediments at a later stage. This is due to the fact that the fresh recharge water moves below the sediments following a tongue shape as shown in Figure 50, and the original salty groundwater in the deep granite is only replaced when almost complete flushing is achieved above it. As a matter of fact, both the results of the 3D model and the 2D cross sections are consistent and show the same buoyancy effect.

An additional effect that it is worth mentioning is that the flushing of the sediments is enhanced when fresh water is underneath them. The density difference between the "native" water of the sediments and the water recharging through the granite enhances the movement of the former, which in any case is mainly promoted by the recharge water.

It is also worth noticing that the presence of the Tsukiyoshi Fault, although relevant for the flow conditions, is not important for the flushing of the salinity, at least for very long time scales.

In general terms, it could be concluded that the results obtained from the 2D model are consistent with the conceptual model and it was justified to give priority to this model rather than the local 3D model.

A general result from this run is that in fact, with the restrictions of this model, complete flushing is achieved at depths of 1000 m in 10,000 years, regardless of the parameters or materials. If such boundary conditions and material parameters have prevailed for geological times, the present salinity would certainly not be consistent with a marine origin.

The next section further explores such a possibility. A sensitivity analysis was carried out and involved changing model parameters and boundary conditions (recharge).

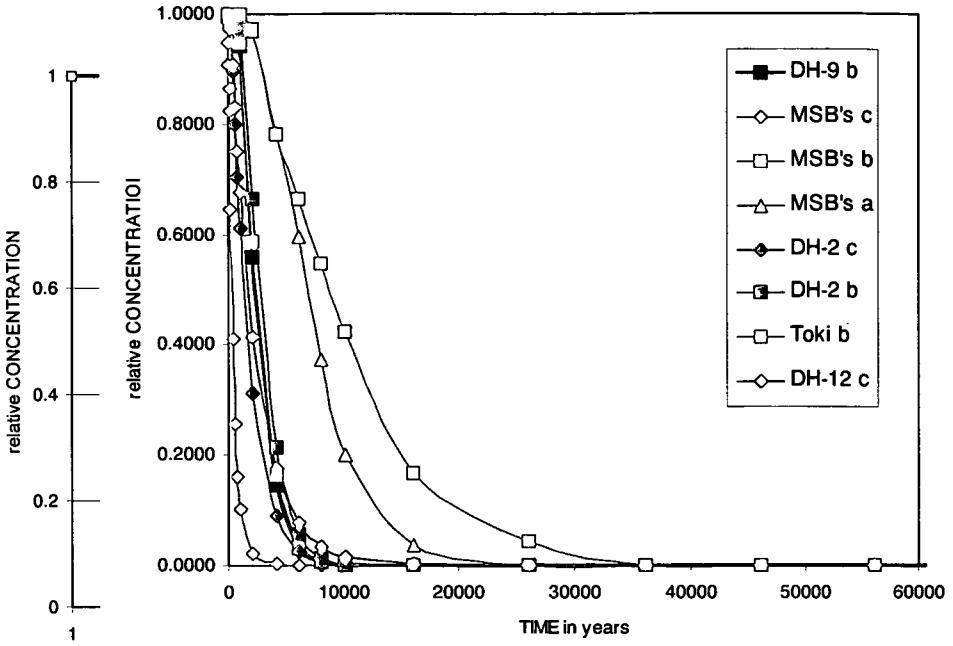

Figure 49. Concentration evolution within time of the selected observation nodes depicted in Figure 48.

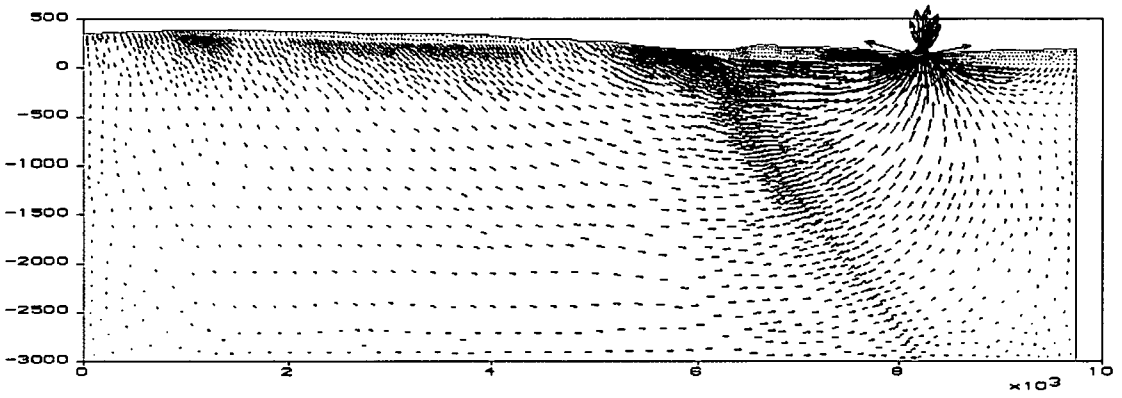

Velocity field at 1009 years.

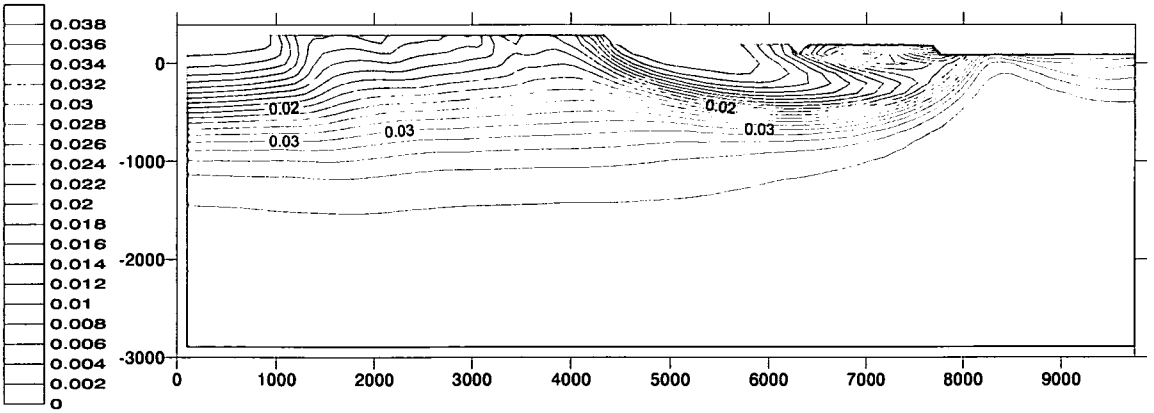

Salinity at t= 1009 years.

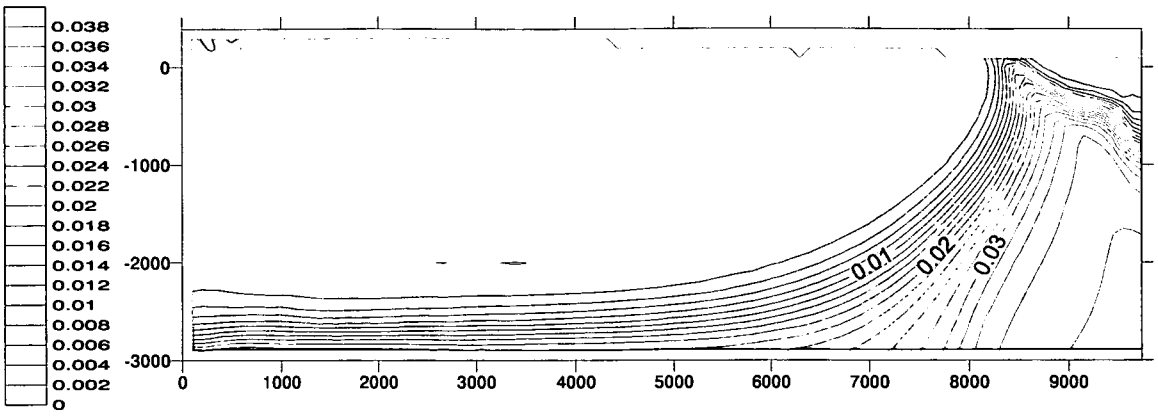

Salinity at t = 10109 years.

Figure 50. Concentration over the entire section at selected times. Note the tongue shape of the fresh recharge water underneath the sediments. Concentration in gl^{-1}.

9.6 2D sensitivity analyses

This section explores the response of the model to changes in fundamental parameters and boundary conditions. Given that the ocean regression and continental emersion is not explicitly modelled, conditions are given to impose flow velocities that are more slowly than the base case presented in section 3.5. It should be kept in mind though, that the recharge value of 12.5 mmy^{-1} which was used in the base case is uncertain.

9.6.1 Cases

Cases have been structured to test the influence of changing the main parameters used in the base case presented in the former section, 9.5. Table 23 shows the cases tested and the changes introduced

Table 23. Summary of the cases used in the sensitivity analyses

Case	Changes in hydraulic conductivity	Changes in recharge
6	= Base case	Base case x 0.1
7	= Base case	Base case x 10
8	Base case x 10	= Base case
9	Base case x 10	Base case x 0.1
10	Base case x 10	Base case x 10
11	Base case x 0.1	= Base case
12	Base case x 0.1	Base case x 0.1
13	Base case x 0.1	Base case x 10
14	Sensitivity to dispersion lengths	= Base case

9.6.2 Results

The results for each case presented in Table 23 are summarised below. Some of the cases did not converge or showed strong numerical instabilities, which prompted us to reduce the time stepping of the calculation, thus conforming to the Courant number (equation (10)). By doing so, the CPU times were increased, making the full run to times of geological significance prohibitive.

Case 6

This case illustrates the effect of reducing the recharge by an order of magnitude. Strong numerical instabilities are observed, which has been solved by reducing the time stepping (Δt) with respect to the original distribution by a factor of 100.

The four plots of Figure 51 show a behaviour that, while resembling the base case, have curves that are shifted to the right one order of magnitude (the flushing takes longer).

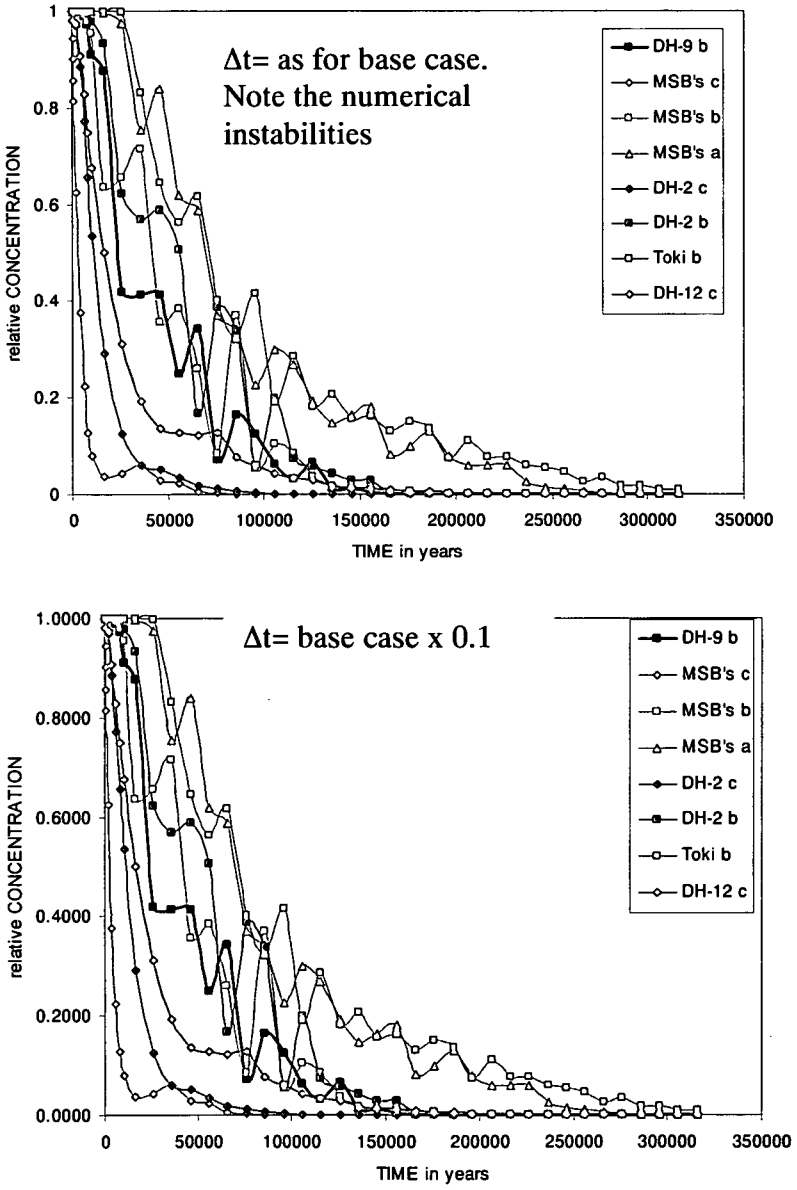

Figure 51. Breakthrough curves for the case 6 using four different sets of Δt.

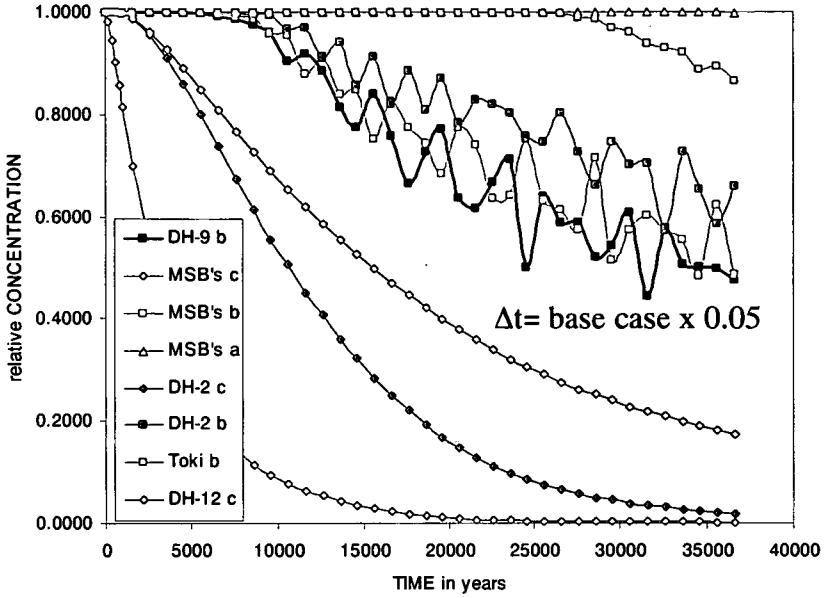

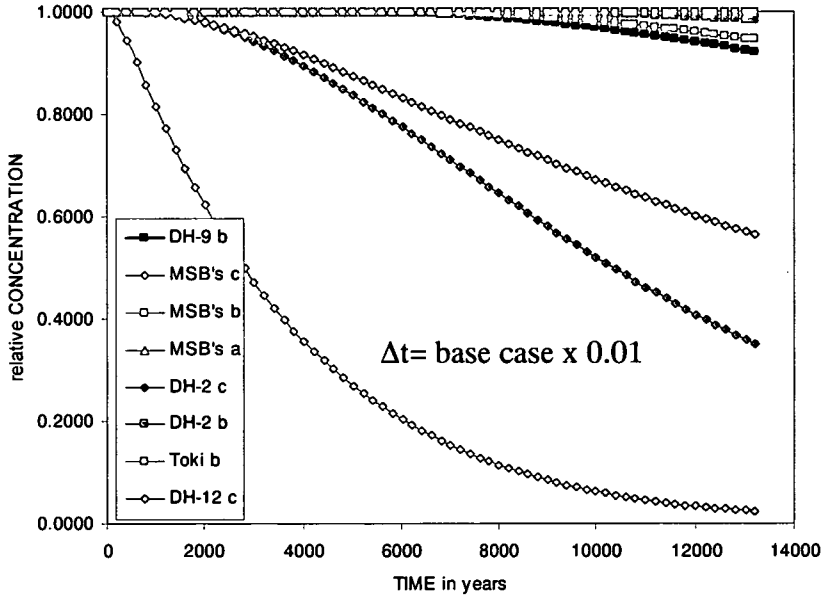

Figure 51. Continued.

Case 7

This case is opposite to the former, in that the recharge has been increased an order of magnitude with respect to the base case. Consequently, complete flushing is accomplished approximately 10 times earlier than in the reference case (Figure 52).

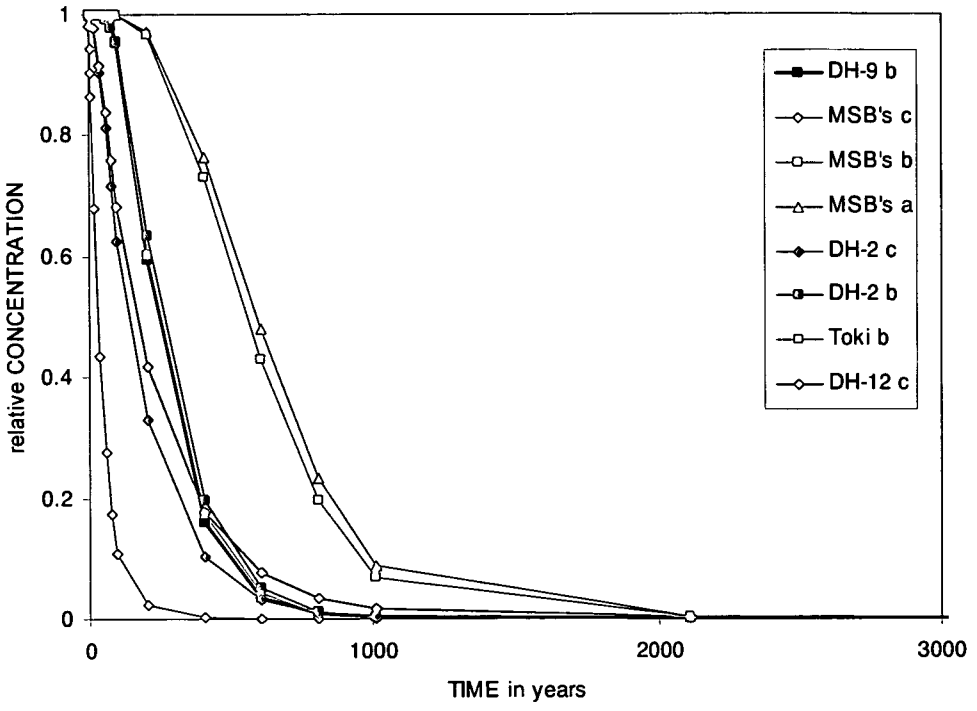

Figure 52. Breakthrough curves for the case 7.

Case 8

Hydraulic conductivities of the 3 different materials have been increased by an order of magnitude, while keeping the recharge as in the base case. Note that in spite of reducing the time stepping by a factor of 1000, a couple of points (perhaps 3, including MSB-b) show a behaviour that can be considered unstable (Figure 53, top). Note that the velocity distribution prevents complete renovation in the deepest part of the domain (point MSB a; Figure 53, bottom). We contend that this effect is caused by the increased hydraulic conductivity of the granite.

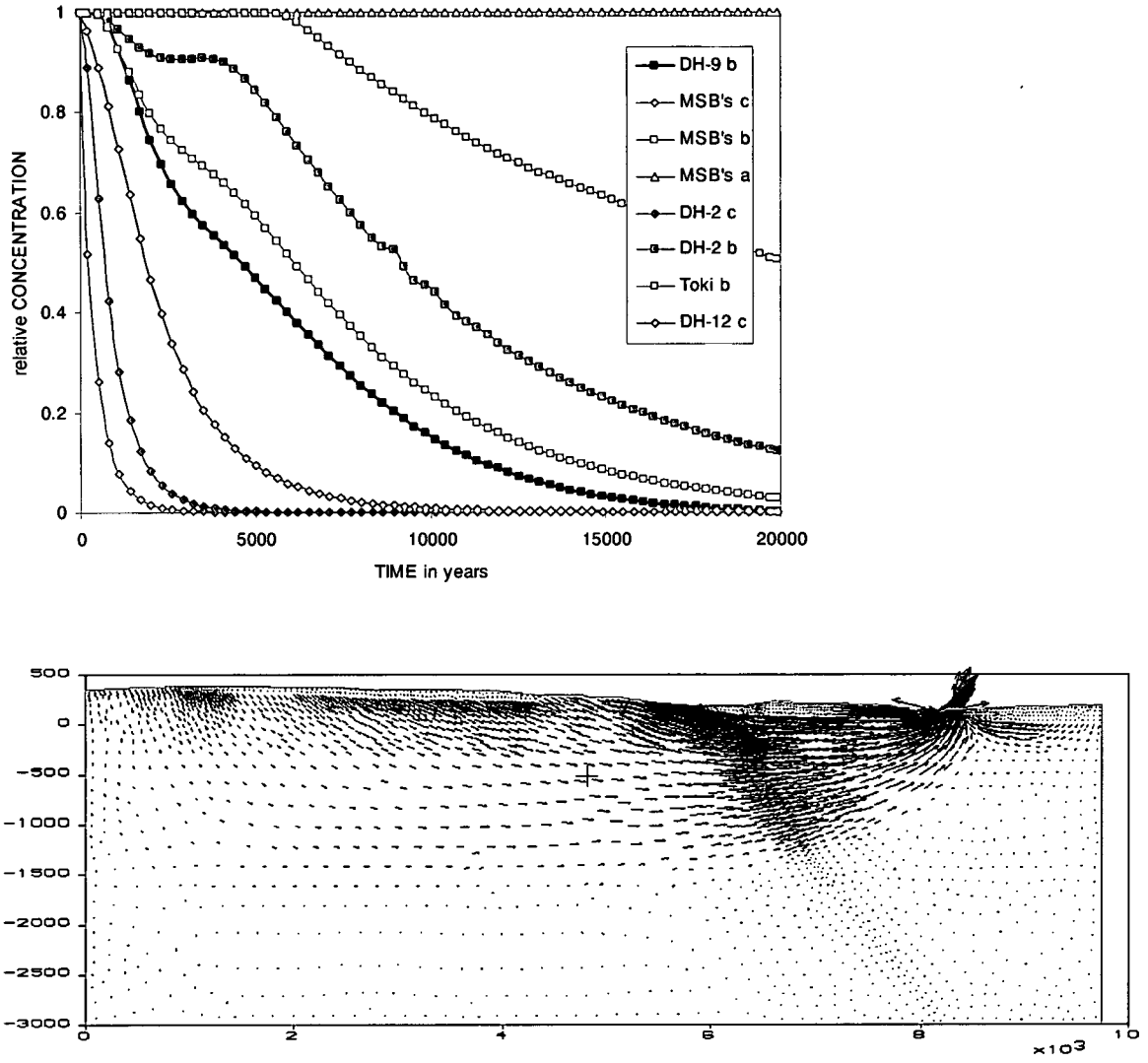

Figure 53. Breakthrough curves and groundwater velocity distribution for the case 8, where Δt= base case x 0.001.

Case 9

In this case, recharge was reduced and conductivity increased both by a factor of 10 with respect to the base case. It could be expected then, that flushing would take place at a similar rate. However, this is not the case. Rather, flushing takes longer, caused by the reduction in recharge (Figure 54).

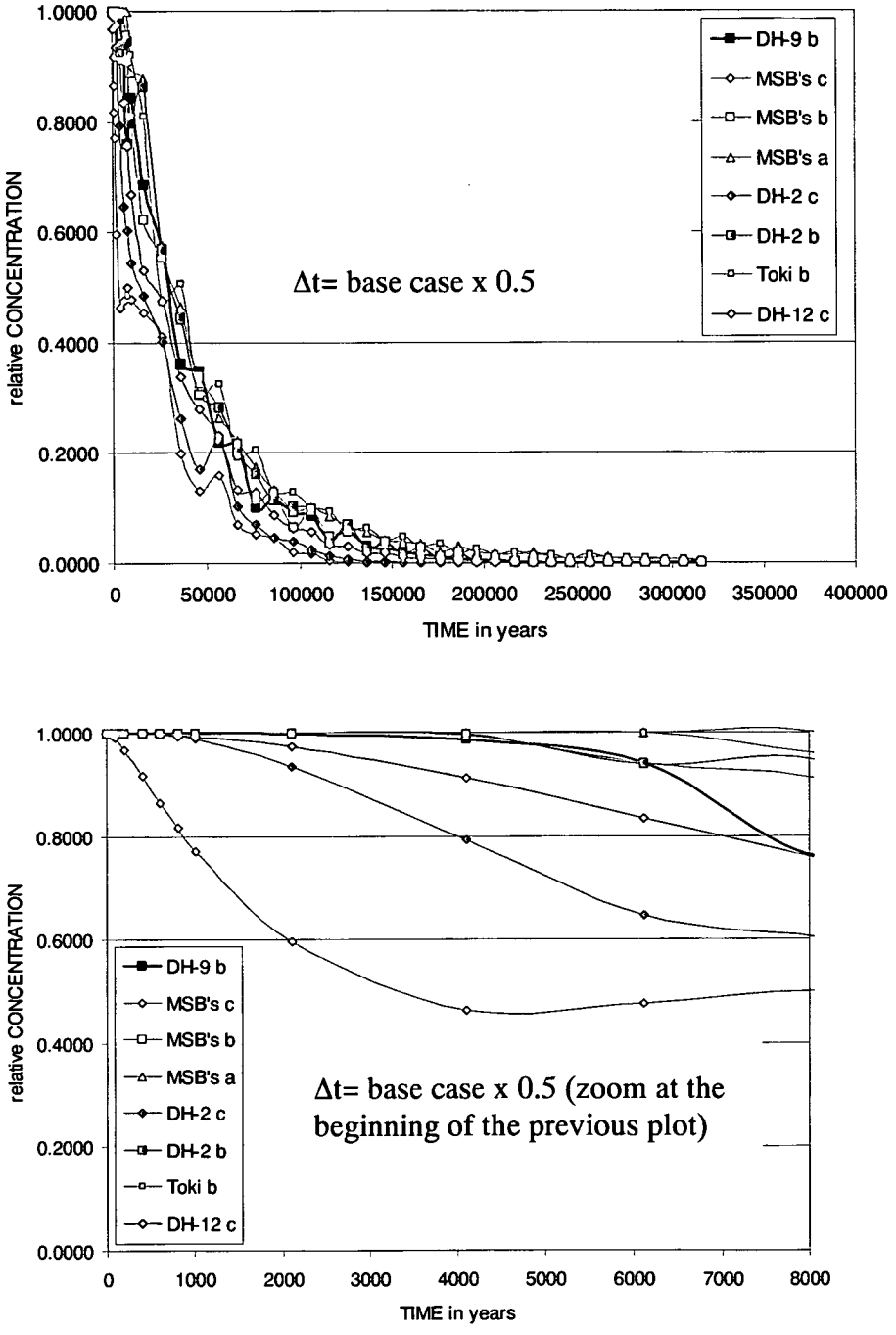

Figure 54. Breakthrough curves for the case 9, using three different Δt.

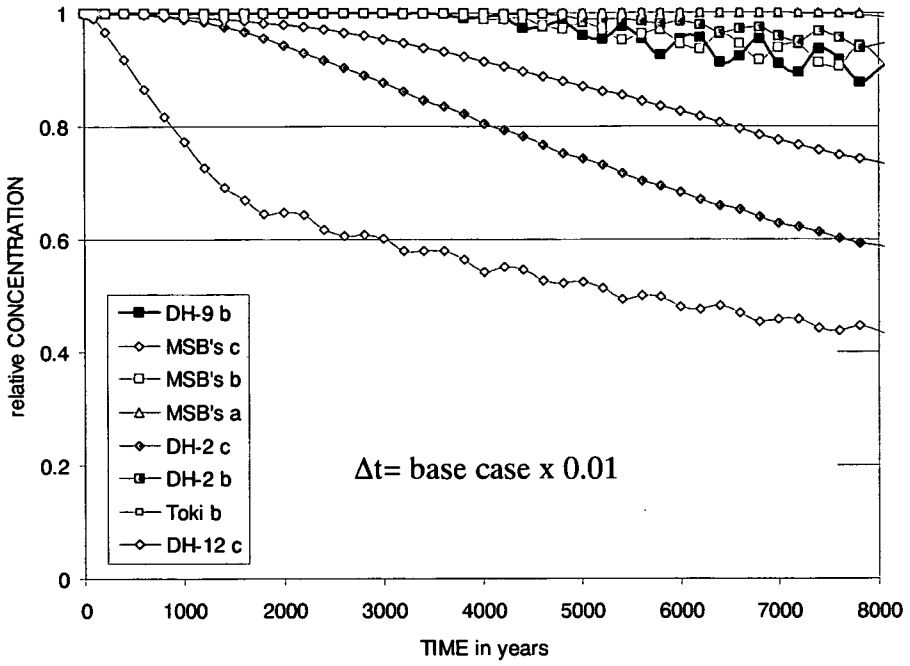

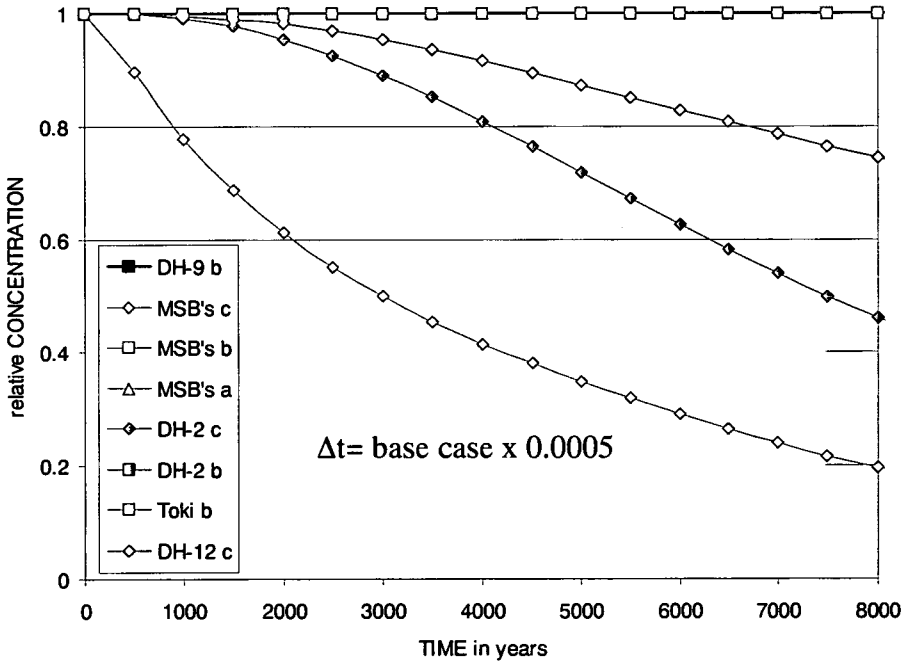

Figure 54. Continued.

Case 10

This case illustrates the effect of increasing both the hydraulic conductivity and the recharge by a factor of 10. While in general terms the flushing is speeded proportionally in time with respect to the base case, it is worth noticing that DH-12-c, one of the deepest points, displays a retarded flushing in the early part of the curve (Figure 55). This is a similar effect to the one observed in case 8, where the increased conductivity enhances the buoyancy effect of the recharge water, which is less dense than the salty water in the domain.

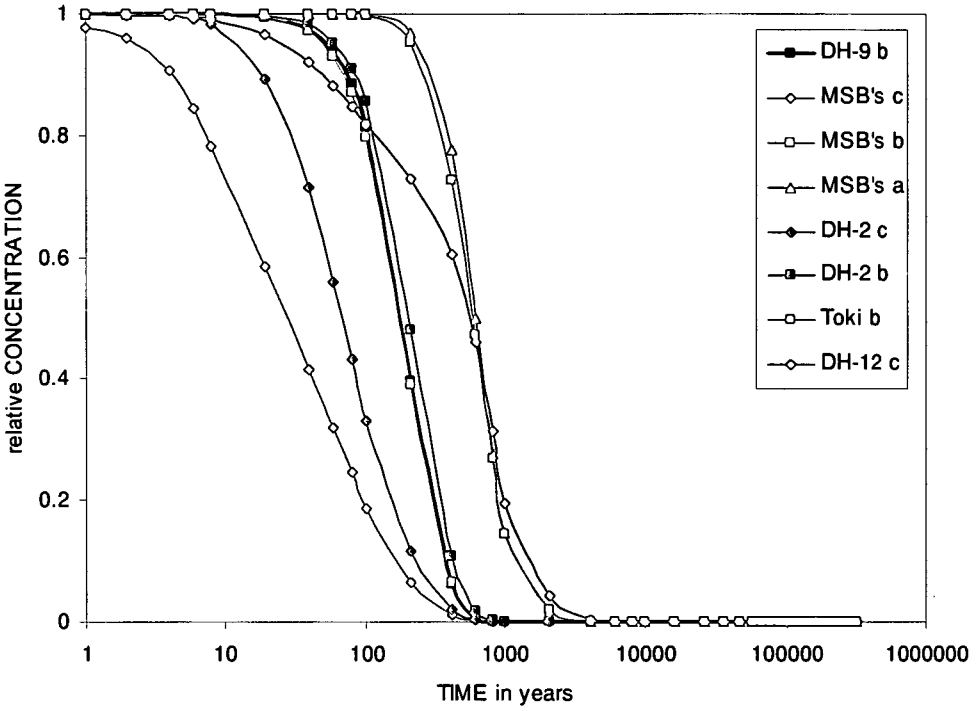

Figure 55. Breakthrough curves for the case 10.

Case 11

The same recharge rate has been maintained for this case, and the hydraulic conductivities have been reduced by a factor of 10. Note that the results are almost equal to the base case (Figure 56).

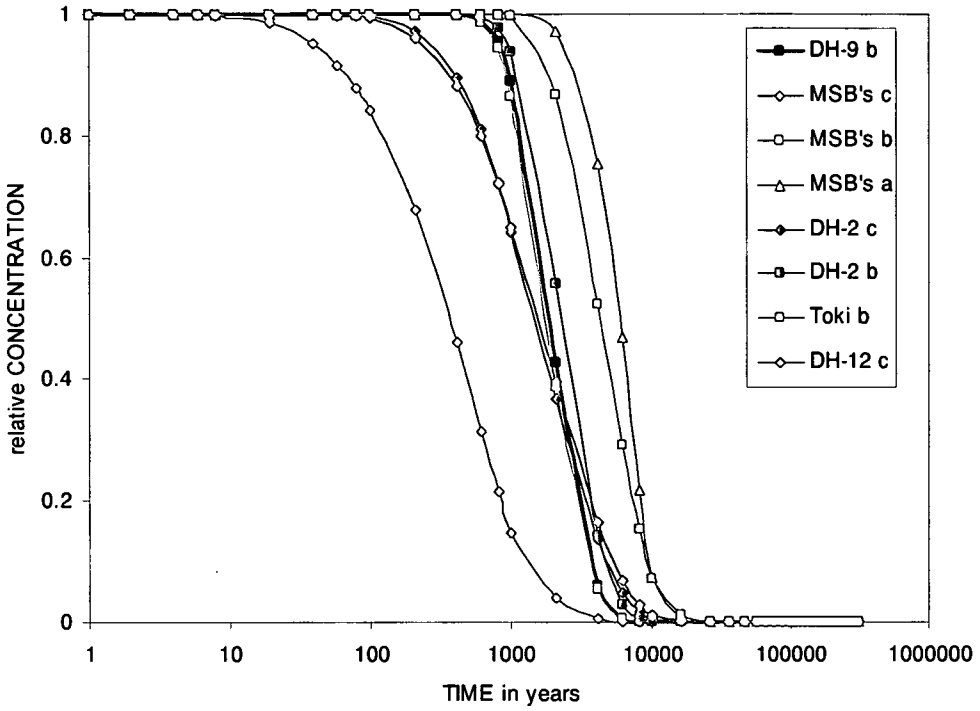

Figure 56. Breakthrough curves for the case 11.

Case 12

Both the recharge and conductivities have been reduced in this case. In accordance with the reduction of the recharge, and similar to other cases, curves are shifted to the right of the plot, since the effective flushing of the domain is retarded (Figure 57). Note that in this case, and in contrast to cases 8 and 10, no buoyancy effects are noted, since the low conductivity prevents more effective flushing in the upper part of the domain.

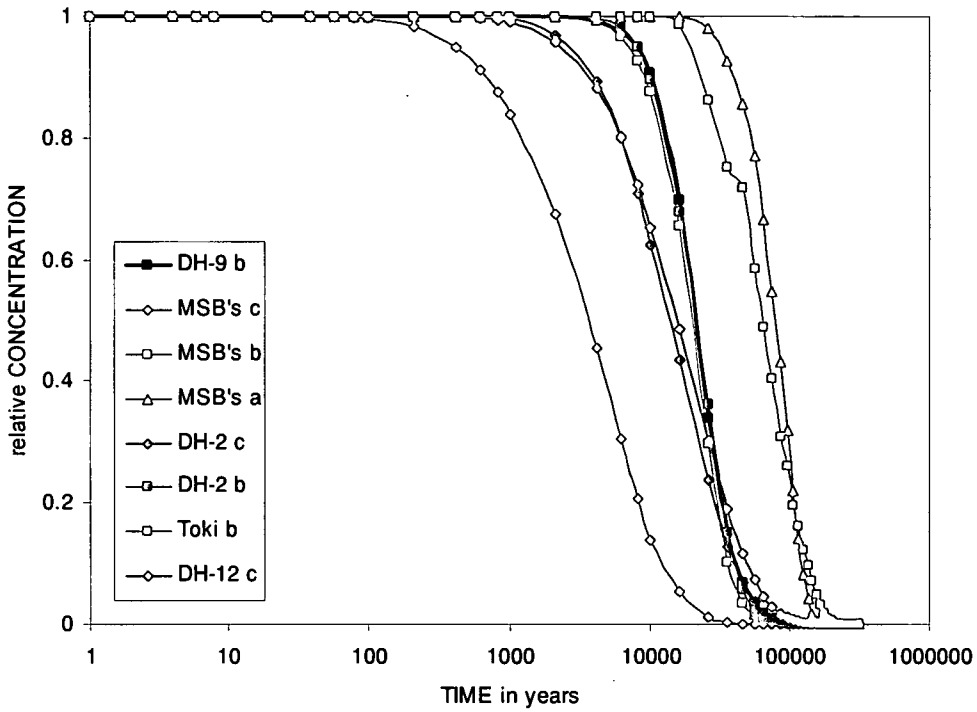

Figure 57. Breakthrough curves for the case 12.

Case 13

The result of this case resembles very much case 7, where recharge was increased and conductivity was maintained equal to the base case (Figure 58).

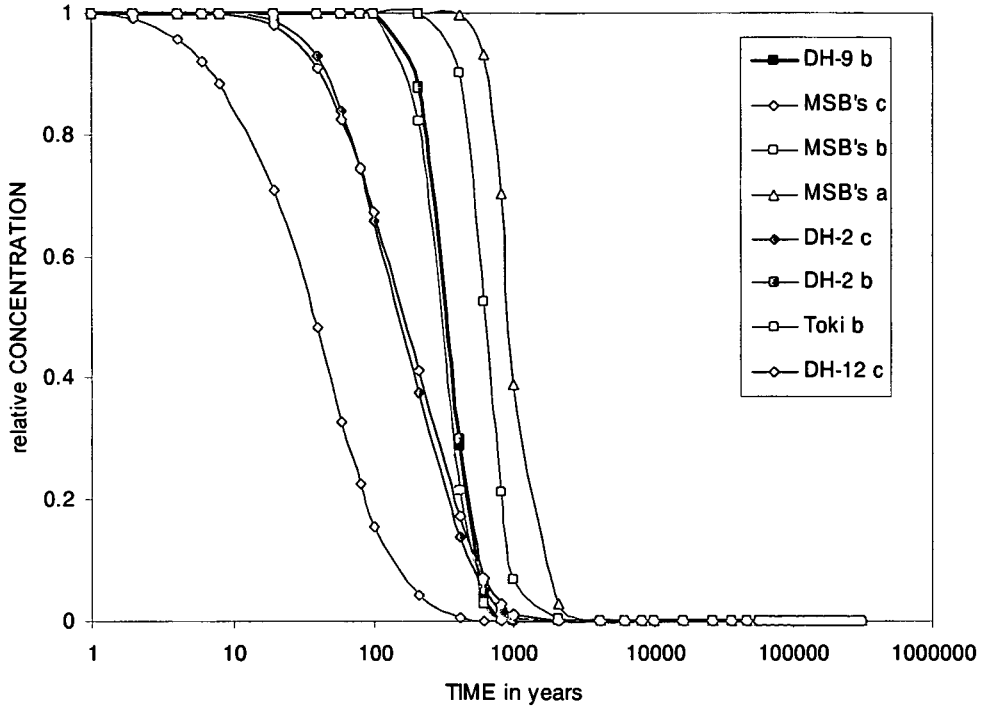

Figure 58. Breakthrough curves for the case 13.

Case 14 Sensitivity to dispersion lengths

Two additional runs under the name of case 14 have been performed to check the effect of the dispersion lengths on the calculations. The base case parameters and recharge have been maintained, while the values of the dispersion lengths have been increased by a factor of 1.5 (Figure 59) and reduced by a factor of 2 (Figure 60). No significant differences were observed at long time scales, although some numerical instabilities were observed when the values were reduced.

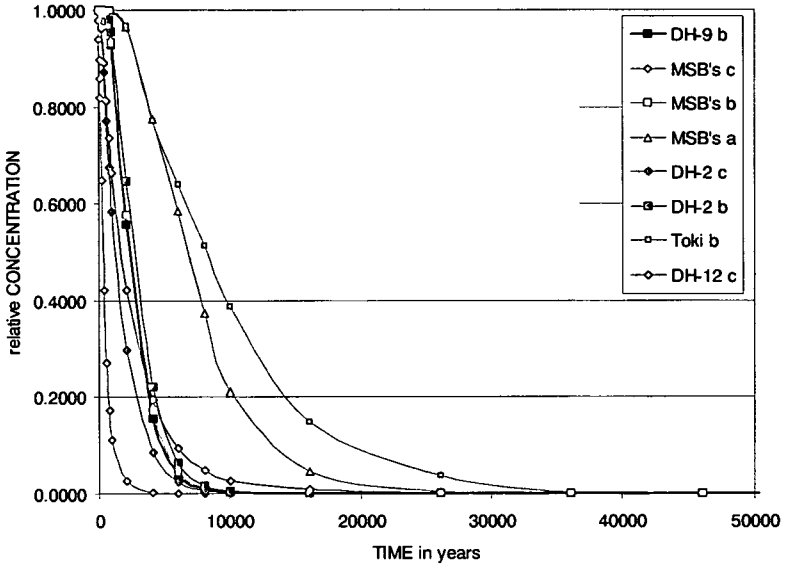

Figure 59. Breakthrough curves for the case 14 with αL = 150 m and αT = 15.

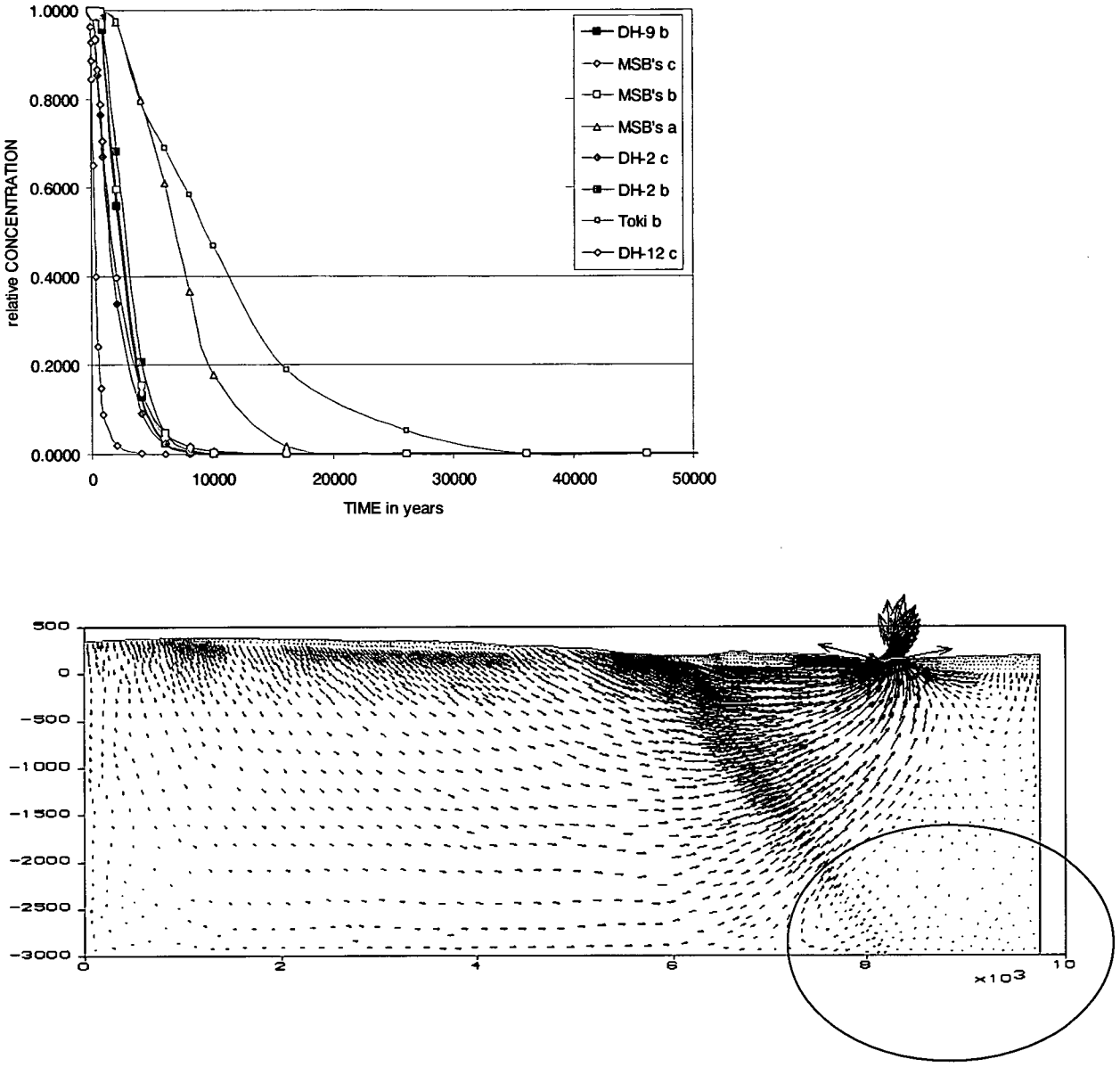

Figure 60. Breakthrough curves and velocity field for the case 14 with αL = 50 m and αT = 5. Note the change in direction of the velocity vectors.

10 Discussion of the models

The models performed present a set of common observations that are discussed below.

The model is very sensitive to the ingress of water on top, that is, to the recharge. The greater is the recharge, the more effectively flushed is the salinity. This has been highlighted in numerous cases of the sensitivity analysis, which is worth exploring in more detail in further models. Similarly, the model is also sensitive to the increase of the hydraulic conductivity of the granite, making evident the effect of buoyancy, since the recharged fresh water flows more effectively through the upper part of the domain. The model is not very sensitive to the increase of the hydraulic gradient when the conductivity of the granite is reduced.

The effect of the hydraulic conductivity distribution on the flushing is relevant though. Considering the granite as a block, if the conductivity gently decreases with depth, which is a common situation in this type of media, then higher salinities can be expected in the deepest parts of the domain than on top. While this origin of salinity has not been supported by the chemical data, this hypothesis can not be completely discarded.

Summing up all the cases, it can be concluded that in all of them complete flushing is achieved earlier than 500000 years. This is consistent with some geochemical observations presented in Section 8, and could also be consistent with some relict salinity in the deepest parts of the domain. However, while consistent with the conceptual understanding, it fails at matching the time scales proposed. In other words, the effective flushing is achieved much early than 1000000 years and hence the present salinity of the sedimentary layer still remains unexplained with the current model. Figure 61 helps to understand the range of possibilities explored in a location which is some 1000 m below the NCS.

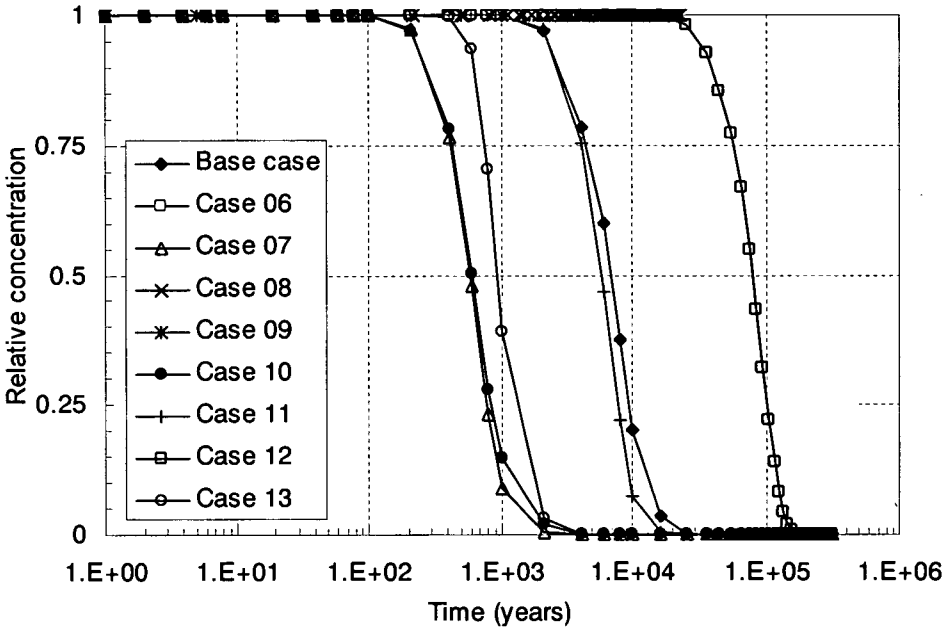

Figure 61. Summary of the runs for MSB_a observation point, 1000 m below surface of the NCS.

It could be contended, however, that the results are an artefact of the recharge distribution adopted. One could expect that if lower recharge rates are adopted for the sedimentary cover than for granite, then the salinity would remain for millions of years. In order to simulate this situation with the model, differences of several orders of magnitude between the recharge occurring on top of both formations should be adopted, which could be inconsistent with the natural understanding of hydrologic phenomena.

11 Conclusions from coupled models of salinity distributions

Several models attempting to simulate the groundwater salinity in the Tono area were developed. The scales of the models ranged from 30 x 40 x 10 km to 9 x 3 km, with different particular objectives.

The assessment of current geometry, geochemistry and hydrodynamic properties of the geological formations in Tono have made evident the presence of salty water at different concentrations depending on the borehole and depth, which origin is at present uncertain. One of the potential origins is relict salty water of Miocene age, when the sedimentary cover of the Toki granite was formed. In order to verify or falsify this hypothesis, the flushing of salty water has been simulated with a model of quite a simplistic nature. The boundary conditions were kept constant through the simulation, instead of varying them according to the recent geological history of the area.

Simulations of variable density groundwater flow and solute transport have been performed without geochemical interactions. In order to account for the likely variable distribution of recharge or hydrodynamic parameters with time, sensitivity analyses were performed to evaluate the significance of the most sensitive parameters of the model.

The conclusions of such a modelling exercise can be summarised as follows:

All cases performed show a complete flushing before simulation times of 500000 years, despite the fact that the recharge has been varied from 1.25 to 125 mmy^{-1}, and hydraulic conductivities over two orders of magnitude as well.

Dispersion lengths play a minor role and porosities were maintained during the simulations.

The model is very sensitive to recharge, and less to changes in hydraulic conductivity. Increasing or decreasing the recharge, changes the flushing regime proportionally. Instead, increasing the conductivity enhances buoyancy effects or preferential circulation on top of the domain. Decreasing conductivity causes little impact on the results.

In general terms, the conceptual understanding has been reproduced properly by the models, and the results show that a seawater origin of the salinity is very unlikely if the model assumptions are valid.

From a PA perspective, it is fundamental to set up a reliable geochemical model that it is consistent with the characterisation results and that integrates the PA hydrogeochemical models. The present understanding of the Tono area needs to enhance the understanding of the salinity, since it is unlikely that, after the few data reviewed and the modelling performed, its origin is relict seawater. The role of post magmatic events and origins must be carefully evaluated. This is important in terms of setting the proper conditions for geochemical stability of a potential repository.

It is fair to say that the model exercise was limited in scope and potential hence, the following recommendations should be given priority if future works are undertaken.

- The flushing of the sediments should be modelled at an appropriate scale.
- The ingress of water in the model should be changed during the simulation.
- To do so, a proper understanding of the changing rates of the boundary conditions is needed (based on an evaluation of recent geomorphology).
- Several alternative origins to salinity of seawater origin need to be considered, such as other origins of a geological nature, for example magmatic origins.
- The possibility that the salinity is a mixture of several components, each with a distinct origin, needs to be considered.

Part 3: Integrated evaluation of results from 1D, 2D and 3D coupled models

12 Approach to developing an integrated evaluation

Evidential Support Logic (ESL) is used to undertake an integrated evaluation of the results from the 1D, 2D and 3D modelling. The approach is to treat each model's output as a piece of evidence for or against the hypothesis that there is a self-consistent understanding of hydrogeology and geochemistry.

If the evaluated scenario, namely that the Tono area was initially saturated with seawater, which was then flushed under hydraulic conditions broadly similar to the present, then the present groundwater system should have certain hydrogeological and geochemical features. The approach is to evaluate to what extent the various codes can actually reproduce these conditions, indicating that the underlying understanding is self-consistent. This approach cannot lead to the scenario being proved, since self-consistency does not in itself prove validity. However, in contrast, inconsistency would effectively disprove the validity of the scenario, thereby leading to a reduction in overall uncertainty.

13 Background to Evidential Support Logic (ESL)

The version of ESL used is based on computational methods that were proposed by Baldwin (1987) and that have since been applied in the petroleum and civil engineering industries (e.g. Foley, et al. 1997; Hall et al. 2004).

An assessment is made of evidence from a number of sub-processes in support of a process of interest (e.g. Cui and Blockley, 1990; Foley et al. 1997; Hall et al. 1998). Compared to classical (point) probability theory, ESL has the major advantage that uncertainty in an actual evaluation of support is taken into account (Figure 62).

The initial step in an evaluation using ESL is to construct a hierarchy of processes (a process model) to link the process of interest to data or information, usually via intermediate sub-processes (Figure 63).

To evaluate the 'evidence' for the process of interest, which is the degree that it is dependable or not, the extent to which information (i.e. evidence) leads to confidence in the dependability of each sub-process corresponding to data (i.e. support for the process) is estimated. The evidence at this latter level is then propagated through the process model (Figure 63). The evaluation of confidence in each process is made relative to a criterion for the success of the process.

To represent evidence and propagate the uncertainties, ESL uses Interval Probability Theory. This theory allows statements of the type: 'The degree of confidence that evidence supports the proposition lies between p and p+u'. Here, p is the minimum probability that evidence supports a proposition and u is the uncertainty in this probability. The minimum degree of confidence that some evidence does not support the proposition is 1-p-u (Figure 63). In contrast, the classical (point) probability theory requires that if evidence supports a proposition with probability p, then the probability against the proposition is automatically 1-p (Figure 62).

In practice, in ESL the evidence for and against each process corresponding to data is usually elicited from experts. Linguistic confidence scales are typically used to achieve this goal. For example, the confidence in the evidence for a process could be expressed using terms such as 'Very confident', 'Confident', 'Intermediate', 'Not confident', 'Not at all confident'.

In Figure 63 'sufficiency' of an individual piece of evidence or supporting proposition can be regarded as the corresponding conditional probability. That is, the 'sufficiency' of some process as support for another process is the probability of the latter proposition being true when the supporting proposition is true and other processes are false. A parameter called 'dependency' represents the degree of overlap in the sources of the evidence for the process. This parameter is introduced to avoid double counting of support from any mutually dependent pieces of evidence. In addition, a Boolean operator, 'necessity'

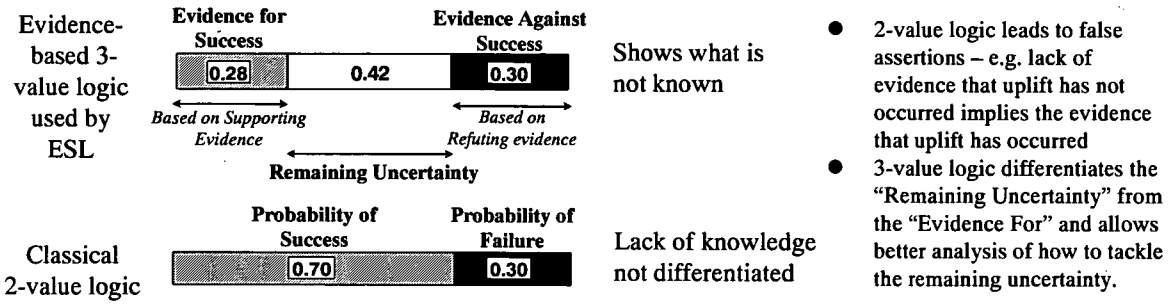

Figure 62. Distinction between the ESL approach (above) and the classical approach (below).

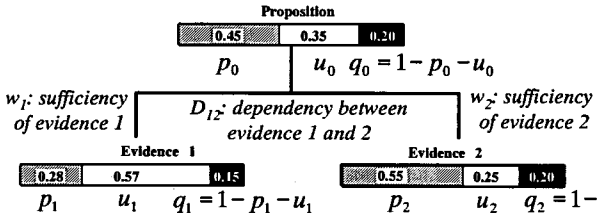

$$p_0 = w_1 p_1 + w_2 p_2 - \rho_{12} Min(w_1 p_1, w_2 p_2)$$

$$q_0 = w_1 q_1 + w_2 q_2 - \rho_{12} Min(w_1 p_1, w_2 p_2)$$

where

$$\rho_{12} = (1 - D_{12}) Max(w_1 p_1, w_2 p_2) + D_{12}$$

Figure 63. Evaluation of confidence using Interval Probability Theory.

is sometimes used to represent evidence without which the top process cannot proceed. The values assigned to the 'sufficiency' and 'dependency' parameters are once again subjective and are obtained by expert judgment.

Though the structure of a process model is subjective, it enables information from diverse sources to be integrated and sensitivity calculations performed to assess the relative importance of different types of information.

14 An evaluation using ESL

The computer code TESLA, developed by Quintessa, was used to construct a process model to assess the hypothesis that hydrogeological and geochemical concepts are consistent (Figure 64). In this process model, this appears in the top left corner and the supporting information is given towards the right margin. The processes in this model and their criteria for success are listed in Table 24.

The information in Figure 64 is also summarised in the ratio plot given in Figure 65. This plot shows the ratio of evidence for a process divided by evidence against the process on the vertical axis. The horizontal axis shows the residual uncertainty. Finally, the sensitivity of the hypothesis of interest to each type of evidence was evaluated using a tornado plot (Figure 66).

Figure 64. An ESL process model to evaluate the degree to which the hypothesis that the hydrogeological and geochemical concepts are consistent (process 1, top left) is valid.

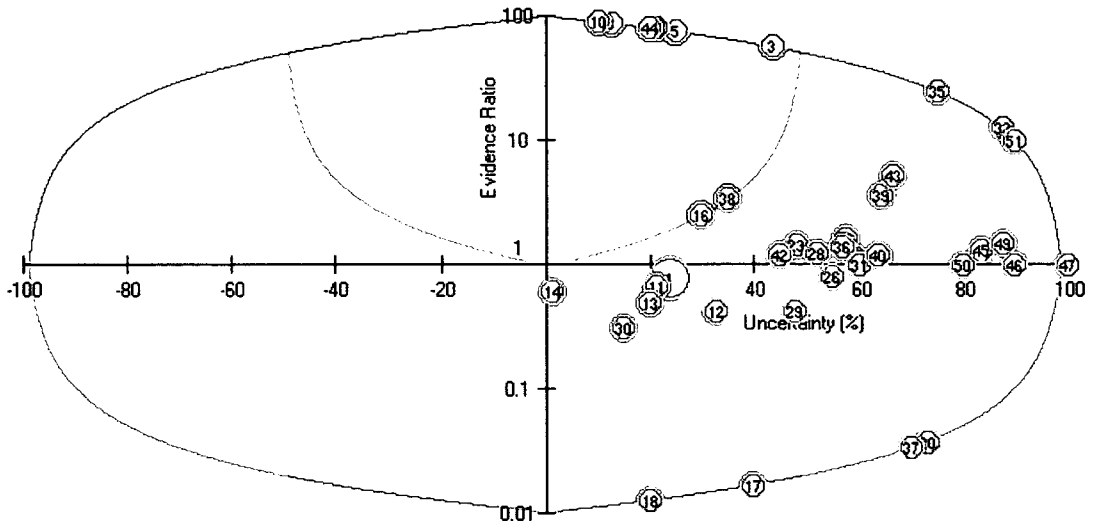

Figure 65. Ratio plot corresponding to the process model in Figure 64. The vertical axis represents the ratio of evidence for to evidence against, whereas the horizontal axis represents uncertainty.

From this evaluation, the following conclusions can be drawn:

- The balance of evidence indicates the hypothesis that seawater has been flushed under conditions broadly similar to the present to be invalid (there is more evidence against than evidence for the hypothesis), but there is still a large uncertainty (Figures 64 and 65).

- The greatest deficiency in the hypothesis is that it cannot explain the time taken to flush the seawater. The calculated flushing times are generally too fast. Some of the 1D dual-porosity simulations could explain the actual long flushing time, but this in itself lends indirect support to the suggestion that the rocks do not behave as equivalent porous media. This is a contradiction of the evaluated hypothesis.

- There is generally greater uncertainty associated with the interpretation of mineralogical fronts than with the interpretation of aqueous geochemical gradients.

- There is no evidence that the hydraulic properties of the rock would vary during the simulated time intervals.

1. Hydrogeological and geochemical concepts are consistent

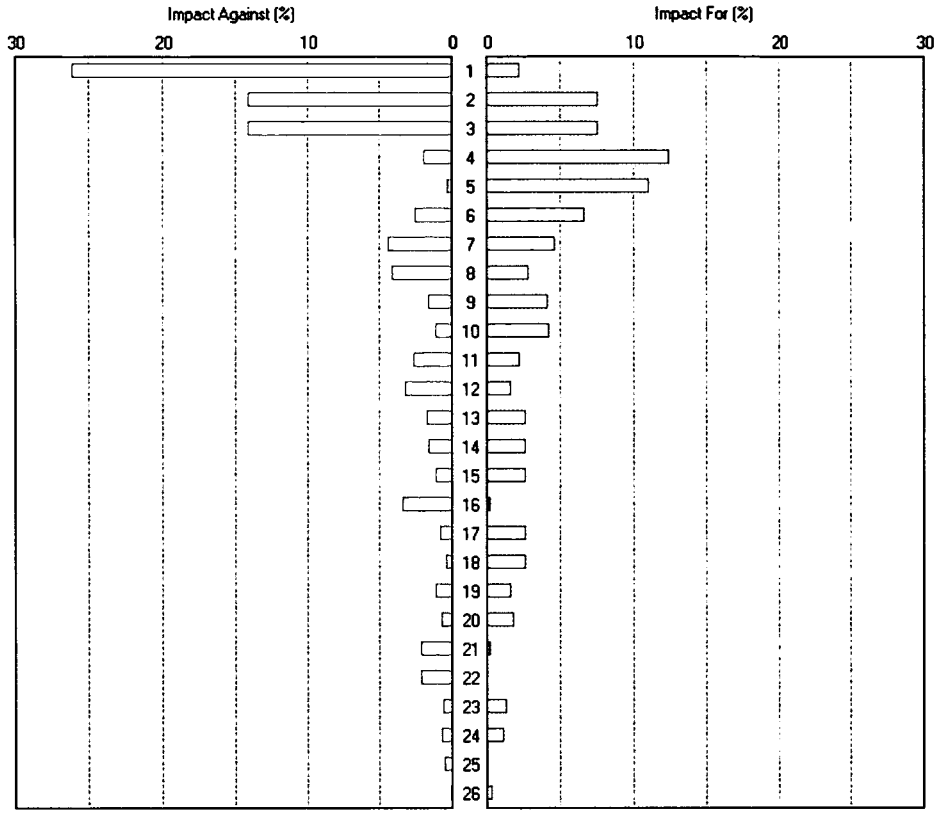

1 : 18. Evaluating time taken to flush seawater in 3D simulations
2 : 21. Evaluating time taken to flush seawater in 1D simulations
3 : 22. Evaluating salinity gradients calculated in 1D simulations
4 : 38. Evaluating chemical gradients calculated in fully-coupled flow and chemical models
5 : 16. Evaluating salinity gradients calculated in 2D simulations
6 : 27. Evaluating output from kinetic reaction-path models
7 : 37. Evaluating time taken to produce present chemical conditions in fully-coupled flow and chemical models
8 : 10. Evaluating output from fully-coupled flow and salinity transport models
9 : 35. Evaluating chemical gradients calculated in semi-coupled flow and chemical models
10 : 44. Evaluating output from 1D coupled models of redox and salinity variations
11 : 19. Evaluating salinity gradients calculated in 3D simulations
12 : 15. Evaluating time taken to flush seawater in 2D simulations
13 : 50. Evaluating time taken to produce present mineral assemblages in fully-coupled flow and chemical models
14 : 34. Evaluating time taken to produce present chemical conditions in semi-coupled flow and chemical models
15 : 30. Evaluating time taken to produce present redox conditions in 1D coupled models of redox and salinity variations
16 : 9. Evaluating output from semi-coupled flow and salinity transport models
17 : 51. Evaluating mineral fronts calculated in fully-coupled flow and chemical models
18 : 31. Evaluating chemical gradients calculated in 1D coupled models of redox and salinity variations
19 : 48. Evaluating mineral fronts calculated in semi-coupled flow and chemical models
20 : 26. Evaluating output from equilibrium geochemical models
21 : 5. Evaluating output from kinetic reaction-path models
22 : 4. Evaluating output from equilibrium geochemical models
23 : 42. Evaluating output from kinetic reaction-path models
24 : 47. Evaluating time taken to produce present mineral assemblages in semi-coupled flow and chemical models
25 : 7. Evaluating output from 1D coupled models of redox and salinity variations
26 : 41. Evaluating output from equilibrium geochemical models

Figure 66. A tornado plot showing the sensitivity of the hypothesis 1 in Figures 64 and 65 to each of the processes corresponding to information (those towards the right of Figure 64). Process 18 (evaluating the time taken to flush the seawater using 3D models) has the greatest impact against the hypothesis, whereas Process 38 (evaluating chemical gradients calculated using fully-coupled flow and chemical models) has the greatest impact in favour of the hypothesis.

Table 24. Criteria for success of processes in Figure 64.

No.	Description	Criteria for success
1.	Hydrogeological and geochemical concepts are consistent	The concept that the rocks of the area behave as equivalent porous media which were initially saturated with seawater and then flushed by fresh water under hydraulic conditions similar to the present, is consistent with the observed variations in groundwater salinity and rock mineralogy and with the inferred chemical evolution of the groundwater system.
2.	Chemical processes could not change hydraulic properties	During the time required to flush the seawater present initially, the hydraulic properties of the rocks did not change due to chemical processes.
3.	Evaluating output from geochemical models	Geochemical models suggest that no significant volume changes would occur during water/rock reactions.
4.	Evaluating output from equilibrium geochemical models	Equilibrium geochemical models suggest that no significant volume changes would occur during water/rock reactions.
5.	Evaluating output from kinetic reaction-path models	Simulations using kinetic reaction-path models suggest that no significant volume changes would occur during water/rock reactions over the time interval required to flush seawater from the rock.
6.	Evaluating output from 1D coupled chemical-flow models	Simulations with 1D coupled chemical-flow models suggest that no significant volume changes would occur during water/rock reactions over the time interval required to flush seawater from the rock.
7.	Evaluating output from 1D coupled models of redox and salinity variations	Simulations with 1D coupled models of redox and salinity variations suggest that no significant volume changes would occur during water/rock reactions over the time interval required to flush seawater from the rock.
8.	Evaluating output from coupled flow and chemical models	Simulations with fully-coupled flow and chemical models of redox and salinity variations suggest that no significant volume changes would occur during water/rock reactions over the time interval required to flush seawater from the rock.
9.	Evaluating output from semi-coupled flow and salinity transport models	Simulations using semi-coupled flow and salinity transport models suggest that no significant volume changes would occur during water/rock reactions over the time interval required to flush seawater from the rock.
10.	Evaluating output from fully-coupled flow and salinity transport models	Simulations using fully-coupled flow and salinity transport models suggest that no significant volume changes would occur during water/rock reactions over the time interval required to flush seawater from the rock.
11.	Evaluating whether understanding of chemical gradients and hydrogeology are consistent	Flushing of uniformly distributed seawater under hydraulic conditions similar to the present would produce the present salinity and chemical gradients in the time since seawater was last in the area.
12.	Evaluating whether understanding of salinity gradients and hydrogeology is consistent	Flushing of uniformly distributed seawater under hydraulic conditions similar to the present would produce the present salinity gradients in the time since seawater was last in the area.
13.	Evaluating output from equivalent porous medium models	The simulated past and present salinity gradients predicted by equivalent porous medium models are consistent with the observed salinity gradients and the palaeohydrogeological evidence for the timescales over which they evolved.
14.	Evaluating output from 2D coupled transport models	2D coupled models produce salinity gradients that are consistent with the present salinity gradients and with the past evolution of these gradients.
15.	Evaluating time taken to flush seawater in 2D simulations	There was a 2D simulation in which the time taken for salinity to be flushed to presently observed levels in the Toki River valley was similar to the time that has elapsed since the last occurrence of seawater in the Tono area.
16.	Evaluating salinity gradients calculated in 2D simulations	There was a 2D simulation that produced salinity gradients similar to the present natural gradients.
17.	Evaluating output from 3D coupled transport models	3D coupled models produce salinity gradients that are consistent with the present salinity gradients and with the past evolution of these gradients.

Table 24. Continued.

No.	Description	Criteria for success
18.	Evaluating time taken to flush seawater in 3D simulations	There was a 3D simulation in which the time taken for salinity to be flushed to presently observed levels in the Toki River valley was similar to the time that has elapsed since the last occurrence of seawater in the Tono area.
19.	Evaluating salinity gradients calculated in 3D simulations	There was a 3D simulation that produced salinity gradients similar to the present natural gradients.
20.	Evaluating dual-porosity models (1D coupled models of redox and salinity variations)	The simulated past and present salinity gradients predicted by dual porosity models are INconsistent with the present salinity gradients and the palaeohydrogeological evidence for the timescales over which they evolved.
21.	Evaluating time taken to flush seawater in 1D simulations	There were NO 1D simulations in which the time taken for salinity to be flushed to presently observed levels in the Toki River valley was similar to the time that has elapsed since the last occurrence of seawater in the Tono area.
22.	Evaluating salinity gradients calculated in 1D simulations	There were NO 1D simulations that produced salinity gradients similar to the present natural gradients at some time during the simulated time interval.
23.	Evaluating whether understanding of chemical gradients (other than salinity) and hydrogeology is consistent	Flushing of uniformly distributed seawater under hydraulic conditions similar to the present would produce the present chemical gradients in the time since seawater was last in the area.
24.	Evaluating whether understanding of aqueous geochemical gradients and hydrogeology is consistent	The simulated past and present aqueous chemical gradients are consistent with the observed aqueous chemical gradients (pCO_2, Eh etc) and the palaeohydrogeological evidence for the timescales over which they evolved.
25.	Evaluating geochemical models	There are geochemical models that predict the evolution of groundwater chemistry and mineralogy along the temperature gradients occurring along plausible groundwater flow paths.
26.	Evaluating output from equilibrium geochemical models	There are equilibrium models that predict the evolution of groundwater chemistry along the temperature gradients occurring along plausible groundwater flow paths.
27.	Evaluating output from kinetic reaction-path models	There are kinetic reaction-path models in which the temporal evolution of water chemistry is similar to the observed variation in water chemistry along an estimated flow line.
28.	Evaluating output from 1D coupled chemical-flow models	1D coupled models produce chemical gradients (other than salinity gradients) that are consistent with the present chemical variations and with the past evolution of these gradients.
29.	Evaluating output from chemical balance-flow models	1D coupled models of redox and salinity variations produce redox gradients that are consistent with the present redox variations and with the past evolution of these gradients.
30.	Evaluating time taken to produce present redox conditions in 1D coupled models of redox and salinity variations	There was a 1D coupled simulation of redox and salinity variations in which the time taken for redox conditions to acquire their presently observed levels was similar to the time that has elapsed since the last occurrence of seawater in the Tono area.
31.	Evaluating chemical gradients calculated in 1D coupled models of redox and salinity variations	There was a 1D coupled simulation of redox and salinity variations that produced redox gradients similar to the present natural gradients.
32.	Evaluating output from coupled chemical thermodynamic-flow models	Coupled flow and chemical thermodynamic models produce chemical gradients that are consistent with the present geochemical variations and with the past evolution of these gradients.
33.	Evaluating output from semi-coupled flow and chemical models	Semi-coupled flow and chemical models produce chemical gradients that are consistent with the present geochemical variations and with the past evolution of these gradients.

Table 24. Continued.

No.	Description	Criteria for success
34.	Evaluating time taken to produce present chemical conditions in semi-coupled flow and chemical models	There was a semi-coupled flow and chemical simulation in which the time taken for chemical conditions to aquire their presently observed levels was similar to the time that has elapsed since the last occurrence of seawater in the Tono area.
35.	Evaluating chemical gradients calculated in semi-coupled flow and chemical models	There was a semi-coupled flow and chemical simulation that produced chemical gradients similar to the present natural gradients.
36.	Evaluating output from fully-coupled flow and chemical models	Fully-coupled flow and chemical models produce chemical gradients that are consistent with the present geochemical variations and with the past evolution of these gradients.
37.	Evaluating time taken to produce present chemical conditions in fully-coupled flow and chemical models	There was a fully-coupled flow and chemical simulation in which the time taken for chemical conditions to acquire their presently observed levels was similar to the time that has elapsed since the last occurrence of seawater in the Tono area.
38.	Evaluating chemical gradients calculated in fully-coupled flow and chemical models	There was a fully-coupled flow and chemical simulation that produced chemical gradients similar to the present natural gradients.
39.	Evaluating whether understanding of mineralogical fronts and hydrogeology is consistent	The simulated past and present mineralogical fronts are consistent with the observed mineralogical fronts and the palaeohydrogeological evidence for the timescales over which they evolved.
40.	Evaluating geochemical models	Geochemical models predict mineral stabilities that are consistent with the present mineralogical distributions and the past evolution of these distributions.
41.	Evaluating output from equilibrium geochemical models	Equilibrium models that predict the evolution of groundwater chemistry along the temperature gradients occurring along plausible groundwater flow paths include minerals that actually occur in the rock along these flow paths.
42.	Evaluating output from kinetic reaction-path models	There are kinetic reaction-path models in which the temporal evolution of rock mineralogy is similar to the observed variation in rock mineralogy along an estimated flow line.
43.	Evaluating evidence from 1D coupled chemical-flow models	Coupled chemical-flow models produce mineralogical variations that are consistent with the present mineralogical variations and the past evolution of these variations.
44.	Evaluating evidence from 1D coupled chemical-flow models	There was a 1D coupled simulation of redox and salinity variations in which the time taken for a mineralogical redox front to reach its present observed depth was similar to the time that has elapsed since the last occurrence of seawater in the Tono area.
45.	Evaluating evidence from coupled chemical thermodynamic-flow models	Coupled chemical thermodynamic-flow models produce mineralogical variations that are consistent with the present mineralogical variations and the past evolution of these variations.
46.	Evaluating output from semi-coupled flow and chemical models	Semi-coupled flow and chemical models produce mineralogical variations that are consistent with the present mineralogical variations and the past evolution of these variations.
47.	Evaluating time taken to produce present mineral assemblages in semi-coupled flow and chemical models	There was a semi-coupled flow and chemical simulation in which the time taken for the mineral assemblage at any locality to become similar to the observed assemblage was similar to the time that has elapsed since the last occurrence of seawater in the Tono area.
48.	Evaluating mineral fronts calculated in semi-coupled flow and chemical models	There was a semi-coupled flow and chemical simulation that produced mineralogical fronts at locations similar to the present natural mineralogical fronts.
49.	Evaluating output from fully-coupled flow and chemical models	Fully-coupled flow and chemical models produce mineralogical variations that are consistent with the present mineralogical variations and with the past evolution of these variations.

Table 24. Continued.

No.	Description	Criteria for success
50.	Evaluating time taken to produce present mineral assemblages in fully-coupled flow and chemical models	There was a fully-coupled flow and chemical simulation in which the time taken for the mineral assemblage at any locality to become similar to observed assemblage was similar to the time that has elapsed since the last occurrence of seawater in the Tono area.
51.	Evaluating mineral fronts calculated in fully-coupled flow and chemical models	There was a fully-coupled flow and chemical simulation that produced mineralogical fronts at locations similar to the present natural mineralogical fronts.

15 Summary conclusions

The work reported here has yielded important new insights into the groundwater flow system in the Tono area.

All types of flow models indicated the hypothesis that seawater has been flushed under hydrogeological conditions broadly similar to the present ones to be invalid, unless the behaviour of the host rock behaves differently to an equivalent porous medium. It is more likely that the boundary conditions have changed substantially during the time frame considered and/or that there is at least partly an alternative origin of Na-dominated salinity besides sea water.

The work has also given valuable insights into the best ways of integrating geochemical and hydrogeological information. Fully-coupled modelling codes exist that can in principle simulate 3D groundwater flow and reactions, but a limitation of these codes is that impractically long computational times would usually be required for such simulations. Therefore, the alternative approach developed in the work reported here is proposed as a generic methodology for developing internally consistent models for groundwater flow and variations in groundwater chemistry. It is suggested that this generic methodology could have the following components:

- Several different kinds of simulation are carried out, each of which is targeted at understanding a specific aspect of the coupling between chemical and physical processes. These simulations are summarised in Table 25.
- The simulated flow field should be selected as far as possible to ensure that it contains data that could enable the simulation results to be checked.
- Following the varied simulations, an integrated interpretation of the output from such simulations is then developed in order to understand the coupling between all processes. This interpretation should combine both qualitative and quantitative information and take into account uncertainties. It is suggested that Evidential Support Logic (ESL) provides a suitable framework for carrying out such integrated interpretations.

Table 25. Summary of major steps recommended for developing an understanding of coupled geochemical-hydrogeological processes.

Order	Non-coupled flow simulations	Coupled flow and transport simulations	Non-coupled chemical reaction simulations	Coupled flow-transport-chemical reaction simulations
1	3D large-scale non-coupled simulations intended to establish the hydraulic boundary conditions of smaller-scale simulations		Equilibrium calculations (could be carried out at any stage before 4)	
2		3D smaller-scale (local) coupled simulations, in which salinity transport is simulated together with flow	Non-kinetic reaction-path models (could be carried out at any stage after equilibrium calculations and before 4)	
3		2D coupled simulations, constructed through the domain of the local 3D models in such a way as to minimise inaccuracies caused by approximating 3D flow in a 2D section (that is the section is chosen to lie approximately parallel to flow in the 3D model)	Kinetic reaction-path models (could be carried out at any stage after non-kinetic reaction-path calculations equilibrium calculations and before 4)	
4				1D semi-coupled flow-transport and water/rock reaction simulations constrained to simulate flow lines in the 3D and 2D coupled transport simulations.
5				1D fully-coupled flow-transport and water/rock reaction simulations constrained to simulate flow lines in the 3D and 2D coupled transport simulations.

One aspect of the coupling between chemical and hydrogeological processes is the possible effect of chemical reactions on the hydraulic properties of the rock mass. The basic methodology that has been used to evaluate this possibility has the following components:

- Equilibrium chemical models are constructed to gain an understanding of the reactions that are likely to be important.
- Kinetic reaction-path simulations are then undertaken to establish which of these reactions are likely to occur sufficiently rapidly to be important.
- Coupled 1D flow-reaction simulations are carried out to evaluate the likely timescales required to cause variations in the hydrogeological properties of the rock mass. These simulations consider only reactions suggested by the kinetic reaction-path models to be potentially important during the time frame considered.

A key point is that in this methodology, the coupled simulations consider only those reactions that are likely to be important. In this way, the duration of the time frame that can be practically considered by the coupled modelling is maximised.

The models reported here were necessarily limited in several respects, notably:

- Only one conceptual model could be evaluated.
- It was not possible to model flushing of the sedimentary rocks at an appropriate scale.
- Boundary conditions did not change during the simulations.
- Only an equivalent porous medium representation of the rock mass was considered (except in some of the simple 1D models).
- The 1D coupled simulations were carried out in parallel with the 2D and 3D simulations, so that all the information regarding flow path geometry from the 2D and 3D simulations could not be included in the 1D simulations.
- The complexity of fully-coupled flow-reaction calculations necessarily requires that each simulation should be very simplified.
- Thermodynamic data and (more importantly) kinetic data are uncertain.

Any future simulations could usefully build upon the work presented here by:

- modelling the flushing of the sediments at an appropriate scale (for example, the scale of the MIU area);
- similarly, modelling the migration of mineralogical fronts (e.g. redox fronts, kaolinitization fronts, calcite dissolution fronts) at a much smaller scale (i.e. within a few hundred metres of the recharge zone) than was done in the present study;
- changing the inflow of water in the model during each simulation;
- considering several alternative origins to the groundwater salinity, such as other origins of a geological nature, for example magmatic origins;
- representing the rock mass as a dual-porosity system;
- focussing on using mass-balances of chemical reactions to place limits on the migration rates of geochemical fronts (e.g. by adopting the approach of Lichnter (1988), as was done for redox fronts in the present study), rather than the actual rates of individual reactions.

A major limitation on the simulations that were carried out is a lack of data suitable for direct comparison with the output of the models. This limitation arises because the boreholes from which groundwater data were obtained do not apparently lie along lines that are parallel to the major flow direction.

The following recommendations are made for future acquisition of data:

- It would be have been valuable to obtain groundwater chemical data from boreholes that are situated along profiles orientated more parallel to the flow lines than the boreholes actually drilled. Data from only two boreholes along a flow-parallel profile would be useful, if one is located close to the inferred discharge area (near the Toki River) and one is located approximately mid-way between the this point and the recharge area.

- It is recognised that there have been practical limitations with siting boreholes in such a way. Therefore, an alternative approach is to obtain information from a relatively deep borehole in the southern part of the Tono area. The water that is penetrated by such a borehole is expected to lie along a number of different flow lines of differing lengths; the distances between recharge zones and the shallower water samples from the borehole will be shorter than the distances between recharge zones and the deeper water samples. Such a borehole should penetrate both the shallower Na-Ca-HCO_3 waters and the deeper Na-Cl waters. It is recommended that consideration is given to:

  - using the results from the MIZ-1 borehole;
  - attempting to use these MIZ-1 data to constrain more localised coupled models of the MIU area.

- Additional data from which the variations in past boundary conditions can be interpreted should be obtained. Such data include:

  - geomorphological evidence for the uplift history of the area;
  - regional palaeo-environmental information;
  - potentially, apatite fission-track data from which the uplift history can be deduced.

- Additional information from which the origins of the groundwater salinity can be constrained more confidently should be obtained. Possibly useful data include:

  - stable Cl-isotope data ($^{37}Cl/^{35}Cl$), which could help to establish whether there is indeed a component of marine Cl in the area;
  - stable B-isotopic data ($^{11}B/^{10}B$), which could also help to establish whether there is a component of marine salinity in the area and whether water/rock interactions have occurred in the granite;
  - palaeogeographical information to establish more clearly whether marine water could have entered the groundwater system more recently than the time of deposition of the Akeyo Formation.

16 References

Appelo, C.A.J. and Postma, D. 1994. Geochemistry, groundwater and pollution. Balkema, Rotterdam, 536pp.

Arthur, R.A. 2003. Empirical constraints on theoretical models of the chemical evolution of groundwaters in the Tono area (Draft Final Report). Montor Scientific LLC Report.

Arthur, R.A. Iwatsuki, T., Hama, K., Amano, K., Metcalfe, R. and Ota, K. In Press. The Redox Environment of Deep Groundwaters Associated with the Tono Uranium Deposit, Japan. Materials Research Society Proceedings.

Baldwin, J,F. 1987. Evidental Support Logic Programming. Fuzzy Sets and Systems, 24, 1-26.

Banwart S., Tullborg E.-L., Pedersen K., Gustafsson E., Laaksoharju M., Nilsson A.-C., Wallin B., and Wikberg P. (1996) Organic carbon oxidation induced by large-scale shallow

water intrusion into a vertical fracture zone at the Äspö Hard Rock Laboratory (Sweden). J.Contaminant Hydrol. 21, 115-125.

Bethke, C.M. 1996. Geochemical reaction modelling. Oxford University Press, Oxford. 397pp.

Burnham, C.H. and Ohmoto, H. 1980. Late-stage of felsic magmatism. Mining Geol. Special Issue, 8, 1-11.

Burnham, C.W. 1997. Magmas and hydrothermal fluid. In: Barnes, H.L. (ed.) Geochemistry of hydrothermal ore deposits. Wiley & Sons, 63-123.

Brady, P.V. and Walther, J.V. 1989. Controls on silicate dissolution rates in neutral and basic pH solutions at 25 °C. Geochimica et Cosmochimica Acta, 53, 2823-2830.

Brandt, F., Bosbach, D., Krawczyk-Bärsch, E., Arnold, T. and Bernhard, G. 2003. Chlorite dissolution in the acid pH range: a combined microscopic and macroscopic approach. Geochimica et Cosmochimica Acta, 67, 1451-1461.

Carpenter A. B. 1978. Origins and chemical evolution of brines in sedimentary basins, pp. 78-88. Oklahoma Geological Survey.

Carrera, J and 22 more authors, 1997. The Hydrogeology of El Berrocal site, Spain. Nuclear Science and Technology, El Berrocal project, TGR 2, EUR 17478 EN.

Carrera, J., Vives, L., Tume, P., Saaltink, M., Galarza, G., Guimerà, J. and Medina, M. 1996. Interpretation of field tests in low permeability fractured media: Recent experiences. In: Gottlieb, J. and Duchateau, P. (eds), Parameter identification and inverse problems in hydrology, geology and ecology. Water Science and Technology Library 23, 53-70 Kluwer Academic Publications, Dordrecht. ISBN 0-7923-4089-2.

Cui, W. and Blockley, D.I. 1990. Interval Probability theory for evidential support. International Journal of Intelligence Systems. 5, 183-192.

Drever, J.I. (1997) The geochemistry of natural waters. Surface and groundwater environments. 3rd edition, Prentice Hall, 436 pp.

Edmunds W. M. 1996. Bromine geochemistry of British groundwaters. Mineralogical Magazine 60, 275-284.

Edmunds W. M., Kay R. L. F., and McCartney R. A. 1985. Origin of saline groundwaters in the Carnmenellis Granite: natural processes and reaction during Hot Dry Rock reservoir circulation. Chemical Geology 49, 287-301.

Edmunds W. M. 1975. Geochemistry of brines in the Coal Measures of northeast England. Transactions of the Institution of Mining and Metallurgy 84B, B39-B52.

EMRL 2001. GMS 3.1 Tutorials. Brigham Young University - Environmental Modeling Research Laboratory.

Evans, W.C., Mariner, R.H., Ingebritsen, S.E., Kennedy, B.M., van Soest, M.C. and Huebner, M.A. 2002. Report of hydrologic investigations in the three sisters area of Central Oregon, Summer 2001. U.S. Geol. Surv., Water-Resources Investigations Report 02-4061.

Foley, L, Ball, L. Hurst, A. Davis, J and Blockley, D. 1997. Fuzziness, incompleteness and randomness: classification of uncertainty in reservoir appraisal. Petroleum Geoscience, 3, 203-209.

Giggenbach, W.F. 1995. Composition of magmatic components in hydrothermal fluids. In: Thompson, J.F.H. (ed.), Magmas, fluids, and ore deposits. Mineralogical Association of Canada, Short Course Series, 23, 247-261.

Giggenbach, W.F. 1997. The origin and evolution of fluids in magmatic-hydrothermal systems. In: Barnes, H.L. (ed.), Geochemistry of hydrothermal ore deposits. 3rd edition. Wiley & Sons, 737-796.

Gillespie, M.R., Milodowski, A.E., Hama, K., Amano, K., Metcalfe, R., Hards, H.L., Darbyshire, D.P.F., Iwatsuki, T., Kunimaru, T. and Yoshida, H. 2000. Characterisation of the Tsukiyoshi Fault Phase I (1999-2000): The Tsukiyoshi Fault intersections in the Toki Formation, the Toki Formation-Toki Granite unconformity and preliminary investigations in the Toki Granite. British Geological Survey Technical Report CR/00/37.

Guimerà, J., Ruiz, E., Luna, M., Arcos, D. And Jordana, S. 2003. Development of a coupled geochemical / hydrogeological model of the Tono area. Final Report. Enviros Report R-0412.1.

Guimerà, J. and 29 more authors 1997. Tracer tests at El Berrocal site, Spain. Nuclear Science and Technology, El Berrocal project, TGR 6, EUR 17478 EN.

Hall, J.W., Blockley, D.I. and Davis, J.P. 1998. Uncertain inference using interval probability theory. International Journal of Approximate Reasoning, 19, 247-264.

Hall, J.W., le Masurier, J.W., Baker-Langman, E.A.B., Davis, J.P. and Taylor, C.A. 2004. A decision-support methodology for performance-based asset management. Civil Engineering and Environmental Systems, 21, 51-75.

Hanor J. D. 1994. Origins of saline fluids in sedimentary basins. In Geofluids: origin, migration and evolution of fluids in sedimentary basins, Vol. 78 (ed. J. S. Parnell), pp. 151-174. Geological Society of London.

Henderson, P. 1982. Inorganic geochemistry. Pergamon Press. Oxford. 353pp.

Henley, R.W., Truesdell, A.H. and Barton Jr., P.B. 1984. Fluid-mineral equilibria. In: Hydrothermal Systems. Society of Economic Geologists, Reviews in Economic Geology, 1.

Iwatsuki, T., Satake, H., Metcalfe, R., Yoshida, H. and Hama, K. 2002. Isotopic and morphological features of fracture calcite from granitic rocks of the Tono area, Japan: a promising palaeohydrogeological tool. Applied Geochemistry, 17, 1241-1257.

Iwatsuki, T., Metcalfe, R., Amano, K., Hama, K., Noda, N., Arthur, R.C. and Sasamoto, H. 2001. (draft). Data book on groundwater chemistry in the Tono area. JNC TN 7450 2001-003, Japan Nuclear Cycle Development Institute, Tono Geoscience Center, Toki, Gifu-ken, Japan.

Iwatsuki T., Metcalfe R., Amano K., Hama K., Arthur R. C., and Sasamoto H. 2000. The Tono Geochemistry Research Project Hydrochemical Database, pp. 300. Japan Nuclear Cycle Development Institute.

Iwatsuki, T. and Yoshida, H. 1999. Characterising the chemical containment properties of the deep geosphere: water-rock interactions in relation to fracture systems within deep crystalline rock in the Tono area, Japan. In: Metcalfe, R. and Rochelle (eds) Chemical containment of wastes in the geosphere. Geological Society of London Special Publications, 157, 71-84.

JNC 2000. H12: Project to establish the scientific and technical basis for HLW disposal in Japan. Second Progress Report on Research and Development for the Geological Disposal of HLW in Japan. JNC Technical Report JNC TN1410 2000-002. (4 volumes plus a supplementary report).

Kamineni D. C., Gascoyne M., Melnyk T. W., Frape S. K., and Blomqvist R. 1992. Cl and Br in mafic and ultramafic rocks: significance for the origin of salinity in groundwater. 7th International Conference on Water-Rock Interaction (WRI-7), 801-804.

Knauss, K.G. and Wolery, T.J. 1988. The dissolution kinetics of quartz as a function of pH and time at 70°C. Geochimica et Cosmochimica Acta, 52, 43-53.

Lichtner, P.C. 1988. The quasi-stationary state approximation to coupled mass transport and fluid-rock interaction in a porous medium. Geochemica et Cosmochimica Acta, 52, 143-165.

Lin, H-C. Richards, J., Talbot, D.R., Yeh, C.A., Cheng, J-R., Cheng, H-P. and Jones, N. L. 2001. FEMWATER Version 3.0: A three dimensional finite element computer model for simulating density-dependent flow and transport in variably saturated media.

Mahon, T. Harvey, C. and Crosby, D. 2000. The chemistry of geothermal fluids in Indonesia and their relationship to water and vapour dominated systems. Proceedings of the World Geothermal Congress 2000, 1389-1394.

Mailloux, B. J., Person, M., Kelley, S., Dunbar, N., Cather, S., Strayer, L. and Hudleston, P. 1999. Tectonical controls on the hydrogeology of the Rio Grande Rift, New Mexico. Water Resources Research, 35 , 2641-2659.

Malmström, M. and Banwart, S. 1997. Biotite dissolution at 25°C: the pH dependence of dissolution rate and stoichiometry. Geochimica et Cosmochimica Acta, 61, 2779-2799.

Metcalfe, R., Hama, K., Amano, K., Iwatsuki, T. and Saegusa, H. 2003. Geochemical approaches to understanding a deep groundwater flow system in the Tono area, Gifu-ken, Japan. In: Nishigaki, M. (ed). Proceedings of an International Symposium on Ground Water Problems related to Geo-Environment(IS-Okayama2003). Balkema. Rotterdam. In Press.

Nirex. 1997. Sellafield geological and hydrogeological investigations - The hydrochemistry of Sellafield: 1997 update. United Kingdom Nirex Limited. Report SA/97/089.

Parkhurst, D.L. and Appelo, C.A.J. 1999. User's guide to PHREEQC (Version 2) – A computer program for speciation, batch-reaction, one-dimensional transport and inverse geochemical calculations. United States Geological Survey, Water-Resources Investigations Report 99-4259. 312pp.

Plummer, L.N., Wigley, T.M.L. and Parkhurst, D.L., 1978. The kinetics of calcite dissolution in CO_2-water systems at 5° to 60°C and 0.0 to 1.0 atm CO_2. American Journal of Science, 278, 179-216.

Rochelle, C.A. et al., 1995. Experimental determination of chlorite dissolution rates. In: T. Murakami and R.C. Ewing (Editors), Scientific Basis for Nuclear Waste Management XVIII. Materials Research Society, Kyoto, Japan, pp. 149-156.

Roedder, E. 1984. Fluid inclusions. Mineralogical Society of America; Reviews in Mineralogy, 12, 646 pp.

Santamarina, J.C., Klein, K.A., Wang, Y.H. and Prencke, E. 2002.Specific surface: determination and relevance. Canadian Geotechnical Journal, 39, 233–241.

Sasaki, M., Fujimoto, K., Sawaki, T., Tsukamoto, H., Muraoka, H., Sasada, M., Ohtani, T., Yagi, M., Kurosawa, M., Doi, N., Kato, O., Kasai, K., Komatsu, R. and Muramatsu, Y. 1998. Characterization of a magmatic / meteoric transition zone at the Kokkonda geothermal system, northeast Japan. In: Arehart, G.B. and Hulston, J.R. (eds.), Proceedings of the 9th International Symposium on Water- Rock Interaction. A.A. Balkema. 483-486.

Sasamoto, H., ,Metcalfe, R. and Arthur, R.A. 2000. TGRP Thermodynamic Database (thermo.tgrp, ver. 1: 12/2000) .

Schweda, P. 1989. Kinetics of alkali feldspar dissolution at low temperature. In: Miles, D.L. (Editor), Proceedings of Water-Rock Interaction 6. Malvern, UK. Balkema, Rotterdam pp. 609-612.

Sheppard, S.M.F. 1986. Characterization and isotopic variations in natural waters. in: Stable isotopes in high temperature geological processes. J.W. Valley, H.P. Taylor, Jr., and J.R. O'Neil (eds.). Min. Soc. Amer.; Rev. Mineral., vol. 16: 165-183.

Shinohara, H., Giggenbach, W.F., Kazahaya, K. and Hedenquist, J.W. 1993. Geochemistry of volcanic gases and hot springs of Satsuma-Iwojima, Japan: Following Matsuo. Geochemical Journal, 27, 271-285.

Stoessell R. K. and Carpenter A. B. 1986. Stochiometric saturation tests of NaCl1-xBrx and KCL1-XBrX. Geochimica et Cosmochimica Acta 50, 1465-1474.

Sturchio, N.C., Ohsawa, S., Sano, Y., Arehart, G., Kitaoka, K. and Yusa, Y. 1996. Geochemical characteristics of the Yufuin outflow plume, Beppu hydrothermal system, Japan. Geothermics, 25, 215-230.

Toupin, D., Eadington, P.J., Person, M., Morin, P., Wieck, J. and Warner, D. 1997. Petroleum hydrogeology of the Cooper and Eromanga basins, Australia: Some insights from mathematical modelling and fluid inclusion data. American Association of Petroleum Geologists Bulletin, 81 (4), 577-603.

Uzumasa Y. 1965. Chemical investigations of hot springs in Japan. Tsukiji Shokan Co. Ltd.

Vengosh A., Starinsky A., Kolodny Y., Chivas A. R., and McCulloch M. T. 1990. Boron isotopes geochemistry as a tracer for the evolution of brines from the Dead Sea (Israel) and associated hot springs. Israel Geological Society Annual Meeting, 84.

Voss, C. I. 1984. A finite element simulation model for saturated-unsaturated fluid-density-dependent groundwater flow with energy or chemically-reactive single species solute transport. U.S. Geological Survey Report WRIR 84-4369, 409 pp.

White, A.F. 1995. Chemical weathering rates of silicate minerals in soils. In: White, A.F. and Brantley, S.L. (eds), Chemical weathering rates of silicate minerals. Reviews in Mineralogy, 31, 407-461.

Wilkin, R.T. and Barnes, H.L. 2000. Nucleation and growth kinetics of analcime from precursor Na-clinoptilolite. American Mineralogist, 85, 1329-1341.

Wieck, J., Person, M. and Strayer, L. 1995. A finite element method for simulating fault block motion and hydrothermal fluid flow with rifting basins. Water Resources Research, 31 (12), 3241-3258.

Yoshida, H., Seo, T., Nohara, T., Ota, K., Hama, K., Kodama, K. And Iwatsuki, T. Data compilation of geoscientific studies of Tono uranium deposits, central Japan. PNC Report PNC TN7410 94-015.

APPENDIX 1: OUTPUT FROM COUPLED SIMULATIONS

Table A1.1. Summary of the coupled simulations undertaken using PHREEQC.

Simulation Number	No. of cells	Lengths of cells	Temperature	Dispersion	Diffusion coefficient	Porosity	Primary minerals	Secondary minerals	Initial groundwater Chemistry	Recharge water chemistry
		m	°C	m	m^2y^{-1}					
JNC 2073A Phq coup inst v4	100	Arbitrary	25	0	9.46e-3	0.1	Quartz, K-feldspar, Anorthite, Albite, Annite, Phlogopite, Pyrite	Calcite, Kaolinite, $Fe(OH)_3(am)$	Saline, modified seawater	Fresh, reducing
JNC 2073A Phq coup inst v5		10	25	100						
JNC 2073A Phq coup inst v6		Arbitrary	25 to 40 (uniform gradient across 100 cells)	0						

Variations in K-feldspar abundances calculated by the three PHREEQC simulations

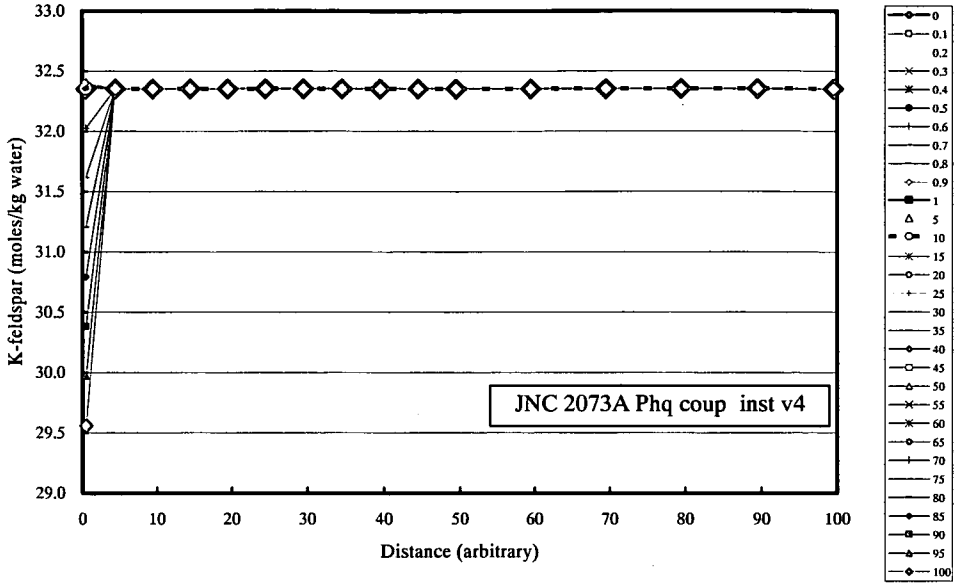

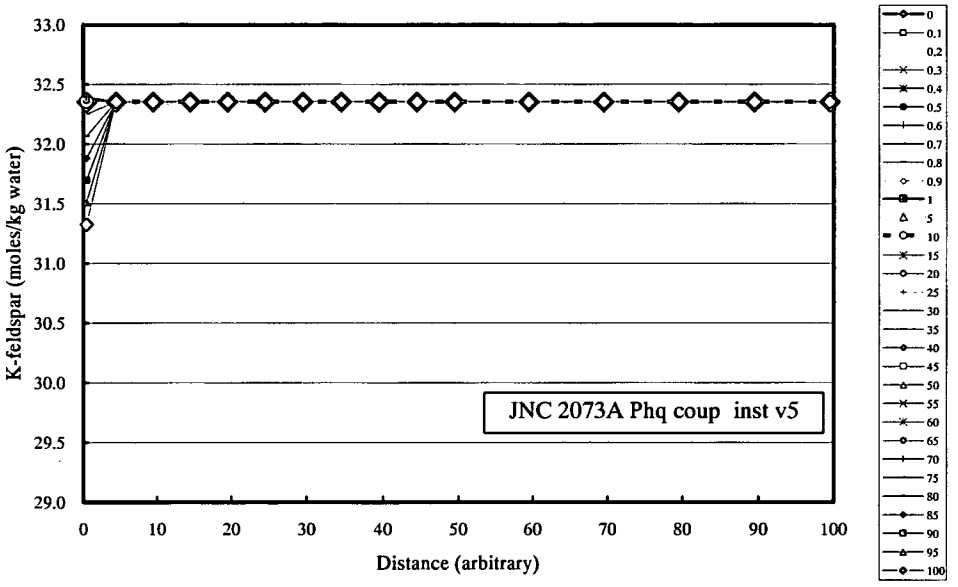

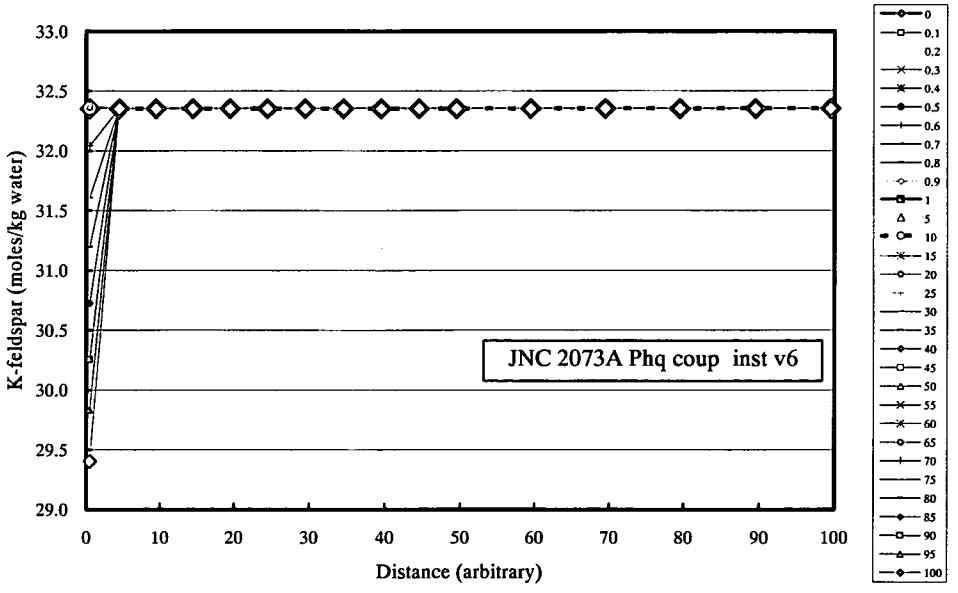

Variations in albite abundances calculated by the three PHREEQC simulations

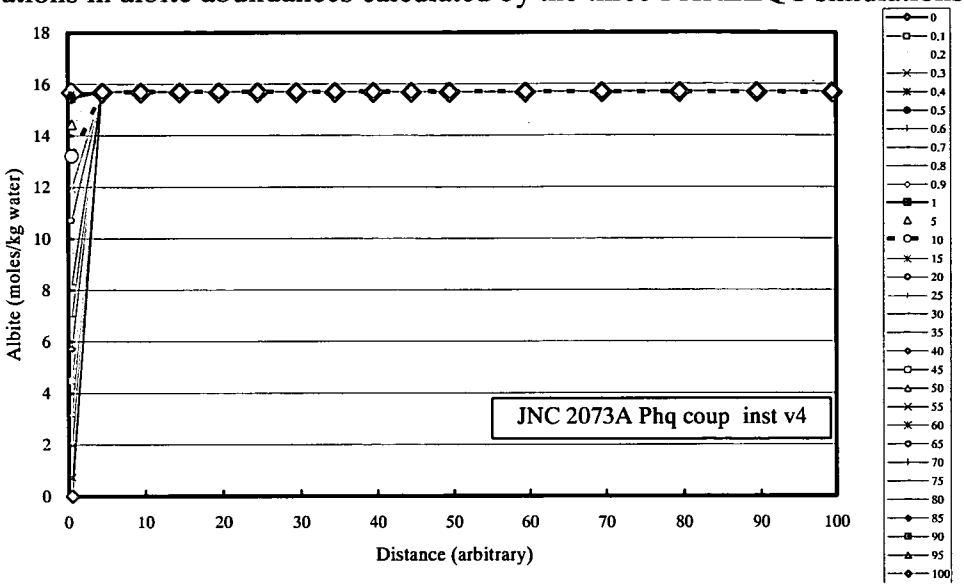

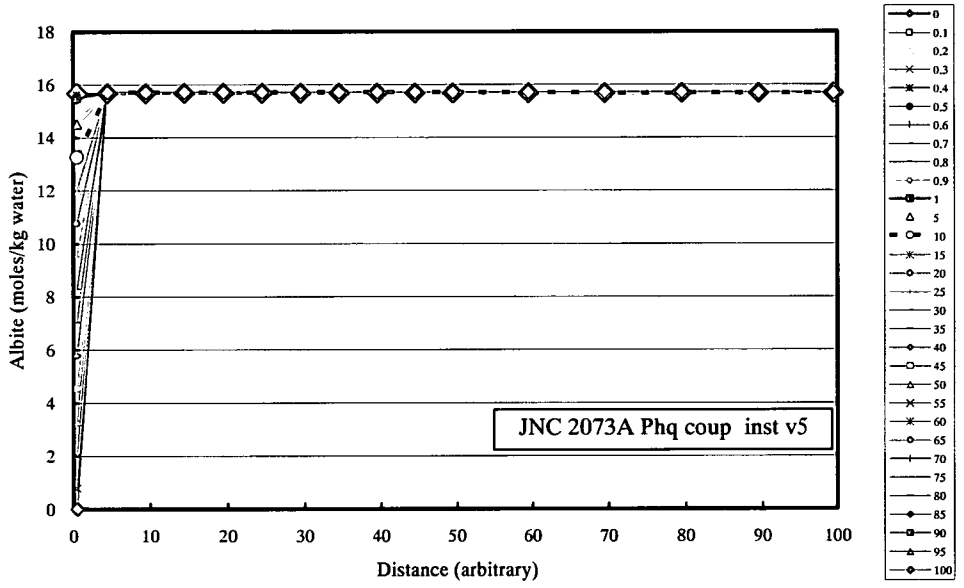

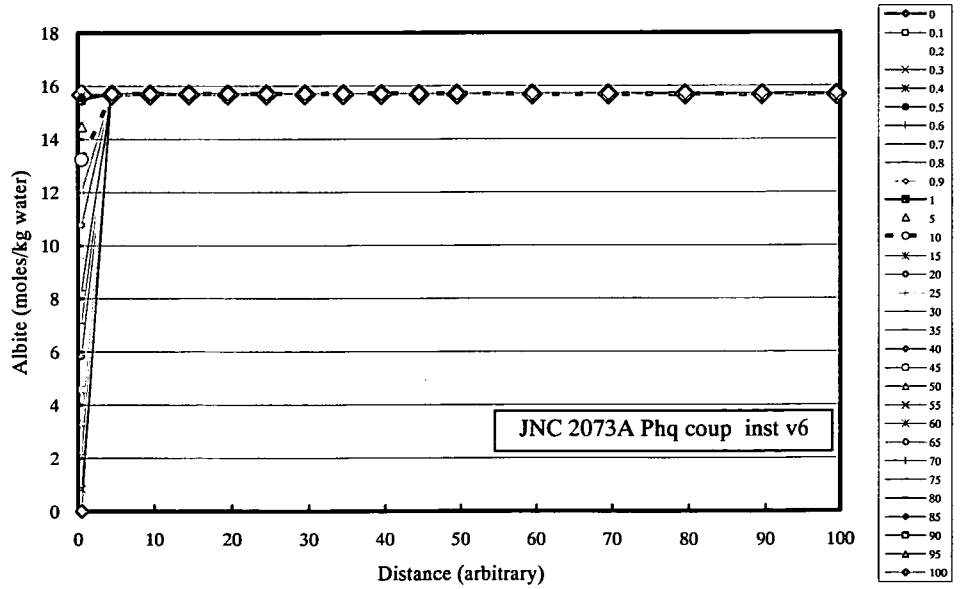

Variations in anorthite abundances calculated by the three PHREEQC simulations

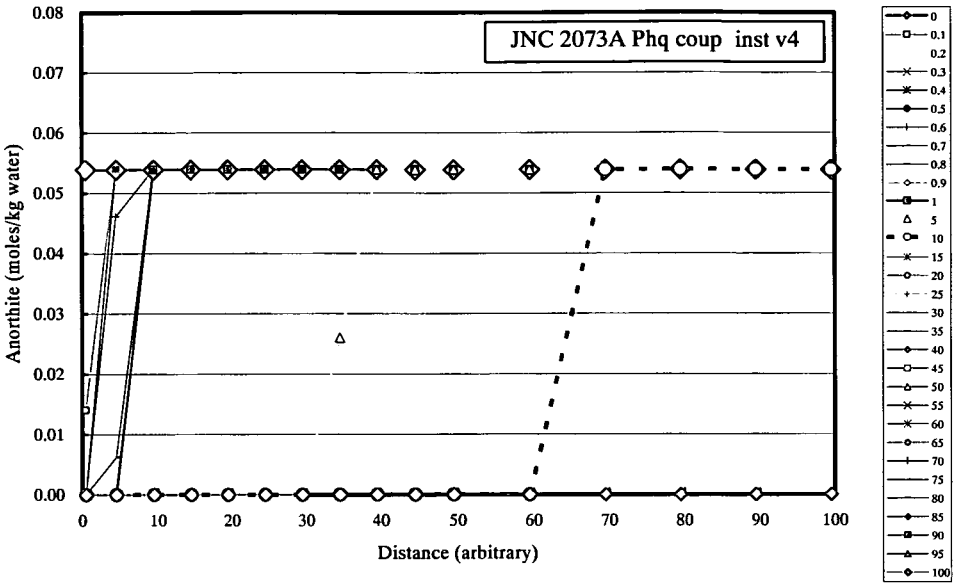

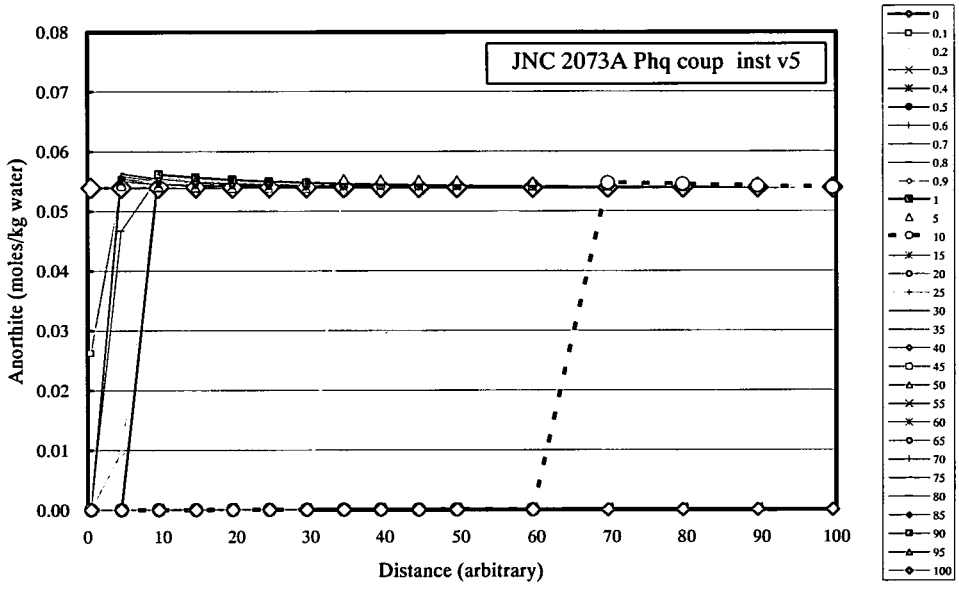

Fractional travel time

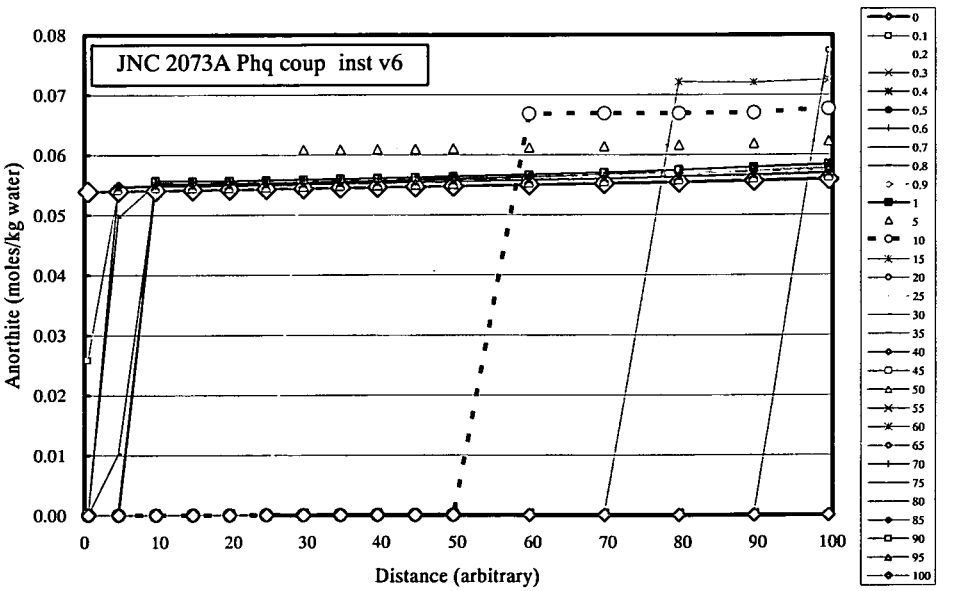

Variations in phlogopite abundances calculated by the three PHREEQC simulations

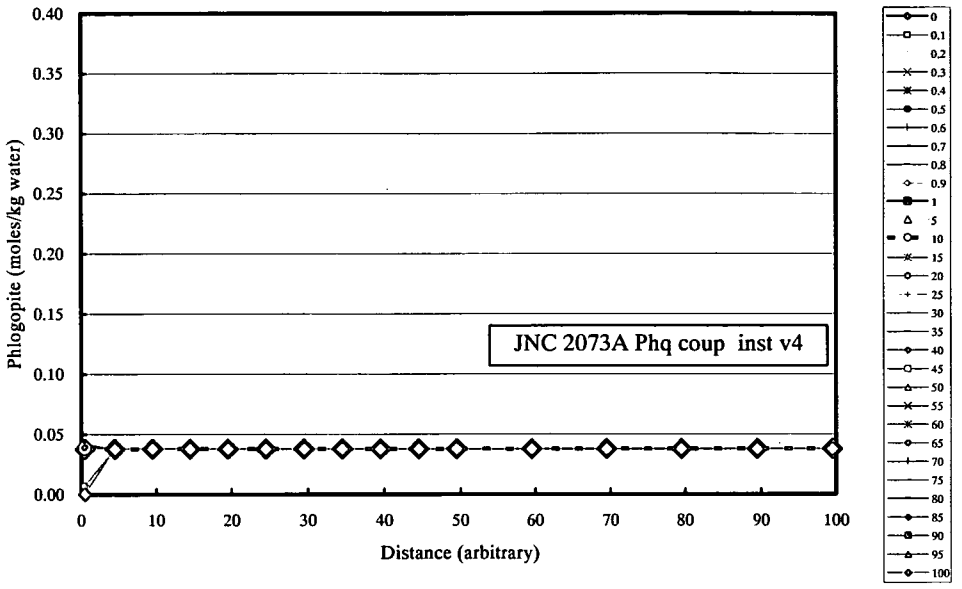

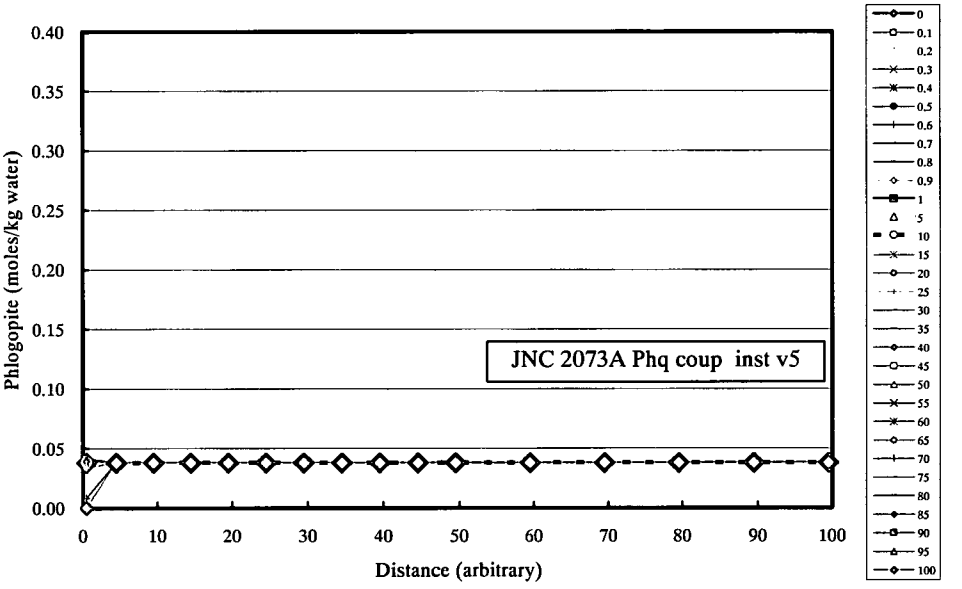

Fractional travel time

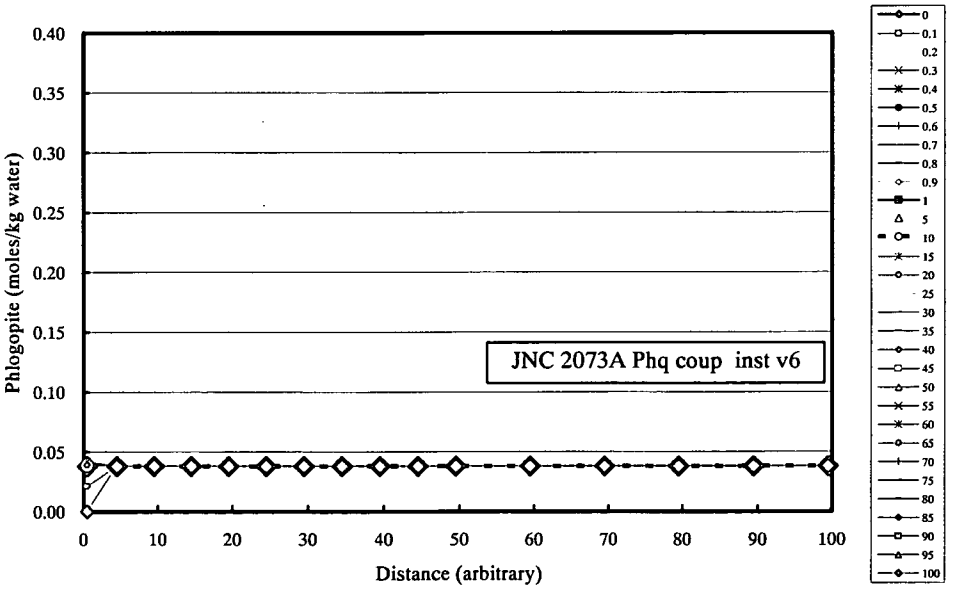

Variations in annite abundances calculated by the three PHREEQC simulations

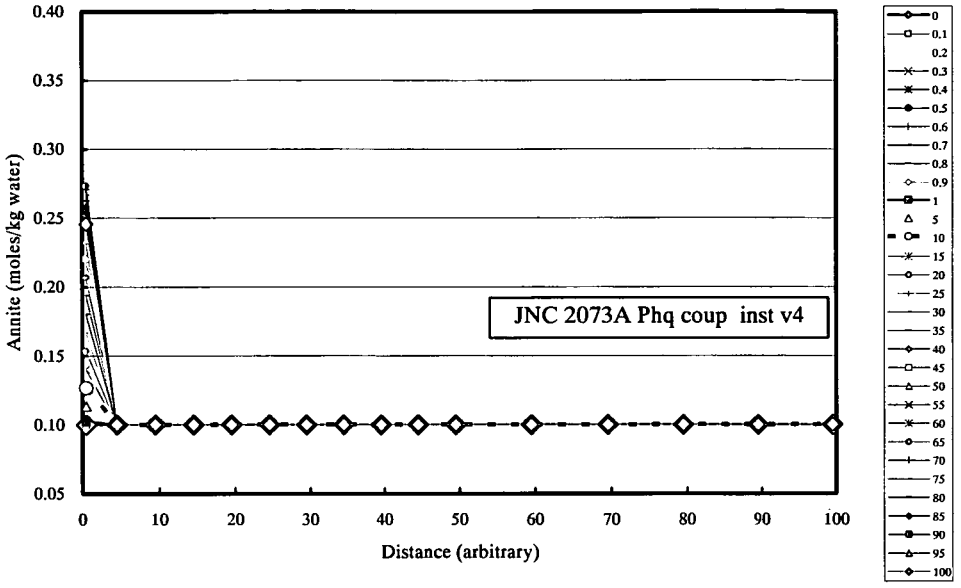

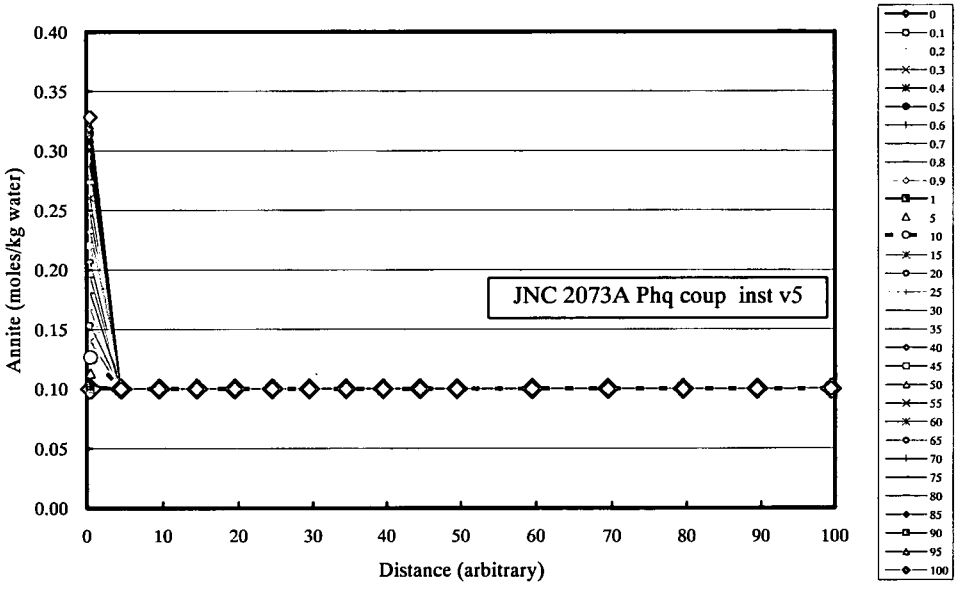

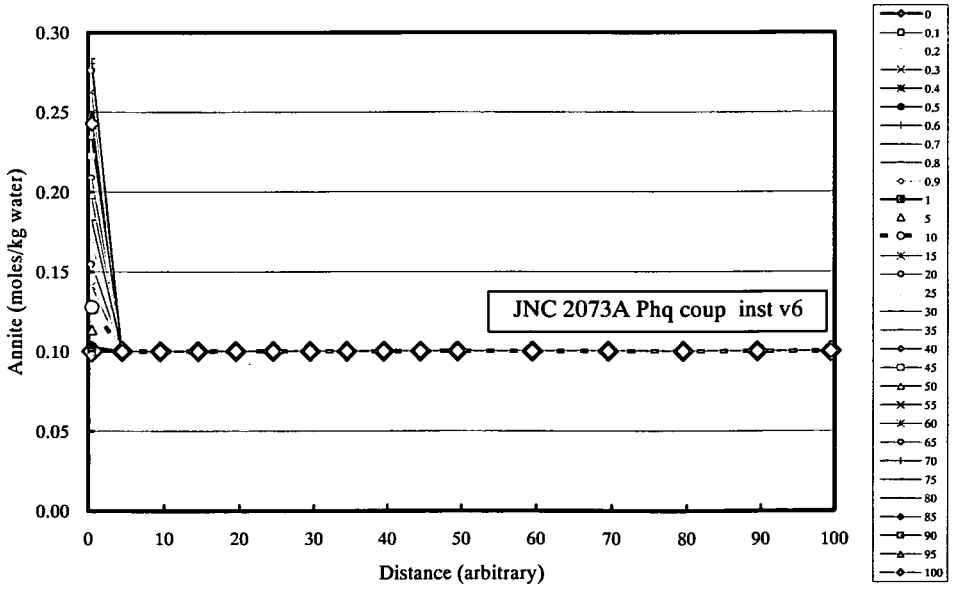

Variations in kaolinite abundances calculated by the three PHREEQC simulations

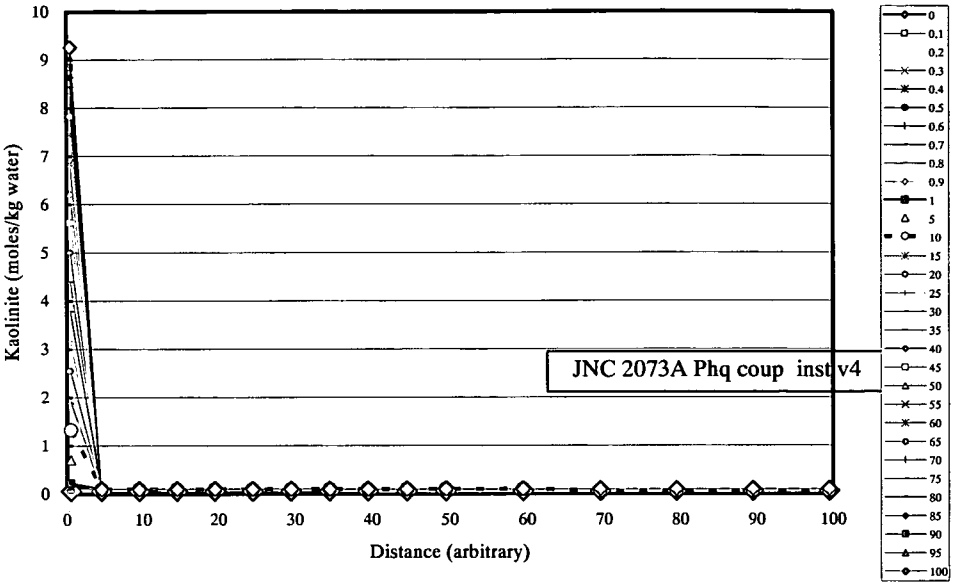

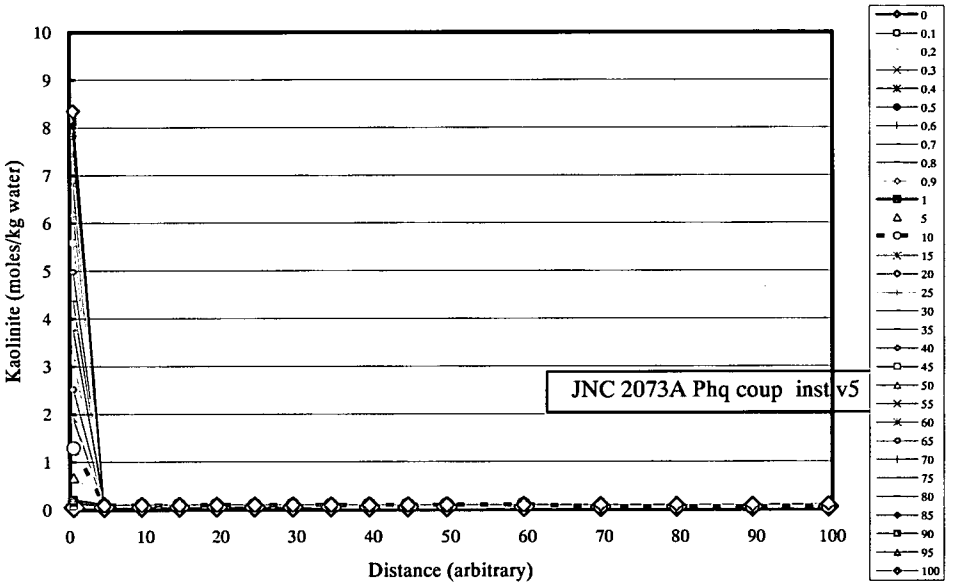

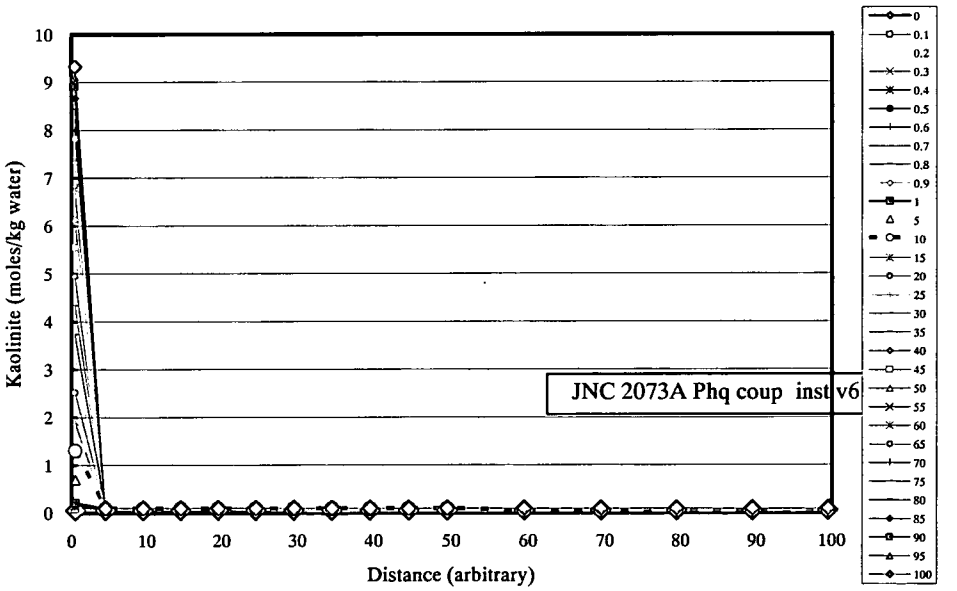

Variations in calcite abundances calculated by the three PHREEQC simulations

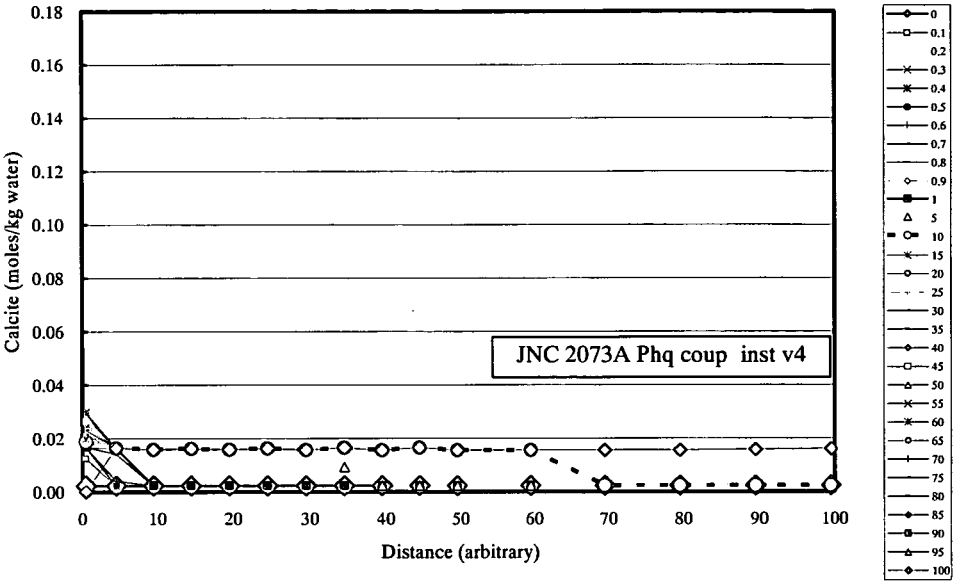

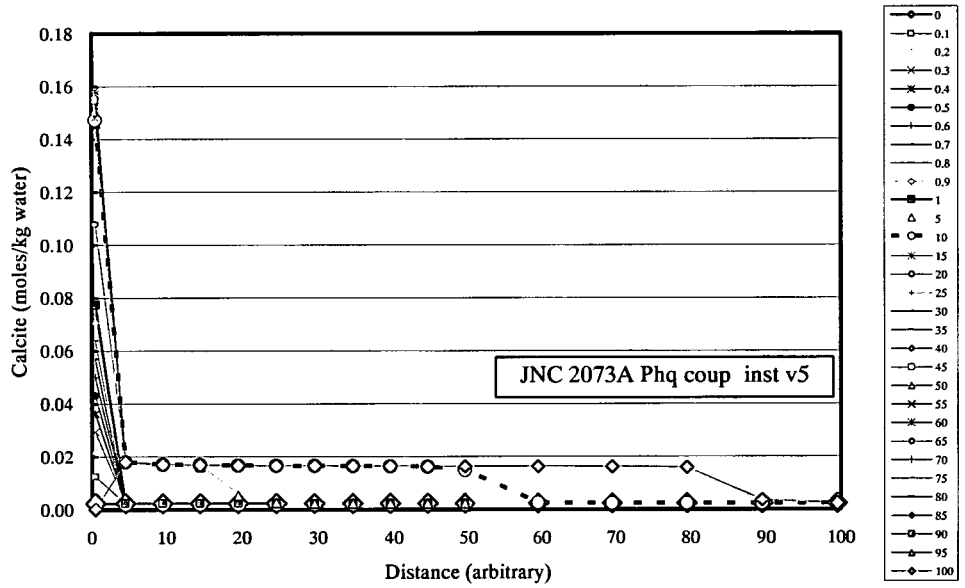

Fractional travel time

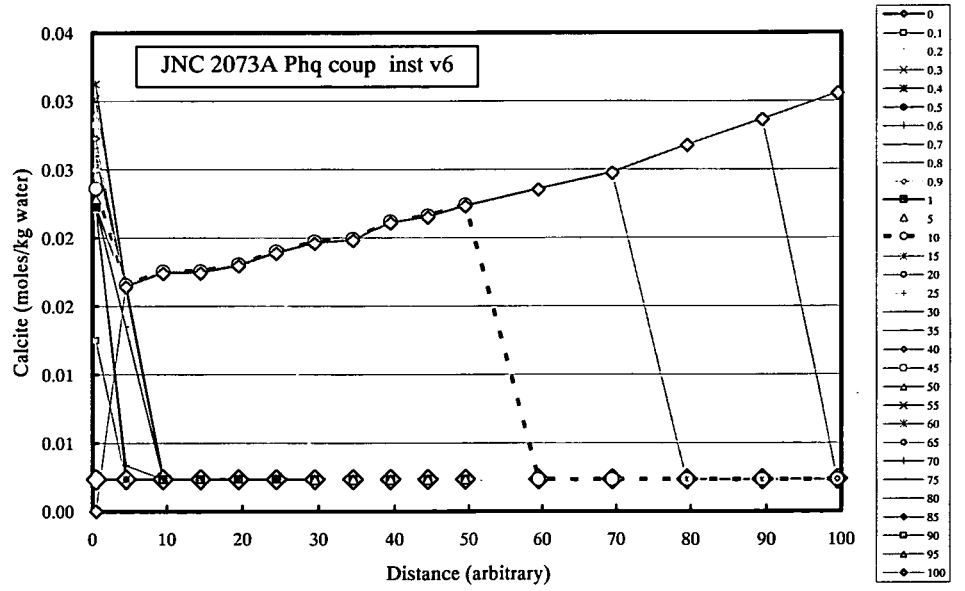

Variations in pyrite abundances calculated by the three PHREEQC simulations

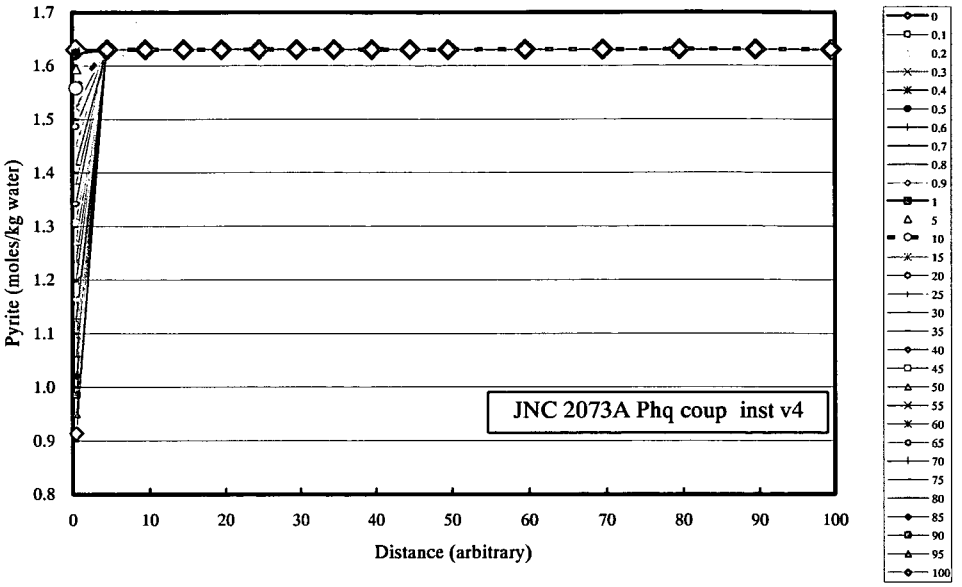

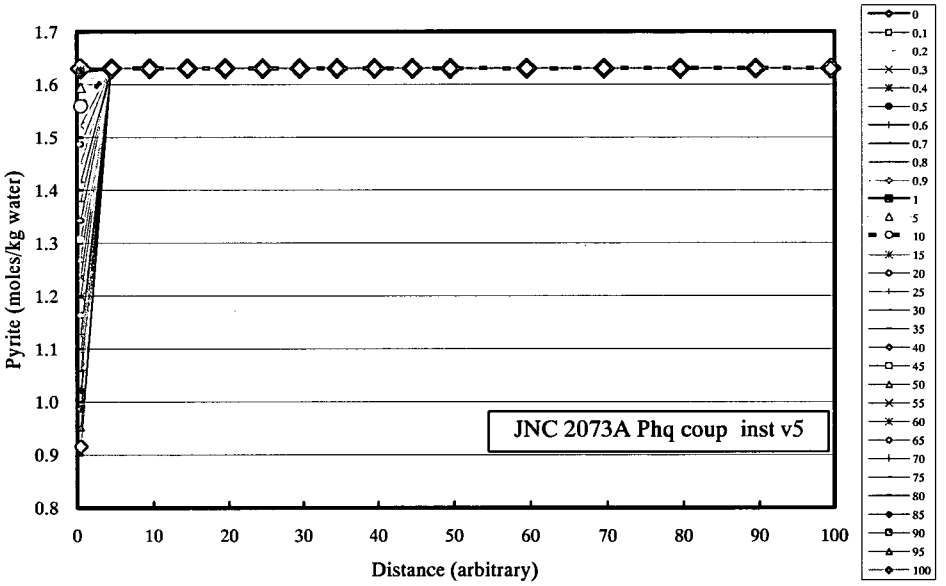

Fractional travel time

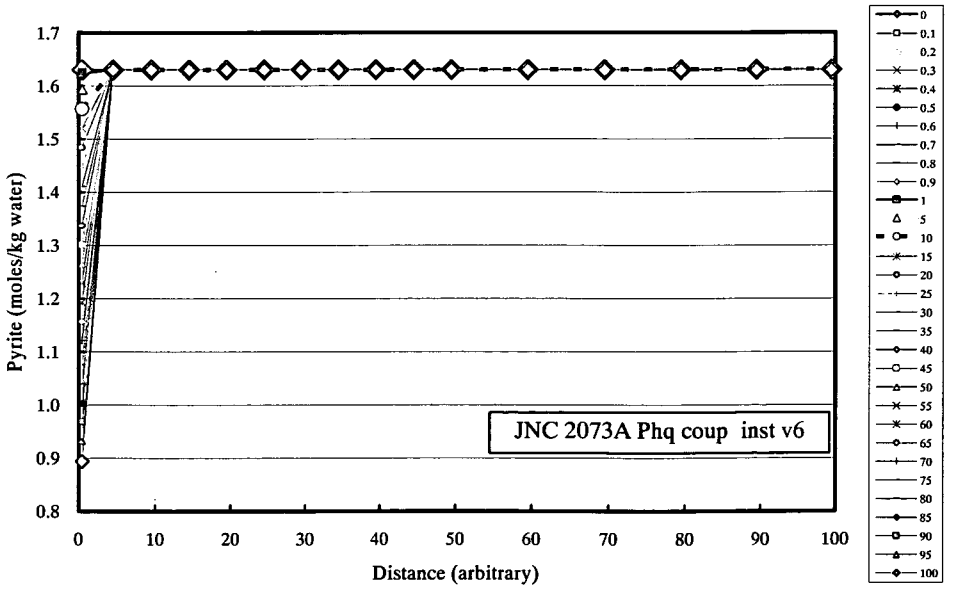

Variations in total Ca concentrations calculated by the three PHREEQC simulations

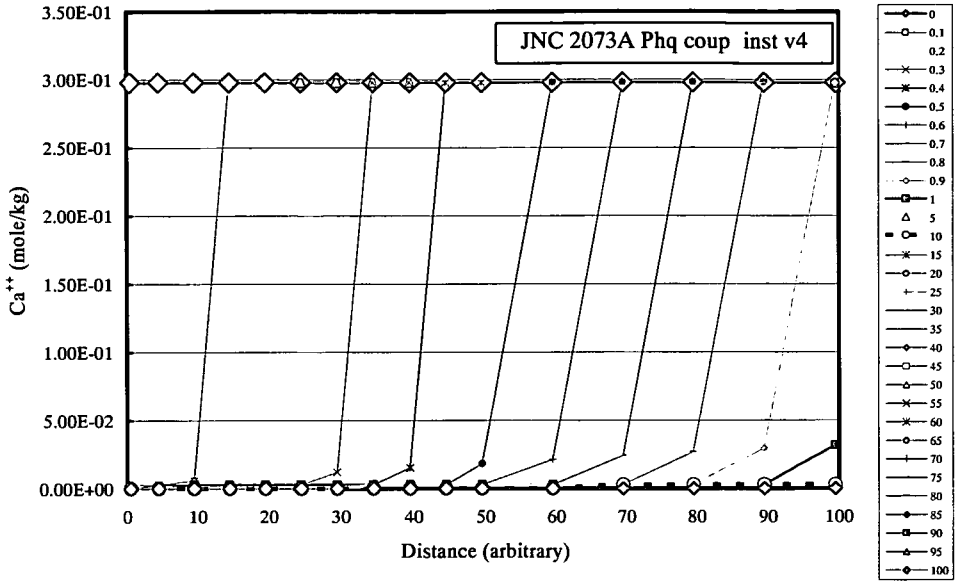

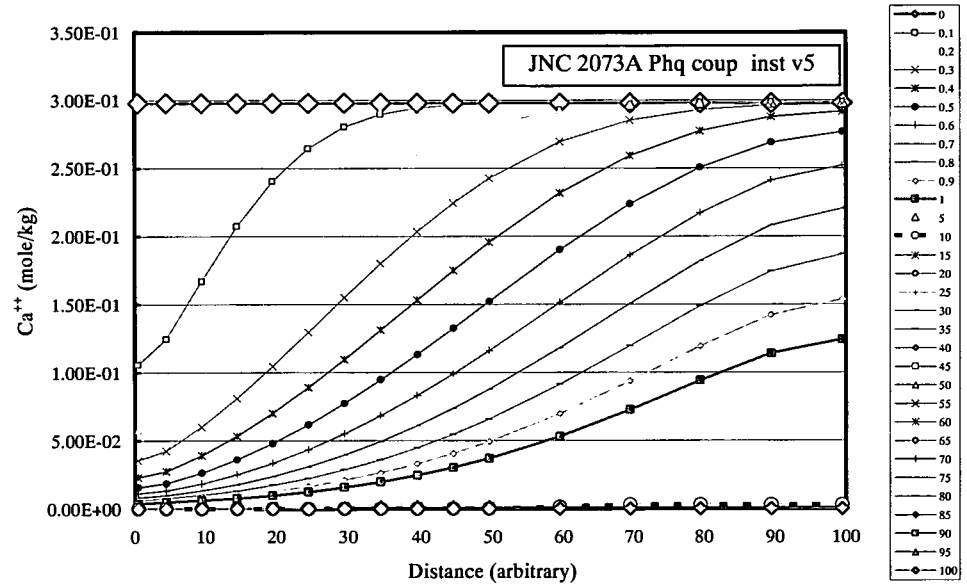

Fractional travel time

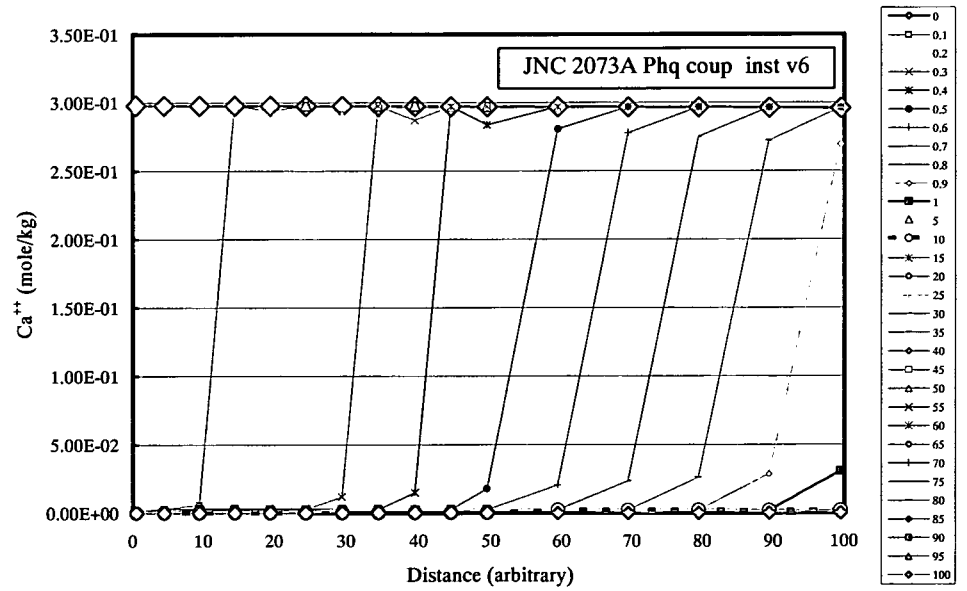

Variations in total Cl concentrations calculated by the three PHREEQC simulations

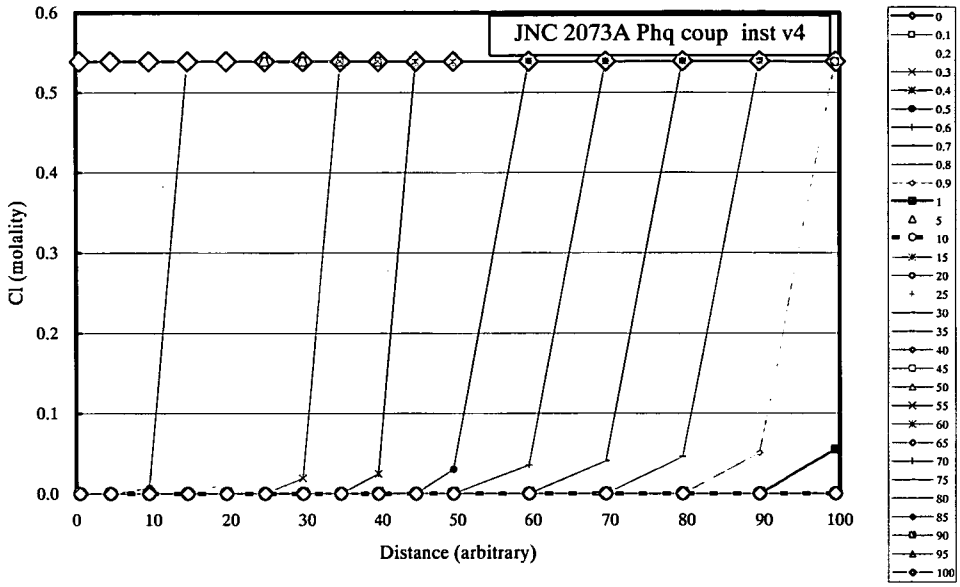

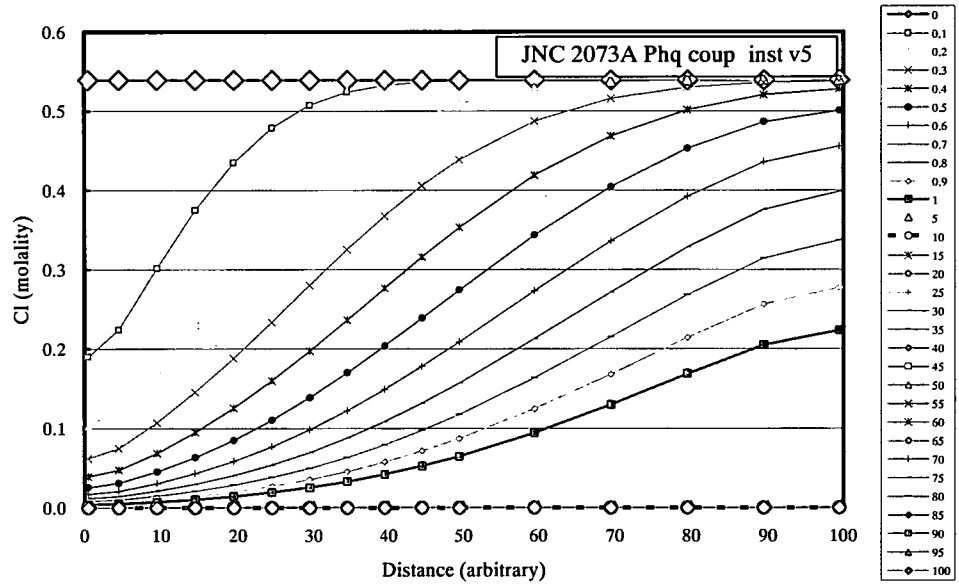

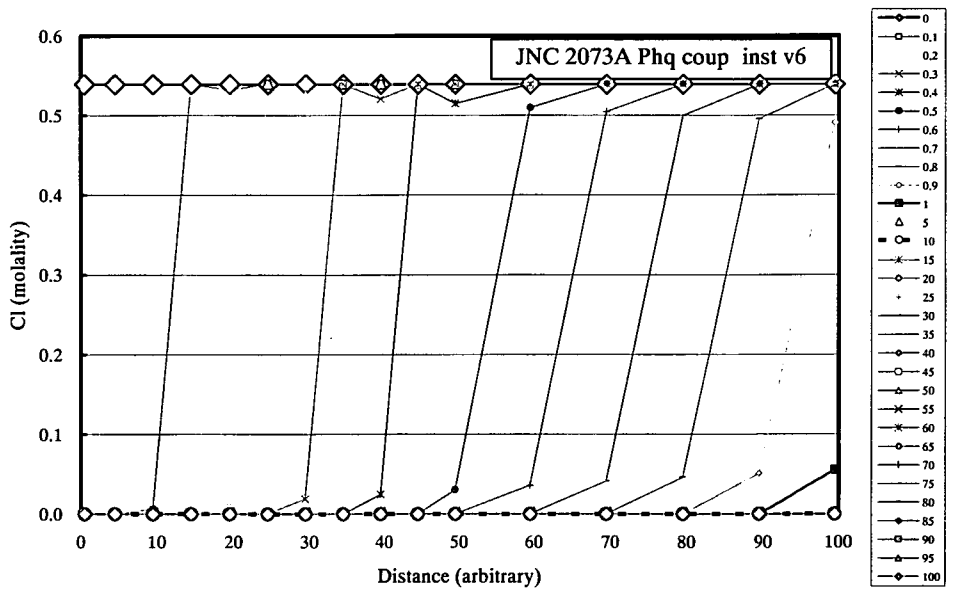

Dependency of pH and CO_2(g) fugacity calculated by PHREEQC

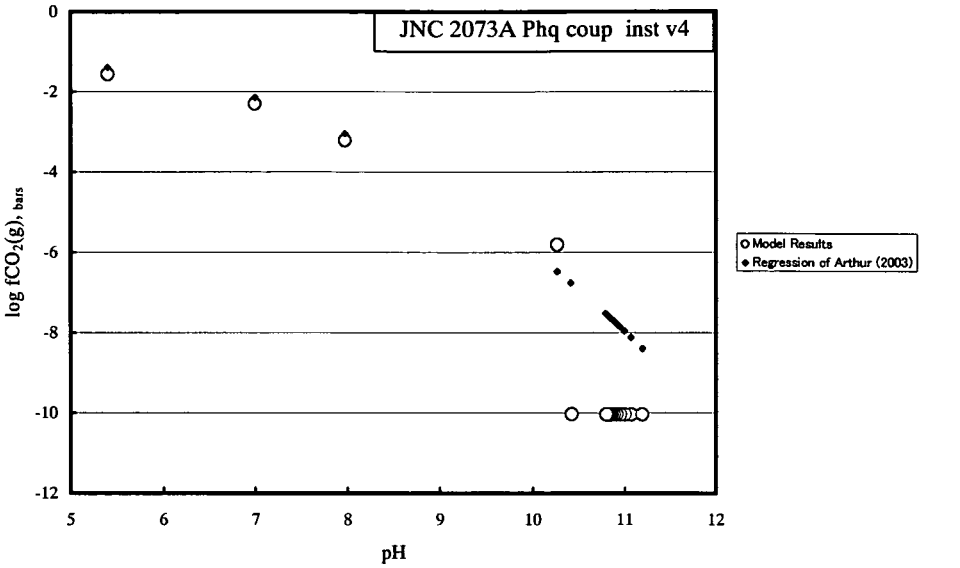

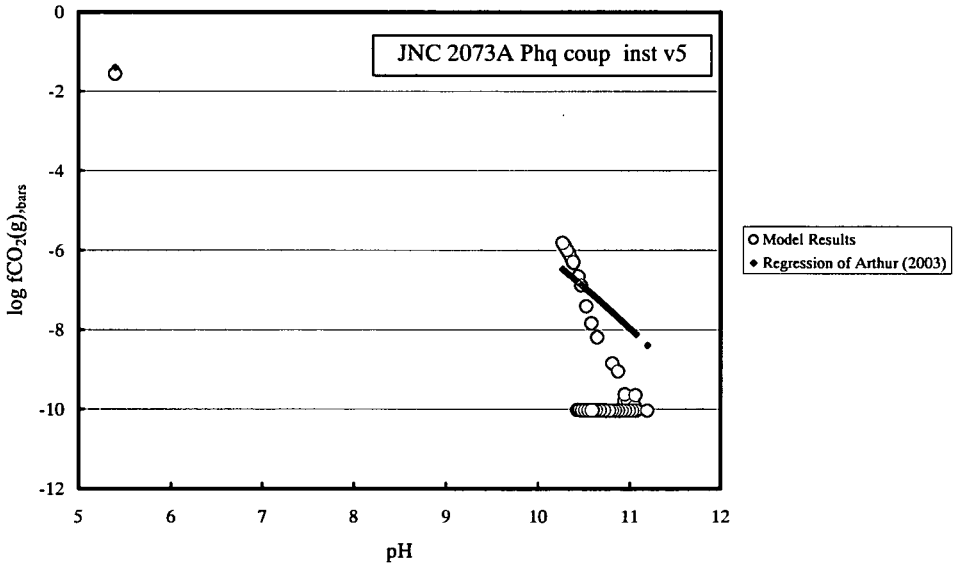

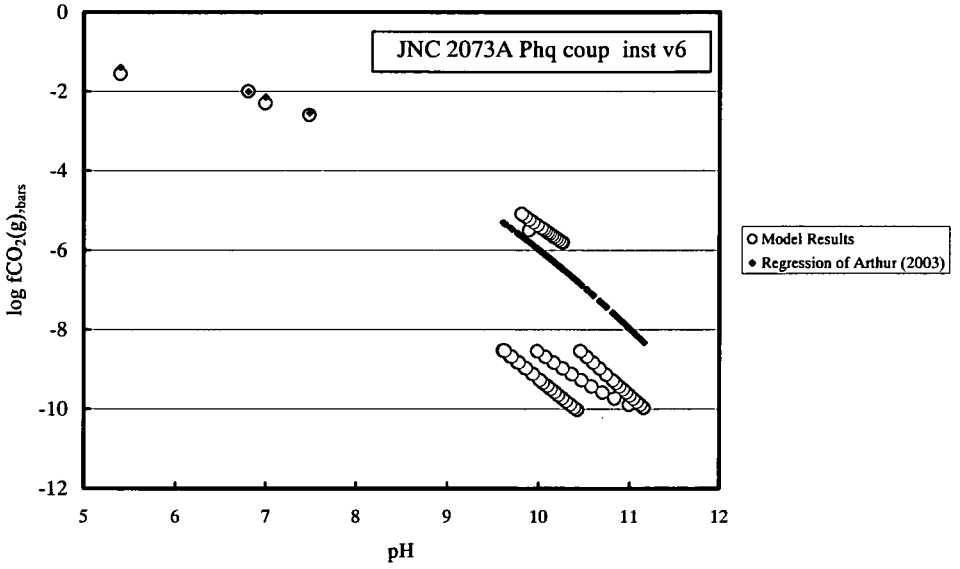

Variations in pH calculated by the three PHREEQC simulations

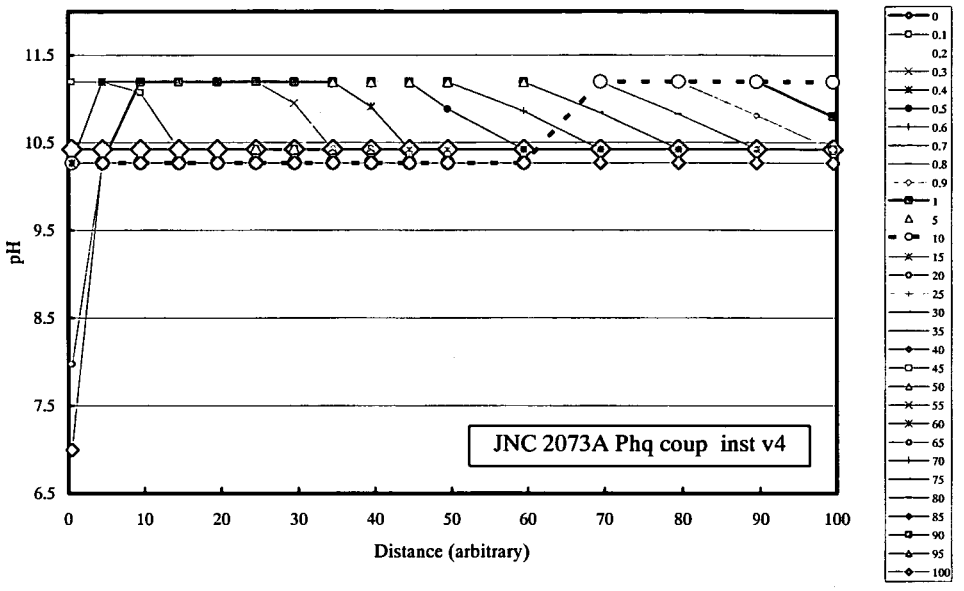

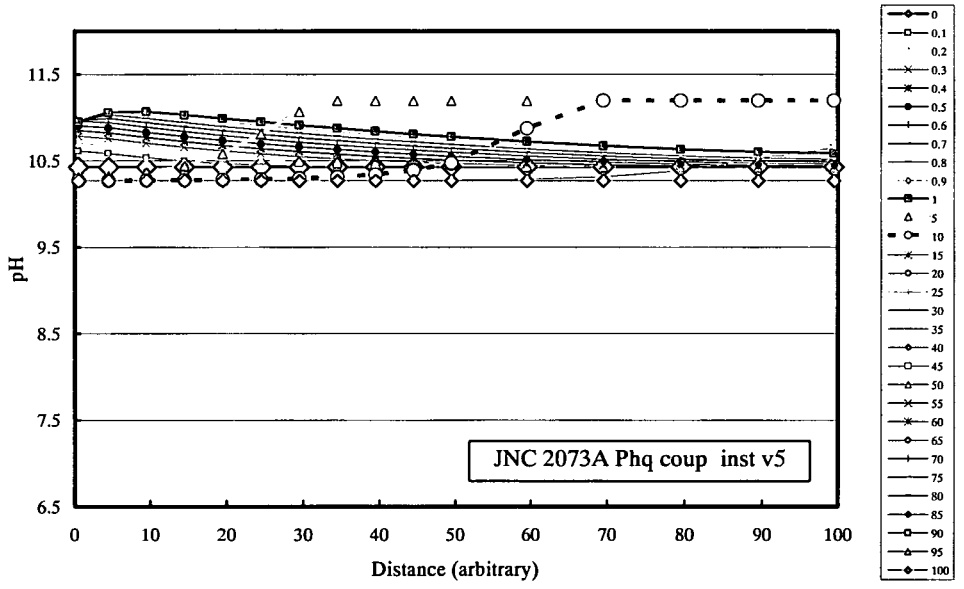

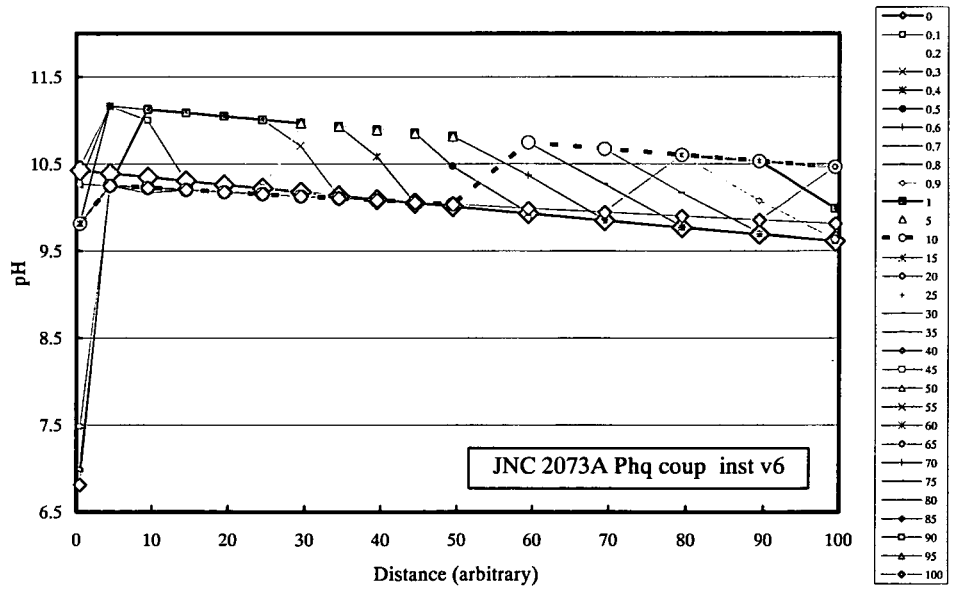

Variations in $CO_2(g)$ fugacity calculated by the three PHREEQC simulations

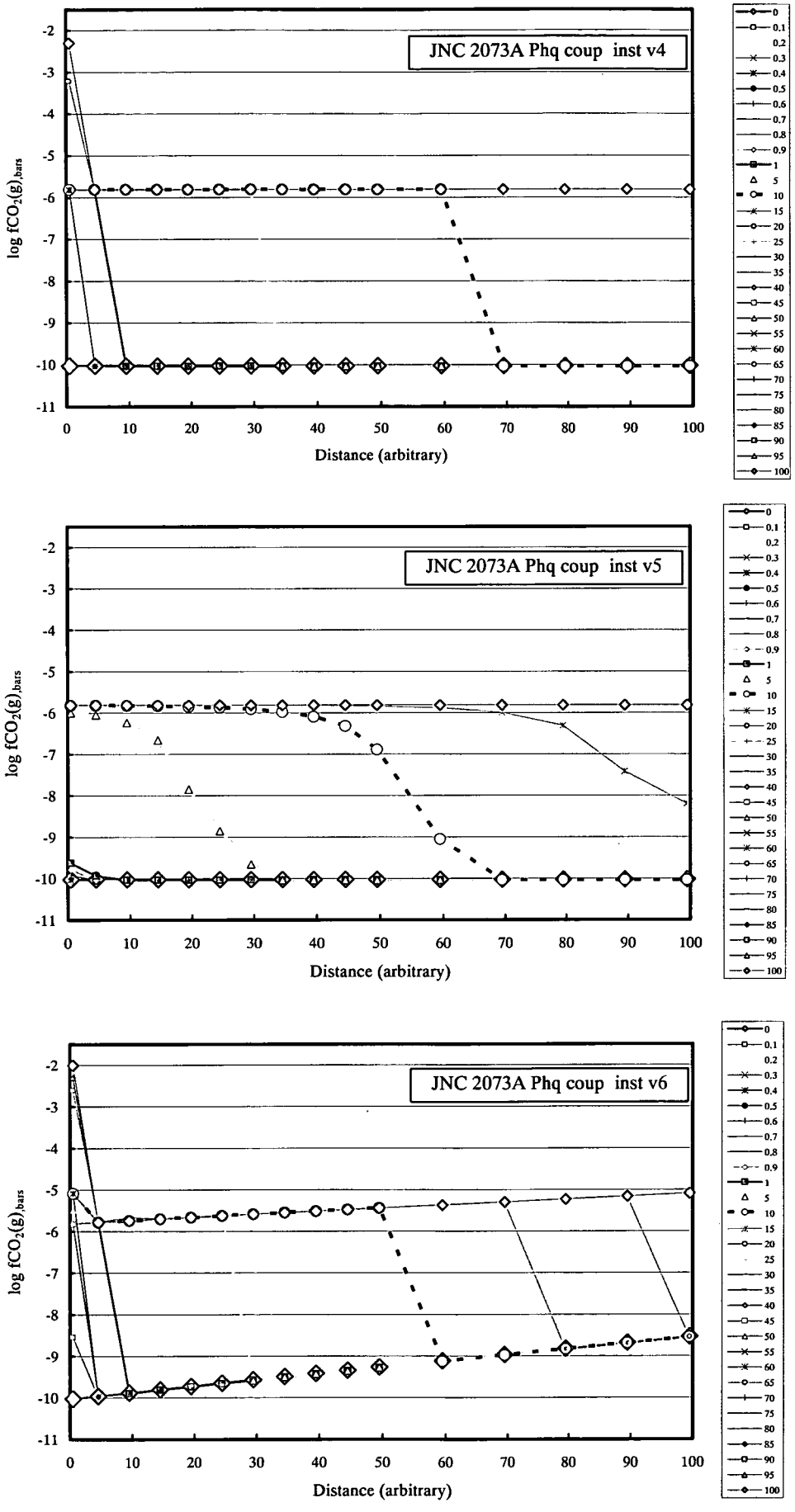

Variations in hematite saturation index calculated by the three PHREEQC simulations

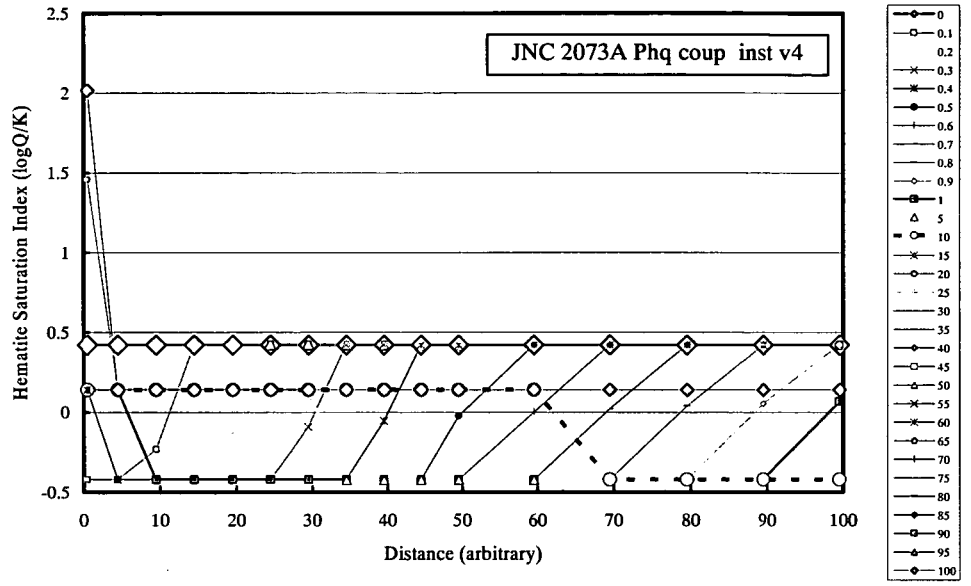

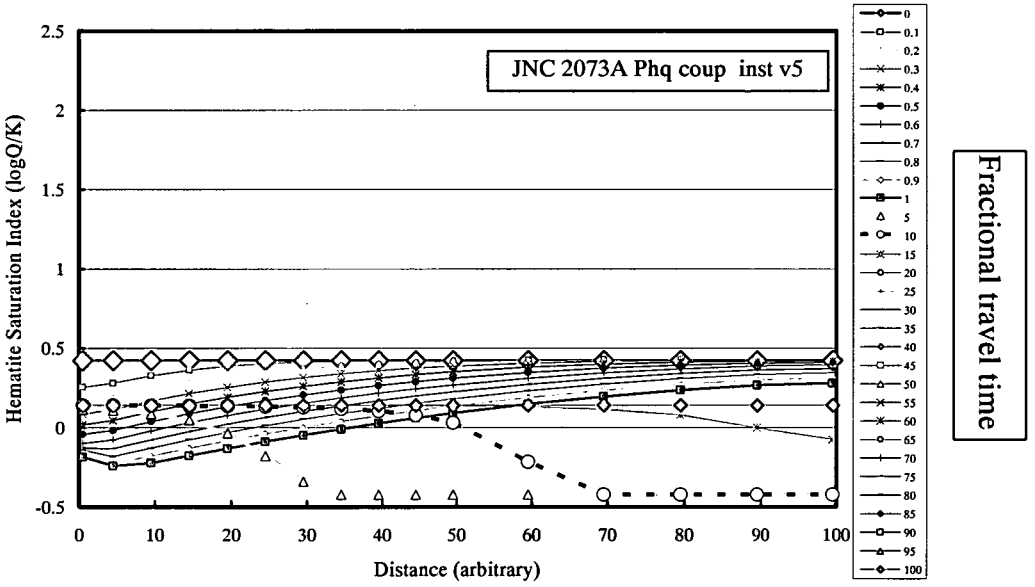

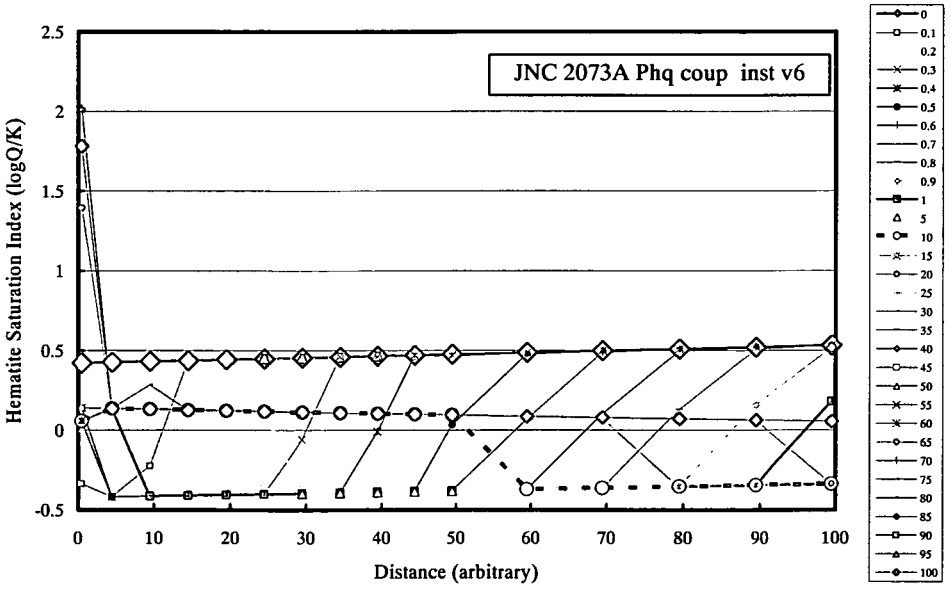

Table A1.2. Summary of the coupled simulations undertaken using Raiden.

Simulation Number	No. of cells	Lengths of cells	Temperature	Dispersion	Diffusion coefficient	Hydraulic Conductivity	Head difference	Porosity	Primary minerals	Secondary minerals	Initial groundwater Chemistry	Recharge water chemistry
		m	°C	m	m^2y^{-1}	my^{-1}	m					
fwpCO2pH25Kav1	1	10000	25	0	3.15e-03	20.4	950	0.1	Quartz, Anorthite	Kaolinite	Fresh, reducing	Fresh, oxidising
fwpCO2pH25Kap01v1	1	10000	25	0	3.15e-03	20.4	950	0.01	Quartz, Anorthite	Kaolinite	Fresh, reducing	Fresh, oxidising
fwpCO2pH25v2	1	10000	25	0	3.16e-04	20.4	950	0.1	Quartz, Anorthite	Kaolinite	Fresh, reducing	Fresh, oxidising
fwpCO2pH25Kadfe5v1	1	10000	25	0	3.15e-05	20.4	950	0.01	Quartz, Anorthite	Kaolinite	Fresh, reducing	Fresh, oxidising
fwpCO2pH25Kah105v1	1	10000	25	0	3.15e-05	20.4	105	0.01	Quartz, Anorthite	Kaolinite	Fresh, reducing	Fresh, oxidising
fwpCO2pH25Kak1.7v1	1	10000	25	0	3.15e-05	1.79	105	0.01	Quartz, Anorthite	Kaolinite	Fresh, reducing	Fresh, oxidising
fwpCO2pH25PhMmv1	1	10000	25	0	3.15e-05	1.79	105	0.01	Quartz, Anorthite, Phlogopite	Ca-Montmorillonite	Fresh, reducing	Fresh, oxidising
fwpCO2pH25PhMmv1a	1	10000	25	0	3.15e-05	1.79	105	0.01	Quartz, Anorthite, Phlogopite	Ca-Montmorillonite, Calcite	Fresh, reducing	Fresh, oxidising
fwpCO2pH25Lmd100v1	1	10000	25	100	3.15e-05	1.79	105	0.01	Quartz, Anorthite	Laumontite	Fresh, reducing	Fresh, oxidising
fwpCO2pH25Kad100	1	10000	25	100	3.15e-05	1.79	105	0.01	Quartz, Anorthite	Kaolinite	Fresh, reducing	Fresh, oxidising
fwpCO2pH25Kad100a	1	10000	25	100	3.15e-05	1.79	105	0.01	Quartz, Anorthite	Kaolinite, Calcite	Fresh, reducing	Fresh, oxidising
fwpCO2pH60Kad100v1	1	10000	60	100	3.15e-05	1.79	105	0.01	Quartz, Anorthite	Kaolinite	Fresh, reducing	Fresh, oxidising

Table A1.2. Continued.

Simulation Number	No. of cells	Lengths of cells	Temperature	Dispersion	Diffusion coefficient	Hydraulic Conductivity	Head difference	Porosity	Primary minerals	Secondary minerals	Initial groundwater Chemistry	Recharge water chemistry
		m	°C	m	m^2y^{-1}	my^{-1}	m					
fwpCO2pH60Kad100v1a	1	10000	60	100	3.15e-05	1.79	105	0.01	Quartz, Anorthite	Kaolinite, Calcite	Fresh, reducing	Fresh, oxidising
fwpCO2pH 25Ka 10 c 270803v1	10	1000	25	100	3.15e-05	1.79	105	0.01	Quartz, Anorthite	Kaolinite	Fresh, reducing	Fresh, oxidising
fwpCO2pH 25Ka 10 c 270803v1a	10	1000	25	100	3.15e-05	1.79	105	0.01	Quartz, Anorthite	Kaolinite, Calcite	Fresh, reducing	Fresh, oxidising
swpCO2pH 25Ka 10 c 270803v2	10	1000	25	100	3.15e-05	1.79	105	0.01	Quartz, Anorthite	Kaolinite	Saline, modified seawater	Fresh, oxidising
swpCO2pH 25Ka 10 c 270803v2a	10	1000	25	199	3.15e-05	1.79	105	0.01	Quartz, Anorthite	Kaolinite, Calcite	Saline, modified seawater	Fresh, oxidising
a28cv2	28	1st 20 cells 100 m, then 8 cells of 1000 m	25	100	3.15e-05	1.79	105	0.01	Quartz, Anorthite	Kaolinite, Calcite	Saline, modified seawater	Fresh, oxidising

Output from simulation fwpCO2pH25Kav1

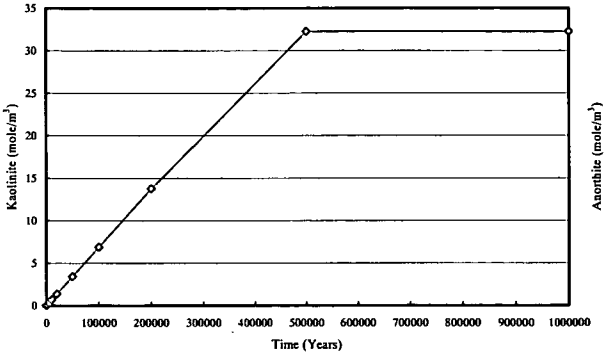

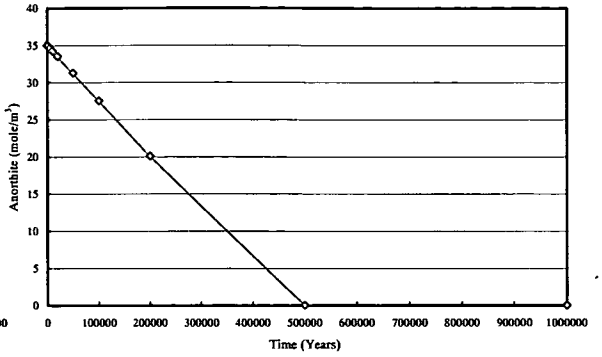

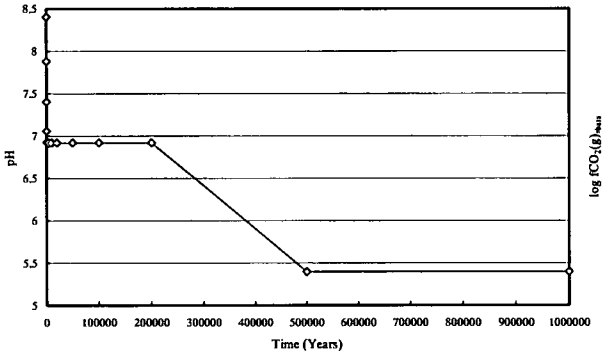

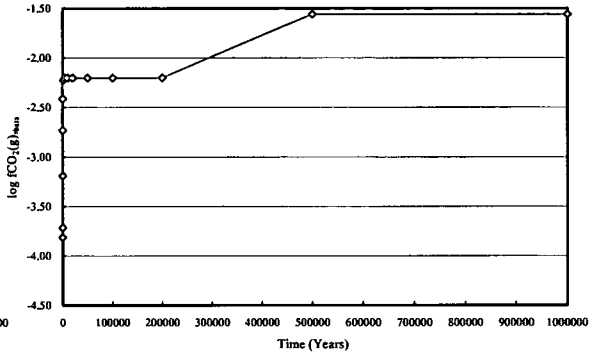

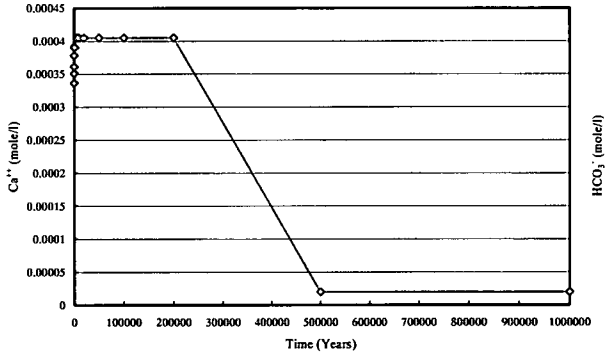

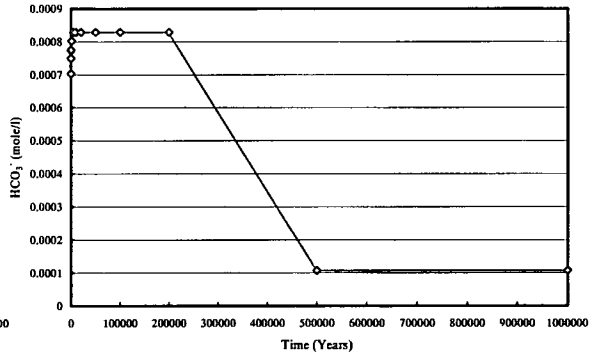

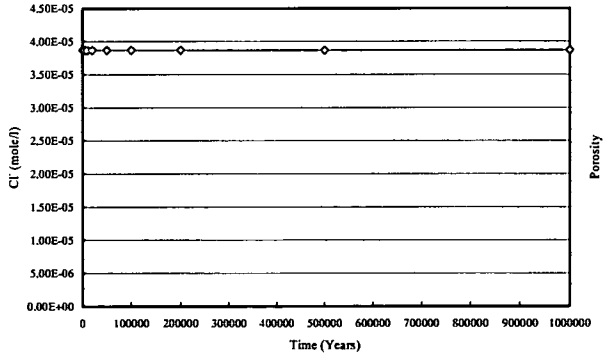

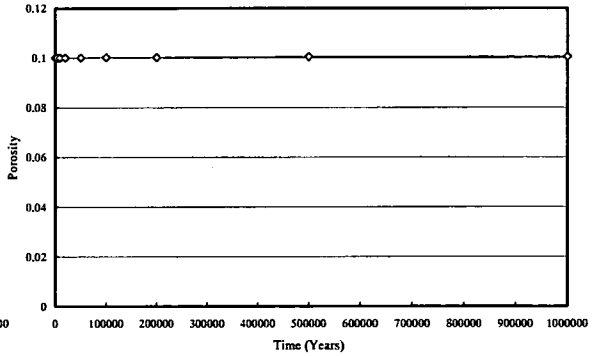

Output from simulation fwpCO2pH25Kap01v1

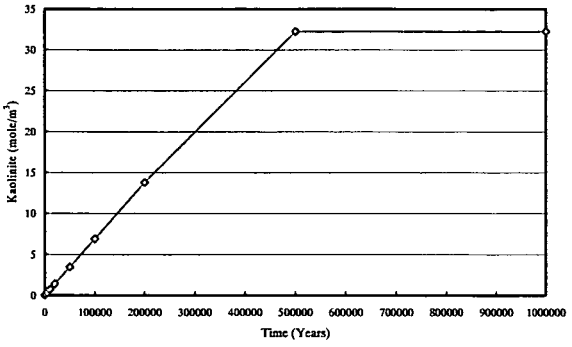

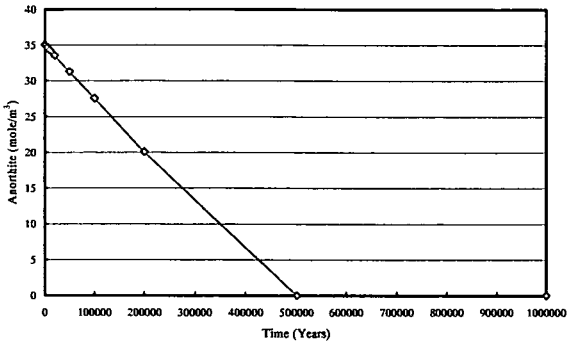

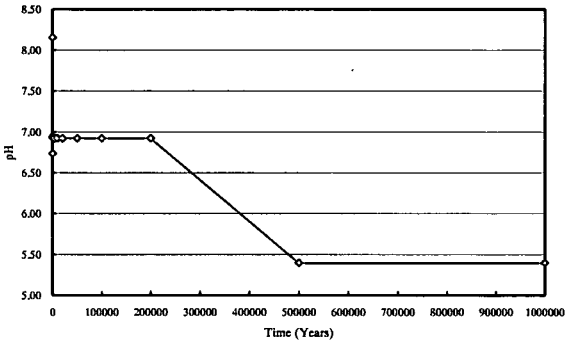

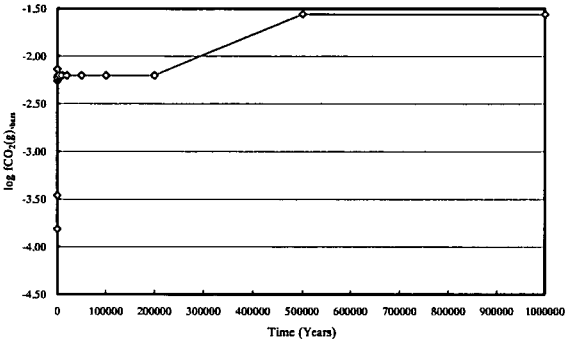

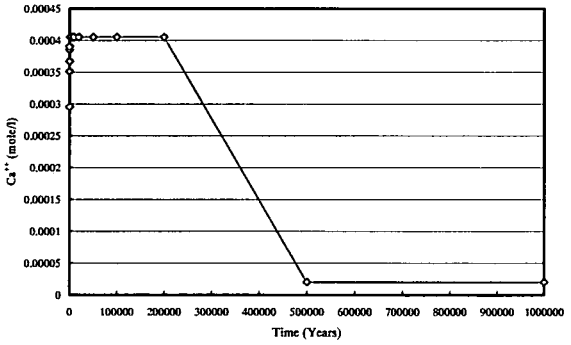

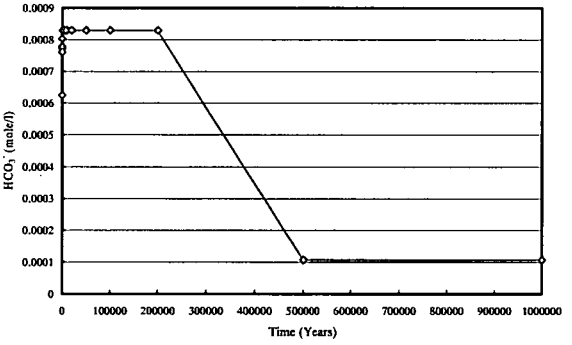

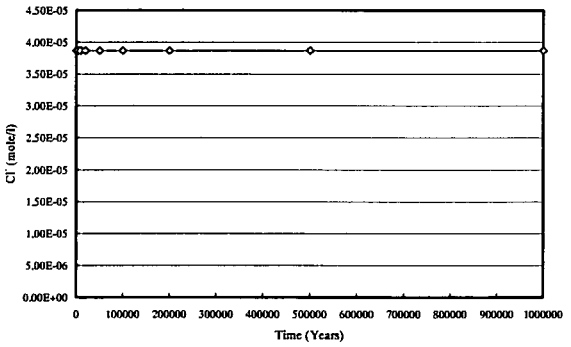

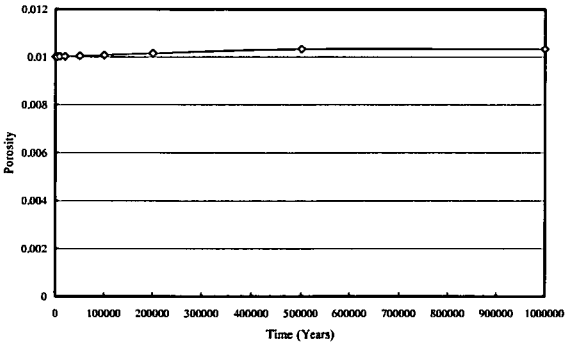

Output from simulation fwpCO2pH25v2

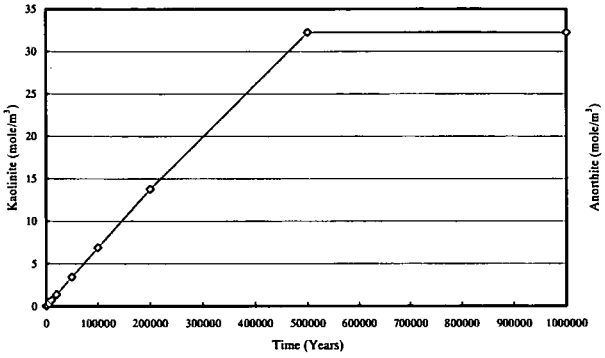

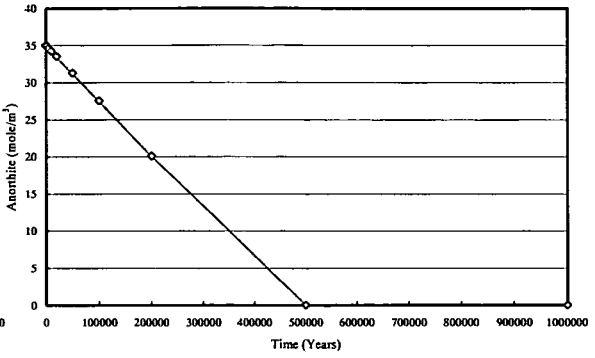

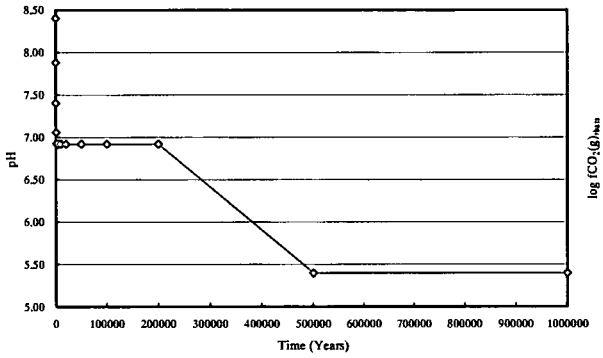

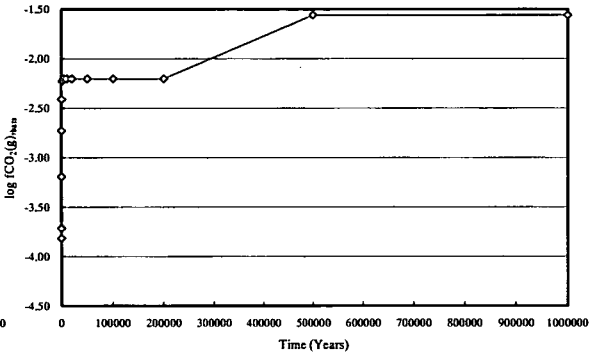

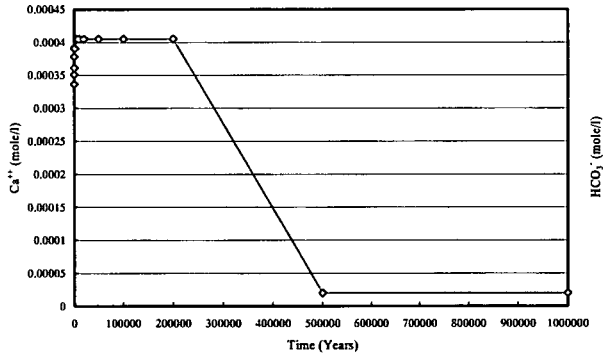

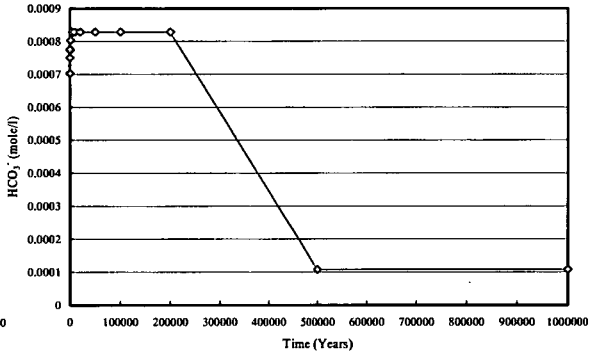

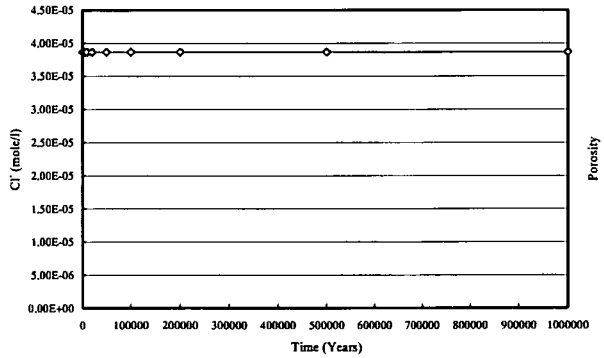

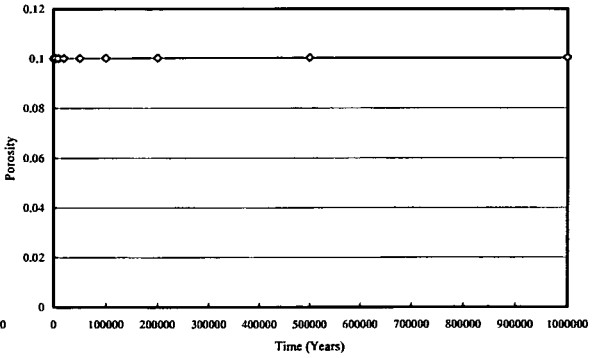

Output from simulation fwpCO2pH25Kadfe5v1

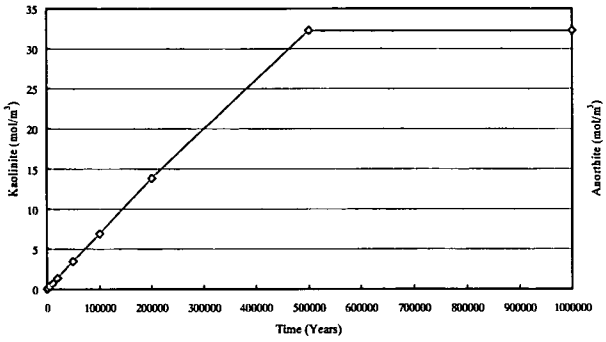

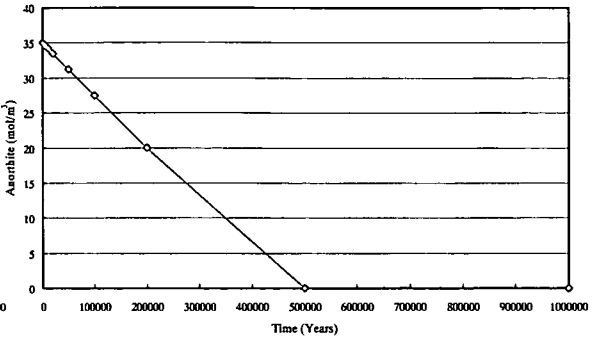

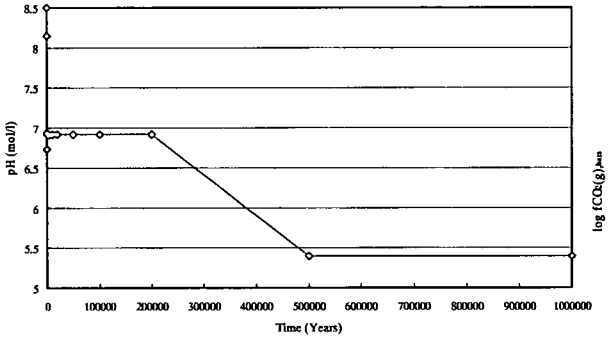

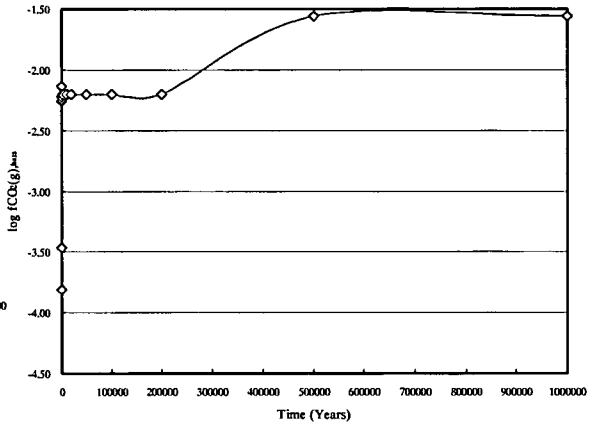

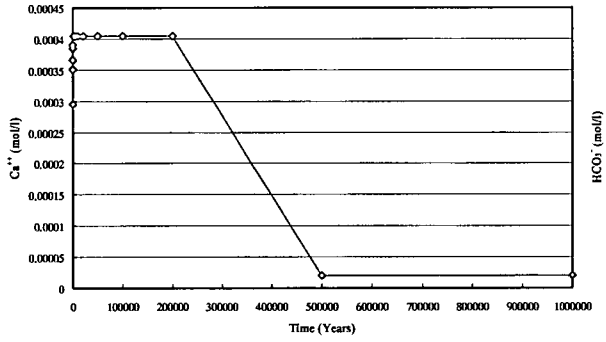

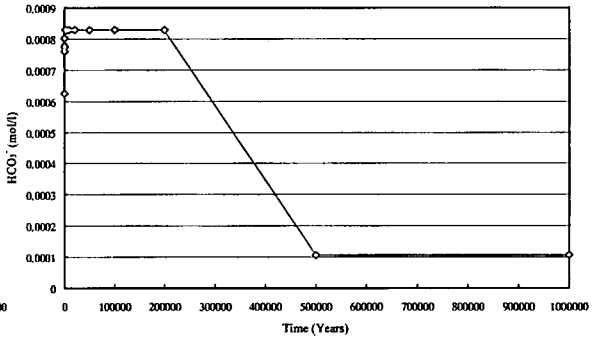

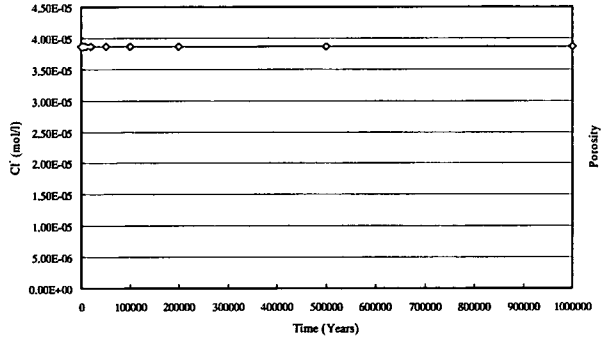

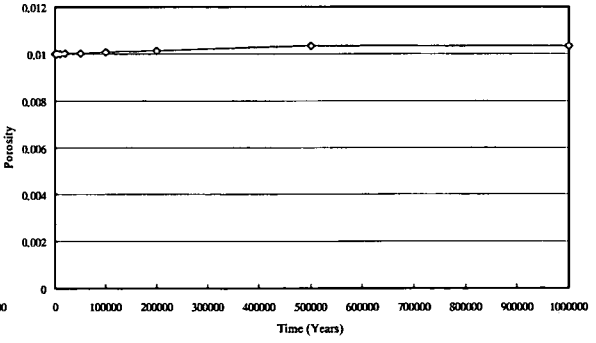

Output from simulation fwpCO2pH25Kah105v1

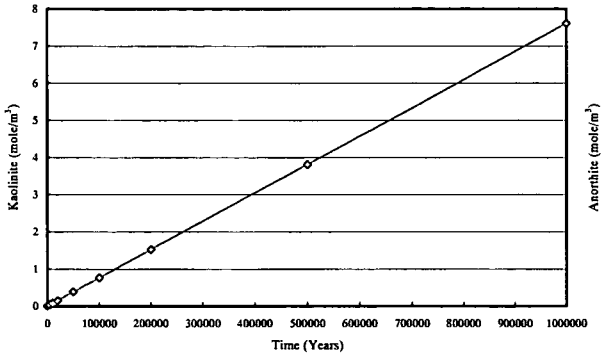

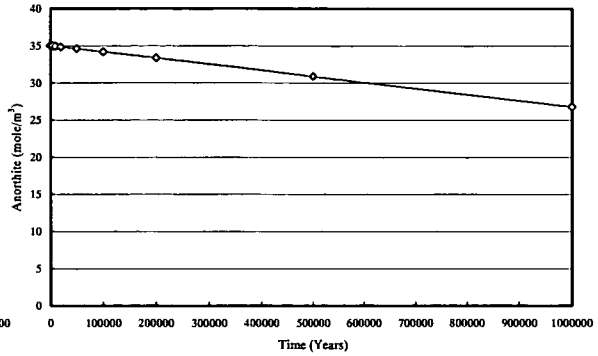

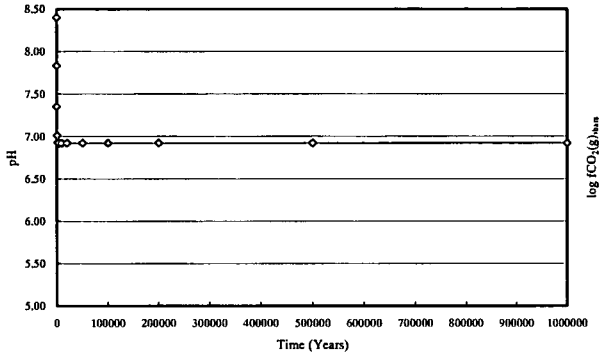

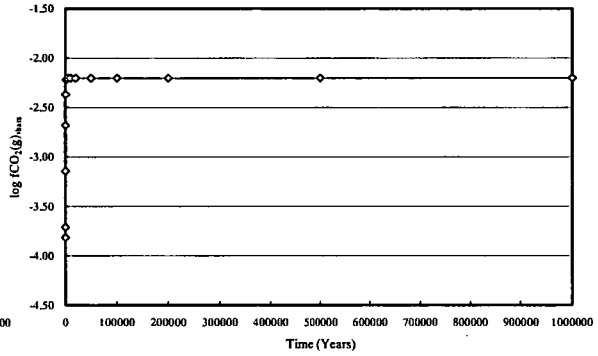

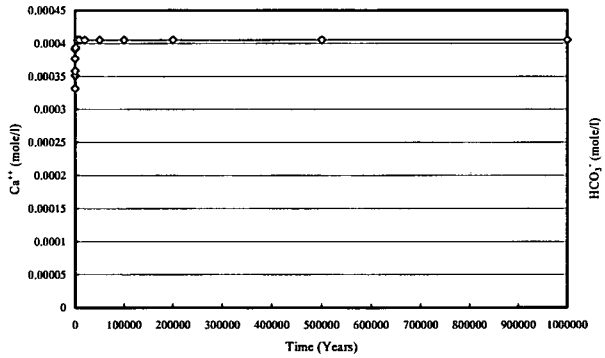

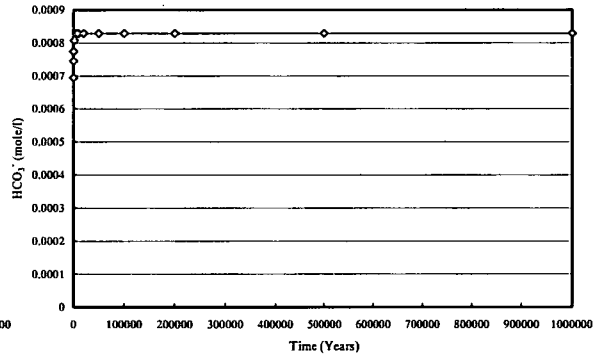

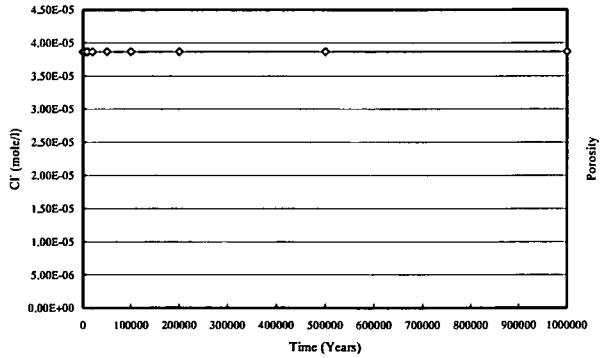

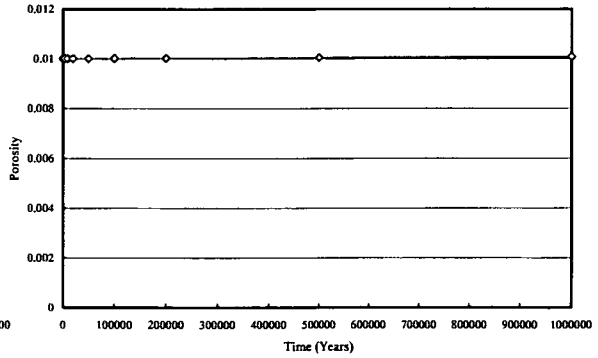

Output from simulation fwpCO2pH25Kak1.7v1

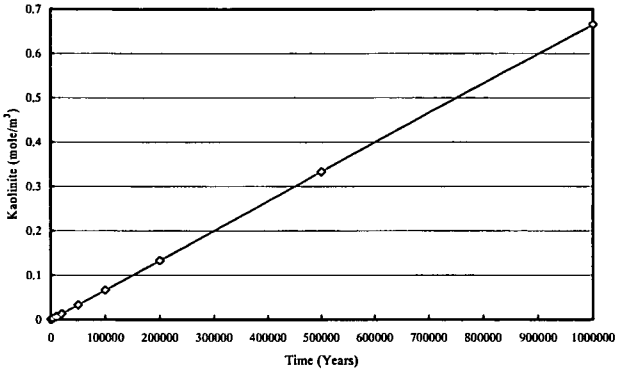

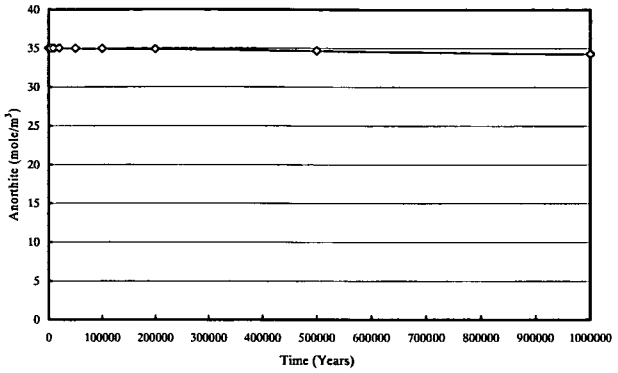

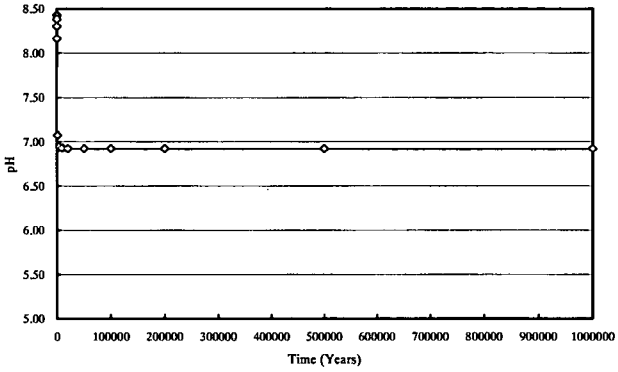

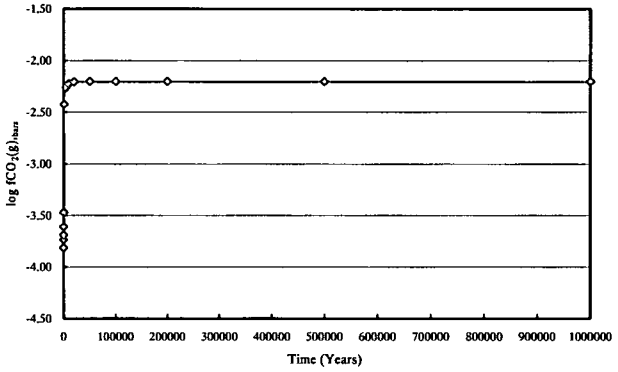

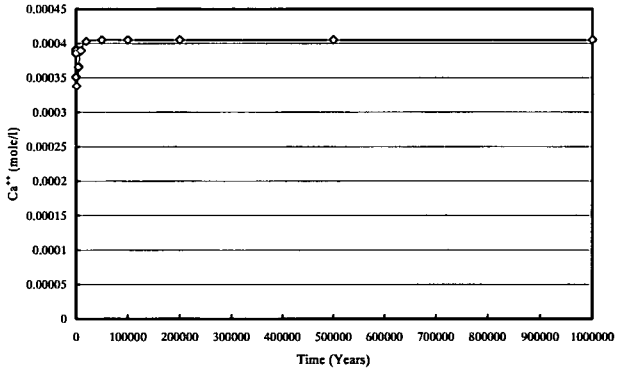

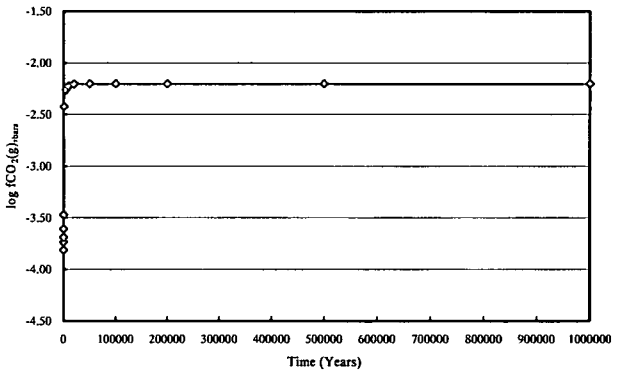

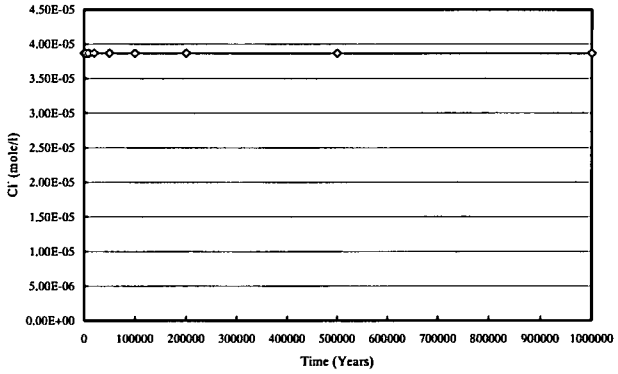

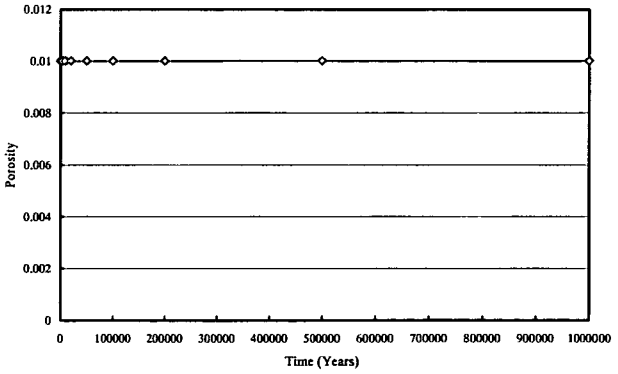

Output from simulation fwpCO2pH25PhMmv1

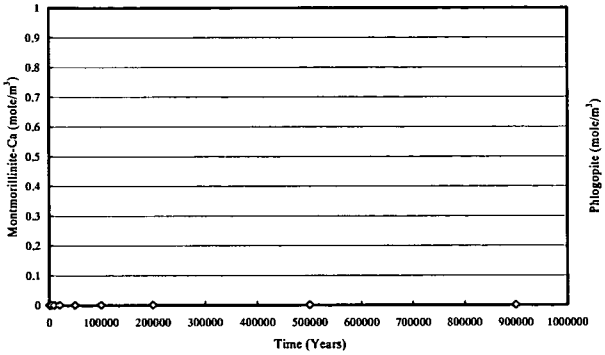

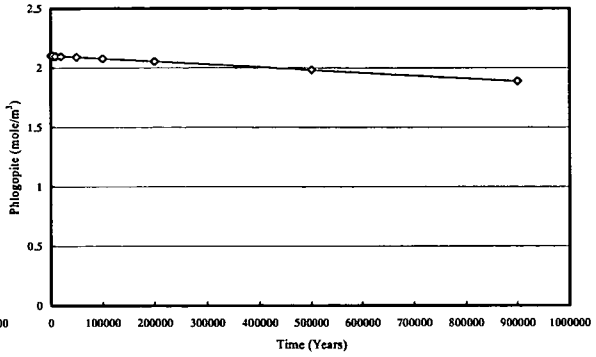

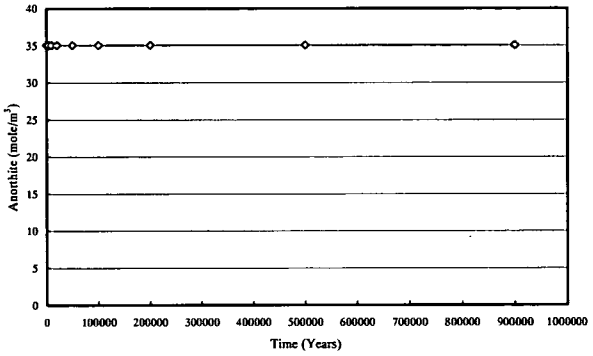

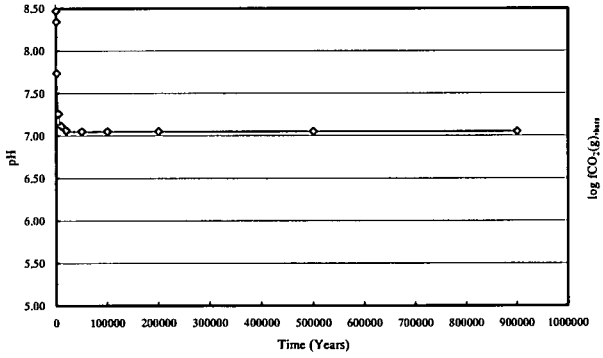

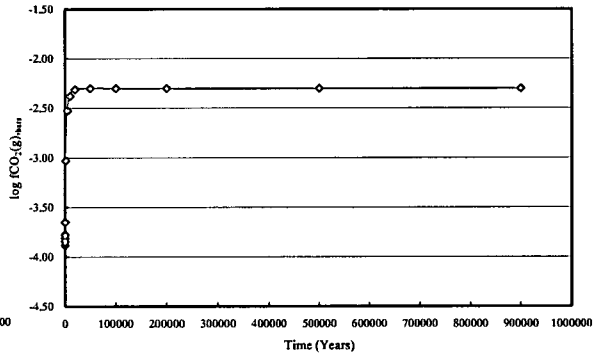

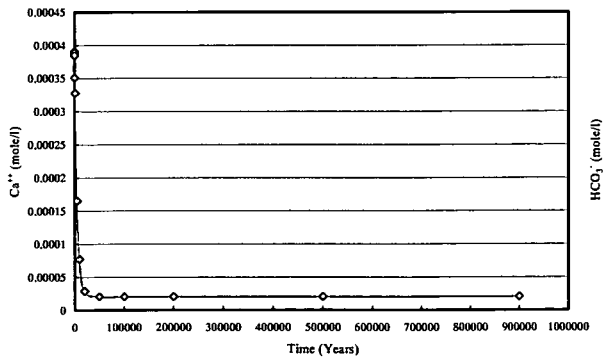

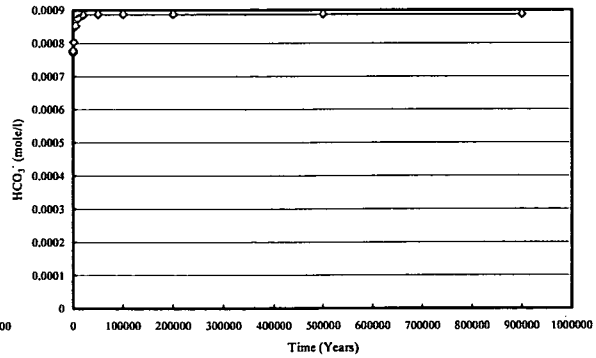

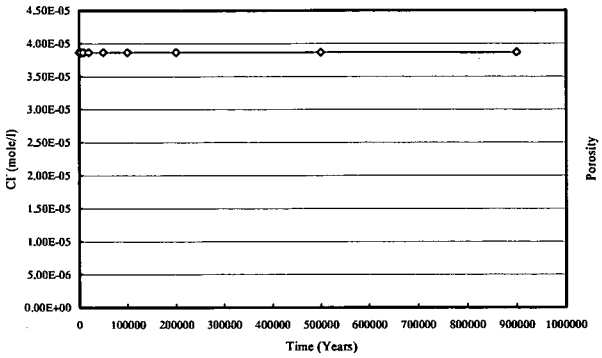
4.50E-05
4.00E-05
3.50E-05
3.00E-05
2.50E-05
2.00E-05
1.50E-05
1.00E-05
5.00E-06
0.00E+00
Cl (mole/l)
0
100000
200000
300000
400000
500000
600000
700000
800000
900000
1000000
Time (Years)

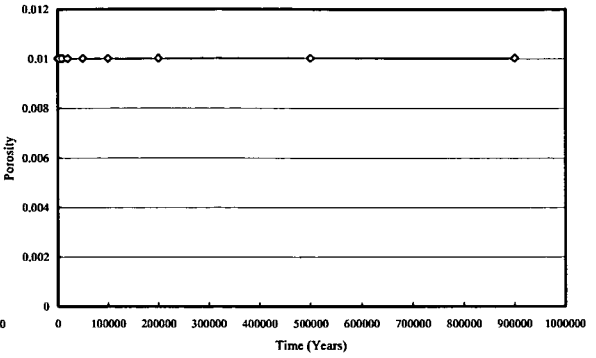
0.012
0.01
0.008
0.006
0.004
0.002
0
Porosity
0
100000
200000
300000
400000
500000
600000
700000
800000
900000
1000000
Time (Years)

Output from simulation fwpCO2pH25PhMmv1a

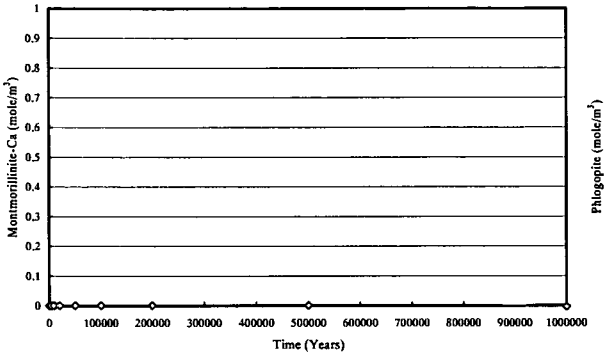

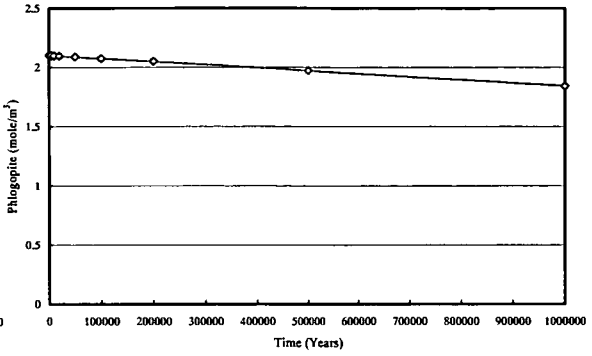

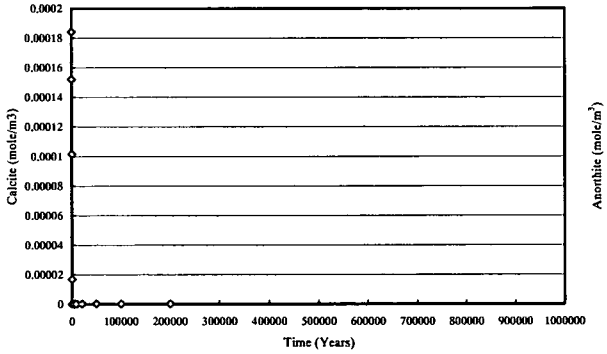

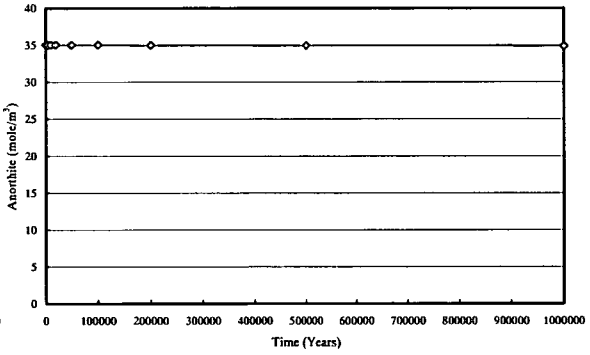

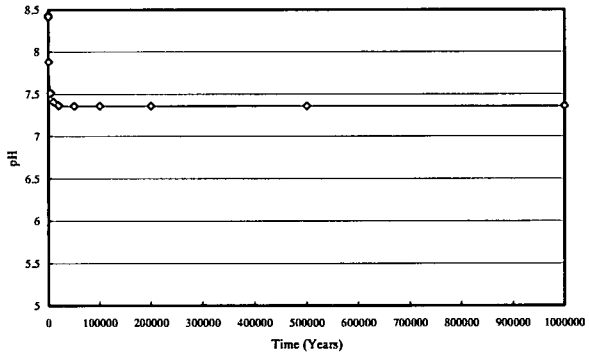

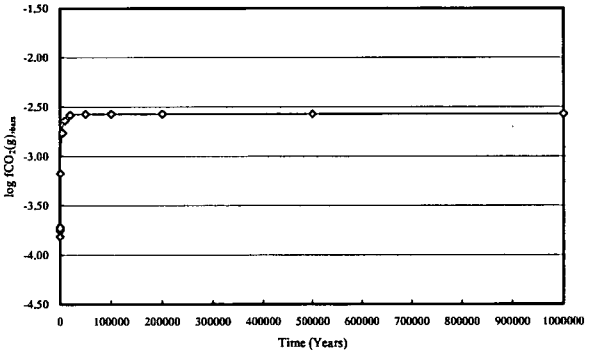

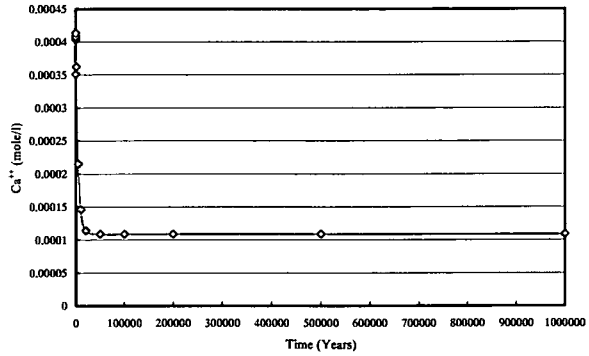

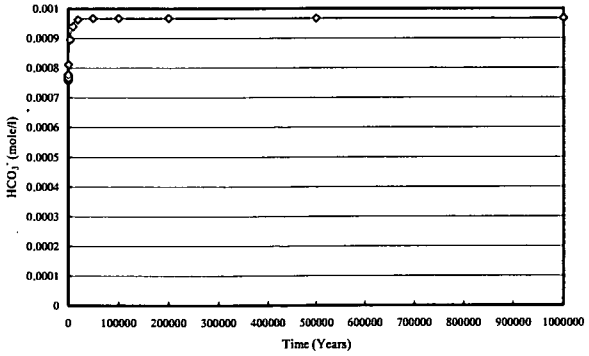

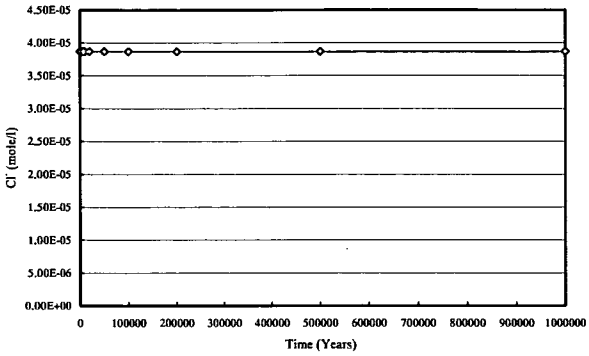
4.50E-05
4.00E-05
3.50E-05
3.00E-05
2.50E-05
2.00E-05
1.50E-05
1.00E-05
5.00E-06
0.00E+00
Cl⁻ (mole/l)
0
100000
200000
300000
400000
500000
600000
700000
800000
900000
1000000
Time (Years)

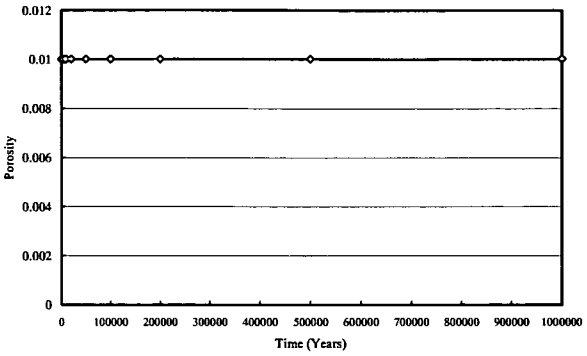
0.012
0.01
0.008
0.006
0.004
0.002
0
Porosity
0
100000
200000
300000
400000
500000
600000
700000
800000
900000
1000000
Time (Years)

Output from simulation fwpCO2pH25Lmd100v1

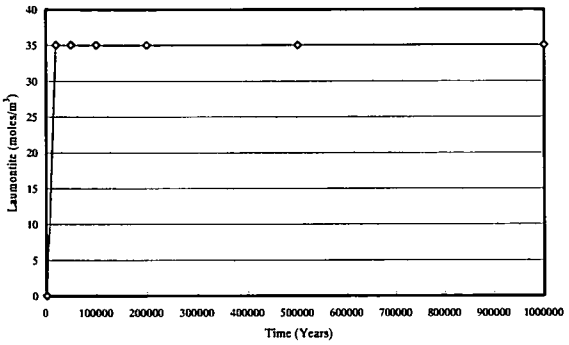

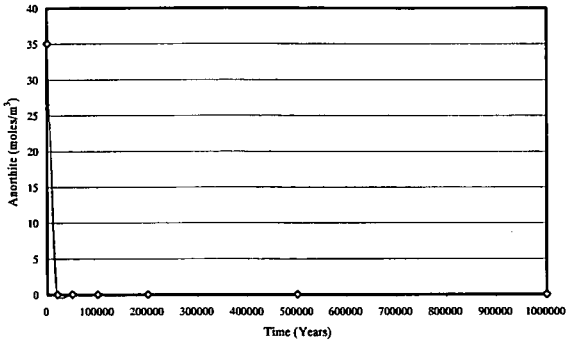

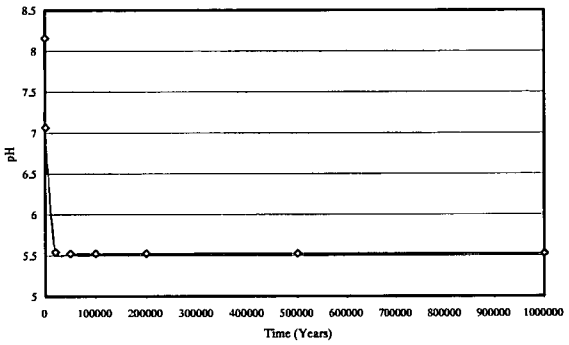

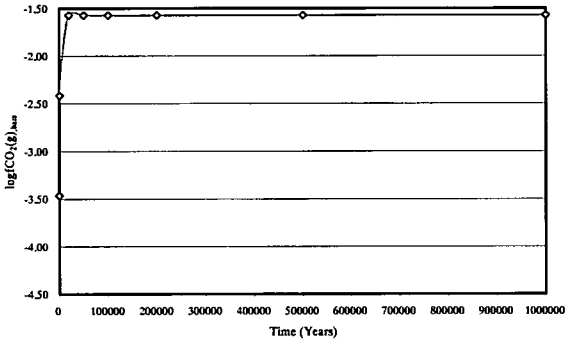

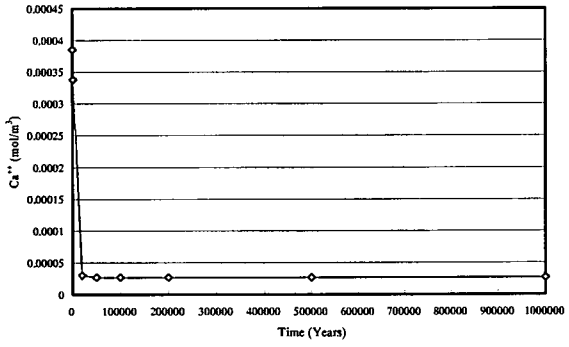

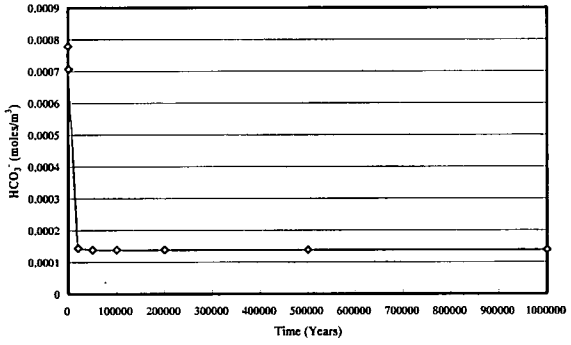

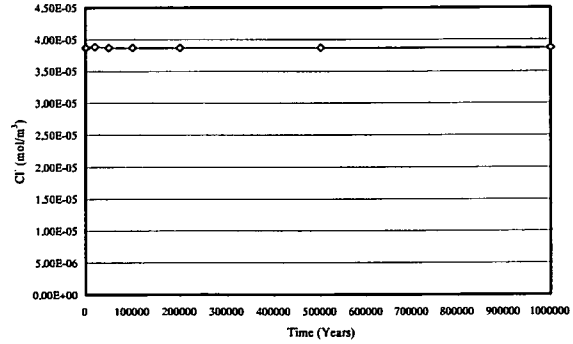

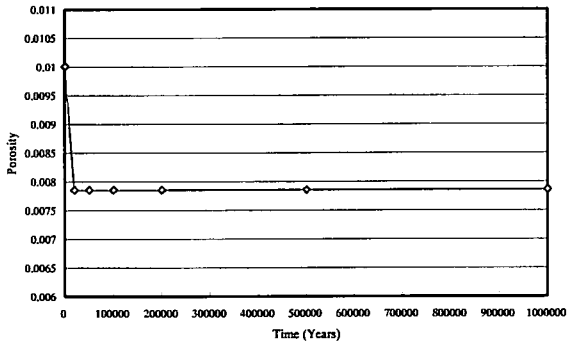

Output from simulation fwpCO2pH25Kad100

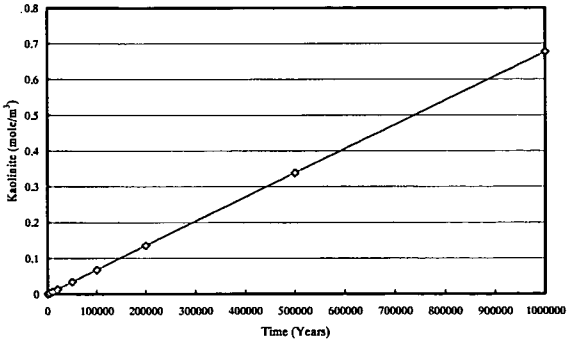

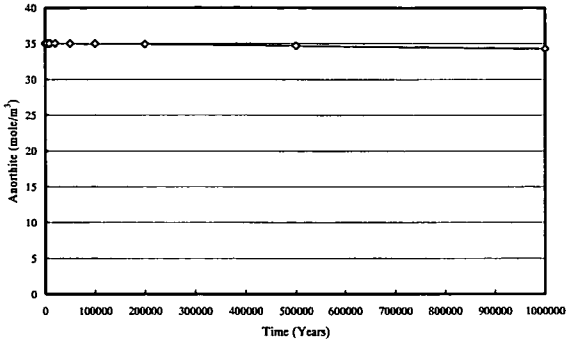

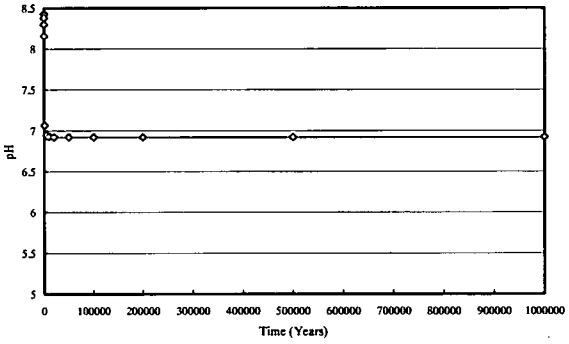

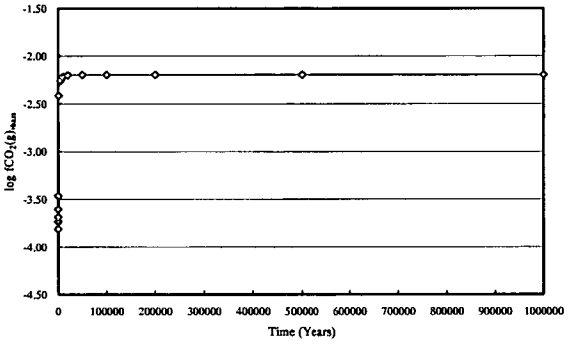

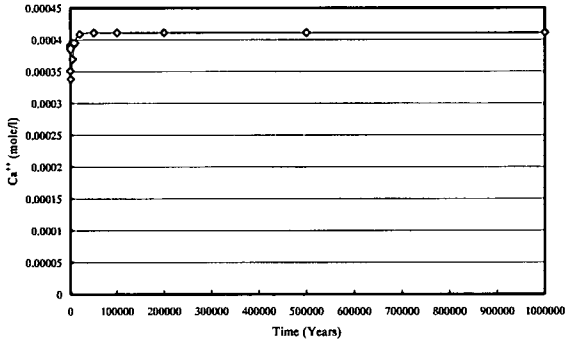

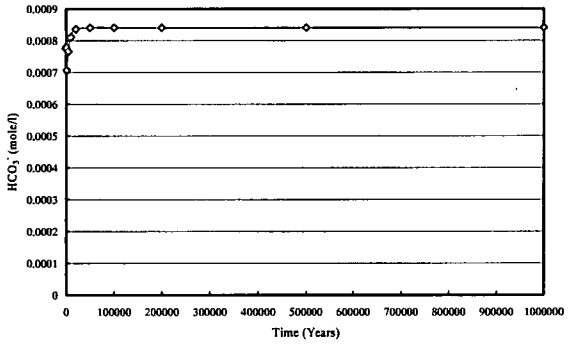

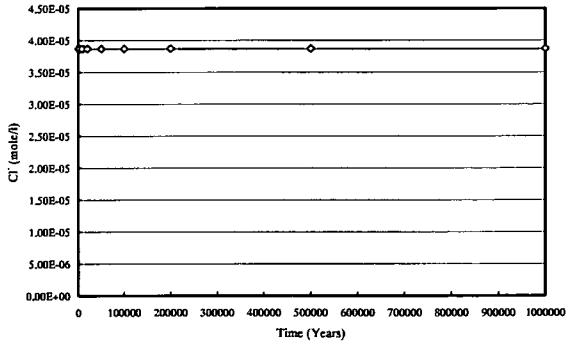

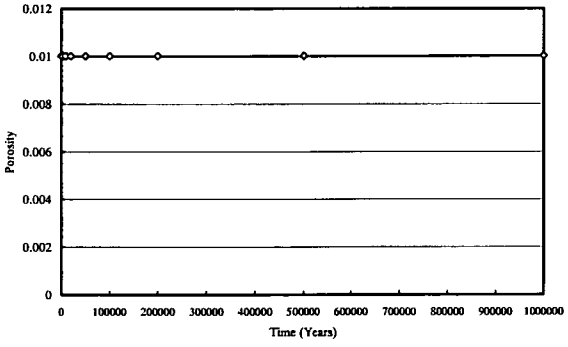

Output from simulation fwpCO2pH25Kad100a

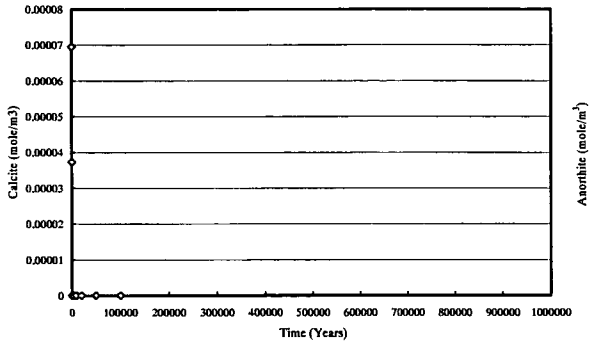

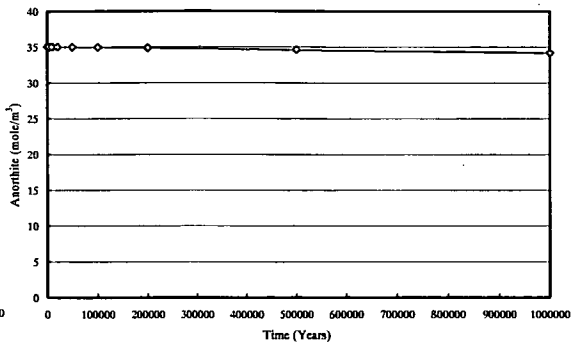

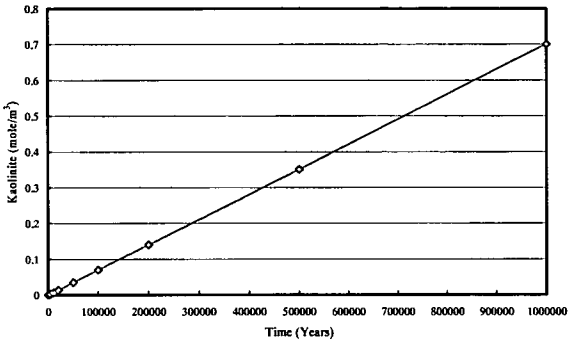

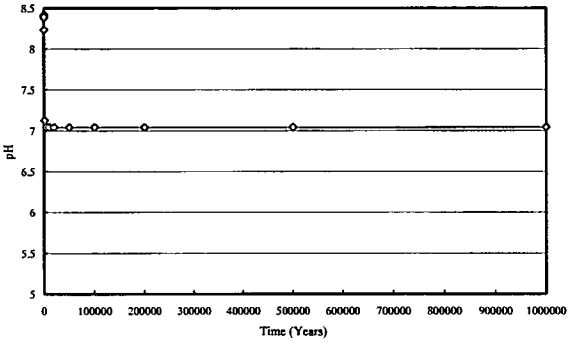

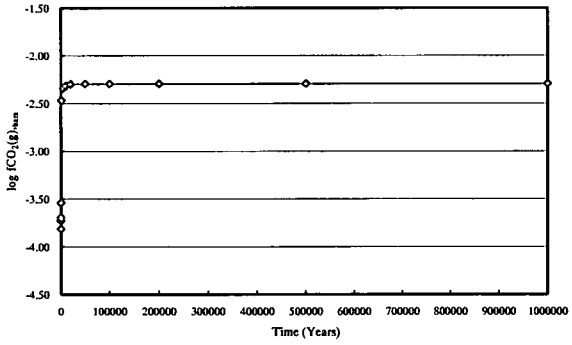

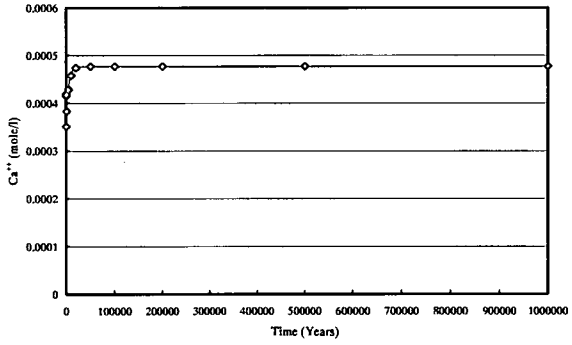

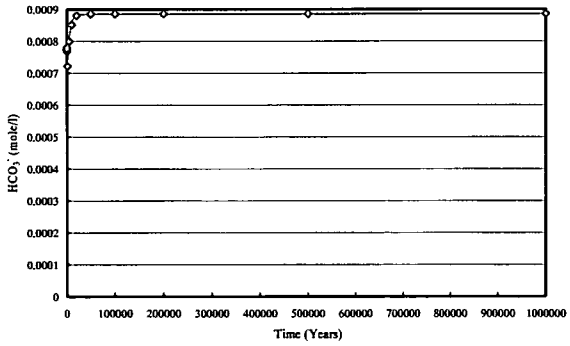

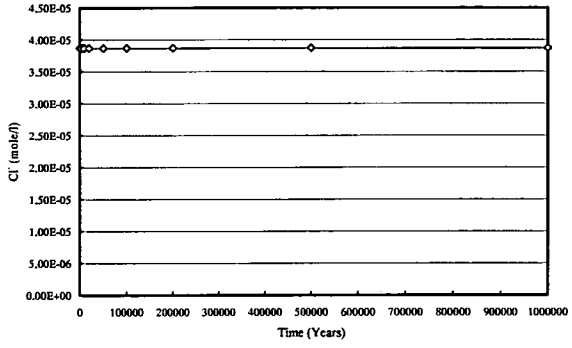

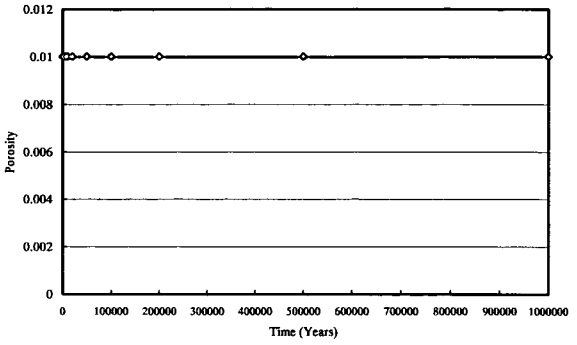
0.012
0.01
0.008
0.006
0.004
0.002
0
Porosity
0
100000
200000
300000
400000
500000
600000
700000
800000
900000
1000000
Time (Years)

Output from simulation fwpCO2pH60Kad100v1

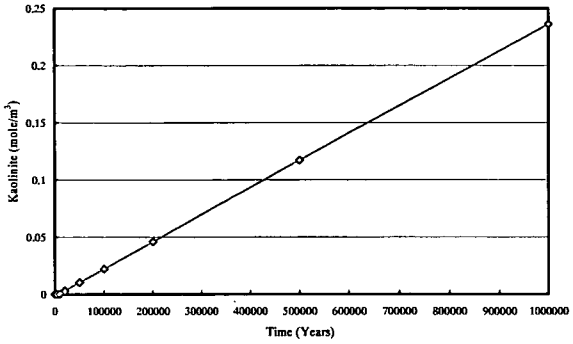

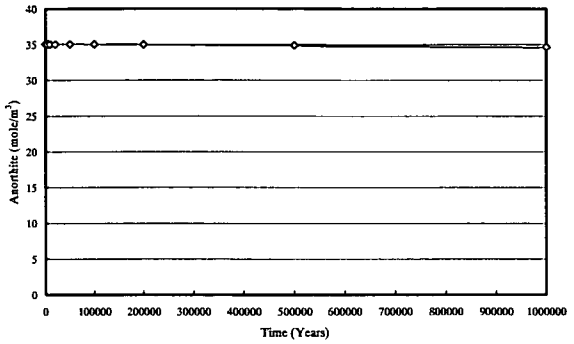

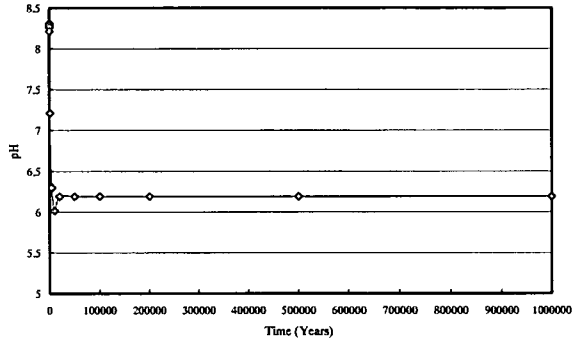

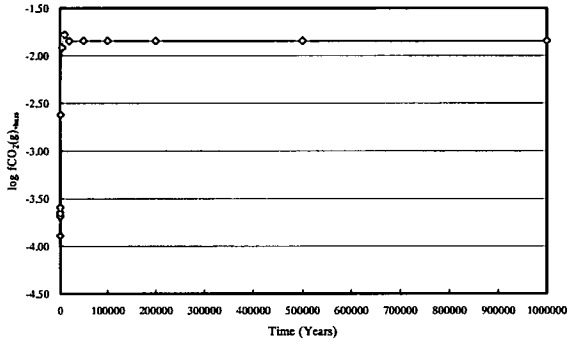

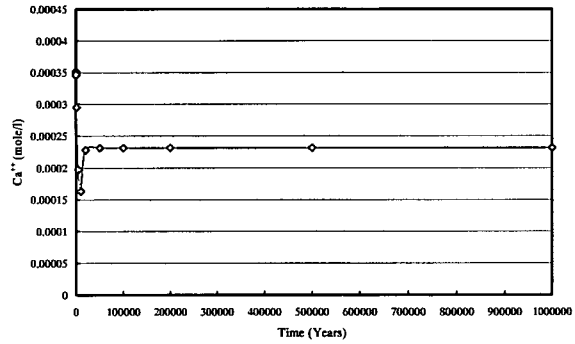

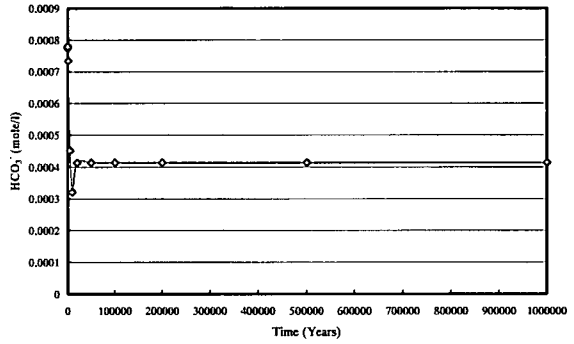

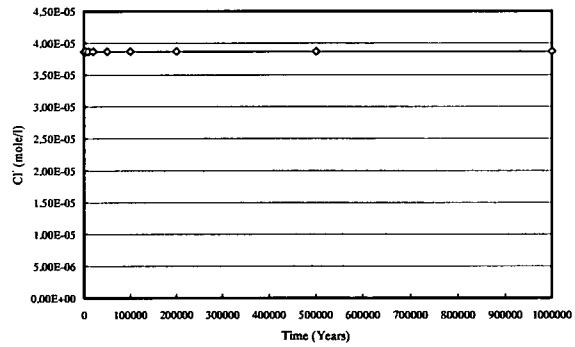

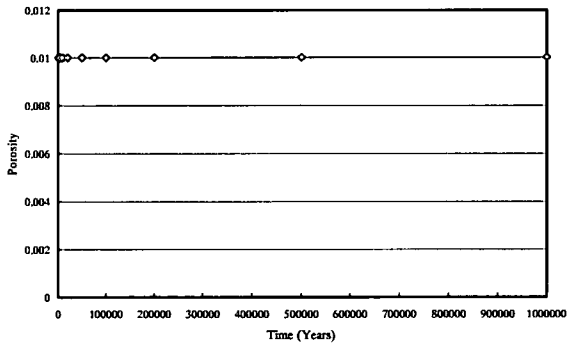

Output from simulation fwpCO2pH60Kad100v1a

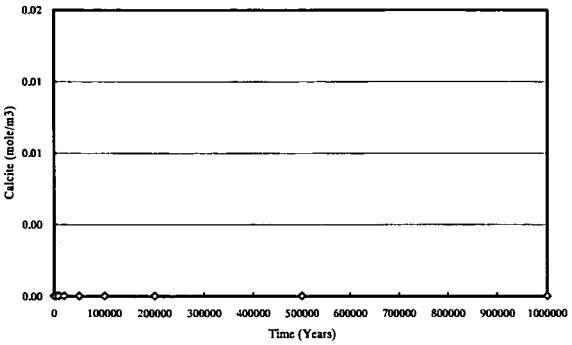

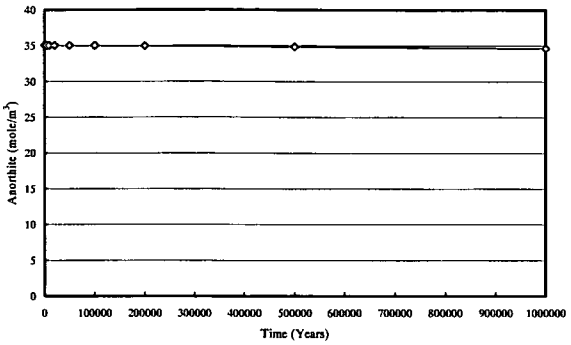

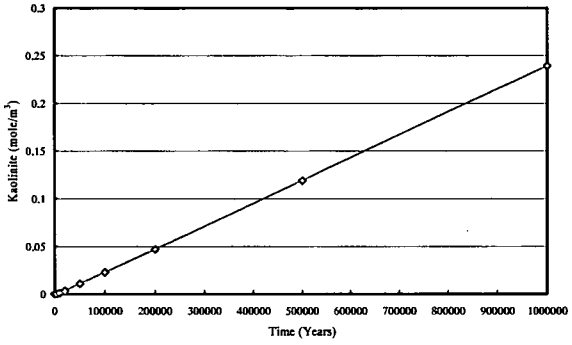

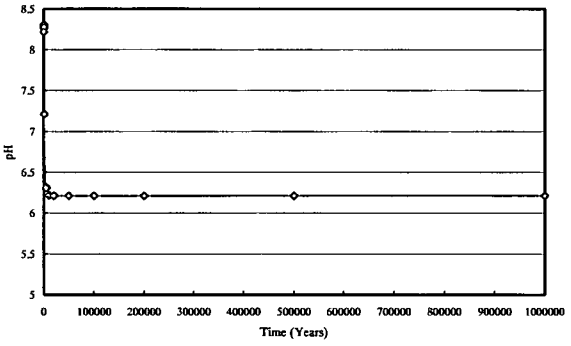

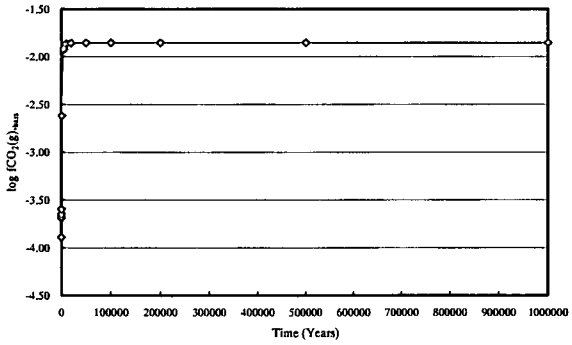

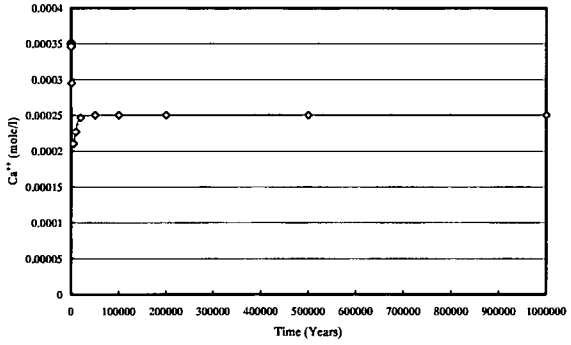

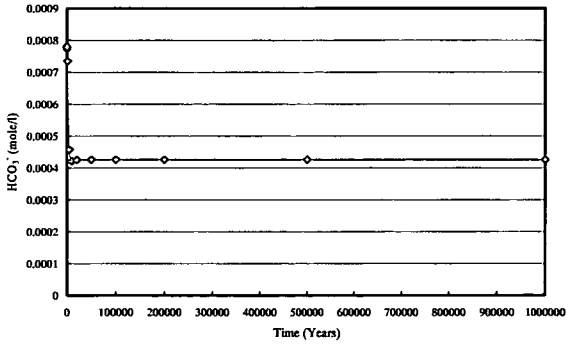

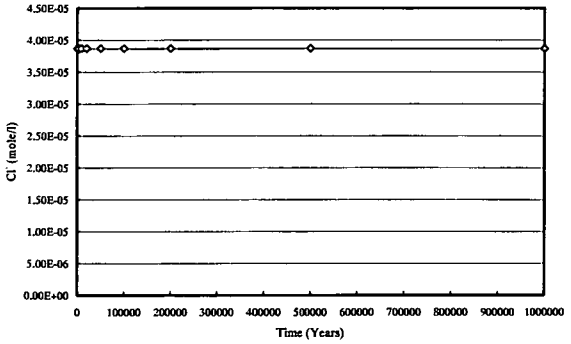

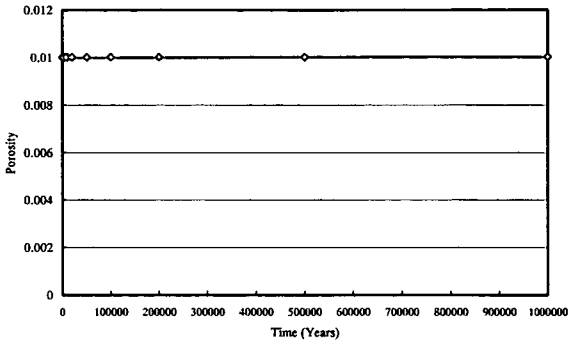
0.012
0.01
0.008
0.006
0.004
0.002
0
Porosity
0
100000
200000
300000
400000
500000
600000
700000
800000
900000
1000000
Time (Years)

Output from simulation fwpCO2pH 25Ka 10 c 270803v1

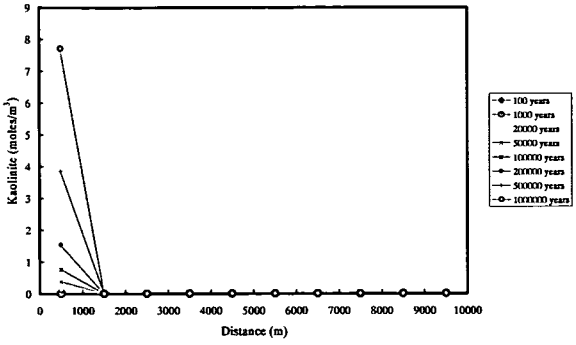

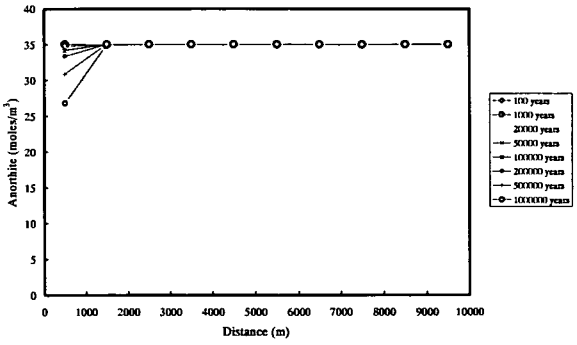

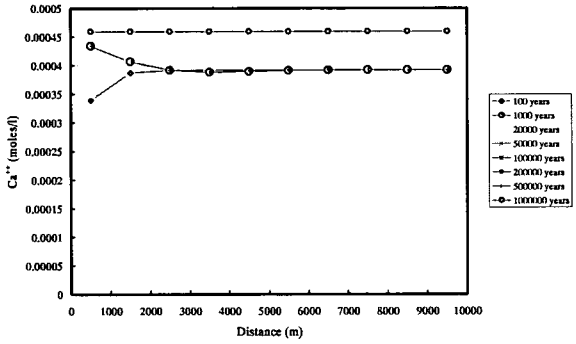

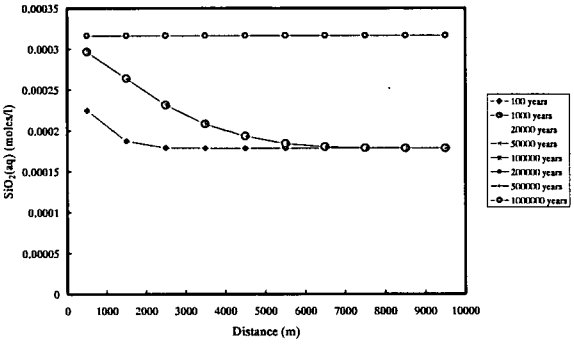

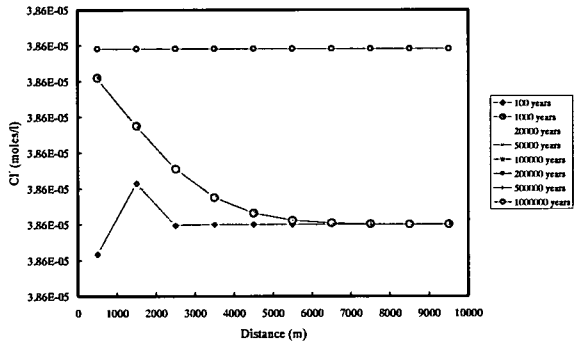

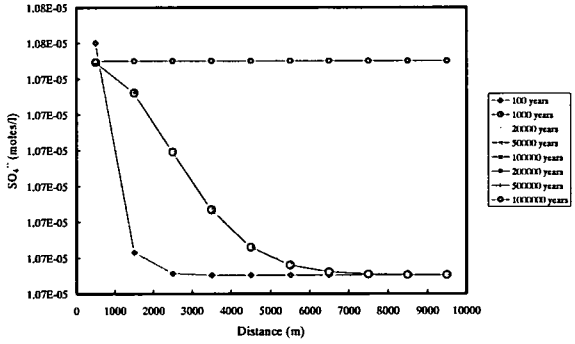

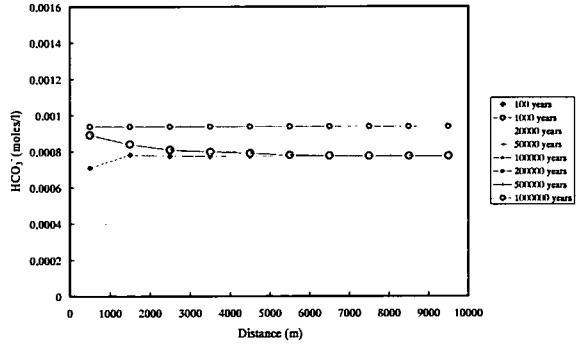

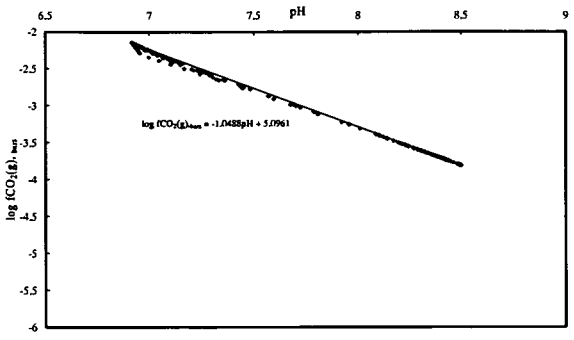
pH
log fCO2(g)
log fCO2(g)sea = -1.0488pH + 5.0961

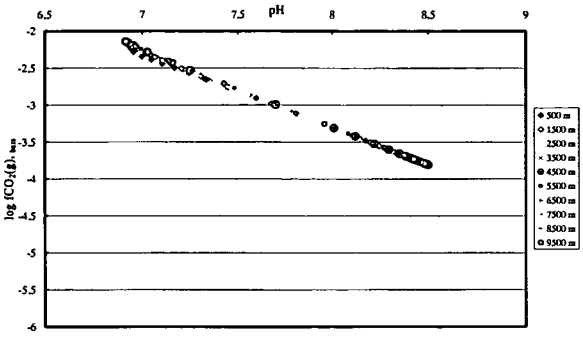
pH
log fCO2(g)
500 m
1500 m
2500 m
3500 m
4500 m
5500 m
6500 m
7500 m
8500 m
9500 m

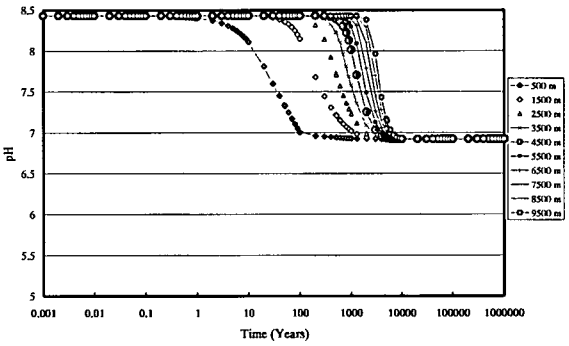
pH
Time (Years)
500 m
1500 m
2500 m
3500 m
4500 m
5500 m
6500 m
7500 m
8500 m
9500 m

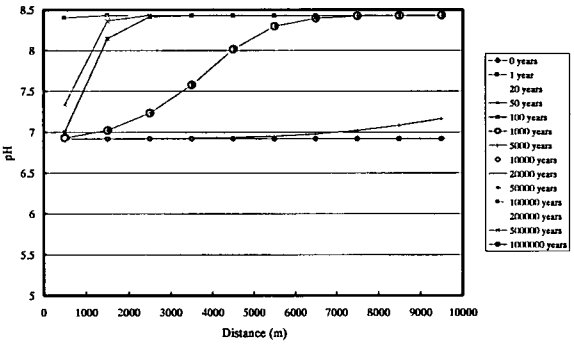
pH
Distance (m)
0 years
1 year
20 years
50 years
100 years
1000 years
5000 years
10000 years
20000 years
50000 years
100000 years
200000 years
500000 years
1000000 years

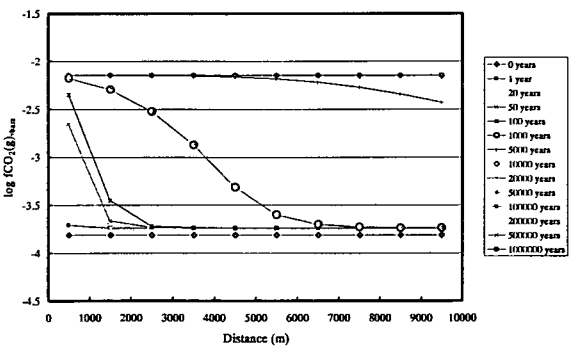
log fCO2(g)
Distance (m)
0 years
1 year
20 years
50 years
100 years
1000 years
5000 years
10000 years
20000 years
50000 years
100000 years
200000 years
500000 years
1000000 years

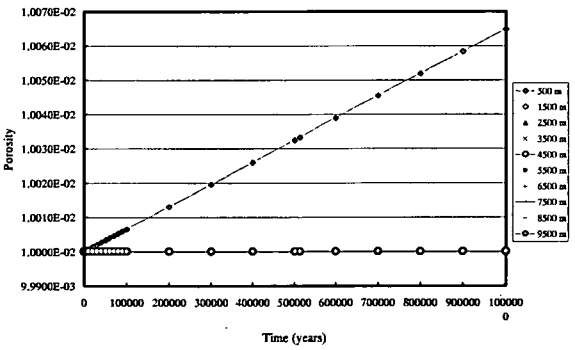
Porosity
Time (years)
500 m
1500 m
2500 m
3500 m
4500 m
5500 m
6500 m
7500 m
8500 m
9500 m

Output from simulation fwpCO2pH 25Ka 10 c 270803v1a

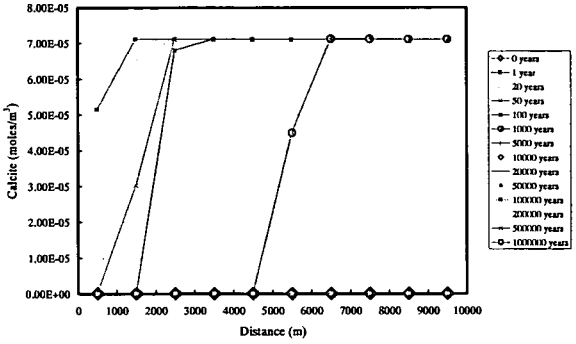

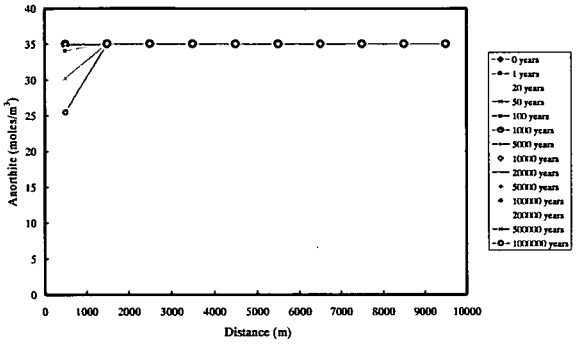

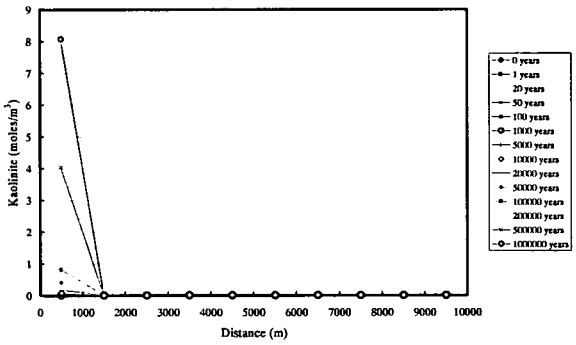

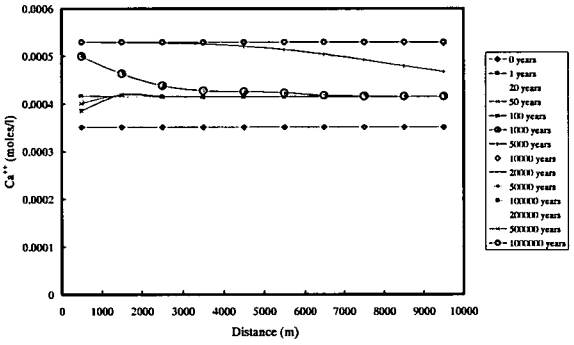

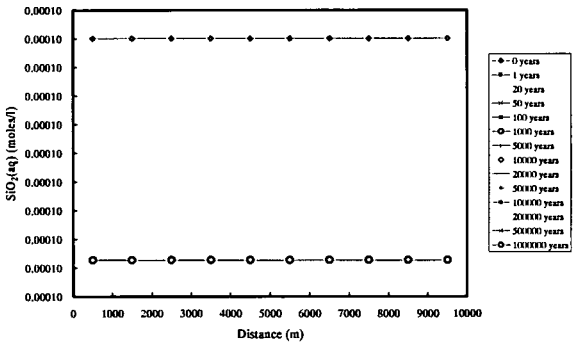

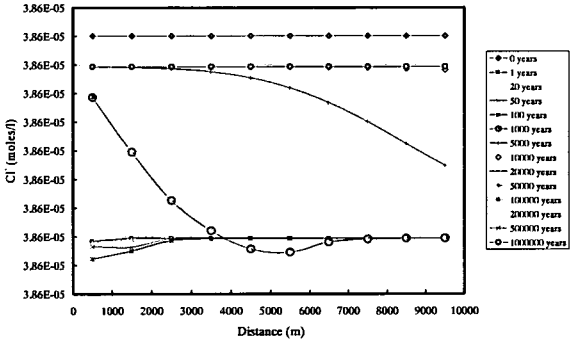

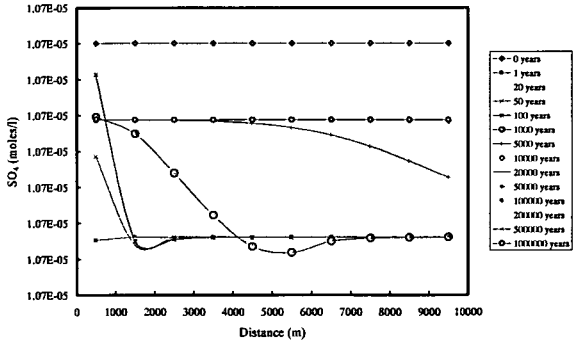

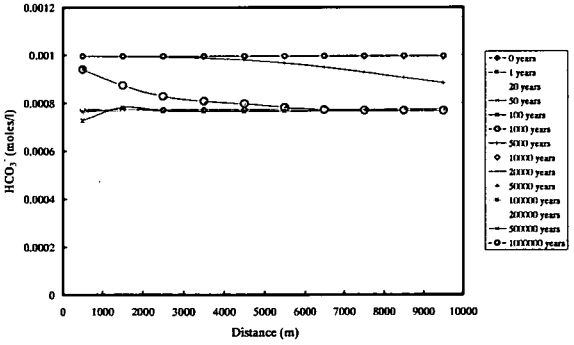

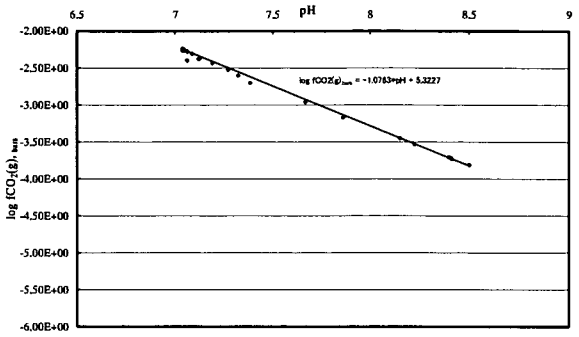
pH
log fCO2(g), bars
log fCO2(g)bars = -1.0763*pH + 5.3227

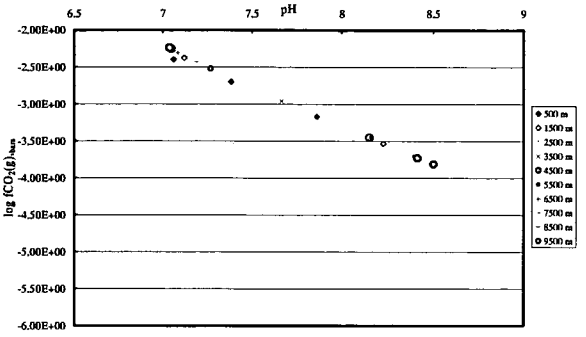
pH
log fCO2(g)bars
500 m
1500 m
2500 m
3500 m
4500 m
5500 m
6500 m
7500 m
8500 m
9500 m

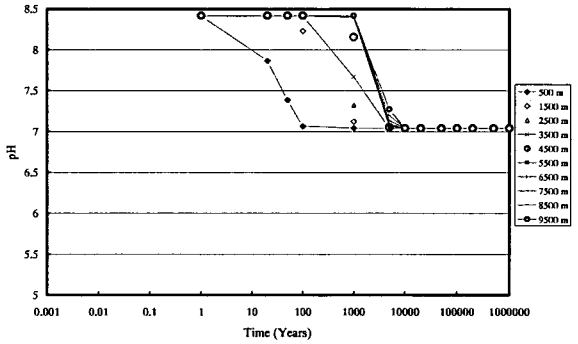
pH
Time (Years)
500 m
1500 m
2500 m
3500 m
4500 m
5500 m
6500 m
7500 m
8500 m
9500 m

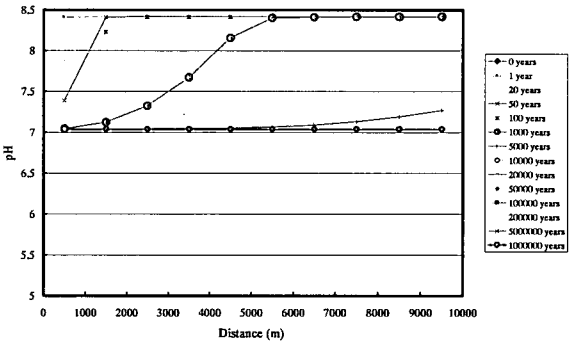
pH
Distance (m)
0 years
1 year
20 years
50 years
100 years
1000 years
5000 years
10000 years
20000 years
50000 years
100000 years
200000 years
500000 years
1000000 years

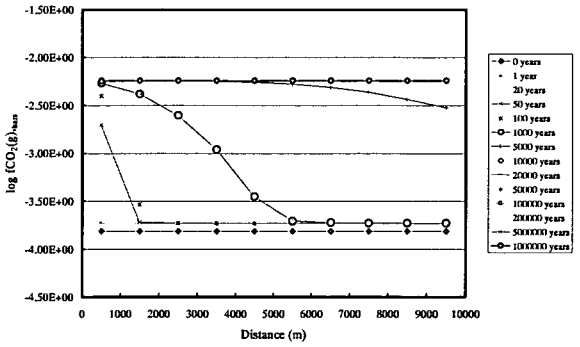
log fCO2(g)bars
Distance (m)
0 years
1 year
20 years
50 years
100 years
1000 years
5000 years
10000 years
20000 years
50000 years
100000 years
200000 years
500000 years
1000000 years

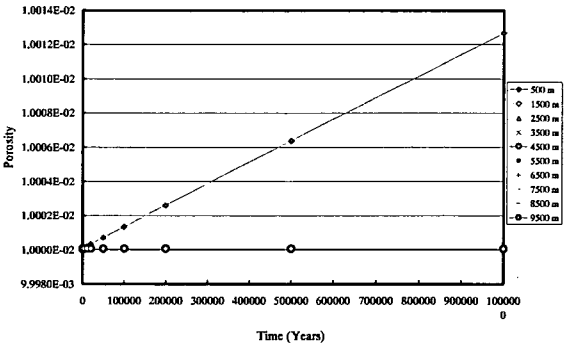
Porosity
Time (Years)
500 m
1500 m
2500 m
3500 m
4500 m
5500 m
6500 m
7500 m
8500 m
9500 m

Output from simulation swpCO2pH 25Ka 10 c 270803v2

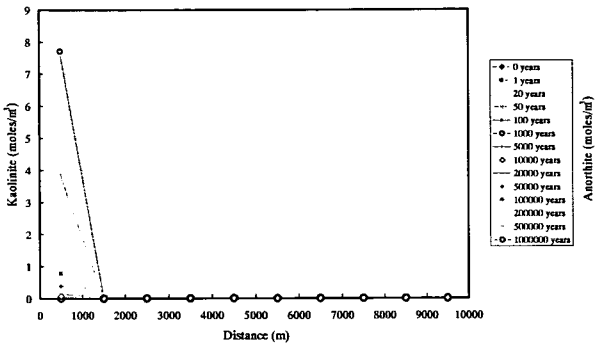

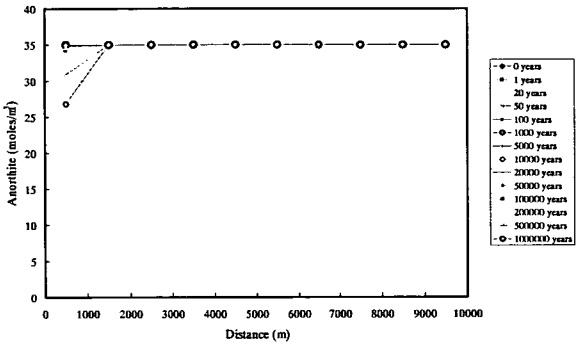

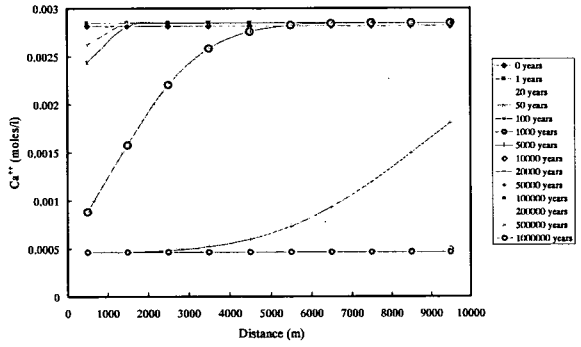

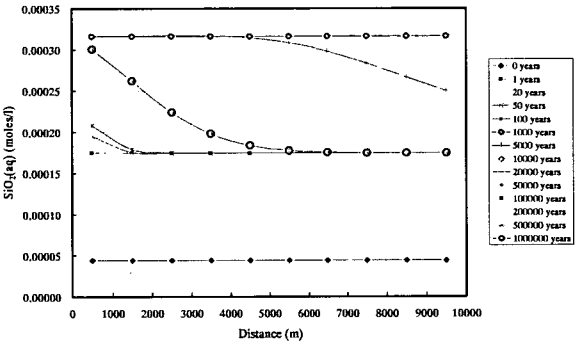

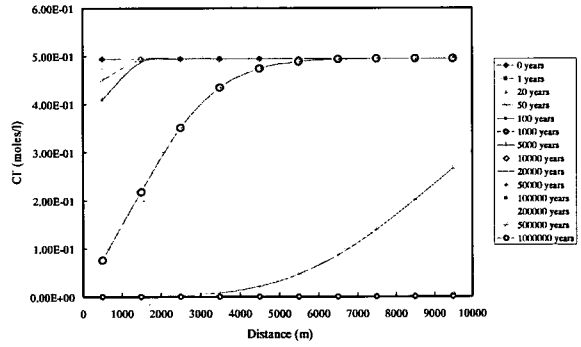

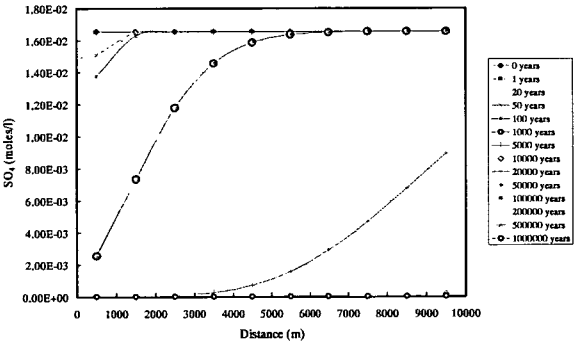

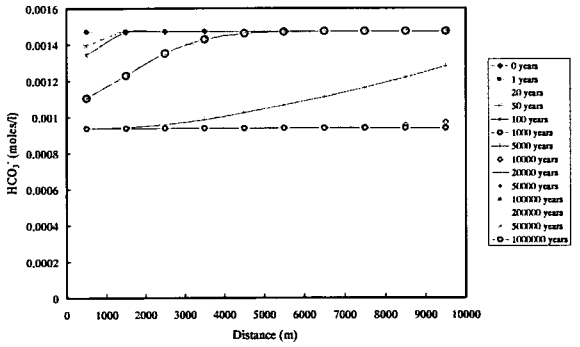

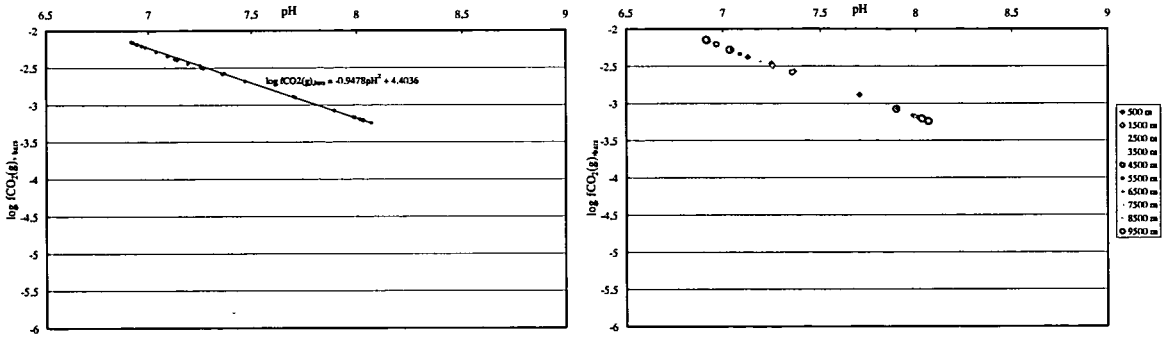
pH
log fCO2(g)
log fCO2(g) = -0.9478pH² + 4.4036
500 m
1500 m
2500 m
3500 m
4500 m
5500 m
6500 m
7500 m
8500 m
9500 m

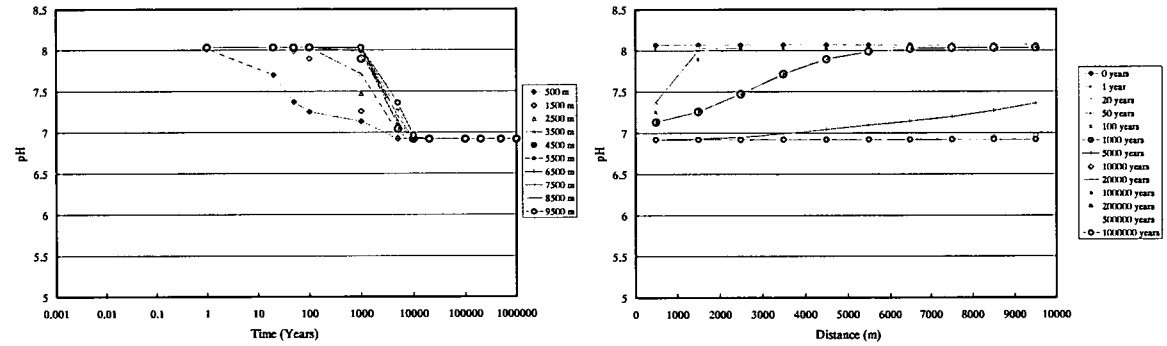
pH
Time (Years)
Distance (m)
0 years
1 year
20 years
50 years
100 years
1000 years
5000 years
10000 years
20000 years
100000 years
200000 years
500000 years
1000000 years

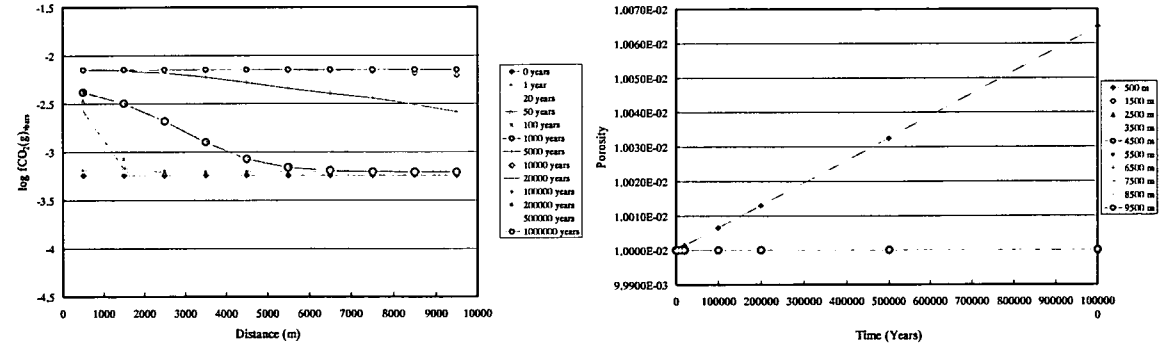
log fCO2(g)
Distance (m)
Porosity
Time (Years)

Output from simulation swpCO2pH 25Ka 10 c 270803v2a

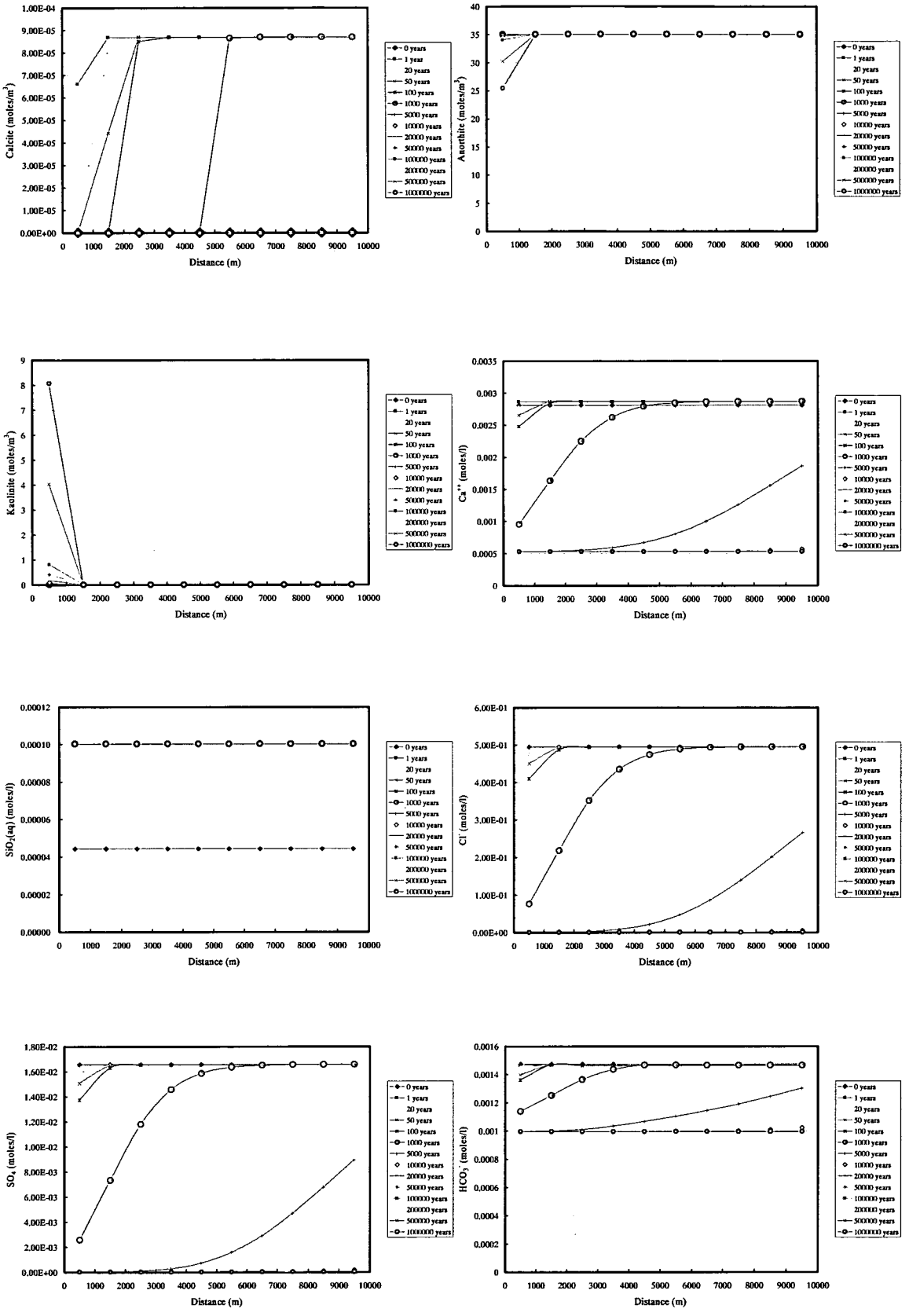

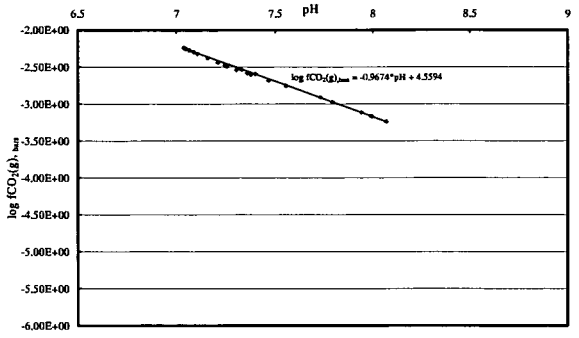
pH
log fCO2(g)
log fCO2(g)max = -0.9674*pH + 4.5594

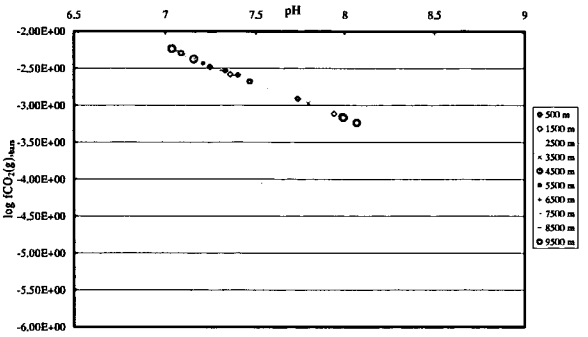
pH
log fCO2(g)
500 m
1500 m
2500 m
3500 m
4500 m
5500 m
6500 m
7500 m
8500 m
9500 m

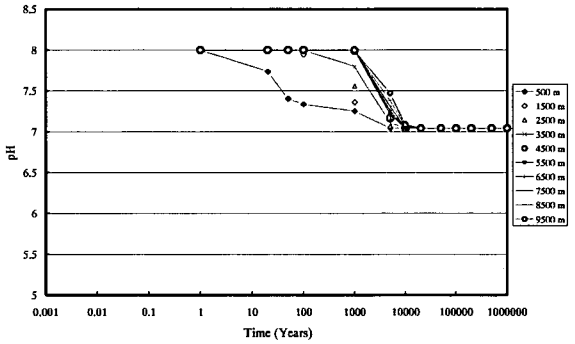
pH
Time (Years)
500 m
1500 m
2500 m
3500 m
4500 m
5500 m
6500 m
7500 m
8500 m
9500 m

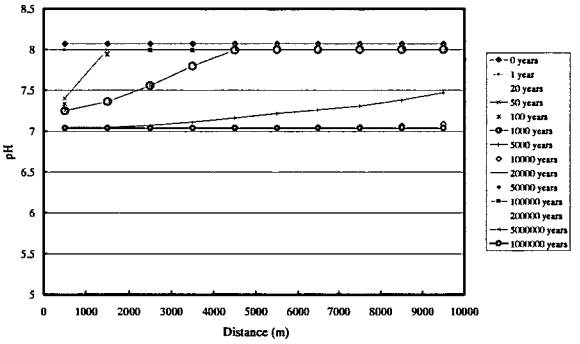
pH
Distance (m)
0 years
1 year
20 years
50 years
100 years
1000 years
5000 years
10000 years
20000 years
50000 years
100000 years
200000 years
500000 years
1000000 years

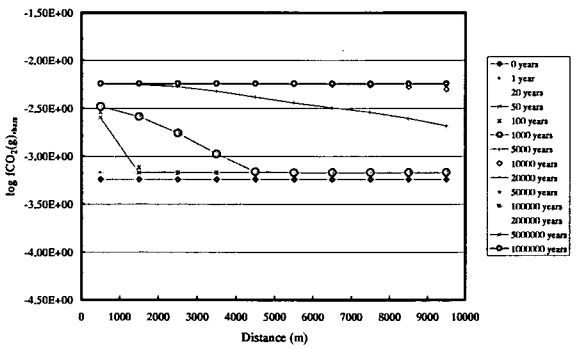
log fCO2(g)
Distance (m)
0 years
1 year
20 years
50 years
100 years
1000 years
5000 years
10000 years
20000 years
50000 years
100000 years
200000 years
500000 years
1000000 years

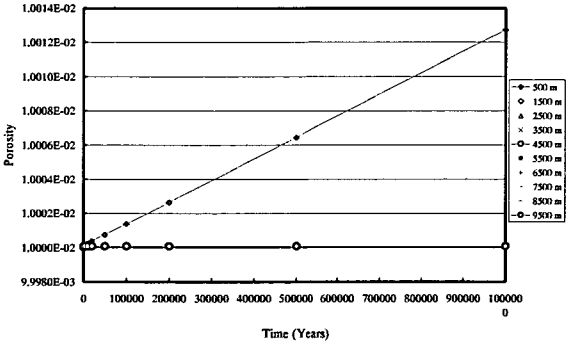
Porosity
Time (Years)
500 m
1500 m
2500 m
3500 m
4500 m
5500 m
6500 m
7500 m
8500 m
9500 m

Output from simulation a28cv2

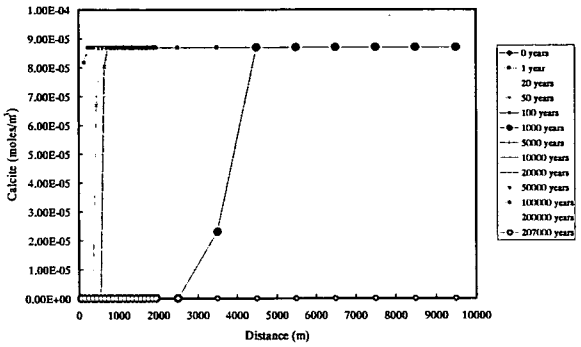

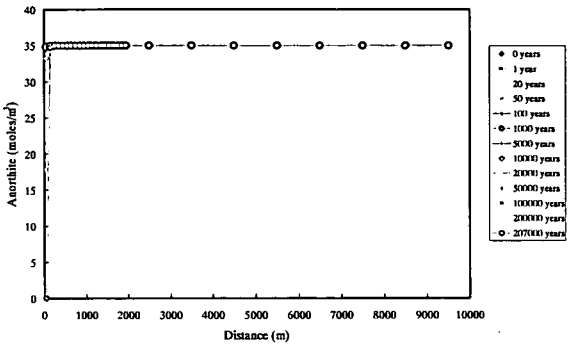

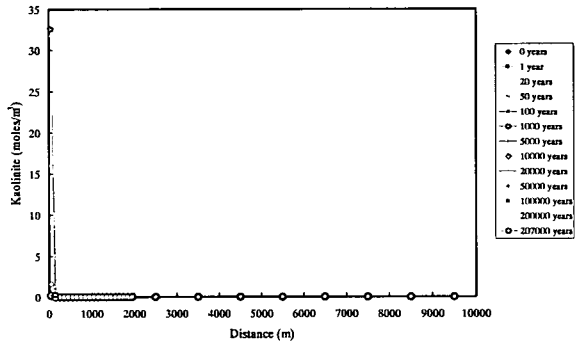

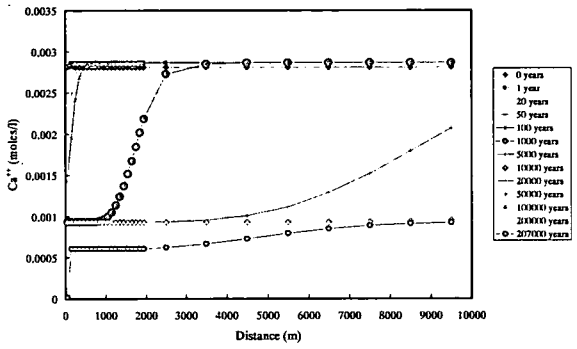

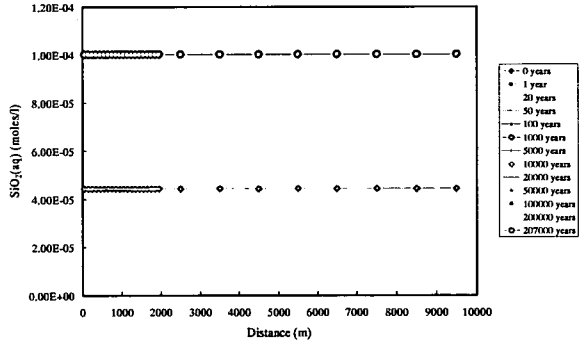

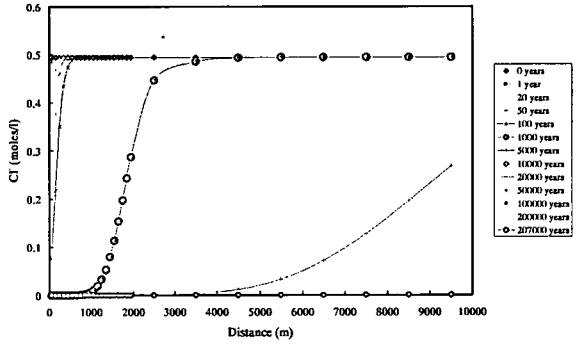

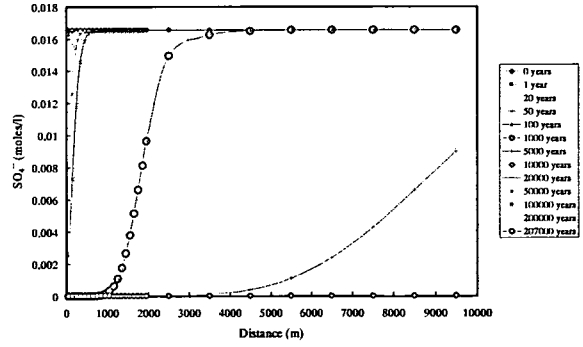

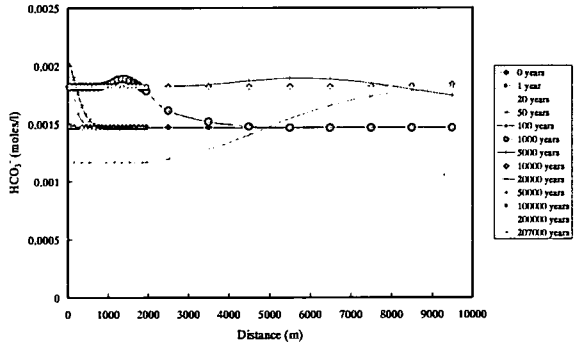

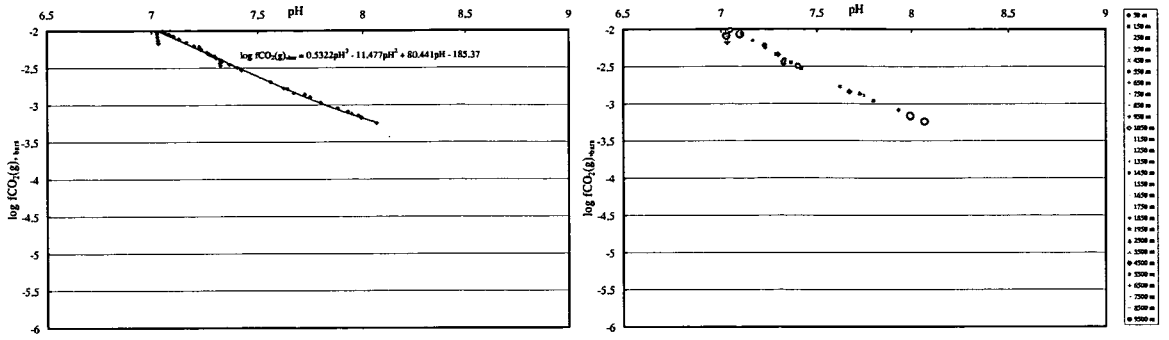
pH
log fCO2(g)
log fCO2(g) = 0.5322pH3 - 11.477pH2 + 80.441pH - 185.37

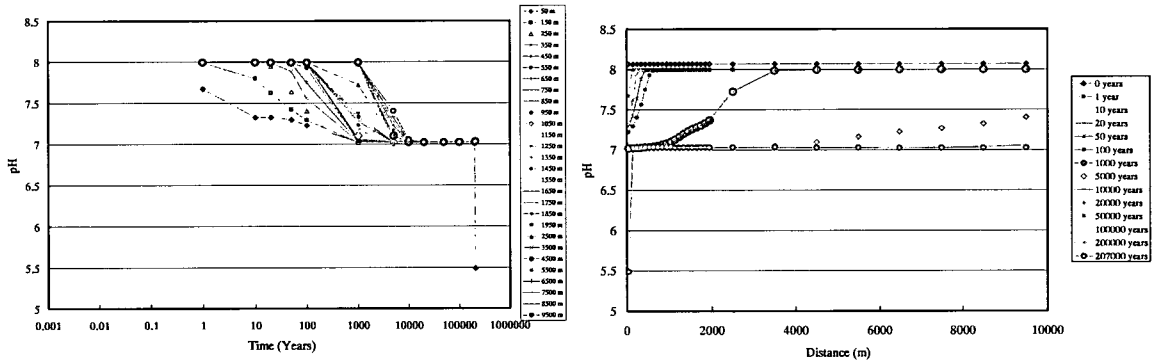
pH
Time (Years)
Distance (m)
0 years
1 year
10 years
20 years
50 years
100 years
1000 years
5000 years
10000 years
20000 years
50000 years
100000 years
200000 years
207000 years

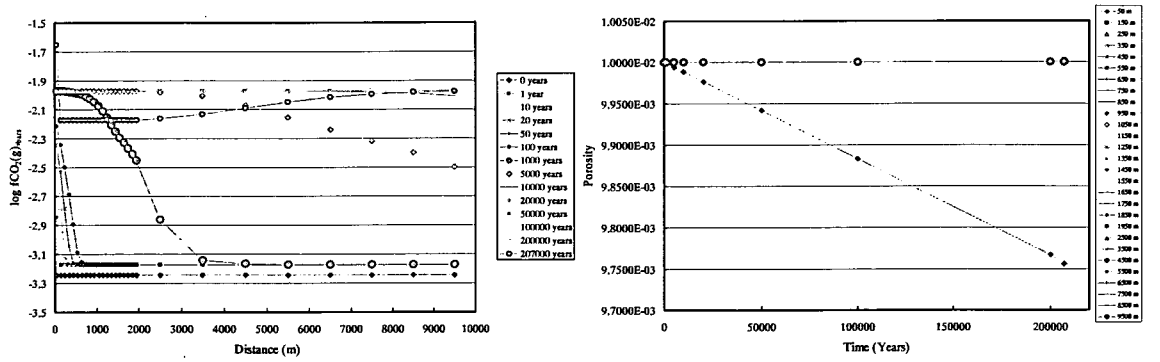
log fCO2(g)
Distance (m)
Porosity
Time (Years)